MULTI-SPHERE HYDRODYNAMIC MODELS OF SUSPENSIONS AND POROUS MEDIA

by

Ronald Jefferson Phillips

B.S., University of California, Davis
(1984)

Submitted to the Department of Chemical Engineering
in partial fulfillment of the requirements
for the degree of

DOCTOR OF PHILOSOPHY

at the

MASSACHUSETTS INSTITUTE OF TECHNOLOGY

October 13, 1989

Signature of Author ______________________________
Department of Chemical Engineering
October 13, 1989

Certified by ______________________________
William M. Deen
Thesis Supervisor

Accepted by ______________________________
William M. Deen
Chemical Engineering Graduate Officer

MULTI-SPHERE HYDRODYNAMIC MODELS OF SUSPENSIONS AND POROUS MEDIA

by

Ronald Jefferson Phillips

Submitted to the Department of Chemical Engineering
on October 13, 1989 in partial fulfillment of the
requirements for the degree of Doctor of Philosophy in
Chemical Engineering

ABSTRACT

A method has been derived for calculating hydrodynamic interactions in unbounded suspensions and porous media comprised of spherical particles. The method relies upon a separation of these interactions into far-field and near-field components. The far-field, or long-range, interactions are calculated in terms of an expansion in moments of the force density of each particle surface about its center, and in principle can be carried out to any level of accuracy that is desired. These far-field interactions are properly renormalized and are summed using an accelerated convergence scheme known as the Ewald summation technique. The near-field, or short-range, interactions are accounted for in a pairwise additive fashion using the exact, two-sphere interaction results available in the literature.

This new method of calculation, referred to as the "Stokesian dynamics" method, has been used to calculate transport properties of both spatially periodic and disordered suspensions and porous media. The studies on spatially periodic media allowed the accuracy of the method to be examined through comparisons with the relatively complete set of results available for those systems. Properties such as the hydraulic permeability, sedimentation velocity, and shear viscosity were calculated for cubic arrays of spheres. It was found that, in almost every case, Stokesian dynamics gave highly accurate results over the full range of volume fractions possible for hard spheres.

Calculations for disordered media were accomplished by Monte Carlo simulation, in which a series of disordered samples were generated and their transport properties calculated and averaged. In addition to the properties mentioned above for periodic media, short-time self-diffusion coefficients and short-time hindered diffusion coefficients were calculated for single, Brownian particles in disordered suspensions and porous media, respectively. The results were compared with other theoretical and experimental results reported in the literature, and again excellent agreement was obtained in almost every case. It should be emphasized here that Stokesian dynamics allowed all the transport properties listed above to be calculated from a single theoretical framework, and also permitted what theoretical predictions do exist for disordered systems to be extended to arbitrarily high volume fractions.

Finally, two approaches have been developed for calculating long-time, macroscopic transport coefficients for a spherical solute in a matrix of fibers. The first method is an effective medium approach based on Brinkman's equation, and has the advantage of being applicable to systems for which very little microstructural information is available. In the second, and more rigorous calculation, the Stokesian dynamics method is used to obtain short-time, or local hydrodynamic coefficients for spherical particles in arrays of bead-and-string fibers. These local coefficients are used to evaluate global coefficients, which govern transport over macroscopic length scales, through application of generalized Taylor dispersion theory. Numerical results have been obtained for two different spatially periodic fiber lattices over a wide range of volume fractions, and for ratios of solute radius to fiber radius ranging from 0.5 to 5. Comparisons between the effective medium model and the generalized Taylor dispersion theory results consistently showed good qualitative agreement, and agreed quantitatively at volume fractions low compared to the critical volume fraction (*i.e.*, the volume fraction where macroscopic transport ceases). In addition, the effective medium model predictions of hindered transport coefficients were found to be in excellent agreement with experimental data obtained from the literature, without the use of adjustable parameters.

Thesis Supervisor: William M. Deen
Professor of Chemical Engineering

To my mother and father

ACKNOWLEDGEMENTS

The development of the Stokesian dynamics method as described in Chapter 2, and the results for spatially periodic systems presented in Chapter 3, were obtained through collaboration with Dr. John F. Brady and Dr. Julia C. Lester at the California Institute of Technology.

This work was supported by a grant from the National Institutes of Health and a grant of computer time from the John von Neumann Center, Princeton, NJ. In addition, the author is the recipient of a fellowship from the National Science Foundation.

I would like to thank Professors William M. Deen and John F. Brady for the technical assistance, support and guidance they have given me throughout my graduate education. Their patience and willingness to help will always be deeply appreciated.

I would like to thank my ex-roommate John Wasson for being a much needed friend during the time I was studying for my Ph.D. qualifying exams (and afterwards).

I would like to thank Marc Davidson for a series of interesting and intense discussions on both technical and non-technical subjects.

I would to thank Nelson Lin for leading our group to the championship in the departmental three-on-three basketball tournament, and for being a great friend both on and off the court.

I would like to thank Nikola Juhasz for many enjoyable hours spent reading the Boston Globe.

I would like to thank my parents, my brother, and my sister for their interest and encouragement before and during my time in graduate school.

Finally, I would like to thank my fiancee Stephanie Dungan, who has made the last two years of my life so interesting and enjoyable. My love and admiration for you are deep and everlasting.

TABLE OF CONTENTS

LIST OF FIGURES

LIST OF TABLES

CHAPTER 1

INTRODUCTION

The determination of the effective transport properties of suspensions and porous media has been a topic of theoretical and practical interest for over a century. The presence of a solid phase immersed in a continuous, fluid phase drastically alters both fluid flow and solute transport in such systems. In general, these effects depend strongly on complex, hydrodynamic interactions that occur between the various substituents of the solid phase. These interactions decay slowly with distance and are significantly influenced by the overall configuration of the system of interest. Thus, the focus of past, as well as present, efforts has been on developing methods for calculating these interactions, thereby allowing the subsequent calculation of the effective transport parameters themselves. Research in this area has made significant advances in recent years, particularly with regard to suspensions and porous media that can be modeled as dilute suspensions of hard spheres. However, there are many important applications in which these requirements are overly restrictive, and a more general approach would be of great use.

One important application is the transport of large solutes through fibrous media in which the interfiber spacing is comparable to the dimensions of the diffusing macromolecule. Such media include gels and a variety of membranes. In systems of this type, transport is hindered by the aforementioned hydrodynamic interactions which take place between the solute and fiber surfaces. In addition, steric interactions reduce the volume accessible to the solute relative to that in bulk solution, resulting in a partitioning effect. Partition coefficients for spherical solutes in random arrays of fibers can be predicted theoretically both in the dilute limit (Ogston, 1958) and for finite concentrations (Fanti and Glandt, 1989). In contrast, little or no information on the increased hydrodynamic resistance experienced by a sphere in a fibrous medium has been available, and hence previous attempts to model transport in such systems have neglected the effects of hydrodynamic interactions entirely (Ogston *et al.*, 1973; Curry and Michel, 1980; Peppas and Reinhart, 1983). However, the increased hydrodynamic drag experienced by a solute surrounded by a fibrous medium could be at least as important an effect as steric partitioning; clearly its overall significance cannot be known without further study.

A useful starting point for studying the effects of hydrodynamic interactions in suspensions, fibrous media, and other porous media is to examine previous hydrodynamic investigations of simpler systems. Such studies have by and large concentrated on examining the transport properties of dilute dispersions of hard spheres. Thus, it would be helpful to explore ways of extending the existing understanding of hard-sphere hydrodynamic interactions, and to employ that new knowledge towards gaining insights on problems with different geometries.

Perhaps the first and most influential contribution to our understanding of hard-sphere hydrodynamics was Stokes' celebrated calculation of the settling velocity of a hard sphere in an unbounded, pure fluid under creeping flow conditions (Stokes, 1851). If the sphere is considered to be settling under the influence of gravity, it could be thought of as one particle in a sedimenting suspension. Alternatively, if the particle is held fixed while surrounded by a moving fluid, then it could be thought of as modeling a particle in a porous medium. Stokes' calculation thus provides the starting point for all subsequent modeling of hard-sphere dispersions. However, corrections to such single-particle models, which can be significant even for volume fractions much less than unity, can only be obtained by properly accounting for the particle-particle interactions that occur in both suspensions and porous media.

The transport properties commonly associated with suspensions include the sedimentation velocity, the dispersion coefficient of the suspended particles, and the viscosity of the fluid-particle continuum. Recent developments in calculating hydrodynamic interactions in such systems have significantly advanced our ability to calculate each of these properties. In particular, the solution to the theoretical problem of two spheres interacting under conditions of low Reynolds number has made an important contribution (Jeffrey and Onishi, 1984; Kim and Mifflin, 1985), principally through the application of pairwise additivity assumptions. Examples of studies applying pairwise additivity are Batchelor's (1972, 1976) and Glendinning and Russel's (1982) calculation of sedimentation velocities and particle dispersion coefficients, and Batchelor and Green's (1972) calculation of the effective viscosity of a suspension to $O(\phi^2)$, where ϕ is the particle volume fraction. Unfortunately, the use of pairwise additivity is only accurate for very dilute systems, in which the interaction between two particles is likely to be unaffected by the presence of a third particle. For higher volume fractions, at which three or more particles interact simultaneously, it is important that many-particle interactions be accounted for properly.

At first glance there appears to be little difference between sedimentation of a suspension, in which particles are settling through a stagnant fluid, and flow through a porous medium, in which fluid is flowing past particles that are held immobile by externally applied forces and torques. However, as discussed by Saffman (1973), interactions between particles under these two types of conditions are fundamentally different. These differences essentially result from the fact that the externally applied forces and torques present in a porous medium have the effect of screening hydrodynamic interactions between particles, causing them to decay more rapidly with distance than in free suspensions. Previously developed theories concerning interactions in porous media often incorporate this screening behavior directly by considering interactions within an *effective medium* of particles and fluid. Examples of this include the hydraulic permeability calculations of Brinkman (1947) and Kim and Russel (1985), and the calculation by Freed and Muthukumar (1978) of the mobility of a sphere moving through a bed of stationary spheres. These effective medium approaches are quite accurate when the influences that dominate the behavior of the solute can be attributed to the presence of the porous medium as a whole, and not to specific geometric characteristics of the microstructure. This is the case when the dominant hydrodynamic interactions occur over distances large compared to the solute dimensions, such as in a dilute dispersion of hard spheres of equal radii.

Due to the contributions of these earlier works, several features that one expects to find in a general method for evaluating hard-sphere interactions are now evident. To extend existing calculations of properties of hard-sphere suspensions beyond the dilute limit, the simultaneous, many-particle interactions present in such systems must be properly taken into account. These interactions must also account for the strong, lubrication forces that can act upon nearly touching spheres if the method is to be useful at high volume fractions, where dense clusters of particles are most likely to be present. Finally, the screening behavior characteristic of porous media should be exhibited by any model for infinite dispersions of spheres held fixed in space.

The Stokesian dynamics method described by Brady *et al.* (1988) combines these desirable characteristics. The method relies upon a separation of hydrodynamic interactions into far-field and near-field components. The far-field, or long-range, interactions are calculated in terms of an expansion in moments of the force density on each particle surface about its center, and in principle can be carried out to any level of accuracy that is desired by including more terms in the expansion. The near-field, or short-range, interactions are included in a pairwise additive fashion. In other words, near-field interactions between two spheres are calculated under the assumption that the effects of the other spheres in the system are negligible, an assumption justified by the short-range nature of these interactions. Thus, far-field, many particle interactions are calculated rigorously in a manner that does yield screening behavior in porous media (Durlofsky and Brady, 1987), and near-field interactions are included in a manner that preserves the strong, lubrication interactions between nearly touching spheres.

Stokesian dynamics was originally used as a method of performing dynamic simulations of suspensions of spherical particles in which the sphere centers all lie in the same plane (*i.e.*, a monolayer). These early simulations used only pairwise additivity to calculate hydrodynamic interactions. However, unlike the work of Batchelor (1972, 1976) and Glendinning and Russel (1982), pairwise additivity of forces rather than velocities was used, as it was found that the lubrication interactions necessary to prevent sphere overlap are preserved by that approach (Brady and Bossis, 1985). The more accurate method of including far-field interactions using a moment expansion was developed by Durlofsky *et al.* (1987), and is valid for systems with finite numbers of spherical particles. This dissertation extends the work of Durlofsky *et al.* to fully three-dimensional, hard-sphere dispersions that are infinite in extent. It is this latter method, which is valid for unbounded systems, that shall henceforth be referred to as Stokesian dynamics (*cf.* Brady *et al.*, 1988).

Several means are available for examining the accuracy of this method. These include calculations of the hydraulic permeability (Zick and Homsy, 1982) and viscosity (Zuzovsky *et al.*, 1983; Nunan and Keller, 1984) of spatially periodic arrays of spheres, and experimental measurements of the self-diffusion coefficient (Pusey and van Megen, 1983; Ottewill and Williams, 1987) and viscosity (van der Werff *et al.*, 1989) of disordered suspensions of spherical particles. In addition, there are the previously mentioned analytical results for dilute systems that can be used for comparison at low volume fractions.

One advantage of the Stokesian dynamics method is that it places no restrictions on the locations of the particles. Thus, it can be readily applied either to dynamic simulations, in which particle trajectories are followed over time, or to Monte Carlo simulations, in which transport properties for instantaneous configurations of particles are calculated and averaged over several realizations. Futhermore, the Stokesian dynamics method allows the simultaneous investigation of diffusion, sedimentation, permeability, rheology, etc.; all of the previously mentioned transport coefficients for both suspensions and porous media can be determined for any microstructural arrangement of spherical particles.

This ability to calculate hydrodynamic interactions for any system of hard spheres has important implications for systems, such as fibrous media, that resemble neither spatially periodic nor disordered hard-sphere dispersions. The usual approach to modeling hindered transport in media with unknown or highly complex microstructures has been to represent the porous medium as an assemblage of straight, cylindrical pores (Deen, 1987). However, the precise meaning of model parameters such as pore radius is unclear when applied to fibrous media. Thus, one important goal of theories of hindered transport, which is to relate transport parameters to the microstructure of the system, is very difficult to achieve with such an approach.

To construct a more appropriate model, one can represent polymeric chains as rows of aligned spheres that form "bead-and-string" fibers. Interactions between spherical solutes and arrays of these "bead-and-string" fibers can then be calculated using the Stokesian dynamics method, since only hard spheres are present in the system. The interactions between the mobile solute and the immobile fibers at any given location will determine both the local mobility and the local velocity of that solute. These coefficients can be calculated for different ratios of solute-to-fiber radius as well as for different microstructural arrangements of the fibers, thus allowing a variety of system geometries to be examined.

The term "local" used to describe the transport properties obtained using Stokesian dynamics refers to the fact that these parameters are valid over time scales so short that a solute does not move a distance comparable to its own size. However, typically one would like to calculate global coefficients, governing transport over macroscopic length scales. Generalized Taylor dispersion theory, as developed by Brenner and Adler (1982), provides a convenient way of calculating global coefficients from the local coefficients obtained using Stokesian dynamics. A rigorous theoretical framework for calculating hindered transport coefficients in fibrous media can therefore be developed and applied to specific fiber configurations.

It has been mentioned that effective medium models are particularly useful in porous media, since hydrodynamic interactions are strongly screened in those systems. Since a fibrous medium is a type of porous medium, one might expect that such an approach could be used as an alternative to the hindered transport calculations just described. An effective medium model can be constructed in which Brinkman's equation (Brinkman, 1947) is used to calculate the hydrodynamic drag on a spherical macromolecule in a fibrous medium. This approach has been successfully applied to the calculation of hydraulic permeabilities in disordered, hard-sphere dispersions (Brinkman, 1947; Kim and Russel, 1985), but has yet to be used to evaluate hindered transport parameters. The relative simplicity of Brinkman's equation allows one to predict such parameters knowing only the radius of the diffusing solute and the hydraulic permeability of the fibrous medium. Thus, an effective medium model could be of great use, particularly when dealing with systems for which very little structural information is available.

In Chapter 2, the details of the Stokesian dynamics method are described, including the approach used to sum hydrodynamic interactions in an infinite medium in a convergent and computationally efficient manner. Results for transport parameters of spatially periodic suspensions and porous media are then presented and compared with other theoretical results in Chapter 3. In Chapters 4 and 5, transport parameters for disordered dispersions of hard spheres, as determined by Monte Carlo simulation, are presented and compared with a different set of theoretical results as well as with experimental data.

Following this work on hard-sphere dispersions, two approaches to calculating global coefficients for fibrous membranes and gels are described in Chapter 6. The first is an effective medium approach based on Brinkman's equation. The second, more rigorous approach involves using the Stokesian dynamics method to obtain local coefficients, and then using generalized Taylor dispersion theory to calculate global coefficients valid over macroscopic length scales. The results of these two approaches will be compared for spatially periodic arrays of fibers, and comparisons will be made between the predictions of the effective medium model and experimental data reported in the literature.

Many of the results to be discussed in the following chapters have been published in the scientific literature. A summary of the theoretical development in Chapter 2 and the results for spatially periodic systems in Chapter 3 can be found in Brady *et al.* (1988). The Monte Carlo simulation results presented in Chapters 4 and 5 were reported in Phillips *et al.*

(1988*a*,*b*). Finally, the theoretical development and calculations regarding hindered transport in fibrous media, which comprise Chapter 6 of this thesis, are presented in Phillips *et al.* (1989*a*,*b*).

CHAPTER 2

THE STOKESIAN DYNAMICS METHOD

Calculations of hydrodynamic interactions between particles at low Reynolds number are often classified as "mobility" problems and "resistance" problems. In a mobility problem, particle forces and torques are prescribed, and particle translational and rotational velocities are unknown. The inverse, resistance problem corresponds to calculating particle forces and torques given the velocities. Under creeping flow conditions these dynamic and kinematic quantities are linearly related, and solutions for the mobility and resistance problems for two hydrodynamically interacting spheres are available in the literature (Jeffrey and Onishi, 1984; Kim and Mifflin, 1985). In addition, a method has recently been proposed that gives a very accurate approximation to the solutions for a finite number of interacting spherical particles (Durlofsky *et al.*, 1987). The goal of this chapter is to extend the method of Durlofsky *et al.* to an infinite number of interacting particles.

Calculation of hydrodynamic transport properties of infinite or unbounded media is complicated by the long-range nature of hydrodynamic interactions. These interactions decay as $1/r$ in suspensions of freely mobile particles, where r is the distance between two spheres. Even in porous media, where hydrodynamic interactions are screened, the rate of decay is k/r^3, where k is the hydraulic permeability. The difficulties caused by these slow rates of decay become apparent if, for example, one attempts to sum the interactions experienced by a particle sedimenting in a suspension of overall dimension R, where R is allowed to grow without bound while the number density of particles n is held constant. As the value of R is increased, the number of new particles being added to the system grows as $O(R^3)$, while the slowest decaying interactions contributed by each new particle decay as $O(1/R)$. Thus, the sum of all interactions diverges as R^2, suggesting that this sum is an ill-defined quantity.

This problem has been recognized by several researchers in the past, and so-called "renormalization" schemes have been successfully applied to obtain expressions for such quantities as sedimentation velocities and the bulk stress in a suspension (Batchelor, 1972; Batchelor and Green, 1972; Hinch, 1977; O'Brien, 1979). The goal of these renormalization methods is to account for the qualitative changes that affect how particles interact in infinite as opposed to finite media. Of the various methods that have been proposed, the one most convenient for use in conjunction with Stokesian dynamics is that of O'Brien. This is because, unlike the other methods, O'Brien's approach involves no preaveraging of hydrodynamic interactions, and thus the capability for calculating hydrodynamic interactions for a given, specific configuration of particles is preserved.

The use of O'Brien's method will insure that fully convergent expressions are obtained for the sum of particle-particle interactions. However, in order to obtain meaningful results, the actual evaluation of those sums must be achieved in an accurate and computationally efficient manner. If the infinite nature of the system is modeled using periodic boundary conditions, then the Ewald summation technique (Ewald, 1921) can be used for this purpose. Ewald's method, first employed by Beenakker (1986) to sum hydrodynamic interactions, accelerates the convergence of lattice sums and can be easily incorporated into O'Brien's renormalization procedure.

Finally, the interactions rendered convergent through the use of O'Brien's method and summed using the technique of Ewald are far-field, or long-range interactions. Near-field, or short-range, interactions decay rapidly with distance and therefore can be calculated the same way for an infinite as for a finite system. Thus, the method of including near-field effects proposed by Durlofsky *et al.* (1987) can be used here with essentially no modification.

2.1 RENORMALIZED HYDRODYNAMIC INTERACTIONS

As stated above, the linearity of Stokes' equations allows one to use a linear expression in defining the relationship among the forces, torques, and velocities of N' particles under creeping flow conditions:

$$\begin{pmatrix} \mathbf{U} - \langle \mathbf{u} \rangle \\ \mathbf{\Omega} - \langle \boldsymbol{\omega} \rangle \end{pmatrix} = \begin{pmatrix} \hat{M}_{UF} & \hat{M}_{UL} \\ \hat{M}_{\Omega F} & \hat{M}_{\Omega L} \end{pmatrix} \cdot \begin{pmatrix} \mathbf{F} \\ \mathbf{L} \end{pmatrix} . \tag{2.1}$$

Here **U** and **Ω** are vectors of dimension $3N'$ containing the particle translational and rotational velocities, respectively. Similarly, **F** and **L** are $3N'$ vectors containing the forces and torques applied to the particles. The angle brackets denote *suspension averages*, or volume averages over a region (including both fluid and particles) large enough to represent the local microstructure of the medium. The vectors $\langle \mathbf{u} \rangle$ and $\langle \boldsymbol{\omega} \rangle$ are the suspension-average velocity and vorticity, respectively, and are related by $\langle \boldsymbol{\omega} \rangle = 1/2(\nabla \times \langle \mathbf{u} \rangle)$. The mobility matrix $\hat{M}$, shown in partitioned form, relates the two vector quantities.

To derive expressions for the mobility matrix, one can begin with the integral representation of the solution to Stokes' equations (Ladyzhenskaya, 1963):

$$u_i(\mathbf{x}) = -\frac{1}{8\pi\mu} \sum_{\alpha=1}^{N'} \int_{S_\alpha} J_{ij}(\mathbf{x}-\mathbf{y})\sigma_{jk}(\mathbf{y})n_k(\mathbf{y})\, dS_y$$

$$-\frac{1}{8\pi\mu} \int_{S_{\Gamma'}} \{J_{ij}(\mathbf{x}-\mathbf{y})\sigma_{jk}(\mathbf{y}) + 2\mu K_{ijk}(\mathbf{x}-\mathbf{y})u_j(\mathbf{y})\}\, n_k\, dS_y . \tag{2.2}$$

Here **u**(**x**) is the fluid velocity at some field point **x** in the fluid, μ is the fluid viscosity, and **n** is a unit normal pointing outward from the surfaces. Also, the vector operations are expressed using the summation convention (Whitaker, 1981), which requires that repeated indices be summed from 1 to 3. The first integral in (2.2) is an integral over the surface of particle α, S_α, while the second is an integral over a macroscopic boundary $S_{\Gamma'}$. The region bounded by $S_{\Gamma'}$ contains the N' particles of the sum, and the surface itself exists only in the fluid phase (*i.e.*, the surface $S_{\Gamma'}$ does not cross any particle boundaries S_α). The tensor $\underset{\approx}{J}$ is the Green function for Stokes flow, given by

$$J_{ij}(\mathbf{r}) = \frac{\delta_{ij}}{r} + \frac{r_i r_j}{r^3} , \tag{2.3}$$

while

$$K_{ijk}(\mathbf{r}) = -3\, \frac{r_i r_j r_k}{r^5} . \tag{2.4}$$

Here δ_{ij} is the identity tensor, and the vector **r** is equal to **x**-**y**, where **y** is a vector to a point on either S_α or $S_{\Gamma'}$ (hence the subscript y on dS_y). The stress tensor $\underset{\approx}{\sigma}$ for a Newtonian, incompressible fluid is given by

$$\sigma_{ij} = -p\delta_{ij} + 2\mu e_{ij} \quad , \tag{2.5}$$

where p is pressure and the rate-of-strain $e_{ij} = 1/2(\nabla_i u_j + \nabla_j u_i)$.

In the renormalization method proposed by O'Brien (1979) it is assumed that, if the radius of the region bounded by $S_{\Gamma'}$ is very large, then the quantities $J_{ij}(\mathbf{x}-\mathbf{y})$ and $K_{ijk}(\mathbf{x}-\mathbf{y})$ will change very little over an element of area $dS_{\Gamma'}$ that is large enough to contain both fluid and particles. Thus, the integration can be performed using appropriately averaged values for the stress and velocity terms. If one replaces $S_{\Gamma'}$ by an analogous surface S_Γ, which differs from $S_{\Gamma'}$ in that it is allowed to cross particle boundaries, then the appropriate averages to be used in place of $\underset{\approx}{\sigma}$ and **u** in (2.2) are the suspension averages $\langle\underset{\approx}{\sigma}\rangle$ and $\langle\mathbf{u}\rangle$. However, making this transformation from primed to unprimed surface also has the effect of generating a third, quadrupolar contribution to the surface integral as shown by Glendinning and Russel (1982). Replacing $\underset{\approx}{\sigma}$ and **u** by their averages and including this additional term yields for the velocity

$$\begin{aligned} u_i(\mathbf{x}) = - \frac{1}{8\pi\mu} \sum_{\alpha=1}^{N'} \int_{S_\alpha} J_{ij}(\mathbf{x}-\mathbf{y})\sigma_{jk}(\mathbf{y})n_k(\mathbf{y})\ dS_y \\ - \frac{1}{8\pi\mu} \int_{S_\Gamma} \left(J_{ij}(\mathbf{x}-\mathbf{y})\langle\sigma_{jk}\rangle n_k + 2\mu K_{ijk}(\mathbf{x}-\mathbf{y})\langle u_j\rangle n_k - n\nabla_k J_{ij}\langle Q'_{klj}\rangle n_l \right) dS_y \ . \end{aligned} \tag{2.6}$$

Here *n* with no subscript is the number density of particles, the derivative $\nabla_k J_{ij}$ is with respect to **y**, and the suspension-average quadrupole density of the particles $\langle Q'_{klj} \rangle$ is given by

$$\langle Q'_{klj} \rangle = \frac{1}{N'} \sum_{\alpha} Q'^{\alpha}_{klj} \quad , \tag{2.7}$$

where

$$Q'^{\alpha}_{klj} = -\frac{1}{2} \int_{S_\alpha} (y_k - x^{\alpha}_k)(y_l - x^{\alpha}_l)\sigma_{jm} n_m \, dS_y \tag{2.8}$$

and $\mathbf{x}^{\alpha}$ is the center of particle α.

The expression (2.6) is a completely convergent solution for the velocity **u** at a field point **x**. However, it remains to relate the suspension average stress to the average rate of strain and other terms contributed by the presence of the particles. Following Hinch (1977), one obtains for the averaged form of Stokes' equations

$$\nabla \cdot \langle \underset{\approx}{\sigma} \rangle = -n\langle \mathbf{F} \rangle \quad , \tag{2.9}$$

where the suspension average of $\underset{\approx}{\sigma}$ is given by

$$\langle \underset{\approx}{\sigma} \rangle = \frac{1}{V} \int_V \underset{\approx}{\sigma} \, dV \tag{2.10}$$

and

$$\langle \mathrm{F} \rangle = \frac{1}{N'} \sum_{\alpha=1}^{N'} \mathrm{F}^{\alpha} \quad . \tag{2.11}$$

The volume in (2.10) includes both fluid and particles, and must be large enough to reflect the local microstructure of the unbounded suspension. An expression for the suspension average stress can be obtained by following the reasoning of Landau and Lifshitz (1959) and Batchelor (1970), yielding

$$\langle \sigma_{ij} \rangle = -\langle p \rangle \delta_{ij} + 2\mu \langle e_{ij} \rangle - n\{\langle S_{ij} \rangle + \langle \mathcal{L}_{ij} \rangle\} \quad , \tag{2.12}$$

where $\langle p \rangle$ and $\langle \underset{\approx}{e} \rangle$ are the suspension average pressure and rate-of-strain, respectively,

$$\langle S_{ij} \rangle = \frac{1}{N'} \sum_{\alpha=1}^{N'} S^{\alpha}_{ij} \quad , \qquad \text{and} \qquad \langle \mathcal{L}_{ij} \rangle = \frac{1}{N'} \sum_{\alpha=1}^{N'} \mathcal{L}^{\alpha}_{ij} \quad . \tag{2.13}$$

The particle stresslet $\underset{\approx}{S}$ is the symmetric portion of the first moment of the force density about the particle surface:

$$S^{\alpha}_{ij} = -\frac{1}{2} \int_{S_{\alpha}} \{\sigma_{ik}(y_j - x^{\alpha}_j) + \sigma_{jk}(y_i - x^{\alpha}_i) - \frac{2}{3}\, \delta_{ij}\sigma_{lk}(y_l - x^{\alpha}_l)\} n_k \, dS_y \quad . \tag{2.14}$$

The rotlet $\underset{\approx}{\mathcal{L}}$ is the antisymmetric complement to $\underset{\approx}{S}$,

$$\mathcal{L}^{\alpha}_{ij} = -\frac{1}{2}\int_{S_\alpha} \{\sigma_{ik}(y_j - x^{\alpha}_j) - \sigma_{jk}(y_i - x^{\alpha}_i)\} n_k \, dS_y \quad , \tag{2.15}$$

and is related to the torque L by

$$L^{\alpha}_i = \epsilon_{ijk}\mathcal{L}^{\alpha}_{jk} \quad , \tag{2.16}$$

where the third-order tensor ϵ_{ijk} is the Levi-Civita tensor. Finally, the average pressure may be obtained via a macroscopic balance between pressure forces and forces exerted by the particles on the fluid, yielding

$$\langle p \rangle = n\langle F_i \rangle (x_i - x^o_i), \tag{2.17}$$

where x^o_i is some reference point at which the pressure is set to zero. The expression (2.12) is valid so long as the externally imposed force is distributed evenly throughout the interior of the particles (*i.e.*, for a suspension sedimenting under the influence of gravity, the density of the particles must be constant).

Using the divergence theorem, the latter, surface integral in (2.6) (*i.e.*, the integral over S_Γ) can be rewritten as

$$\begin{aligned} &\frac{1}{8\pi\mu}\int_{V'} \nabla_k [J_{ij}\langle\sigma_{jk}\rangle + 2\mu K_{ijk}\langle u_j\rangle - n\nabla_l J_{ij}\langle Q'_{klj}\rangle] \, dV_y \\ &- \frac{1}{8\pi\mu}\int_{S_\epsilon} [J_{ij}\langle\sigma_{jk}\rangle n_k + 2\mu K_{ijk}\langle u_j\rangle n_k - n\nabla_k J_{ij}\langle Q'_{klj}\rangle n_l] \, dS_y , \end{aligned} \tag{2.18}$$

where S_ϵ is a spherical surface that is completely enclosed by S_Γ and surrounds the field point $\mathbf{x}$, and V' is the volume between the surfaces S_ϵ and S_Γ. Substituting $\langle \underset{\approx}{\sigma} \rangle$ from (2.12) into the volume integral in (2.18), and using $\langle p \rangle$ from (2.17), one can rewrite that volume integral as

$$- \frac{n}{8\pi\mu} \int_{V'} \{J_{ij} \langle F_j \rangle + R_{ij} \langle L_j \rangle + K_{ijk} \langle S_{jk} \rangle + \nabla_k \nabla_l J_{ij} \langle Q'_{klj} \rangle\} \, dV_y \ , \qquad (2.19)$$

where the Green function, or velocity propagator, for a point torque R_{ij} is given by

$$R_{ij} = \epsilon_{ijk} \frac{r_k}{r^3} = \epsilon_{lkj} \frac{1}{4} (\nabla_k J_{il} - \nabla_l J_{ik}) \ . \qquad (2.20)$$

Finally, taking the limit as the surface S_ϵ shrinks to a point, the volume V' in (2.19) can be replaced by V, the total volume enclosed by S_Γ, and the surface integral in (2.18) becomes

$$\langle u_i(\mathbf{x}) \rangle + \frac{2n}{15\mu} [2 \langle Q'_{jji} \rangle - \langle Q'_{ijj} \rangle] \ . \qquad (2.21)$$

Substituting (2.21) and (2.19) into (2.6) yields the desired convergent expression for $u_i(\mathbf{x})$:

$$u_i(\mathbf{x}) - \langle u_i(\mathbf{x})\rangle = \frac{2n}{15\mu}\,[2\langle Q'_{jji}\rangle - \langle Q'_{ijj}\rangle] - \frac{1}{8\pi\mu}\sum_{\alpha=1}^{N'}\int_{S_\alpha} J_{ij}\sigma_{jk}n_k \; dS_y$$

$$- \frac{n}{8\pi\mu}\int_V \{J_{ij}\langle F_j\rangle + R_{ij}\langle L_j\rangle + K_{ijk}\langle S_{jk}\rangle + \nabla_k\nabla_l J_{ij}\langle Q'_{klj}\rangle\}\; dV_y \quad . \tag{2.22}$$

The expression (2.22) is valid for systems of arbitrarily large size because, as the system size is increased, terms in the volume integral will cancel the divergent terms in the sum, yielding a finite result. For an infinite suspension of sedimenting particles, it is this volume integral which supplies the "backflow" of fluid, relative to zero-flux axes $\langle \mathbf{u}\rangle = 0$, that results from the pressure gradient necessary to balance the excess weight of the particles. The presence of this "backflow" term has been noted previously for periodic (Hasimoto, 1959) and disordered suspensions (Batchelor, 1972).

The quadrupole terms in (2.22) can be greatly simplified by equating the quadrupole moment of each particle with its "mean-field" value proportional to $\langle \mathbf{F}\rangle$. To see how this can be done, it is convenient to express Q'^{α}_{klj} in terms of its trace and the irreducible quadrupole moment density Q^{α}_{klj}, defined by

$$Q^{\alpha}_{klj} = Q'^{\alpha}_{klj} - \frac{a^2}{6} F^{\alpha}_j \delta_{kl} \quad . \tag{2.23}$$

The "mean-field" value of Q^{α}_{klj} can be obtained by replacing $\underset{\approx}{\sigma}$ by $\langle\underset{\approx}{\sigma}\rangle$ and evaluating the integral in (2.8), remembering to subtract off the trace as in (2.23). The result is

$$Q^{\alpha}_{klj} \approx \frac{\phi}{10} \frac{\langle F_m \rangle}{6\pi\mu a} \{\delta_{km}\delta_{jl} + \delta_{lm}\delta_{kj} - \frac{2}{3} \delta_{kl}\delta_{jm}\} \ . \tag{2.24}$$

Making use of (2.23) and (2.24), (2.22) can now be rewritten as

$$\begin{aligned} u_i(\mathbf{x}) - \langle u_i(\mathbf{x}) \rangle = -\frac{\phi}{2} \frac{\langle F_i \rangle}{6\pi\mu a} - \frac{3}{5} \phi \frac{\langle Q_{ijj} \rangle}{6\pi\mu a^3} - \frac{1}{8\pi\mu} \sum_{\alpha=1}^{N'} \int_{S_\alpha} J_{ij}\sigma_{jk}n_k \, dS_y \\ - \frac{n}{8\pi\mu} \int_V \{ (1+\frac{a^2}{6} \nabla^2) J_{ij} \langle F_j \rangle + R_{ij} \langle L_j \rangle + K_{ijk} \langle S_{jk} \rangle \\ + \nabla_k \nabla_l J_{ij} \langle Q_{klj} \rangle \} \, dV_y \ . \end{aligned} \tag{2.25}$$

Here ϕ is the volume fraction of particles, given by $n(4/3\pi a^3)$. The accuracy of using the mean-field approximation given in (2.24) will be examined in the next chapter.

To calculate the mobility matrix of (2.1), it will be necessary to use the fluid velocity given in (2.25) to obtain translational and rotational velocities of particles in terms of applied forces and torques. This can be accomplished by taking two additional steps. First, one expands the surface integral in (2.25) in terms of moments of the force density $\underset{\approx}{\sigma}\cdot\mathbf{n}$:

$$\begin{aligned}\int_{S_\alpha} J_{ij}(\mathbf{x}-\mathbf{y})\sigma_{jk}n_k \, dS_y &= J_{ij}(\mathbf{x}-\mathbf{x}^\alpha)\int_{S_\alpha}\sigma_{jk}n_k \, dS_y \\ &\quad - \frac{\partial}{\partial y_l} J_{ij}(\mathbf{x}-\mathbf{y})\Big|_{\mathbf{y}=\mathbf{x}^\alpha}\int_{S_\alpha}(y_l - x_l^\alpha)\sigma_{jk}n_k \, dS_y \qquad (2.26) \\ &\quad + \frac{1}{2}\frac{\partial}{\partial y_l}\frac{\partial}{\partial y_m} J_{ij}(\mathbf{x}-\mathbf{y})\Big|_{\mathbf{y}=\mathbf{x}^\alpha}\int_{S_\alpha}(y_m - x_m^\alpha)(y_l - x_l^\alpha)\sigma_{jk}n_k \, dS_y \ \ldots\end{aligned}$$

The zeroth moment of $\underset{\approx}{\sigma}\cdot\mathbf{n}$, given by the first integral in (2.32), is the force on particle α. The first moment, given by the second integral in (2.32), is a tensor which can be separated into symmetric and antisymmetric parts. These are given by $\underset{\approx}{S}^{\alpha}$ and $\underset{\approx}{\mathcal{L}}^{\alpha}$ in (2.32) and (2.33), respectively. The second moment, which contributes the quadrupole terms of the expansion, can be broken down as shown in (2.32). The portion of the quadrupole term that is proportional to the force (or to the zeroth moment) can be conveniently included in the first term of the expansion by replacing $J_{ij}(\mathbf{x}-\mathbf{x}^\alpha)$ by $(1+\frac{a^2}{6}\nabla^2)J_{ij}(\mathbf{x}-\mathbf{x}^\alpha)$. Thus, this expansion process relates the fluid velocity to the forces, torques, and stresslets of the particles, and could be carried further to include higher moments (octupoles, hexadecapoles, *etc.*) if desired. For this development, the expansion will be truncated at the level of the first moment (torques and stresslets), but the trace of the quadrupole term that contributes a term proportional to the particle forces will be included since this requires no additional computational effort.

The second step in calculating the mobility matrix is to use (2.25) and (2.26) in conjunction with Faxen formulae (Faxen, 1927) to determine the particle velocities. For systems of equally sized spheres, these formulae are

$$U_i^\alpha - \langle u_i(\mathbf{x}^\alpha)\rangle = \frac{F_i^\alpha}{6\pi\mu a} + \left(1 + \frac{a^2}{6} \nabla^2 \right) u_i'(\mathbf{x}^\alpha) \ , \tag{2.27a}$$

$$\Omega_i^\alpha - \langle \omega_i(\mathbf{x}^\alpha)\rangle = \frac{L_i^\alpha}{8\pi\mu a^3} + \frac{1}{2} \epsilon_{ijk} \nabla_j u_k'(\mathbf{x}^\alpha) \tag{2.27b}$$

and

$$-\langle e_{ij}\rangle = \frac{S_{ij}^\alpha}{(20/3)\pi\mu a^3} + \left(1 + \frac{a^2}{10} \nabla^2 \right) e_{ij}'(\mathbf{x}^\alpha) \tag{2.27c}$$

Here, $u_i'(\mathbf{x}^\alpha)$ is the velocity disturbance caused by all the particles except for particle α, and $e_{ij}'(\mathbf{x}^\alpha)$ is the rate of strain of the disturbance flow, $e_{ij}' = 1/2(\nabla_j u_i' + \nabla_i u_j')$.

Substituting (2.25) and (2.26) into (2.27) will now yield expressions for the particle velocities in terms of forces, torques, and stresslets. Making these substitutions, but leaving the integral in (2.26) in its unexpanded form to simplify the result, one obtains the following convergent expressions:

$$\begin{aligned} U_i^\alpha - \langle u_i(\mathbf{x}^\alpha)\rangle = {} & \phi \frac{\langle F_i\rangle}{6\pi\mu a} - \frac{3}{5} \phi \frac{\langle Q_{ijj}\rangle}{6\pi\mu a^3} + \frac{F_i^\alpha}{6\pi\mu a} \\ & - \frac{1}{8\pi\mu} \sum_{\beta\neq\alpha} \int_{S_\beta} \left(1 + \frac{a^2}{6} \nabla^2 \right) J_{ij} \sigma_{jk} n_k \, dS_y \\ & - \frac{n}{8\pi\mu} \int_V \{ \left(1 + \frac{a^2}{6} \nabla^2 \right) J_{ij} \langle F_j\rangle + R_{ij}\langle L_j\rangle + K_{ijk}\langle S_{jk}\rangle \\ & \qquad + \nabla_k \nabla_l J_{ij} \langle Q_{klj}\rangle \} \, dV_y \end{aligned} \tag{2.28a}$$

$$\Omega_i^\alpha - \langle \omega(\mathbf{x}^\alpha) \rangle = \phi \frac{\langle L_i \rangle}{8\pi\mu a^3} + \frac{L_i^\alpha}{8\pi\mu a^3} - \frac{1}{8\pi\mu} \sum_{\beta\neq\alpha} \int_{S_\beta} \frac{1}{2}\epsilon_{ijk} \nabla_j J_{kl} \sigma_{lm} n_m \, dS_y$$

$$- \frac{n}{8\pi\mu} \int_V \frac{1}{2}\epsilon_{ijk} \nabla_j \{ J_{kl} \langle F_l \rangle + R_{kl} \langle L_l \rangle + K_{klm} \langle S_{lm} \rangle \} \, dV_y \tag{2.28b}$$

and

$$-\langle e_{ij}(\mathbf{x}^\alpha) \rangle = -\phi \frac{\langle S_{ij} \rangle}{(20/3)\pi\mu a^3} + \frac{S_{ij}}{(20/3)\pi\mu a^3} - \frac{1}{8\pi\mu} \sum_{\beta\neq\alpha} \int_{S_\beta} \left(1 + \frac{a^2}{10} \right) \nabla_j^{sym} J_{ik} \sigma_{kl} n_l \, dS_y$$

$$- \frac{n}{8\pi\mu} \int_V \nabla_j^{sym} \{ J_{ik} \langle F_k \rangle + R_{ik} \langle L_k \rangle + K_{ikl} \langle S_{kl} \rangle \} \, dV_y \tag{2.28c}$$

Here the operator ∇_j^{sym} acting on a vector v_i is defined by $\nabla_j^{sym} \equiv 1/2(\nabla_j v_i + \nabla_i v_j)$. In obtaining the term $\phi\langle F_i \rangle / 6\pi\mu a$ in (2.25a), one should note that it is necessary to apply the $(a^2/6)\nabla^2$ operator from (2.27a) to the surface integral of (2.18). This results in a term $\phi\langle F_i \rangle / 12\pi\mu a$ being added to (2.21), which when included yields the result shown. Finally, the quadrupole term in (2.28a) can be evaluated using (2.24), giving

$$- \frac{3}{5} \phi \frac{\langle Q_{ijj} \rangle}{6\pi\mu a^3} = - \frac{1}{5} \phi^2 \frac{\langle F_i \rangle}{6\pi\mu a} \quad . \tag{2.29}$$

Hence, when the approximation (2.24) is used, $\langle Q_{ijj} \rangle$ is proportional to $\langle F_i \rangle$. In addition, quadrupole terms in the volume integral of (2.28a) and in the surface integrals of (2.26) and (2.28a) can be included with terms proportional to $\nabla^2 \underset{\approx}{J}$. Thus, from this point in the development forward it will not be necessary to include quadrupoles in the formulation explicitly.

Making use of (2.28) along with (2.29) and the expansion (2.26), one can now evaluate the terms of a mobility matrix relating particle velocities with forces, torques, and stresslets. This relation can be expressed using a partitioned matrix as follows:

$$\begin{bmatrix} \mathbf{U} - \langle \mathbf{u} \rangle \\ \mathbf{\Omega} - \langle \omega \rangle \\ -\langle \underset{\approx}{e} \rangle \end{bmatrix} = \begin{bmatrix} M_{UF} & M_{UL} & M_{US} \\ M_{\Omega F} & M_{\Omega L} & M_{\Omega S} \\ M_{EF} & M_{EL} & M_{ES} \end{bmatrix} \cdot \begin{bmatrix} \mathbf{F} \\ \mathbf{L} \\ \underset{\approx}{S} \end{bmatrix} . \tag{2.30}$$

If higher moments than those shown in (2.26) were included, then additional terms would be added to the bottom of the vectors on both the left- and right-hand sides of (2.30). For example, if all the quadrupole terms were to be included, a third-order tensor with each element equaling zero could be added below $-\langle \underset{\approx}{e} \rangle$ on the left-hand side (note that $\nabla\nabla\langle \mathbf{u} \rangle$ can only be non-zero in a system with physical boundaries), while the third-order quadrupole tensor Q could be added below the $\underset{\approx}{S}$ on the right-hand side. An additional Faxen formula would be required to evaluate the new components of the mobility matrix.

Stresslets and all higher moments are *induced* moments which are not applied and must be obtained as part of the calculation. For example, given the value of $\langle \underset{\approx}{e} \rangle$ one could solve for $\underset{\approx}{S}$ in terms of F and L, and from that solution derive an equation with the form of (2.1). A suspension sedimenting in an otherwise quiescent fluid has $\langle \underset{\approx}{e} \rangle = 0$, and therefore

$$\left(\underset{\approx}{S} \right) = - \left(M_{ES} \right)^{-1} \cdot \left(M_{EF} \quad M_{EL} \right) \cdot \begin{bmatrix} F \\ L \end{bmatrix} , \tag{2.31}$$

whence

$$\begin{bmatrix} U-\langle u \rangle \\ \Omega-\langle \omega \rangle \end{bmatrix} = \left[\begin{pmatrix} M_{UF} & M_{UL} \\ M_{\Omega F} & M_{\Omega L} \end{pmatrix} - \begin{pmatrix} M_{US} \\ M_{\Omega S} \end{pmatrix} \cdot \left(M_{ES} \right)^{-1} \cdot \left(M_{EF} \quad M_{EL} \right) \right] \cdot \begin{bmatrix} F \\ L \end{bmatrix} . \tag{2.32}$$

The entire matrix in (2.32), including the matrix accounting for stresslet interactions, represents the far-field portion of $\hat{M}$ in (2.1) for any system with $\langle \underset{\approx}{e} \rangle = 0$. In a similar manner, higher moments than those shown in (2.30) can always be incorporated into a solution of a form that allows one to calculate particle velocities given the applied forces and torques, or *vice versa*.

2.2 EWALD SUMS

The solution for the particle velocities given in (2.28) is rigorously correct and absolutely convergent. However, as a practical matter, computation of the difference between the integrals and sums in these equations, which is the convergent quantity that is needed, can prove quite difficult. This is a result of the slow decay of hydrodynamic interactions, and has the effect of requiring one to deal with very large systems and large numbers of spheres. In order to reduce the number of particles needed and accelerate the convergence of the sum and integral terms, one can deal with a finite unit cell containing *N* particles, and impose periodic boundary conditions as a means of modeling the true, infinite nature of the system. Choosing this approach allows one to make use of the Ewald summation technique, first developed by Ewald (1921) and later applied to hydrodynamic problems by Beenakker (1986).

Previous attempts to model three-dimensional, infinite systems using periodic boundary conditions without properly summing all hydrodynamic interactions have at times yielded aphysical results (Dickinson, 1985), a fact that has been attributed to loss of positive definiteness in the mobility matrix. The characteristic of positive definiteness is important in that it insures the dissipative nature of the system (*i.e.*, that mechanical energy is dissipated rather than created). Correctly summing the long-range hydrodynamic interactions, which can be accomplished using Ewald sums, insures that the mobility matrices will never lose positive definiteness.

To demonstrate the procedure, it is convenient to use the form of (2.28a) appropriate for a system so dilute that each sphere only feels the zeroth moment (point-force) interactions of the other spheres. This is obtained by removing all interaction terms related to the finite size of the spheres, resulting in the following expression:

$$U_i^\alpha - \langle u_i(\mathbf{x})\rangle = \frac{F_i}{6\pi\mu a} + \frac{1}{8\pi\mu}\sum_{\gamma}\sum_{\substack{\beta=1\\ \beta\neq\alpha}}^{N} J_{ij}(\mathbf{x}^\alpha - \mathbf{x}^\beta)F_j^\beta - \frac{n}{8\pi\mu}\int_0^\infty J_{ij}\langle F_j\rangle\, dV \qquad (2.33)$$

Here γ labels the unit cells, β labels particles within a given unit cell, and the restriction $\beta\neq\alpha$ only refers to the unit cell $\gamma=1$.

To sum the interactions using the Ewald method, one can use the fact that J_{ij} in (2.3) can be rewritten as

$$J_{ij}(r) = (\nabla^2 \delta_{ij} - \nabla_i \nabla_j) r \quad . \tag{2.34}$$

One can therefore write

$$\frac{3}{4} J_{ij}(r) = M^{(1)}_{ij}(r) + M^{(2)}_{ij}(r) \tag{2.35}$$

where

$$M^{(1)}_{ij}(r) = \frac{3}{4} (\delta_{ij} \nabla^2 - \nabla_i \nabla_j)(r \operatorname{erfc}(\xi r)) \tag{2.36}$$

and

$$M^{(2)}_{ij}(r) = \frac{3}{4} (\delta_{ij} \nabla^2 - \nabla_i \nabla_j)(r \operatorname{erf}(\xi r)) \quad . \tag{2.37}$$

Here ξ is a convergence parameter with units of inverse length, *erf* and *erfc* refer to the error function and the complement of the error function, respectively, and the factor of 3/4 has been included for convenience.

The sum in (2.33) can now be rewritten as

$$\frac{1}{6\pi\mu} \left[\sum_{\gamma} \sum_{\substack{\beta=1 \\ \beta\neq\alpha}}^{N} M^{(1)}_{ij}(\mathbf{x}^\alpha - \mathbf{x}^\beta) F^\beta_j - M^{(2)}_{ij}(\mathbf{r}=\mathbf{0}) F^\alpha_j + \sum_{\gamma} \sum_{\beta=1} M^{(2)}_{ij}(\mathbf{x}^\alpha - \mathbf{x}^\beta) F^\beta_j \right] , \tag{2.38}$$

where the restriction $\beta \neq \alpha$ has been left off the sum over $M^{(2)}_{ij}(\mathbf{x}^\alpha - \mathbf{x}^\beta)$, but the resulting additional term has been cancelled by $M^{(2)}_{ij}(\mathbf{r}=\mathbf{0})$. The advantage of writing the sum of (2.33) in the form shown in (2.38) is that convergence is greatly accelerated. The sum over $\underset{\approx}{M}^{(1)}$, which depends on *erfc*(ξr), decays rapidly with distance and therefore poses no computational difficulties. The second sum, which depends on *erf*(ξr), can be Fourier transformed and converges rapidly in reciprocal space. The sum on the reciprocal space lattice can be related to a sum over real space using the Poisson summation formula (Nijboir and de Wette, 1957), given by

$$\sum_{\gamma} g(\mathbf{r}_\gamma) = \frac{1}{V} \sum_{\lambda} g(\mathbf{k}_\lambda) \quad , \tag{2.39}$$

where *g(k)* is the Fourier transform of *g(r)* according to

$$g(\mathbf{k}) = \int e^{i\mathbf{k}\cdot\mathbf{r}} g(\mathbf{r})\, d\mathbf{r} \quad , \tag{2.40}$$

V is the volume of the unit cell, and $\mathbf{k}_\lambda$ are reciprocal lattice vectors satisfying $exp(\mathbf{k}_\lambda \cdot \mathbf{r}_\gamma) = 1$ (*cf*. Kittel, 1976). Using (2.39) and (2.40), one can write the sum over $M_{ij}^{(2)}$ in (2.38) as

$$\frac{1}{6\pi\mu V} \sum_{\lambda} \sum_{\beta=1}^{N} \exp(-\mathbf{k}_\lambda \cdot \mathbf{x}^\alpha - \mathbf{x}^\beta) M_{ij}^{(2)}(\mathbf{k}_\lambda) F_j^\beta \quad , \tag{2.41}$$

where the Fourier transform of $\underset{\approx}{M}^{(2)}$ can be calculated from (2.37) as (Beenakker, 1986)

$$M_{ij}^{(2)}(\mathbf{k}) = (\delta_{ij} - \hat{k}_i \hat{k}_j)(1 + \frac{1}{4}\, \xi^{-2}k^2 + \frac{1}{8}\, \xi^{-4}k^4) 6\pi k^{-2} \exp(-\tfrac{1}{4}\xi^2 k^2) \quad . \tag{2.42}$$

Here the vector $\hat{\mathbf{k}}=\mathbf{k}/k$. Of the remaining terms in (2.38), $M^{(1)}_{ij}(\mathbf{x}^{\alpha}-\mathbf{x}^{\beta})$ can be found by simple differentiation according to (2.36), while $M^{(2)}_{ij}(\mathbf{r}=0)$ can be found from the inverse of the Fourier transform, giving

$$M^{(2)}_{ij}(\mathbf{r}=0) = \frac{1}{(2\pi)^3} \int M^{(2)}_{ij}(\mathbf{k})\, d\mathbf{k} = \delta_{ij} \frac{6}{\pi^{-1/2}} \xi a \quad , \tag{2.43}$$

where a is the radius of the spheres. Thus, each of the terms needed to evaluate the sum in (2.38) (and hence the sum in (2.33)) is known.

The sum over $M^{(2)}_{ij}$ given in (2.41) appears to be ill-defined for $\mathbf{k}_{\lambda}=0$, since the expression given in (2.42) has a term proportional to k^{-2}. However, closer examination will show that the $\mathbf{k}_{\lambda}=0$ term in (2.41) is exactly cancelled by the "backflow" volume integral in (2.33). As $k\rightarrow 0$, the double sum in (2.41) becomes

$$\frac{1}{6\pi\mu V} M^{(2)}_{ij}(\mathbf{k}\rightarrow 0) \sum_{\beta=1}^{N} F^{\beta}_{j} = \frac{1}{\mu V} (\delta_{ij} - \hat{k}_i \hat{k}_j) k^{-2} \sum_{\beta=1}^{N} F^{\beta}_{j} \quad . \tag{2.44}$$

To evaluate the behavior of the volume integral in (2.33) as $k\rightarrow 0$, one can use the convolution theorem to write

$$\int J_{ij}\, dV = \delta(\mathbf{k})\, \hat{J}_{ij}(\mathbf{k}) \quad , \tag{2.45}$$

where $\delta(\mathbf{k})\hat{\underset{\approx}{J}}(\mathbf{k})$ can be taken as meaning the limit of $\hat{\underset{\approx}{J}}(\mathbf{k})$ as $k\rightarrow 0$. The

Fourier transform $\hat{\underset{\approx}{J}}$ of $\underset{\approx}{J}$ is

$$\hat{J}_{ij}(\mathbf{k}) = (\delta_{ij} - \hat{k}_i\hat{k}_j)8\pi k^{-2} \quad , \tag{2.46}$$

and thus

$$\frac{n}{8\pi\mu} \int_0^\infty J_{ij}\langle F_j\rangle \, dV = \frac{n}{\mu}(\delta_{ij} - \hat{k}_i\hat{k}_j)k^{-2}\langle F_j\rangle \quad . \tag{2.47}$$

Comparing the right-hand sides of (2.44) and (2.47), and using $\langle \mathbf{F}\rangle=(1/N)\sum_\alpha \mathbf{F}^\alpha$, one can see that the volume integral in (2.33) exactly cancels the $\mathbf{k}_\lambda=\mathbf{0}$ term in the reciprocal-space sum. Thus, Beenakker's requirement that $\langle\mathbf{F}\rangle=\mathbf{0}$ is not necessary.

There is a simple and intuitive reason why Beenakker's restriction should be superfluous. The mobility matrix depends only on the geometry of the system, and not on the forces applied to the particles. A mobility matrix describing the interactions for particles in a particular configuration must therefore be valid whatever velocities or forces those particles have. Thus, any mobility matrix derived correctly under the assumption that $\langle\mathbf{F}\rangle=\mathbf{0}$ must also be valid when that condition is no longer true.

The Ewald sums of the terms of M_{UF} associated with the finite size of the particles (*i.e.*, terms resulting from the $(a^2/6)\nabla^2$ operator in Faxen's law (2.27a)) and the terms for the other mobility submatrices in (2.30) can be carried out in much the same manner as used here. The elements of M_{UL}, $M_{\Omega U}$, etc. are easily expressed in terms of gradients of the Green function $\underset{\approx}{J}$, and thus they can be written as gradients of the expression given in

(2.34), and new equations for $M_{ij}^{(1)}(r)$, $M_{ij}^{(2)}(r=0)$, and $M_{ij}^{(2)}(r)$ can be derived. Just as the "backflow" volume integral cancelled out the divergent $\mathbf{k}_\lambda = \mathbf{0}$ term in the point-force sum described above, it will also cancel these same terms in the evaluation of the other submatrices of (2.30), in addition to the terms proportional to $\phi\langle \mathbf{F}\rangle$, $\phi\langle \mathbf{L}\rangle$, and $\phi\langle \underset{\approx}{\mathbf{S}}\rangle$ shown in (2.28). The expressions required for the summation of all the submatrices shown in (2.30) are given in Appendix *A*.

2.3 NEAR-FIELD INTERACTIONS

The interactions calculated thus far have been far-field, or long-range interactions. It is important to calculate and renormalize these interactions properly if one is to obtain a convergent result. However, near-field interactions are short-range, and therefore can be accounted for in a pairwise additive fashion. This is because short-range interactions between two spheres are unlikely to be strongly affected by "reflections" caused by the presence of a third sphere. For nearly-touching spheres, these near-field interactions are responsible for the singular lubrication forces that can dominate the effects of all other interactions. Thus, it is important that they be included when dealing with any but the most dilute systems.

The method used to incorporate these interactions is identical to that described by Durlofsky *et al.* (1987). One begins with the far-field mobility matrix shown in (2.30), which shall henceforth be referred to as M^*, where the superscript * indicates that the interactions have been summed by the Ewald method. It has been shown (Bossis and Brady, 1984) that pairwise additivity of two-sphere resistances, which corresponds to pairwise additivity of forces, preserves lubrication interactions, while pairwise additivity of two-sphere mobilities does not. Thus, Durlofsky *et al.* incorporate near-field interactions by inverting the far-field mobility matrix to form a far-field resistance matrix, and subsequently add in the known, exact two-sphere resistance interactions that have been calculated previously (Jeffrey and Onishi, 1984; Kim and Mifflin, 1985). However, these two-sphere resistances have both far- and near-field components. To avoid counting the far-field interactions twice, the two-sphere, far-field resistance terms must therefore be subtracted off, leaving only the near-field terms. If the total, pairwise additive resistance matrix is designated by R_{2B}, and the two-body, far-field resistance matrix by R^{∞}_{2B}, then the process can be expressed mathematically as

$$\hat{R}^{*} = (M^{*})^{-1} + (R_{2B} - R^{\infty}_{2B}), \tag{2.48}$$

where far-field interactions are contained in $(M^{*})^{-1}$, while near-field interactions are accounted for in $(R_{2B} - R^{\infty}_{2B})$. In Chapters 3, 4 and 5 it will be shown that $\hat{R}^{*}$ is a very accurate approximation to the exact resistance matrix (or equivalently that $\hat{M}^{*}=(\hat{R}^{*})^{-1}$ is an accurate approximation to the exact mobility matrix), and can describe hydrodynamic interactions in hard-sphere dispersions of any configuration. A FORTRAN computer program in which the matrices of (2.48) are evaluated is given in Appendix *B*.

CHAPTER 3

TRANSPORT PROPERTIES OF SPATIALLY PERIODIC DISPERSIONS

Previous studies of the transport behavior of ordered arrays of spheres provide a set of results which can be compared with those obtained using the Stokesian dynamics method. One motivation for choosing such systems for comparison is that a relatively complete set of data is available for these ordered arrangements. In addition, the imposition of periodic boundary conditions, which is necessary when using the Ewald summation technique, complicates studies of disordered systems since the size of the periodic unit cell can affect the system behavior. No such ambiguity is present in studies of completely ordered arrays. Thus, even though the Stokesian dynamics method is applicable to hard-sphere systems of any geometry in a periodic unit cell of arbitrary size, it will be worthwhile to verify the accuracy of that method by performing preliminary calculations using simple cubic (SC), body-centered cubic (BCC), and face-centered cubic (FCC) arrays of hard spheres.

3.1 HYDRAULIC PERMEABILITY AND SEDIMENTATION VELOCITY

The hydraulic permeability of a spatially periodic porous medium and the sedimentation velocity of a spatially periodic suspension are two closely related properties which will serve as a starting point for calculations on ordered systems. The discussion here will be primarily concerned with the former property of porous media. However, calculation of the sedimentation velocity will follow directly as shown in the paragraphs to follow.

The hydraulic permeability k is a parameter commonly used to relate the average velocity and pressure drop for flow through a porous medium, and is defined by Darcy's law:

$$\langle \mathbf{u} \rangle = - \frac{k}{\mu} \nabla \langle p \rangle \ . \tag{3.1}$$

Equation (3.1) is a mathematical expression of a balance between hydrodynamic drag forces and pressure forces. In order to facilitate comparison with data from the literature, the results here will be presented as drag coefficients K defined by

$$\langle \mathbf{F} \rangle = K \langle \mathbf{u} \rangle \ . \tag{3.2}$$

For systems that are not isotropic, the scalar K in (3.2) can be expressed as a tensor $\underset{\approx}{K}$. For isotropic systems, the coefficient K is directly related to the hydraulic permeability k by

$$k = \frac{2}{9\phi} \, \frac{1}{K} \ , \tag{3.3}$$

where ϕ is the volume fraction of particles.

The calculation of the average drag coefficient for a system of spheres can be accomplished by averaging the resistance matrix $\hat{R}^{*}_{FU}$. This averaging process is equivalent to calculating $\langle \mathbf{F} \rangle$ in (3.2) for a medium in which $\mathbf{U}^{\alpha}=0$ for all particles α. The resulting expression for K is

$$K = \frac{1}{3} \operatorname{tr} \left(\frac{1}{N} \sum_{\alpha=1}^{N} \sum_{\beta=1}^{N} \hat{R}^{\alpha\beta}_{FU} \right) . \tag{3.4}$$

Here $\hat{R}^{\alpha\beta}_{FU}$ is the portion of $\hat{R}^{*}$ that relates the force on particle α to the velocity of particle β, and the notation *tr* refers to the trace of the averaged 3×3 matrix. The matrix $\hat{R}^{*}_{FU}$ can be obtained by inverting either $\hat{M}^{*}$ of (2.1) or M^{*} of (2.30), and then removing the terms coupling forces and velocities and grouping them into a matrix of dimension 3N×3N.

For the cubic arrays of interest in this chapter, the forces and velocities of all the spheres in the lattice are the same. Thus, for these systems the angle brackets around **F** in (3.2) and the sum over α given in (3.4) are not necessary, but are included for later use with disordered systems. In addition, for cubic arrays a sedimentation coefficient U_s defined by

$$\langle \mathbf{U} \rangle = U_s \mathbf{F} , \tag{3.5}$$

where **F** is the force applied to all of the particles, is easily calculated using

$$U_s = \frac{1}{K} , \tag{3.6}$$

where, again, U_s and K are expressed as scalars because of the isotropic nature of these arrays. The equality (3.6) is *not* true for disordered systems, since averaging $\hat{R}^*_{FU}$ as in (3.4) and then inverting K is not in general equivalent to first inverting the resistance matrix to obtain $\hat{M}^*_{UF}$ and then averaging that mobility matrix. Only for spatially periodic arrays, in which all particles have the same forces and velocities, do these averaging and inverting operations commute (*cf.* Saffman, 1973). In light of (3.5), it will not be necessary to report sedimentation velocities explicitly for ordered arrays.

The drag coefficient results for SC, BCC, and FCC arrays obtained using (3.4) are plotted in Figure 3.1(a,b,c) along with the results of Zick and Homsy (1982). Zick and Homsy's solution was obtained by expanding the spatially periodic Green function for a periodic array of point forces (Hasimoto, 1959) in moments, an approach that is conceptually similar to that described in Chapter 2, but differs in that it is restricted to use with only periodic systems. For the purposes of this comparison, Zick and Homsy's results can be considered exact since as many as twelve moments were included in their expansion. (Recall that torques and stresslets correspond to only the first moment.)

As can be seen from all three plots of Figure 3.1, the drag coefficients calculated using the Stokesian dynamics method are quite accurate up to moderate volume fractions (20-40%), but significantly underestimate the value of K as the limiting value of ϕ is approached. (The limiting values of ϕ for SC, BCC, and FCC packing are 0.5236, 0.6802, and 0.7405, respectively.) Thus, the far-field interactions included in Stokesian

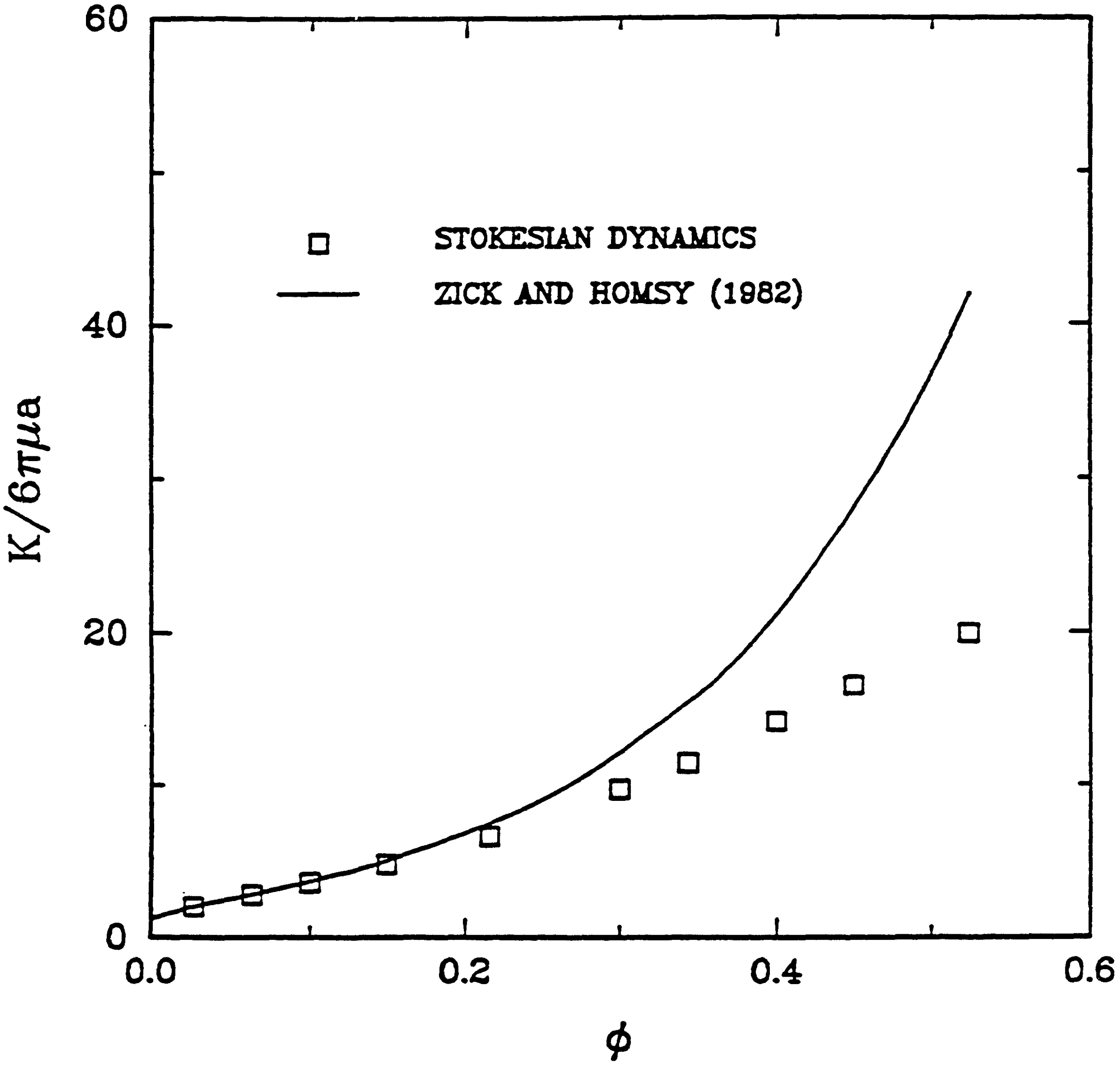

Figure 3.1a - The dimensionless drag coefficient $K/6\pi\mu a$ is plotted as a function of volume fraction ϕ for an SC lattice of spheres. The values reported by Zick and Homsy (1982) are included for comparison.

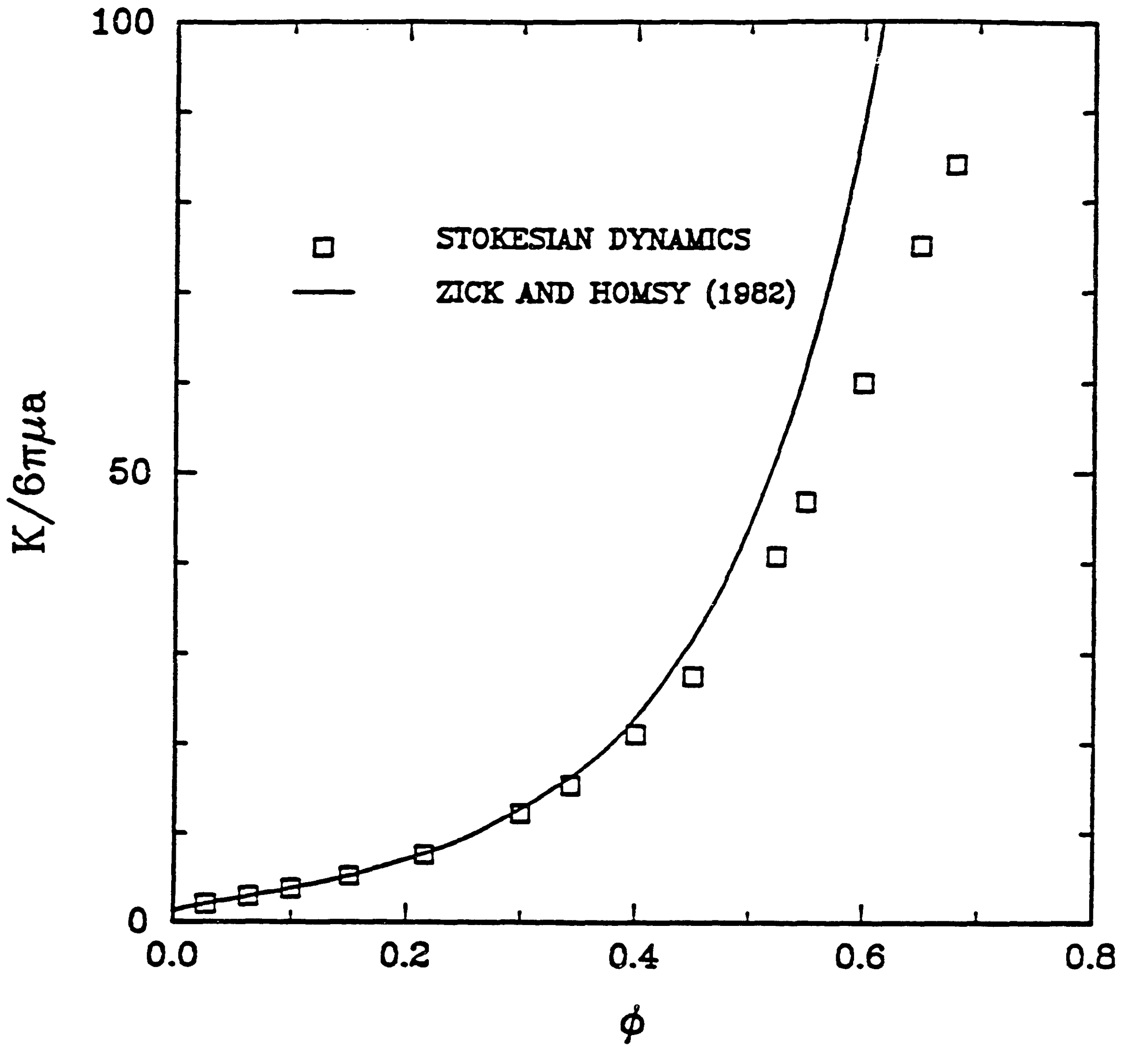

Figure 3.1b - The dimensionless drag coefficient $K/6\pi\mu a$ is plotted as a function of volume fraction ϕ for a BCC lattice of spheres. The values reported by Zick and Homsy (1982) are included for comparison.

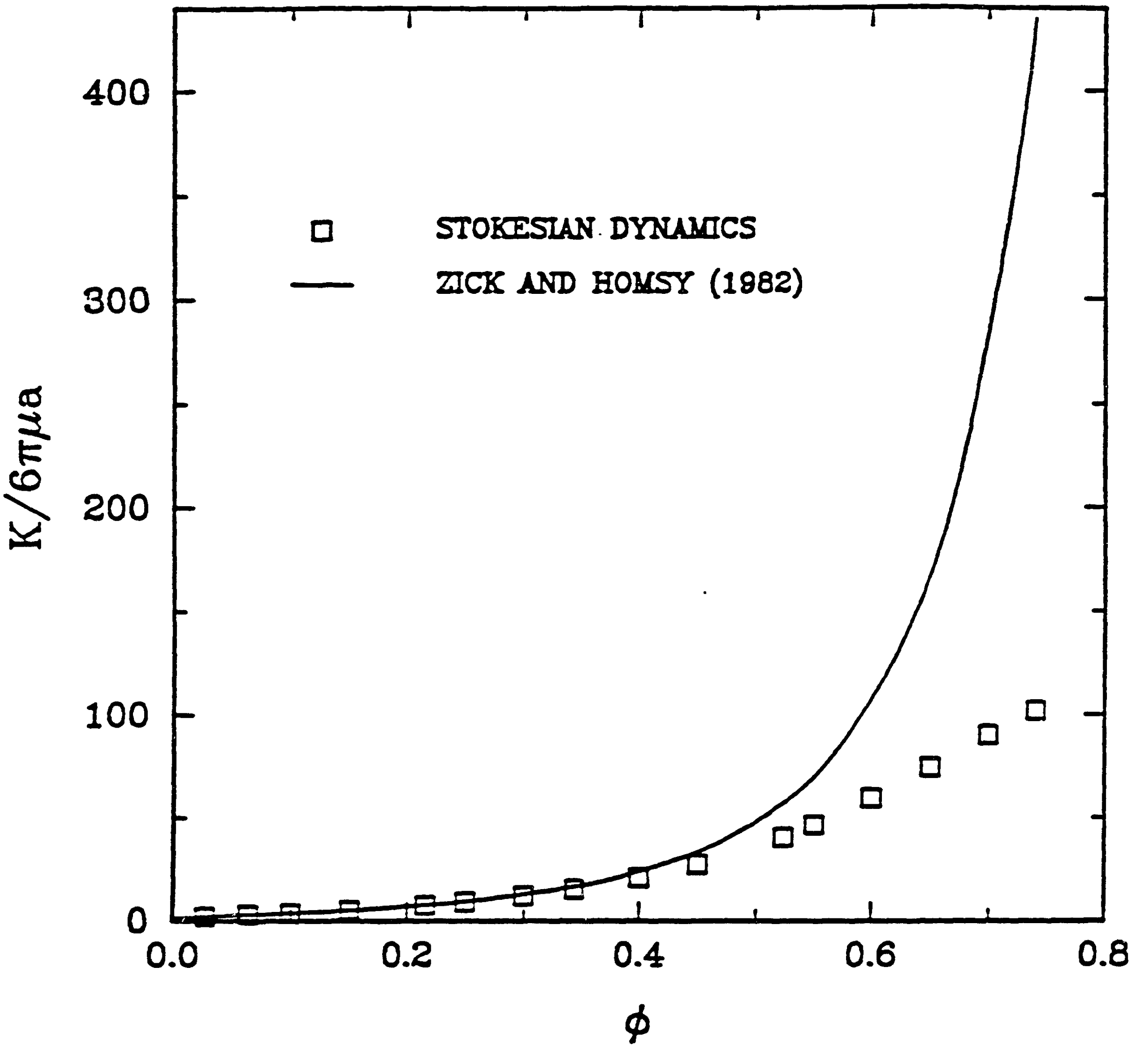

Figure 3.1c - The dimensionless drag coefficient $K/6\pi\mu a$ is plotted as a function of volume fraction ϕ for an FCC lattice of spheres. The values reported by Zick and Homsy (1982) are included for comparison.

dynamics appear to be sufficient to obtain accurate results at the lower volume fractions studied, but the interactions necessary to obtain comparable agreement at high ϕ seem to be lacking.

The discrepancy at high volume fraction can be understood by considering how the resistance matrix $\tilde{R}^*$ is constructed. The basic assumption made is that, for nearly touching spheres, lubrication interactions are dominant, and thus one can safely neglect the higher moments in (2.26). However, for flow through densely packed arrays of spheres, only a negligible fraction of the fluid flow takes place in the small gaps where lubrication is important. This is the reason why K remains finite even in the limit of close packing. The drag force on a given sphere in a tightly packed array results almost entirely from flow through the large interstices that exist even at the highest possible values of ϕ. Thus, lubrication interactions are never dominant for hydraulic permeability (and sedimentation velocity) calculations, and higher moments in the expansion (2.26) cannot be safely neglected for the entire range of ϕ.

The close correspondence between the method used here and that of Zick and Homsy makes it possible to examine the magnitude of these higher moments and, in doing so, assess the accuracy of the mean-field approximation discussed in the previous chapter. In Table 3.1 values of the drag coefficient calculated by expanding to the level of dipoles (torques and stresslets) and quadrupoles are compared for arrays at the limit of close packing. The mean-field approximation (2.24) was used to include the effect of quadrupoles in Stokesian dynamics, whereas Zick and Homsy's results incorporate them exactly. Clearly the mean-field approximation captures a large portion

Table 3.1

Values of $K/6\pi\mu a$ from Stokesian dynamics and from Zick and Homsy are compared for SC, BCC, and FCC lattices at the limit of close packing.

	Stokesian Dynamics		Zick and Homsy (1982)		
# moments[a]	1	2	1	2	COMPLETE
SC	9.53	19.95	9.53	28.04	42.14
BCC	9.6	84.5	9.6	86.1	162.9
FCC	8.4	101.8	8.4	135.8	435

[a] A solution involving only the first moment corresponds to including force, torque, and stresslet terms in the moment expansion (force terms here include the $(a^2/6)F$ contribution from (2.23)). For Stokesian dynamics, the second moment corresponds to including the mean-field quadrupole term of (2.24), while Zick and Homsy account for the quadrupole contribution exactly. The complete results reported by Zick and Homsy were extrapolated from the solution including the first twelve moments.

of the quadrupolar contribution. However, it is also apparent that even the complete solution through the level of quadrupoles is inaccurate at high ϕ. Indeed, in order to obtain 10% accuracy at the limit of close-packing, Zick and Homsy found it necessary to include four, six, and eight moments for SC, BCC, and FCC lattices, respectively. Since including the complete quadrupolar contribution would increase the size of the matrix in (2.30) from 11N×11N to 26N×26N, resulting in a 13-fold increase in computational effort, it is doubtful whether the increase in accuracy justifies a more complete treatment of the quadrupole terms than that offered by the mean-field approximation.

3.2 SHEAR VISCOSITY

Unlike the case of flow through a periodic porous medium, when a cubic array is sheared there is relative motion between the spheres, and thus singular lubrication interactions become dominant as ϕ is increased. Nunan and Keller (1984) have calculated the shear viscosity of such an array over a wide range of ϕ using a method similar to that of Zick and Homsy (1982). However, because of singularities caused by lubrication forces, this method could not be used in the limit of close packing, and as a result the authors also provide asymptotic results valid for comparison at high values of ϕ.

As stated in (2.12), the particle contribution to the bulk stress in a system with $\langle \underset{\approx}{\mathcal{L}} \rangle = 0$ is $n\langle \underset{\approx}{S} \rangle$. (The average rotlet $\langle \underset{\approx}{\mathcal{L}} \rangle$ is zero for particles in a linear shear flow.) The shear viscosity of a suspension relates $\langle \underset{\approx}{S} \rangle$ to $\langle \underset{\approx}{e} \rangle$, and can be found by solving (2.30) for the particle stresslets under the condition that $\mathbf{F}^\alpha = \mathbf{L}^\alpha = 0$ for all α. Solving for the stresslets, and averaging the resulting matrix that relates the stresslets to the average rate-of-strain, one obtains

$$\langle \underset{\approx}{S} \rangle = -\langle A \rangle : \langle \underset{\approx}{e} \rangle \quad , \tag{3.7}$$

where the fourth order tensor A is given by

$$A = \begin{pmatrix} R^*_{SU} & R^*_{S\Omega} \end{pmatrix} \cdot \begin{pmatrix} R^*_{FU} & R^*_{F\Omega} \\ R^*_{LU} & R^*_{L\Omega} \end{pmatrix}^{-1} \cdot \begin{pmatrix} R^*_{FE} \\ R^*_{LE} \end{pmatrix} - \begin{pmatrix} R^*_{SE} \end{pmatrix} \quad . \tag{3.8}$$

The symmetry of periodic lattices guarantees that the first term on the right-hand side of (3.8) (the product of the three matrices shown) will be zero for the calculation considered here, but it is included for generality. The average of A is given by

$$\langle A \rangle = \frac{1}{N} \sum_{\alpha=1}^{N} \sum_{\beta=1}^{N} A^{\alpha\beta} \quad , \tag{3.9}$$

where $A^{\alpha\beta}$ relates the stresslet of particle α to the average rate-of-strain $\langle \underset{\approx}{e} \rangle$.

The symmetry of the cubic lattice also allows one to completely specify all the elements of the tensor A in terms of two scalar coefficients, α and β, according to (*cf*. Nunan and Keller, 1984 and Zuzovsky *et al*., 1983)

$$A_{ijkl} = \frac{\mu}{2}(1+\beta)(\delta_{ik}\delta_{jl}+\delta_{il}\delta_{jk}-\frac{2}{3}\delta_{ij}\delta_{kl}) + \mu(\alpha-\beta)(\delta_{ijkl}-\frac{1}{3}\delta_{ij}\delta_{kl}), \quad (3.10)$$

where δ_{ijkl} is unity when all four indices are the same and zero otherwise. The quantity μ in (3.10) is the viscosity of the pure fluid, and the scalars α and β will be referred to as the α and β coefficients of shear viscosity, respectively. It is important to note that α and β are the viscosity coefficients corresponding to a single, instantaneous configuration of particles, and are not time averages.

The Stokesian dynamics results for α and β and those of Nunan and Keller (1984) are plotted as a function of ϕ for SC, BCC, and FCC lattices of spheres in Figures 3.2(a,b), 3.3(a,b), and 3.4(a,b), respectively. The agreement is excellent for every case except the β coefficient of the FCC lattice. However, Nunan and Keller reported significant difficulty in obtaining convergence with increasing number of moments for that calculation, and thus there is some doubt as to whether their result should be considered exact for that particular case.

For comparisons in the limit of close packing, the aforementioned high volume fraction asymptotic results can be used. These results for the effective viscosity coefficients α and β are as follows:

Simple Cubic Lattices:

$$\begin{aligned} \alpha &= \frac{3}{16}\pi\epsilon^{-1} + \frac{27}{80}\pi\ln(\epsilon^{-1}) + 3.1 + 0.25\epsilon\ln(\epsilon^{-1}) + O(\epsilon) \\ \beta &= \frac{1}{4}\pi\ln(\epsilon^{-1}) + 0.63 + O(\epsilon) \end{aligned} \quad (3.11a)$$

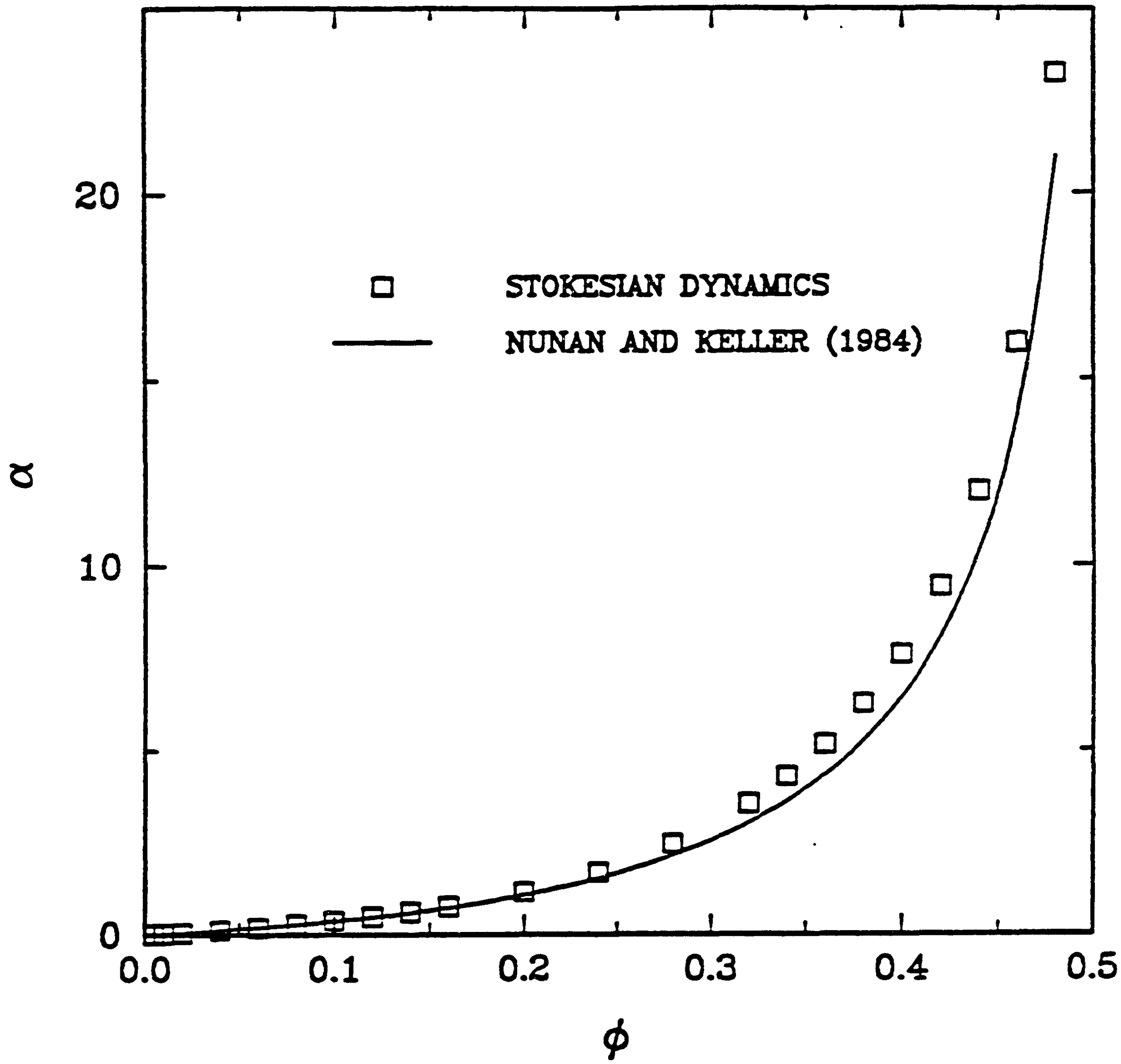

Figure 3.2a - The α coefficient of shear viscosity is plotted as a function of volume fraction ϕ for an SC lattice of hard spheres. The results of Nunan and Keller (1984) are included for comparison.

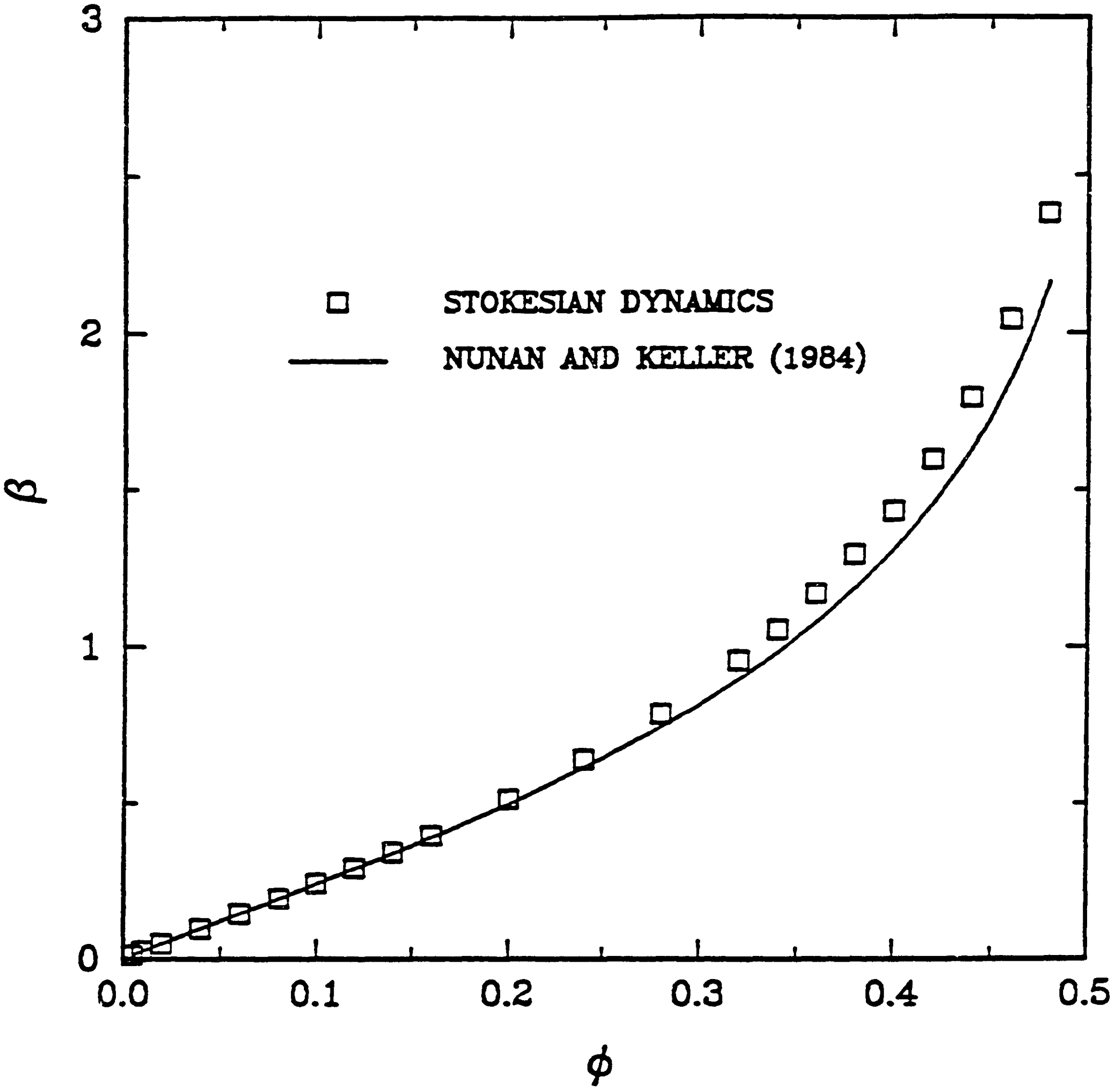

Figure 3.2b - The β coefficient of shear viscosity is plotted as a function of volume fraction ϕ for an SC lattice of hard spheres. The results of Nunan and Keller (1984) are included for comparison.

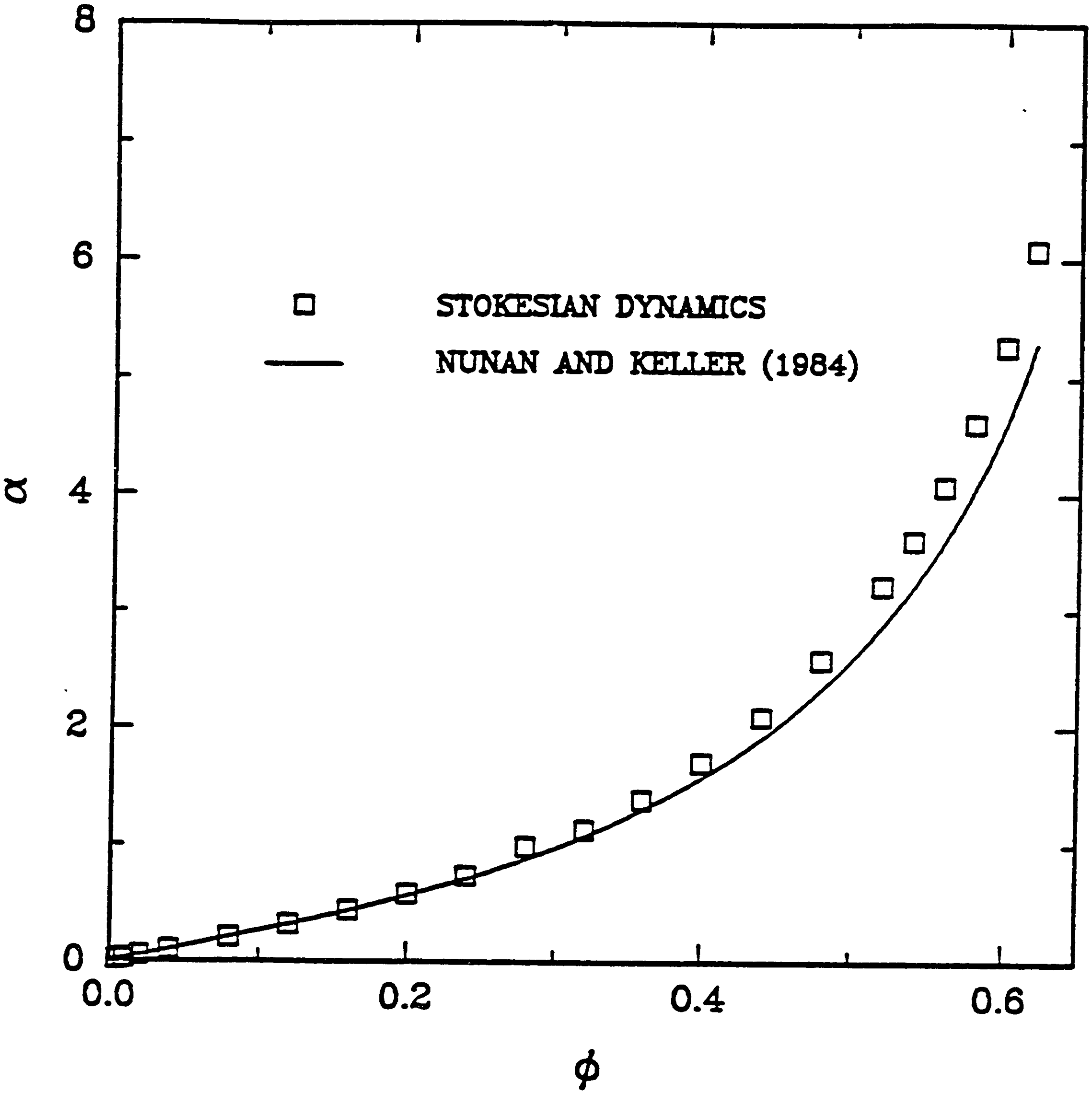

Figure 3.3a - The α coefficient of shear viscosity is plotted as a function of volume fraction ϕ for a BCC lattice of hard spheres. The results of Nunan and Keller (1984) are included for comparison.

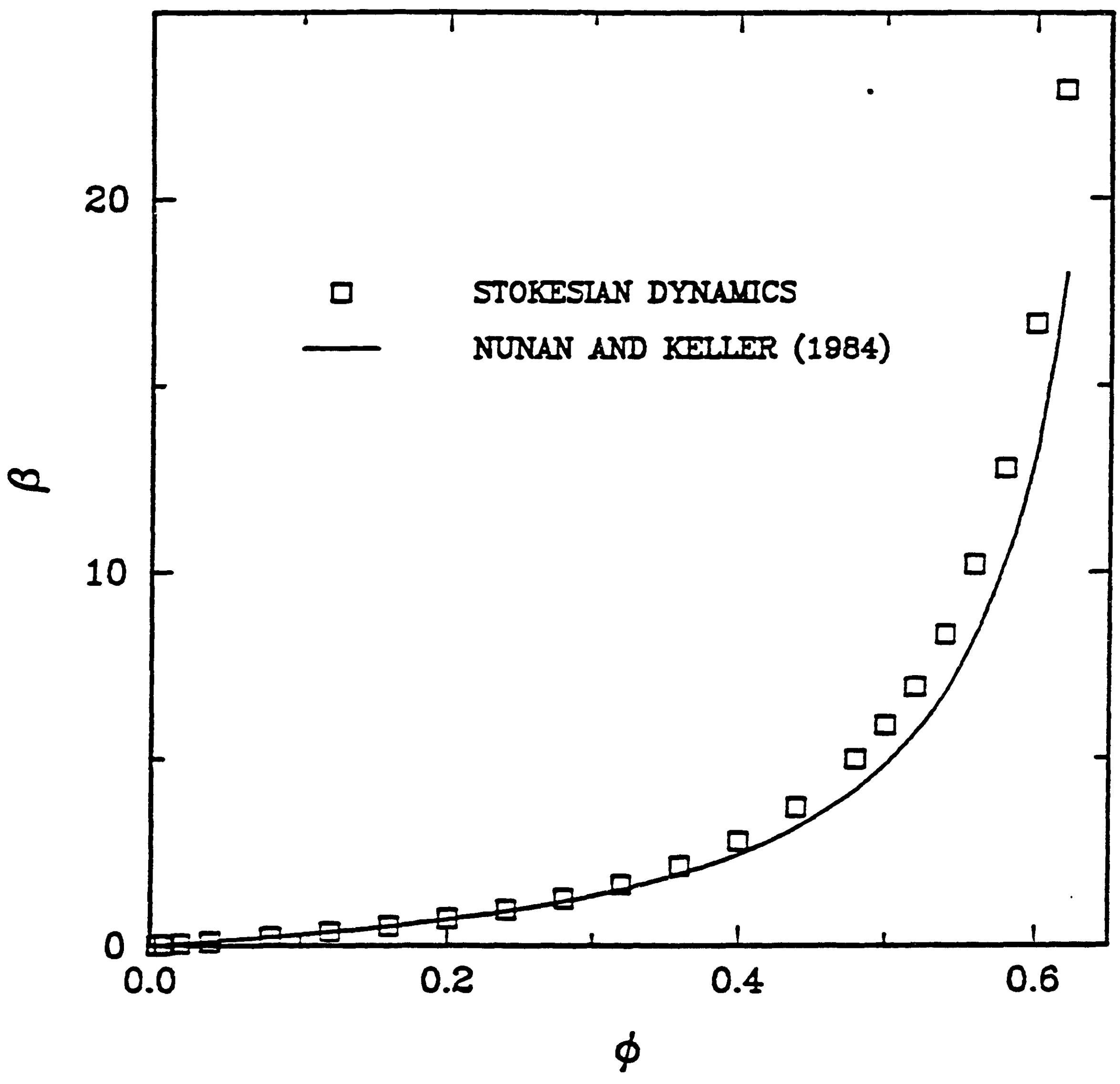

Figure 3.3b - The β coefficient of shear viscosity is plotted as a function of volume fraction φ for a BCC lattice of hard spheres. The results of Nunan and Keller (1984) are included for comparison.

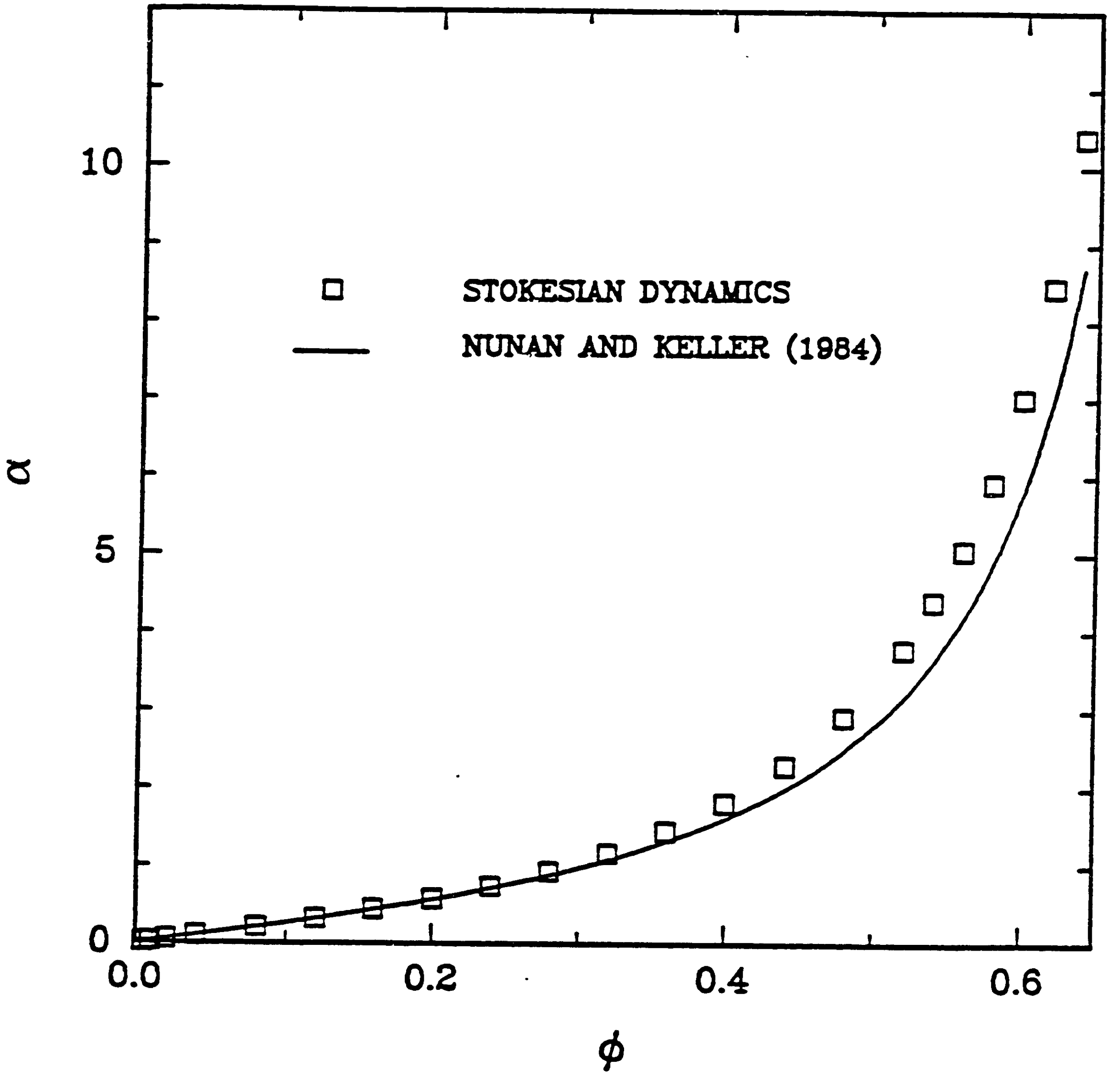

Figure 3.4a - The α coefficient of shear viscosity is plotted as a function of volume fraction ϕ for an FCC lattice of hard spheres. The results of Nunan and Keller (1984) are included for comparison.

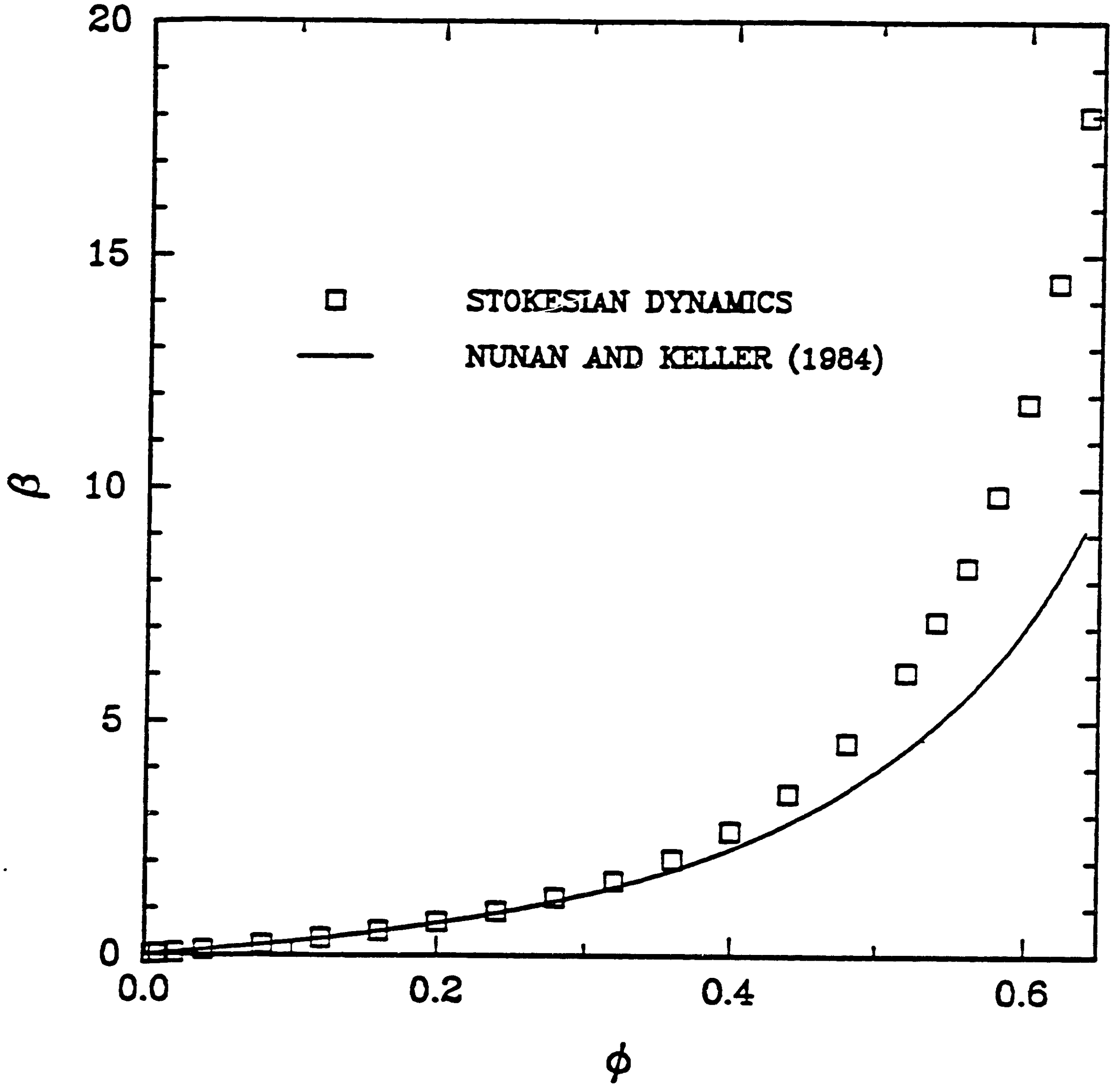

Figure 3.4b - The β coefficient of shear viscosity is plotted as a function of volume fraction ϕ for an FCC lattice of hard spheres. The results of Nunan and Keller (1984) are included for comparison.

Body-Centered Cubic Lattices:

$$\alpha = \frac{1}{4}\sqrt{3}\,\pi\,\ln(\epsilon^{-1}) - 1.73 + 12.3\epsilon\ln(\epsilon^{-1}) + O(\epsilon)$$
$$\beta = \frac{1}{8}\sqrt{3}\,\pi\epsilon^{-1} + \frac{37}{120}\sqrt{3}\,\ln(\epsilon^{-1}) + 12.8 - 35\epsilon\ln(\epsilon^{-1}) + O(\epsilon) \qquad (3.11b)$$

Face-Centered Cubic Lattices:

$$\alpha = \frac{3}{32}\sqrt{2}\,\pi\epsilon^{-1} + \frac{87}{160}\sqrt{2}\,\pi\ln(\epsilon^{-1}) + 9.7 - 15.5\epsilon\ln(\epsilon^{-1}) + O(\epsilon)$$
$$\beta = \frac{3}{16}\sqrt{2}\,\pi\epsilon^{-1} + \frac{47}{80}\sqrt{2}\,\pi\ln(\epsilon^{-1}) + O(1) \qquad (3.11c)$$

Here ϵ is the distance separating the surfaces of neighboring spheres made dimensionless by the sphere radius. Limiting values of α and β obtained from the asymptotic expansions (3.11) and from Stokesian dynamics are compared in Table 3.2(a,b,c).

Again, agreement is excellent for all cases considered. Significantly, however, the two sets of results agree best for cases where the asymptotic expansion has an $O(\epsilon^{-1})$ singularity (α for SC, β for BCC, α and β for FCC) as opposed to an $O(\ln\epsilon^{-1})$ singularity (β for SC, α for BCC). This observation is consistent with the explanation given for the trends in the hydraulic permeability results presented in the previous section. The agreement is better for the more severe, $O(\epsilon^{-1})$ singularity because it dominates the many-particle, far-field interactions more completely than does the logarithmic singularity, and thus the pairwise-additive method of including lubrication used in the Stokesian dynamics method is more accurate

Table 3.2a

Coefficients of shear viscosity for an SC lattice (high ϕ).

ϕ	α_{SD}	$\alpha_{N\&K}$	β_{SD}	$\beta_{N\&K}$
0.520	262.0	136.8	4.943	4.856
0.523	1552	1556	6.242	6.268
0.52359	1.054×10^{5}	1.055×10^{5}	9.378	9.585
0.52359877	1.653×10^{8}	1.653×10^{8}	15.00	15.38

Table 3.2b

Coefficients of shear viscosity for a BCC lattice (high ϕ).

ϕ	α_{SD}	$\alpha_{N\&K}$	β_{SD}	$\beta_{N\&K}$
0.680	16.38	11.01	7952	7970
0.6801	17.48	12.17	1.857×10^{4}	1.859×10^{4}
0.6801747	26.81	20.32	2.254×10^{7}	2.254×10^{7}
0.680174761	33.03	26.21	2.361×10^{9}	2.361×10^{9}

Table 3.2c

Coefficients of shear viscosity for an FCC lattice (high ϕ).

ϕ	α_{SD}	$\alpha_{N\&K}$	β_{SD}	$\beta_{N\&K}$
0.730	96.58	110.1	183.7	189.7
0.740	1941	1955	3867	3873
0.74048	1.890×10^{6}	1.890×10^{6}	3.779×10^{6}	3.779×10^{6}
0.7404848	9.546×10^{7}	9.546×10^{7}	1.909×10^{6}	1.909×10^{6}

The dominance of lubrication forces also becomes more complete as the volume fraction approaches the limiting value, which explains the better agreement shown in Table 3.2 as ϕ is increased.

3.3 ROTATIONAL DRAG COEFFICIENT

By averaging $R^*_{L\Omega}$ in precisely the same manner that R^*_{FU} was averaged in (3.4), one can calculate a rotational drag coefficient that relates the torque and rotational velocity for periodically arranged spheres that are all rotating with the same value of $\boldsymbol{\Omega}$. This coefficient is sometimes called the "spin viscosity" since it can be used to calculate the contribution of the antisymmetric average rotlet $\langle \underset{\approx}{\ell} \rangle$ to the bulk stress $\langle \underset{\approx}{\sigma} \rangle$ (*cf.* equation (2.12)). One practical application of such a parameter lies in the use of ferrofluids, which commonly have antisymmetric stresses (Zuzovsky *et al.*, 1983; Rosensweig, 1988).

Values for the rotational drag coefficient K_r, which is defined by the relation

$$\langle \mathbf{L} \rangle = K_r \boldsymbol{\Omega} \ , \tag{3.12}$$

are plotted in Figure 3.5(a,b,c) together with the asymptotic results of Zuzovsky *et al.* Again, SC, BCC, and FCC lattices are considered. As discussed above, the angle brackets around **L** in (3.12) are not needed for these periodic systems, but are included for later use.

As can be seen in Figure 3.5*a*, the Stokesian dynamics method captures both the low and high ϕ behavior of K_r exactly. As with the shear vis-

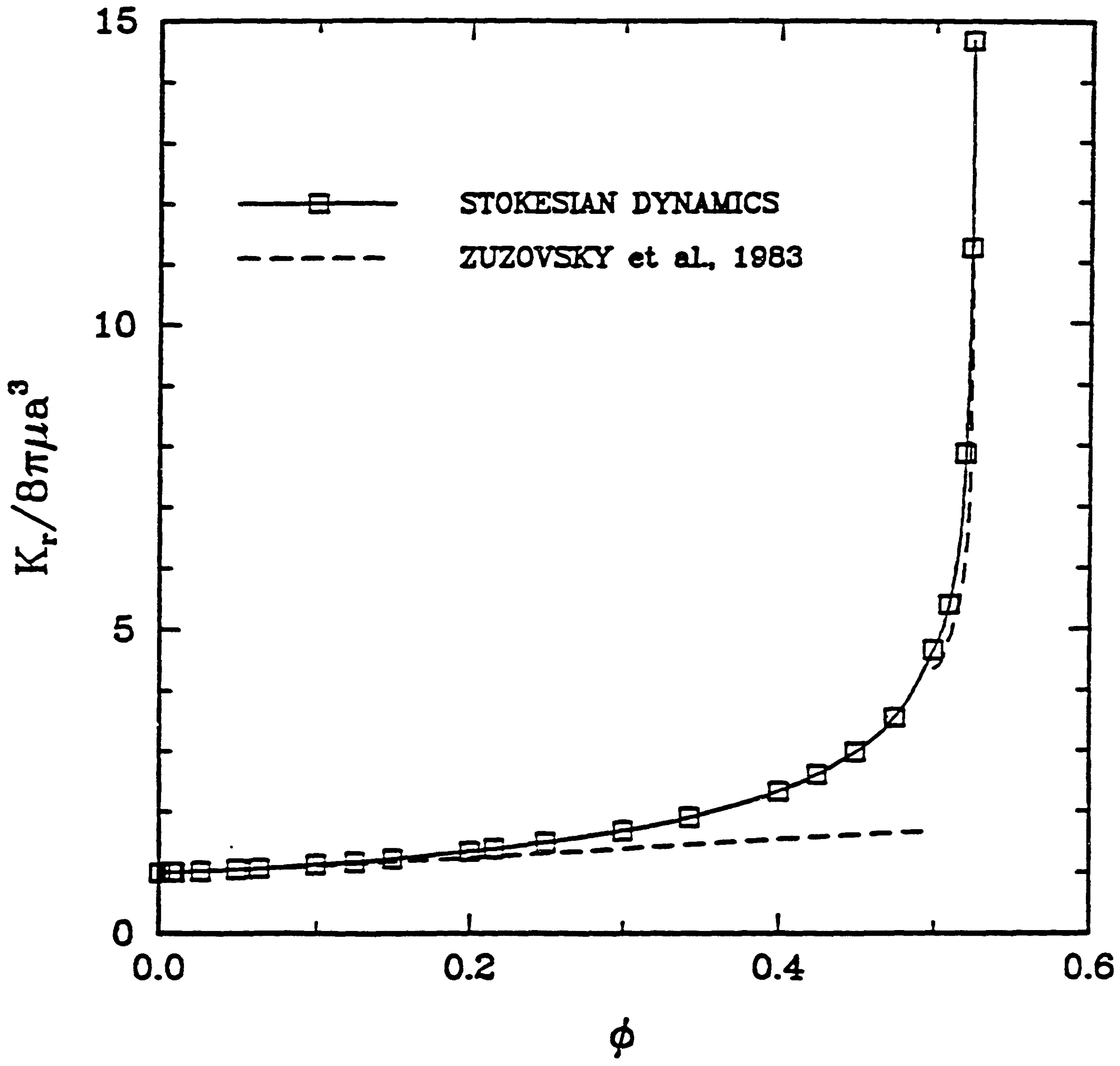

Figure 3.5a - The dimensionless rotational drag coefficient $K_r/8\pi\mu a^3$ is plotted as a function of volume fraction ϕ for an SC lattice of hard spheres. Asymptotic results reported by Zuzovsky *et al.* (1983), valid in the limits of low and high ϕ, are also shown (dashed curves).

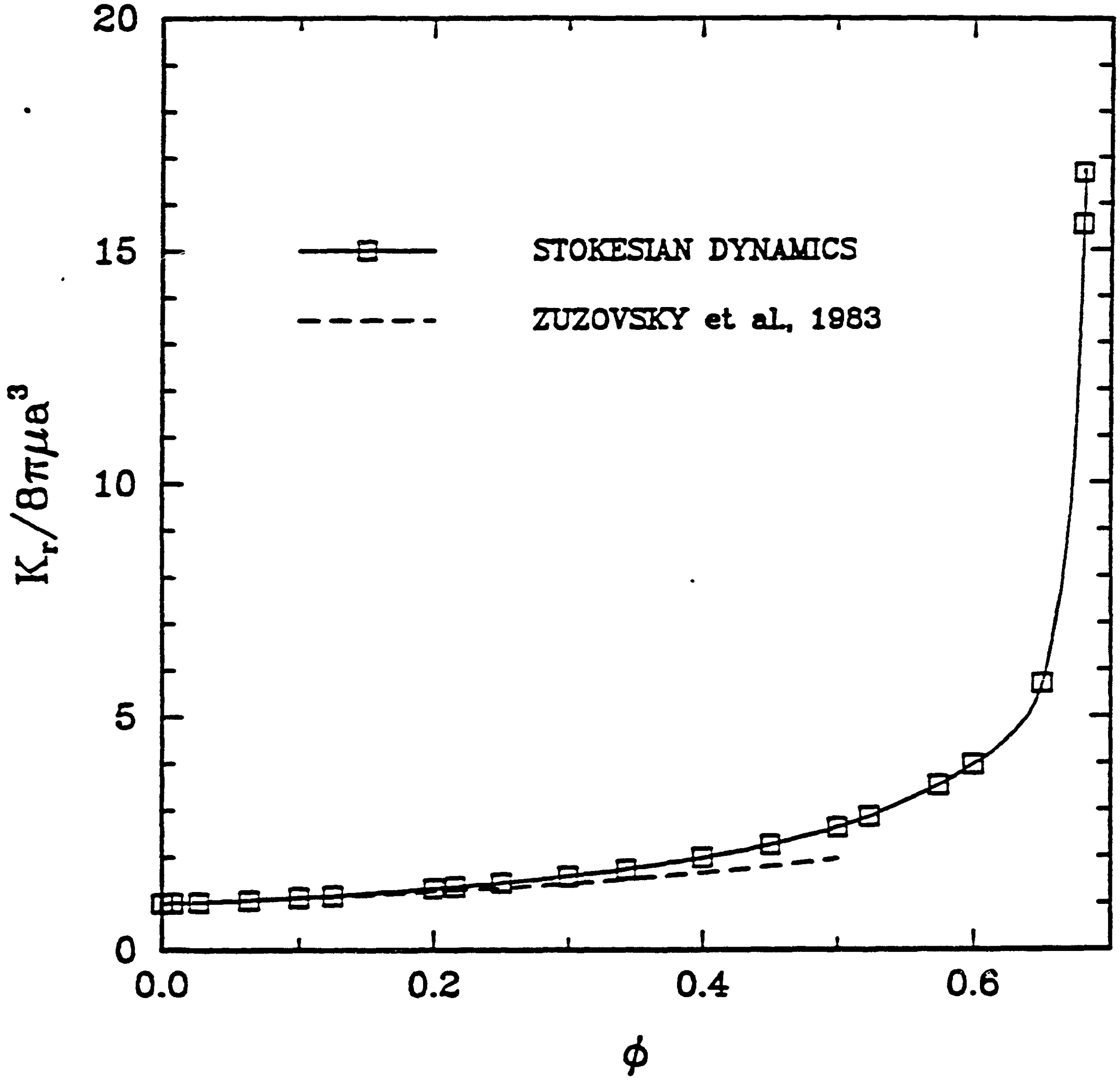

Figure 3.5b - The dimensionless rotational drag coefficient $K_r/8\pi\mu a^3$ is plotted as a function of volume fraction ϕ for a BCC lattice of hard spheres. The low ϕ, asymptotic result reported by Zuzovsky *et al.* (1983) is also shown (dashed curve).

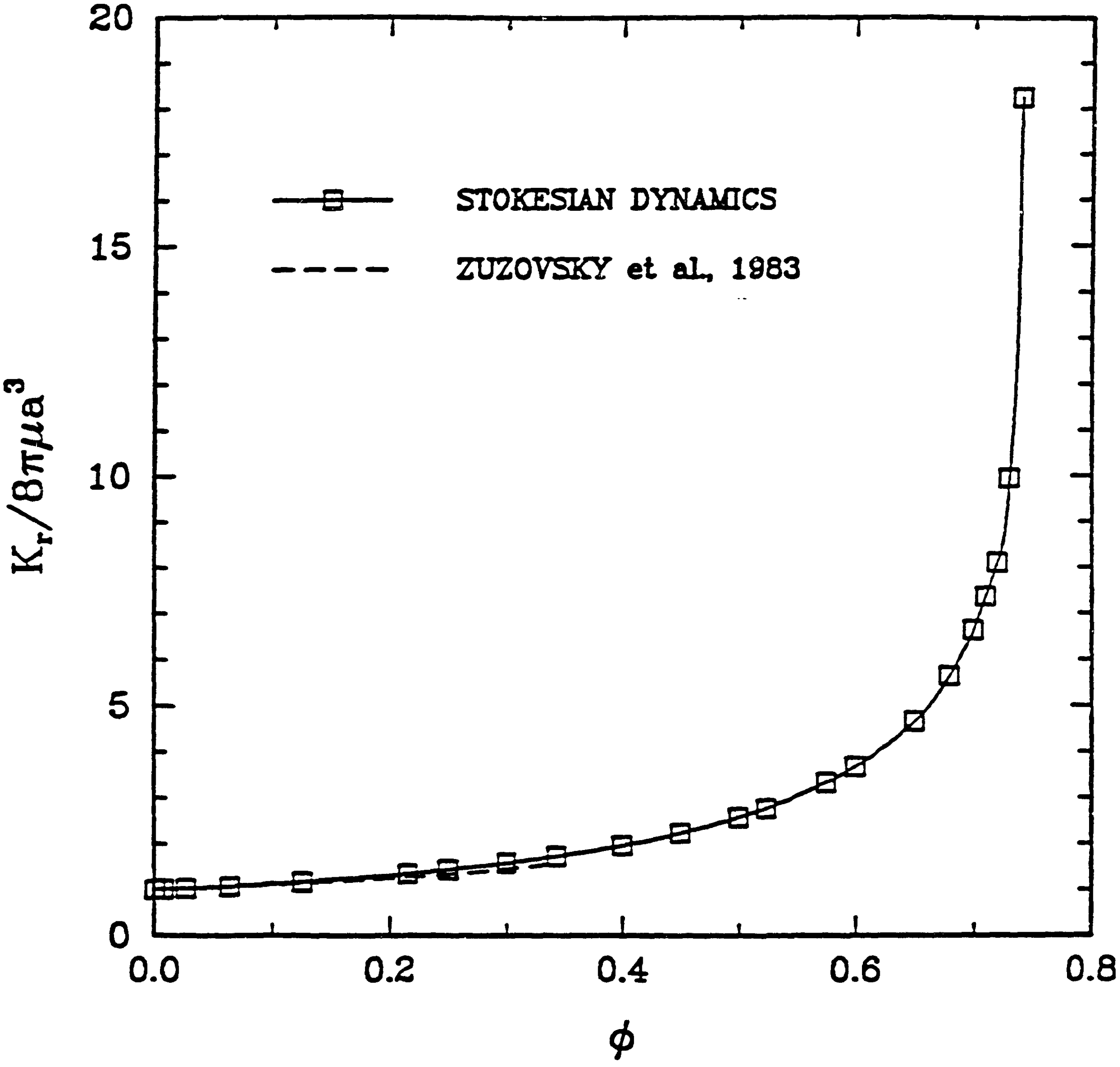

Figure 3.5c - The dimensionless rotational drag coefficient $K_r/8\pi\mu a^3$ is plotted as a function of volume fraction ϕ for an FCC lattice of hard spheres. The low ϕ, asymptotic result reported by Zuzovsky *et al.* (1983) is also shown (dashed curve).

cosity, this accuracy can be attributed to the fact that singular lubrication forces become dominant as periodically arranged, rotating spheres come into contact, just as is assumed in the Stokesian dynamics method. Figures 3.5*b* and 3.5*c* show the same excellent agreement as Figure 3.5*a* at low volume fractions, but Zuzovsky *et al.* do not give the high volume fraction asymptotes for BCC and FCC lattices, and so no comparison is made for those systems in the limit of close packing.

3.4 CONCLUSION

Values for the hydraulic permeability and shear viscosity of spatially periodic dispersions have been calculated using the Stokesian dynamics method. It was seen that the Stokesian dynamics result for the hydraulic permeability was in good agreement with those of Zick and Homsy (1982) up to volume fractions of about 20-40%, after which the Stokesian dynamics method significantly underpredicted Zick and Homsy's results. The disparity can be attributed to the approximations made in the Stokesian dynamics method of calculating hydrodynamic interactions. One key assumption in this method is that, for nearly touching spheres, singular lubrication forces come into play and dominate the effects of other, longer range interactions. However, fluid flowing through densely packed, fixed arrays of spheres avoids the small gaps present in favor of large interstices that offer less hydrodynamic resistance, and thus lubrication forces are never dominant in the hydraulic permeability calculation considered here.

In contrast, when a cubic lattice of spheres is sheared, there is relative motion between the sphere surfaces that insures the dominance of lubrication forces in the limit of high volume fraction. Since Stokesian dynamics accounts for these lubrication forces properly, the correct high ϕ behavior is obtained for the viscosity coefficients, as shown by comparison with the results of Nunan and Keller (1984). Similar behavior was demonstrated by the rotational drag coefficient, or "spin viscosity."

The methods used by Zick and Homsy (1982) and Nunan and Keller (1984) are somewhat less general than the Stokesian dynamics method in that they can only be applied to periodic systems. However, there is a close enough correspondence between Stokesian dynamics and these two methods to allow for the evaluation of the accuracy of the "mean-field" approach to including quadrupoles that was described in Chapter 2. It was found that, using this approximate approach, Stokesian dynamics is able to account for a large portion of the quadrupole effects reported by Zick and Homsy.

For spatially periodic media, many theoretical results are presently available and thus the results given here are included mainly for purposes of comparison. Even so, the rotational drag (or "spin viscosity") calculations shown in Figure 3.5 supplement the existing knowledge of periodic systems in that such values had not yet been reported in the literature for the full range of volume fractions possible. In addition, the generality of the Stokesian dynamics method makes it amenable for use in analyzing systems of arbitrary geometry, provided that they are constructed of hard spheres. The fact that Stokesian dynamics is highly accurate for many transport calculations involving hard-sphere systems presents several possibilities for advancing the current understanding of suspensions and porous media. As will be demonstrated in succeeding chapters, this flexibility can be of great use in a large number of interesting transport problems.

CHAPTER 4

TRANSPORT PROPERTIES OF DISORDERED SUSPENSIONS

One important attribute of the Stokesian dynamics method is that it places no restrictions on the locations of particles other than those required by the imposition of periodic boundary conditions. Thus, it can be used to calculate hydrodynamic transport properties of disordered dispersions as well as periodic arrays such as those considered in the previous chapter. Examining disordered systems will allow this method to be studied more extensively than was possible in Chapter 3 by allowing comparison both with a different set of theoretical results and with experimental data. In addition to these comparisons, the effects of imposing periodic boundary conditions, which pose no ambiguities when modeling a periodic system, can be significant in calculations involving disordered media. Thus, the results presented in the following paragraphs should both demonstrate the application of the newly derived theory and give some indication of the effects of long-range order on disordered systems.

One approach to examining the behavior of disordered systems is dynamic simulation, in which particle trajectories are calculated and followed over time. Several studies involving dynamic simulations can be found in the literature (Brady and Bossis, 1985; Bossis and Brady, 1984; Bossis and Brady, 1987; Brady and Bossis, 1988). Another approach useful for studying disordered systems is the Monte Carlo method, in which transport properties for instantaneous configurations are calculated and averaged over many realizations. This approach is restricted to calculations of transport properties valid over time scales so short that the system configuration does not change. However, because particle interactions are not being recalculated for many time steps, the Monte Carlo approach requires significantly less computer time than does dynamic simulation. In addition, the Monte Carlo method can be used to study simultaneously the properties of suspensions, such as sedimentation velocity, self-diffusion†, and viscosity, and the properties of disordered porous media, such as hydraulic permeability and hindered diffusion. In this chapter results of the Monte Carlo simulations are presented for suspension properties. The corresponding results for properties associated with porous media are given in Chapter 5.

The calculations were carried out over volume fractions ranging from infinite dilution to the fluid-solid transition, which occurs at approximately $\phi = 0.49$ for hard spheres (Hoover and Ree, 1968). Three different levels of approximation in modeling the far-field portion of the hydrodynamic interactions are considered. In addition, the effects of changing the length scale over which periodic boundary conditions are imposed are examined, and scaling laws for these periodicity effects are derived. In all cases where it is possible the results are compared both with alternative theories and with experimental data from the literature, thereby providing some criteria for assessing the accuracy of the method.

---

†The term "self-diffusion" as used in this thesis refers to diffusion of a Brownian sphere in a suspension of identical spheres (*cf.* Rallison and Hinch, 1986). This process is also often referred to as tracer diffusion or intradiffusion (Reid *et al.*, 1987).

4.1 SAMPLING TECHNIQUES

The procedure used to generate the hard-sphere microstructure varied according to the volume fraction of the suspension. For $\phi < 0.25$, sphere locations within a given periodic, cubic unit cell were chosen by "random sequential addition." This process involves the sequential placement of spheres at random positions within a unit cell. If the location chosen for a given sphere overlaps with that of a previously positioned sphere, then a new location is chosen, and the process is repeated until suitable, non-overlapping positions are obtained for each of the N spheres. For $0.25 < \phi < 0.49$, random sequential addition becomes computationally infeasible. Thus, at these volume fractions, the spheres were placed in an arbitrary initial configuration and then moved using a random-stepping routine in order to insure that the sample was disordered. To check that the samples generated using the latter, random-stepping method were sufficiently independent from one another, the linear correlation between the initial and final coordinates ($\mathbf{x}$) of the particles was monitored through the correlation coefficient r_c. For example, the correlation between particle positions in two samples **A** and **B** could be checked by plotting $\mathbf{x}_A$ vs. $\mathbf{x}_B$ for the N particles, and then calculating the three linear correlation coefficients. If the particles had not moved significantly from their previous positions, then one would expect values of r_c close to unity, whereas sufficient randomization should result in a much lower level of correlation. Because this method of monitoring spatial correlation is only approximate and is based primarily on intuitive arguments, the condition $r_c < 0.5$ was accepted as a reasonable criterion for statistical independence and a more rigorous statistical analysis was not attempted. The FORTRAN 200 function RANF was used to generate the random numbers needed for both of the sample-generation techniques used here.

For $\phi = 0.25$ the criterion on r_c was easily met by moving each particle 500 steps between samples, where the length of each step was chosen so that the probability of success (*i.e.*, no overlap) was about 0.5 - 0.7, values that agree closely with those suggested by Binder (1986). Radial distribution functions calculated from samples used for these calculations generally agreed with those of Barker and Henderson (1971) to within 10%, although the maximum values at contact were sometimes in error by as much as 20%. This error could always be eliminated by increasing the number of samples. To check the consistency of the two sample-generating methods used, we performed simulations with each of them at $\phi = 0.25$ and found that the two sets of results did not differ by more than about 2-3%. In addition, our results at $\phi = 0.40$ were found to be independent of the initial configuration chosen, and did not change when the number of randomization steps was doubled from 500 to 1000 steps per particle.

4.2 CALCULATION OF HYDRODYNAMIC INTERACTIONS

Once the locations of the N particles are specified through the sample-generating process, the transport properties can be determined by Stokesian dynamics. Three levels of approximation in the far-field interactions are considered here, and each of these levels is examined both with and without the addition of near-field interactions. The different levels are determined by the point at which the expansion (2.26) is truncated in evaluating the far-field, many-particle interactions. If truncation occurs after the zeroth moment, then the only submatrix of the mobility in (2.30) to be evaluated is M^*_{UF}. This in turn implies that it is M^*_{UF} that must be inverted to add in near-field interactions in (2.48). This lowest level of approximation, at which only particle forces are considered (along with the quadrupole terms that were expressed in terms of particle forces in Chapter 2), will be referred to as the "F method." Similarly, if the moment expansion (2.26) includes torques (the antisymmetric portion of the first moment), then the mobility to be used in (2.30) and (2.48) will include M^*_{UF}, M^*_{UL}, $M^*_{\Omega F}$, and $M^*_{\Omega L}$, and one has what will be referred to as the "F-T method." Finally, including all the interactions discussed in Chapter 2, which consist of forces, torques, and stresslets, results in the "F-T-S method," the most accurate of the three levels of approximation considered. Note that the size of the mobility matrix that must be inverted in (2.48) increases from 3N×3N to 6N×6N to 11N×11N as one progresses from the F to the F-T to the F-T-S method. Since the computation time required to invert a matrix grows as the cube of the matrix dimension, it is clearly desirable to have some idea of how the three methods compare in terms of accuracy. This potential savings thus provides one motivation for the comparisons that will be made in the next section.

The two-sphere, far-field interactions used to form R^{∞}_{2B} of (2.48) included force, torque, and stresslet interactions for each of the three cases described above. In other words, these terms were not included in any of the pairwise-additive calculations of near-field interactions performed in these simulations. Thus, results for the "F method" do not include torque and stresslet interactions, even in a pairwise-additive fashion.

Similarly, results for the "F-T method" do not include any stresslet interactions. Torque and stresslet interactions were not included in the near-field interactions in order to avoid including non-convergent terms in the sums in (2.28). As will be seen in Chapter 5, however, pairwise addition of stresslet interactions between near-neighbors can greatly improve the accuracy of the "F method" for certain calculations. In the following discussion, the definitions and averages given will be valid regardless of whether the F, F-T, or F-T-S methods are used, and whether or not near-field interactions are included. Thus, for simplicity, no explicit reference will be made to the level of approximation used in forming the mobility and resistance matrices that are used in those equations.

All of the calculations described here were done on a CYBER 205 supercomputer. It required 22 seconds of CPU time to fill the complete, Ewald-summed, F-T-S mobility matrix for a single 27 sphere sample, while 6 seconds were required to invert that matrix. The CPU time required to form (R_{2B} - R_{2B}^{∞}) of (2.48) is negligible compared to that needed for the formation and inversion of M^*. Although these requirements might seem prohibitive to those interested in doing dynamic simulations, we should point out that suitable, time-saving approximations can be used to significantly decrease the time requirements of this method. Two such possibilities are: a) only recalculating far-field interactions on a time scale that allows for the particles to move a significant fraction of their own radii, such as every 10 or 100 time steps; or b) using the less accurate F or F-T methods in order to take advantage of the corresponding reduction in the size of the mobility matrix. The former approximation is made possible by the fact that far-field interactions are insensitive to small rearrangements in the system configuration, while some information on the implications of the latter approximation will be obtained by examining the results of the next section. Either or both of these suggestions could be of potential value, depending upon the particular problem being investigated.

For this work, computer time limitations required that averages be performed over only 10 samples for each volume fraction studied. Fortunately, however, 95% confidence intervals calculated using the standard deviations associated with the results were generally within 5% of the average values reported. The statistical errors were decreased by the isotropic nature of the dispersions. That is, the use of the $\frac{1}{3}tr$ operator in (4.1) and (4.7) reflects the fact that, for each realization, three independent values of the coefficients are obtained for the sedimentation velocities and self-diffusion coefficients. Similarly, five independent values of the shear viscosity are obtained for each realization, since there are five independent components of $\langle \underset{\approx}{S} \rangle$ and $\langle \underset{\approx}{e} \rangle$. Thus, although only 10 samples are represented in each data point, that point is actually an average computed from either 30 or 50 values, depending on the transport property in question.

4.3 SEDIMENTATION VELOCITY

The sedimentation velocity $\langle \mathbf{U} \rangle$ of a suspension of particles in some configuration is usually defined as the average translational velocity of the particles relative to zero volume flux (*i.e.*, such that the suspension average velocity $\langle \mathbf{u} \rangle = \mathbf{0}$). The value of $\langle \mathbf{U} \rangle$ can be calculated in a manner directly analogous to that used to obtain $\langle \mathbf{F} \rangle$ in (3.4). Assuming the particles are all identical and are sedimenting under the same applied force, U_s from (3.6) is given by

$$U_s = \frac{1}{3} \operatorname{tr} \left(\frac{1}{N} \sum_{\alpha=1}^{N} \sum_{\beta=1}^{N} M_{UF}^{\alpha\beta} \right) \quad . \tag{4.1}$$

Here $M_{UF}^{\alpha\beta}$ is the portion of M_{UF}^{*} that relates the force on particle β to the velocity of particle α. The velocity $\langle U \rangle$ is an average over all the particles of a particular realization. Thus, to complete the Monte Carlo method described above, $\langle U \rangle$ must be calculated for several instantaneous configurations and averaged, yielding a final result that is an average both over all particles and over all realizations of the suspension microstructure.

The complications associated with inserting some degree of periodicity into a model of a disordered medium are relatively severe in the sedimentation problem. To understand why this is the case, one must look more closely at exactly what problem is being solved in the simulation. Although the goal is to model a random, sedimenting suspension, what one actually has, as a result of the imposed periodic boundary conditions, is N simple cubic lattices of spheres sedimenting among one another. Each sphere "sees" the $N-1$ other sphere positions evenly distributed throughout its periodic box as a result of the averaging that takes place in the Monte Carlo simulations. Thus, the sedimenting suspension has both periodic and random characteristics.

To assess the relative importance of these two components, the ϕ-dependence of the asymptotic, low volume fraction solutions for U_s can be examined for both periodic and random systems. For a random suspension Batchelor (1972) gives, to leading order in ϕ,

$$\frac{U_s^{ran}}{U_s^o} = 1 - 6.55\phi \ , \tag{4.2}$$

while for a suspension of particles in a simple cubic (SC) lattice, Saffman (1973) gives

$$\frac{U_s^{SC}}{U_s^o} = 1 - 1.74\phi^{1/3} \ . \tag{4.3}$$

The $\phi^{1/3}$ dependence of the sedimentation coefficient for periodic lattices suggests that periodic characteristics of our system are likely to be important, particularly at low volume fractions. The sedimentation velocities in (4.2) and (4.3) have been normalized by U_s^o, the sedimentation velocity of an isolated sphere in an unbounded fluid.

A simple approach to determining how the effects of periodicity scale with N is to superimpose a sedimenting, simple cubic lattice of volume fraction ϕ/N on a random, sedimenting suspension of volume fraction $\phi(1 - 1/N)$. That these two effects are superimposable can be shown by considering the calculations of the Ewald sums used in constructing $\underset{\approx}{M}^*_{UF}$ of the mobility matrix in (2.30). In that calculation, the self-terms containing the interactions between the spheres of the simple cubic lattice are contained in the 3×3 diagonal matrices $M_{UF}^{\alpha\alpha}$, and are calculated separately from the calculation of the interactions between those spheres whose positions are averaged throughout the unit cell. The latter interactions are contained in the off-diagonal 3x3 matrices $M_{UF}^{\alpha\beta}$, and are added to the self-terms in the averaging process described by (4.1). The sedimentation velocity at dilute ϕ should therefore be approximated by

$$\frac{U_s}{U_s^o} \approx 1 - 1.74\phi^{1/3}N^{-1/3} - 6.55\phi(1 - N^{-1}) \ . \tag{4.4}$$

The finite-size effects (and the effects of periodicity) should thus decay as $N^{-1/3}$, which is quite slow. From a different perspective, if the periodicity effects are to be small compared to the random results, then one has the requirement

$$N \gg \phi^{-2} \quad , \tag{4.5}$$

a condition which is extremely severe as $\phi \to 0$.

In Figure 4.1 the results of simulations with values of N equal to 14, 27, and 64 spheres are plotted along with the results of Zick and Homsy (1982) for an SC lattice (*cf.* Section 3.1) and Batchelor's low volume fraction result (4.2). The influence of periodicity is clearly evident and, as one might expect, tends to be more severe for the 14 sphere simulations than for the 27 and 64 sphere simulations. Unfortunately, however, there was no discernable trend with the 27 and 64 sphere samples, and thus an extrapolation to infinite N was not possible. Such an extrapolation might be feasible if more than 10 samples were used in the averages and more than 64 particles were included in the periodic unit cells, but the computational cost of such measures was not deemed warranted as this periodicity limitation was unique to the sedimentation calculations.

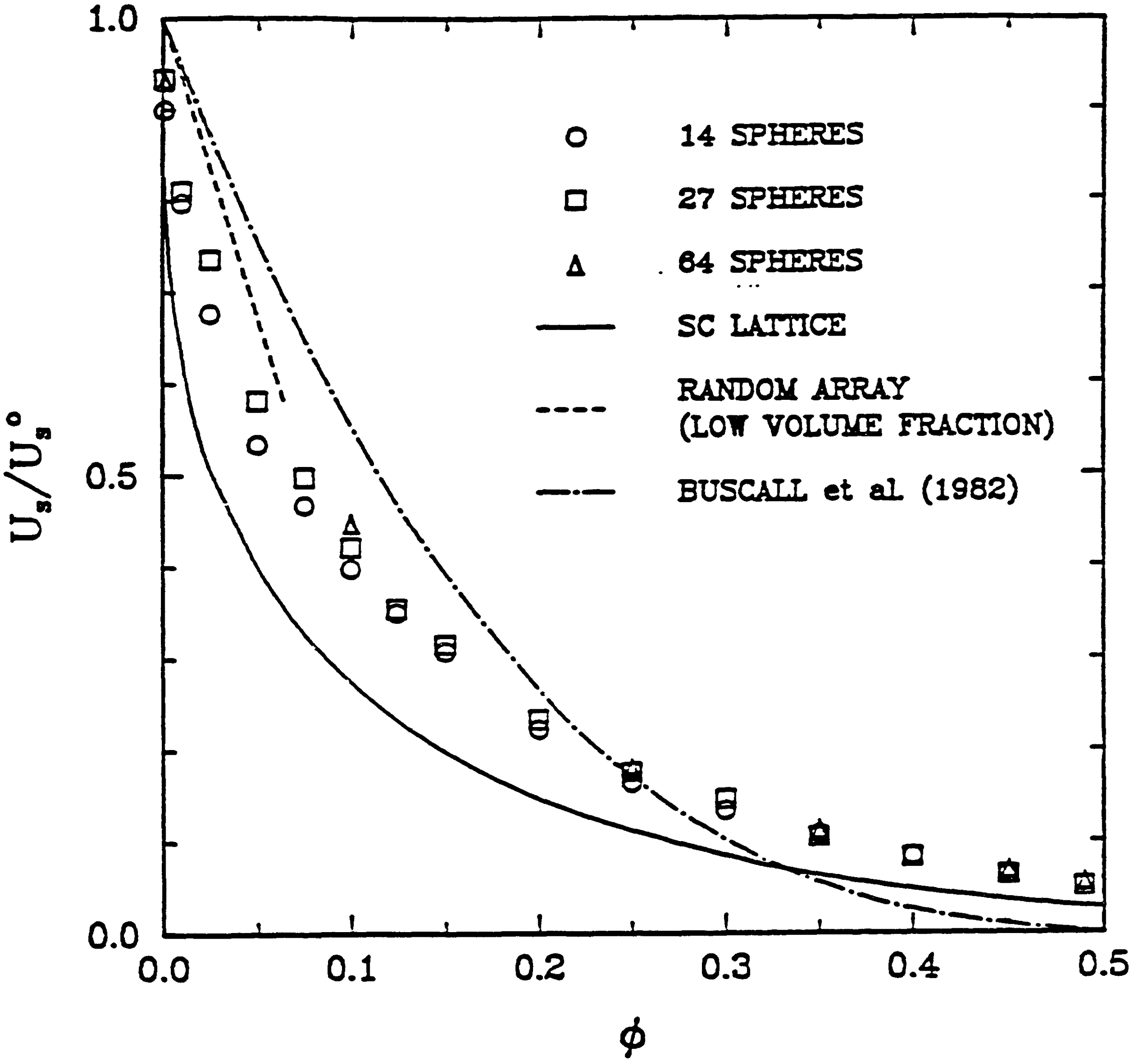

Figure 4.1 - The sedimentation velocity, nondimensionalized by the infinite dilution value U_s^o, is plotted as a function of volume fraction ϕ for several different cases. The open symbols correspond to the Monte Carlo simulation results for $N = 14$, 27, and 64 spheres per periodic unit cell. The solid curve is the result of Zick and Homsy for simple cubic lattices (*cf.* Chapter 3), the dashed-dot curve is a correlation of experimental data (Buscall *et al.*, 1982), and the dotted curve is the low ϕ result of Batchelor (1972).

Also included in Figure 4.1 is a correlation of experimental data reported by Buscall *et al.* (1982), who measured sedimentation velocities for suspensions of polystyrene latices. Note that the $O(\phi)$ coefficient obtained by taking the slope of the experimental data, roughly 5.4, differs from that predicted by Batchelor (*cf.* (4.2)). Slopes between 5.0 and 5.4 have also been measured by Maude and Whitmore (1958) and by Cheng and Schachman (1955), and thus it would appear that the correct result lies somewhere between those values. The roots of the discrepancy between Batchelor's calculation and experimental data are related to errors inherent in the use of pairwise additivity to calculate stresslet interactions. Removal of stresslet and higher order interactions from Batchelor's calculation results in a predicted slope of 5.0, as explained in detail by Brady and Durlofsky (1988).

In Figure 4.2, the results for the 27 sphere simulations using the F method, the F-T-S method, and the F-T-S method without lubrication (*i.e.* without $(R_{2B}-R_{2B}^{\infty})$ in (2.48)) are presented. The F-T method results were essentially identical to those for the F method and so are left out for simplicity. Perhaps the most interesting conclusion to be drawn from this plot is that the near-field interactions have virtually no effect on the sedimentation velocity. The explanation for this behavior is the same as that given in relation to the hydraulic permeability calculations of Chapter 3. Quite simply, the fluid displaced by the falling particles flows up through the interstices between particles. Little fluid flows between the narrow gaps separating the particle surfaces at high ϕ, and therefore the lubrication forces do not come into play. The only way to obtain better agree-

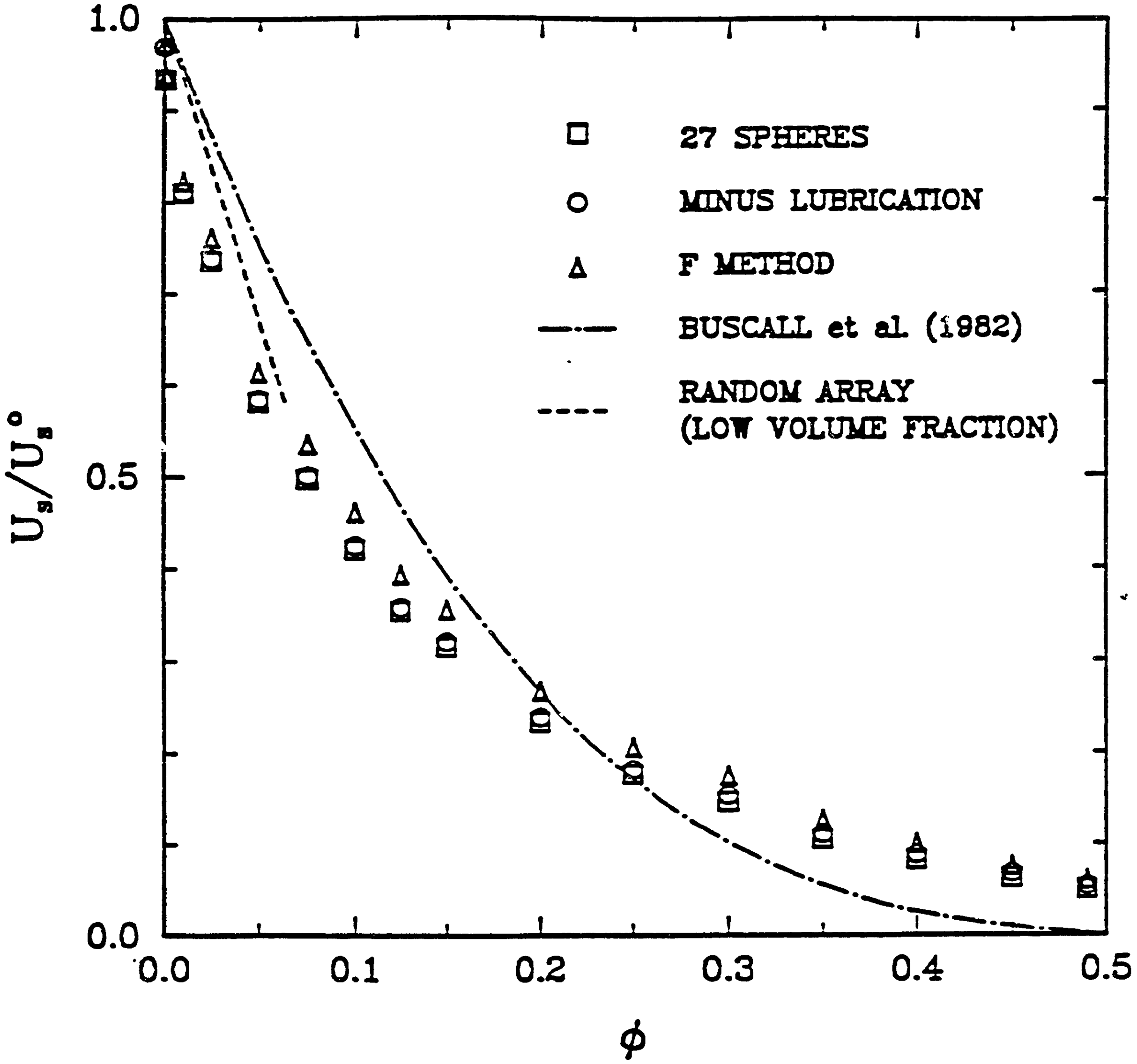

Figure 4.2 - Comparison of the effects of various levels of hydrodynamic approximation on calculation of the sedimentation velocity. The open squares correspond to 27 particles per periodic unit cell using the full F-T-S method with lubrication. The open triangles are results for the F method (*i.e.*, no stresslets, but including lubrication), and the open circles are the F-T-S method results without lubrication. The curves are the same as in Figure 4.1. These results show that stresslet interactions and lubrication play no significant role in sedimentation.

ment with experiment at high ϕ is to include higher multipole moments in the development of the mobility matrix.

Thus, the small number of particles used here causes the effects of periodicity to dominate the sedimentation velocity at small ϕ, and the relatively low number of multipoles included reduces the accuracy at high ϕ. Improvements could be made on both fronts by including more particles on the one hand, and by including more multipoles on the other. Either of these approaches, however, dramatically increases the number of unknowns, or degrees of freedom, and results in prohibitive computation times. Even if the F method is used without lubrication, thereby avoiding the costly $O(N^3)$ inversion required by (2.48), calculating the mobility interactions alone requires $O(N^2)$ operations. Such a computation is still excessive at low volume fractions in light of the criterion given in (4.5).

4.4 SHORT-TIME SELF-DIFFUSION

The procedure for calculating the short-time self-diffusion coefficients for a sphere in a suspension of force- and torque-free particles is very similar to that outlined in the previous section. In this case, however, instead of all the spheres having the same applied force or torque, only the sphere whose mobility is being calculated has a non-zero force. The coefficients relating the velocity and force of the test particle therefore lie along the diagonal of M^*_{UF}. Averaging these 3×3 diagonal elements corresponds to applying a force separately to each sphere in turn, calculating its velocity to obtain its self-mobility, and then averaging the self-mobilities. Note that this average is being performed over instantaneous configurations of the particles. In other words, the time scale of the sampling is so short that the particles do not move a distance comparable to their own size or to the interparticle spacing. Thus, the average described corresponds to the short-time diffusivity. The long-time self-diffusivity, where a particle moves far from its starting point and undergoes many encounters with other particles (*cf*. Rallison and Hinch, 1986), can be obtained through dynamic simulation (*cf*. Bossis and Brady, 1987).

In mathematical terms, the short-time self-diffusivities D^s_o are defined through the Stokes-Einstein relation

$$D^s_o = \frac{k_B T}{f} \quad , \tag{4.6}$$

where the average mobility ($1/f$) appropriate for this case is given by

$$\frac{1}{f} = \frac{1}{3} \, \mathrm{tr} \left(\frac{1}{N} \sum_{\alpha=1}^{N} (M^{\alpha\alpha}_{UF}) \right) \quad . \tag{4.7}$$

The 3×3 matrices $M^{\alpha\alpha}_{UF}$ are the diagonal elements of M^*_{UF} mentioned above. The term $k_B T$ in (4.6) is the product of Boltzmann's constant and absolute temperature. In the dilute limit where the volume fraction $\phi \rightarrow 0$, one has $D^s_o = kT/(6\pi\mu a)$.

The periodicity problems that plagued the sedimentation velocity results also play a role in the calculation of the short-time self-diffusion coefficient. In this case, however, the data follow a perceptible trend with increasing N, so that an extrapolation to obtain the limiting behavior as $N \to \infty$ is possible. To derive the dependence of D_o^s on N, recall that in calculating the self-diffusion coefficient, or self-mobility, one is essentially exerting a force on one sphere and calculating its resulting velocity. Because of the periodic boundary conditions, however, a force exerted on one sphere is also exerted on all the images of that sphere. We thus have, again, a simple cubic lattice of volume fraction ϕ/N "sedimenting" in superposition with the motion of one particle in N-1 neutrally buoyant particles. Hence, the analysis leading to (4.4) is applicable, with (4.2) replaced by Batchelor's calculation (Batchelor, 1976) of the self-diffusion coefficient in a random suspension of identical spherical particles,

$$\frac{D_o^s}{D_o} = 1 - 1.83\phi \ . \tag{4.8}$$

One therefore expects an $N^{-1/3}$ scaling in the data.

In Figure 4.3, self-diffusion data for values of N equal to 14, 27, 32, 49, and 64 are shown. Here a trend is clearly discernable and, assuming an $N^{-1/3}$ dependence, the data have been extrapolated to $N \to \infty$ to give the solid symbols. The linear correlation coefficients obtained by plotting the simulation results versus $N^{-1/3}$ were consistently between 0.98 and 1. The extrapolated results are compared with both experiment (Pusey and van Megen, 1983; Ottewill and Williams, 1987) and an alternative theory proposed by Beenakker and Mazur (1984) in Figure 4.4. Both sets of experimental data were obtained using photon correlation spectroscopy to measure rates of diffusion of colloidal latex particles made of polymethyl methacrylate. The

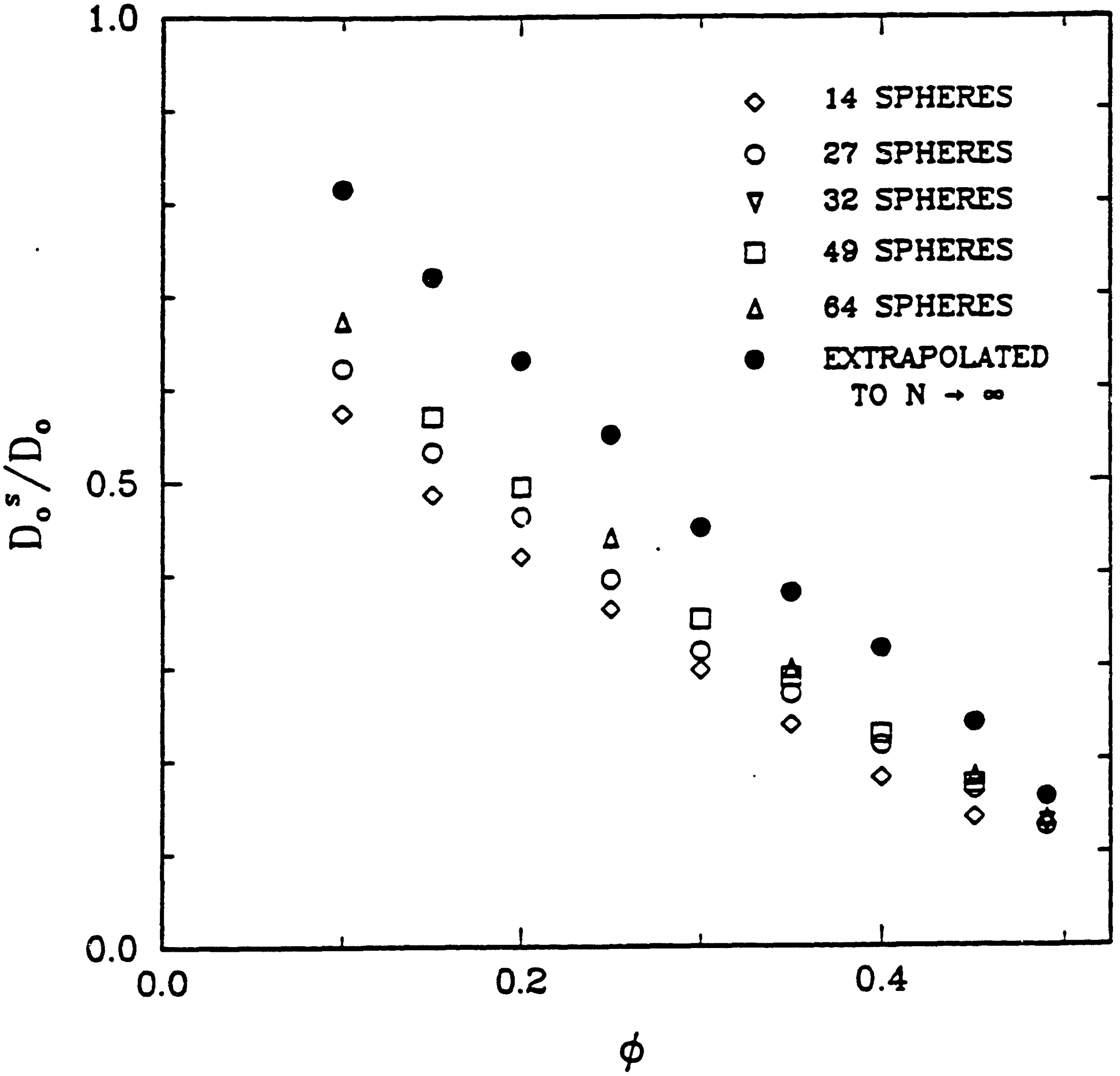

Figure 4.3 - The dimensionless short-time self-diffusion coefficient D_0^s/D_0 is plotted as a function of volume fraction ϕ for different numbers of spheres in the periodic unit cell (open symbols). The solid symbols are the values obtained by extrapolation to $N \to \infty$.

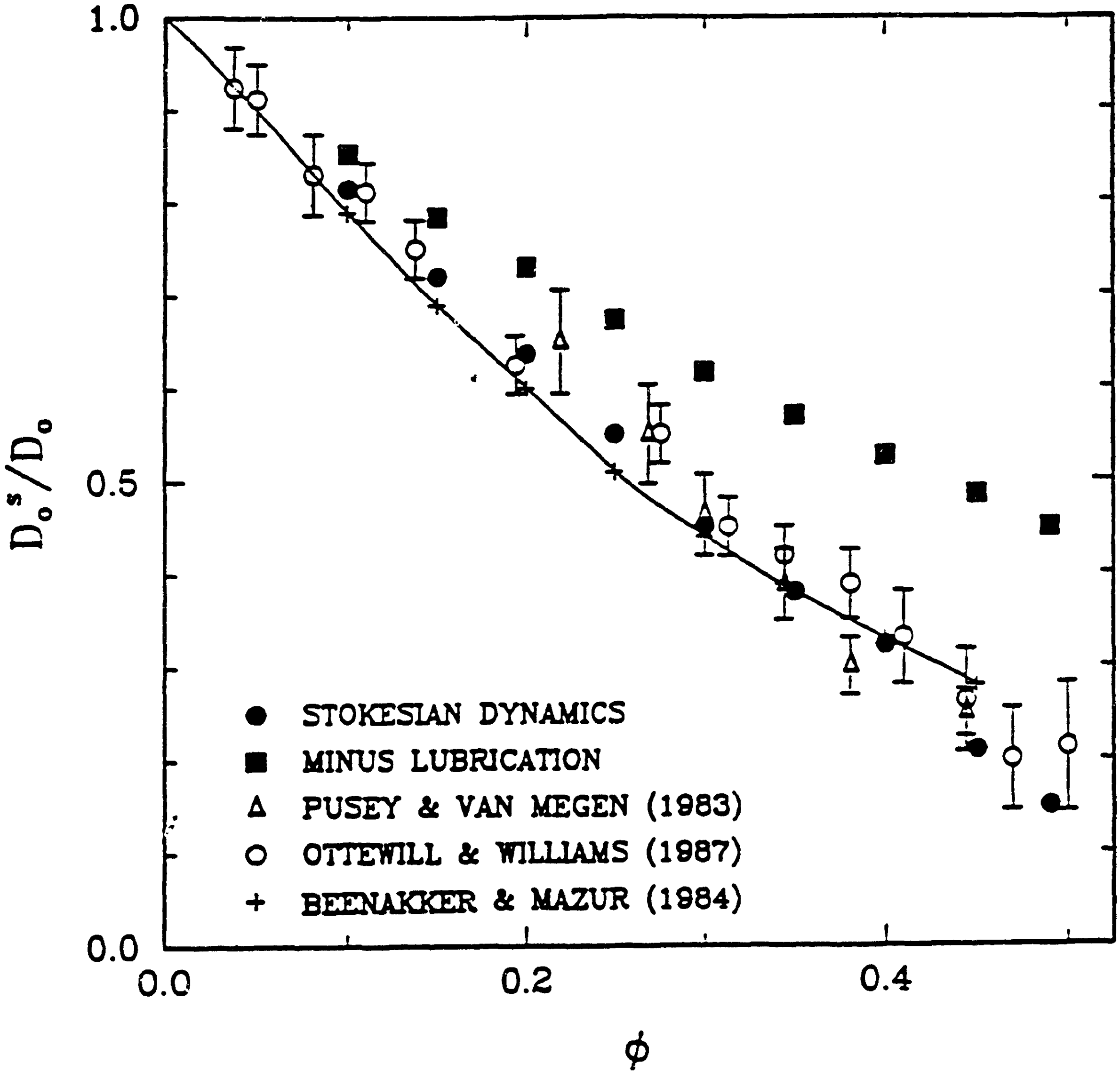

Figure 4.4 - Comparison of the short-time self-diffusion coefficients obtained by simulation (solid circles) with the experimental results of Pusey and van Megen (1983) and Ottewill and Williams (1987). Also included is a theoretical calculation of Beenakker and Mazur (1984). The solid squares are the simulation results without lubrication, showing the importance of the near-field interactions.

theory of Beenakker and Mazur includes only far-field interactions, and can be thought of as an effective medium approach in which lowest order result for D_0^s is obtained by replacing f in (4.6) by $6\pi\mu_s a$, where μ_s is the viscosity of the suspension. The agreement between theory and experiment over the entire range of volume fractions is clearly excellent.

The effects of neglecting the near-field, lubrication interactions in the extrapolated values of the short-time self-diffusion coefficient are also shown in Figure 4.4. In contrast to the sedimentation velocity, lubrication is clearly important in self-diffusion, since at high volume fractions the particle of interest must push against its tightly packed neighbors in order to move. The good agreement with experiment shown by the results of Figure 4.4 also shows that the pairwise additive method of including the near-field interactions used in Stokesian dynamics quantitatively captures the proper physics.

As a final point, one should note that the self-diffusion coefficients extrapolated for $N \to \infty$ at low ϕ agree with Batchelor's prediction for the $O(\phi)$ coefficient, given in (4.8). Specifically, at $\phi = 0.001$, the simulations yielded a value of $D_0^s = 0.998$, while at $\phi = 0.1$, a value of $D_0^s = 0.814$ was obtained. These are to be compared with the results 0.998 and 0.817 predicted by (4.8); the good agreement seems to confirm Batchelor's prediction.

Because of the pronounced effects of periodicity, which scale as $N^{-1/3}$ in this case, one may speculate as to whether it is possible to use the "minimum image convention" (Levesque *et al.*, 1986) without Ewald sums as a better model of a disordered system. This convention corresponds to accounting only for those interactions that occur between each particle and other particles that are in its periodic unit cell (*i.e.*, in a periodic unit cell with the particle of interest at its center), thereby neglecting the influence of particles outside the unit cell. Although it would result in a considerable savings in computation time, this approach has one serious difficulty: mobility matrices constructed using periodic boundary conditions without Ewald sums lose positive definiteness at volume fractions as low as 0.05. Non-positive definite matrices lead to completely aphysical behavior, such as negative diffusion coefficients! Only by properly accounting for the long-range hydrodynamic interactions are the correct physics obtained.

4.5 ROTATIONAL VELOCITY AND ROTATIONAL DIFFUSION

Quantities analogous to the sedimentation velocity and translational self-diffusion coefficient can also be defined for particle rotation. The rotational analog to $\langle \mathbf{U} \rangle$ is $\langle \boldsymbol{\Omega} \rangle$, which is the average rotational velocity of the particles of a suspension in which each particle is subjected to the same applied torque. For an isotropic medium, this rotational velocity is related to the applied torque by

$$\langle \boldsymbol{\Omega} \rangle = \Omega_s \mathbf{L} \ , \tag{4.9}$$

where Ω_s can be calculated by substituting $M^{\alpha\beta}_{\Omega L}$ for $M^{\alpha\beta}_{UF}$ in (4.1). Note that, in calculating U_s it is assumed that $\mathbf{L}^{\alpha}=0$ for all α, while in calculating Ω_s it is assumed that $\mathbf{F}^{\alpha}=0$ for all α. Similarly, a short-time rotational diffusion coefficient can be calculated using the rotational friction factor f_r

in (4.6), where f_r is obtained by substituting $R^{\alpha\alpha}_{L\Omega}$ for $R^{\alpha\alpha}_{FU}$ in (4.7).

There are at present no experimental results for these rotational properties, and the theoretical predictions are limited to periodic systems (Zuzovsky *et al.*, 1983). It should be noted, however, that any of the theoretical approaches used for the translational properties could be extended to the rotational case. It is also noteworthy that rotational diffusion coefficients have been measured for non-spherical particles in a variety of contexts (Berne and Pecora, 1976), and could be obtained for spherical particles if the particles themselves, although spherical, somehow had an anisotropic light scattering ability. The rotational velocities may be directly relevant to ferrofluids (Rosensweig, 1987) where small magnetic colloidal particles are caused to rotate by an applied magnetic field. (The inverse problem of determining the average torque produced by an average rotational velocity, which is discussed in the next chapter dealing with transport properties of porous media, yields the spin viscosity referred to in Chapter 3 and is relevant to the antisymmetric stresses generated in ferrofluids (Brady *et al.*, 1988; Zuzovsky *et al.*, 1983; Rosensweig, 1987)).

As in the translational problems, the periodic boundary conditions and Ewald sums imply that one rotating sphere in a rotational velocity calculation must necessarily be replicated by other rotating spheres arranged in an infinite SC lattice. In Figure 4.5 the results for rotational velocities calculated with N equal to 14, 27, and 64 spheres are shown. The fact that the three sets of results are essentially identical indicates that periodicity is not an important factor in this calculation.

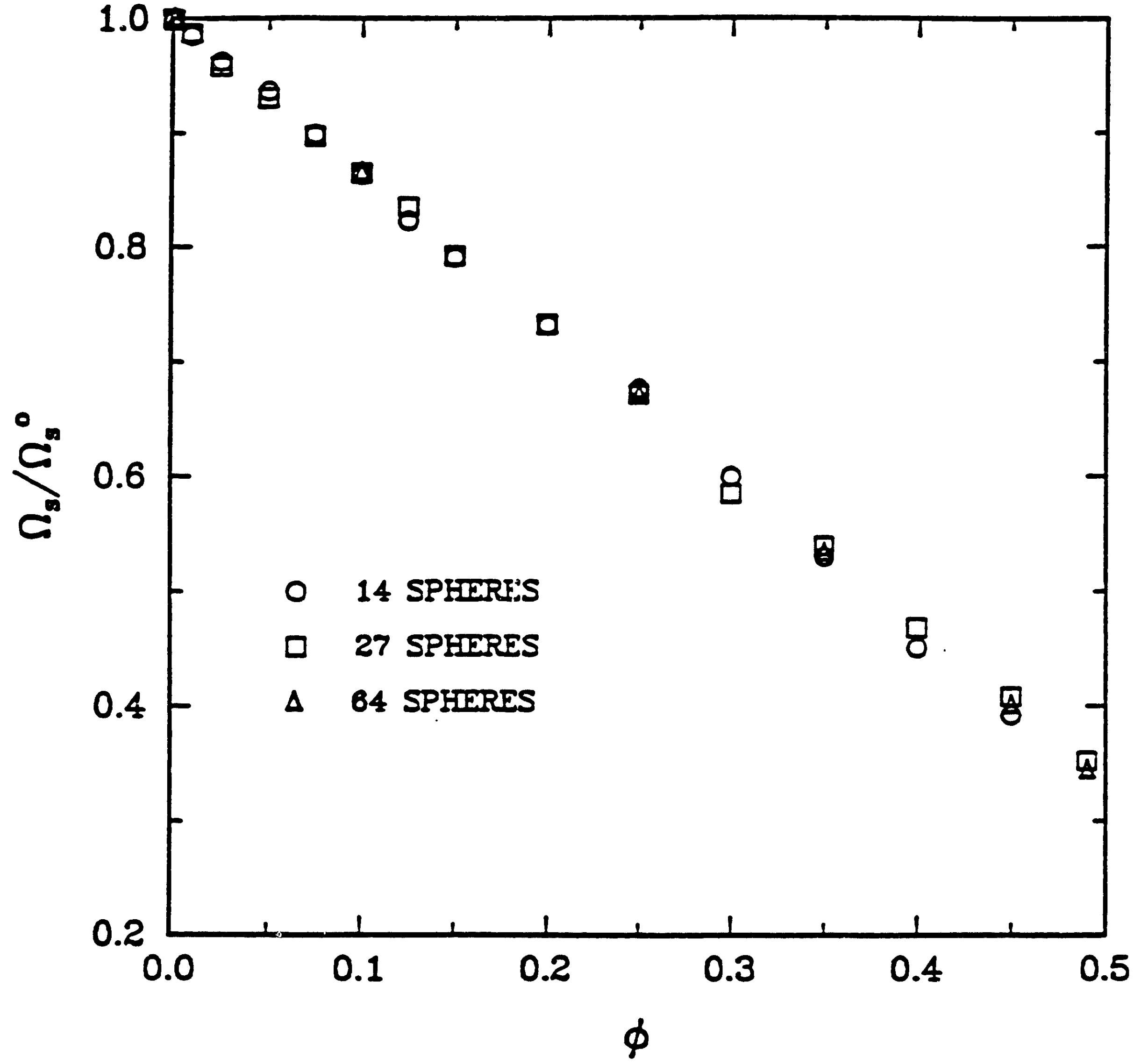

Figure 4.5 - The rotational velocity, normalized by its infinite dilution value Ω_s^o, is plotted as a function of volume fraction ϕ for different numbers of spheres in the periodic unit cell.

To explain this observation, one can follow the approach used to assess the periodicity effects in the sedimentation velocity, and look for a low volume fraction solution for Ω_s. The solution provided by Zuzovsky *et al.* (1983) for a dilute, SC lattice of rotating spheres is independent of structure:

$$\Omega_s = 1 - \phi . \qquad (4.10)$$

The fact that (4.10) is valid for both periodic and disordered systems suggests that the effect of a rotating sphere's periodic self-reflections, all of which are at least one periodic box length away from the central sphere, is no different than if they were located at random positions. Clearly this argument is supported by the data shown in Figure 4.5.

It is known from the work of Durlofsky and Brady (1987) that the resistance matrix formed from the inverse of the mobility has $O(N^{-1})$ errors owing to the effects of the periodic boundary conditions on the satisfaction of overall mass and/or momentum balances. Thus, these $O(N^{-1})$ errors may also be present in the rotational mobility problems, and a conservative estimate is that the periodicity effects scale as N^{-1}. However, the data in Figure 4.5 were not extrapolated with this scaling as the resulting values would not lie outside the error in the results shown.

In Figure 4.6, rotational velocities calculated using the F-T method and using the F-T-S method without including lubrication are shown. As one might expect, the stresslets, which result from a symmetric distribution of force density about the particle surfaces, have only a slight effect on the rotational velocities. In addition, note that the results with no lubri-

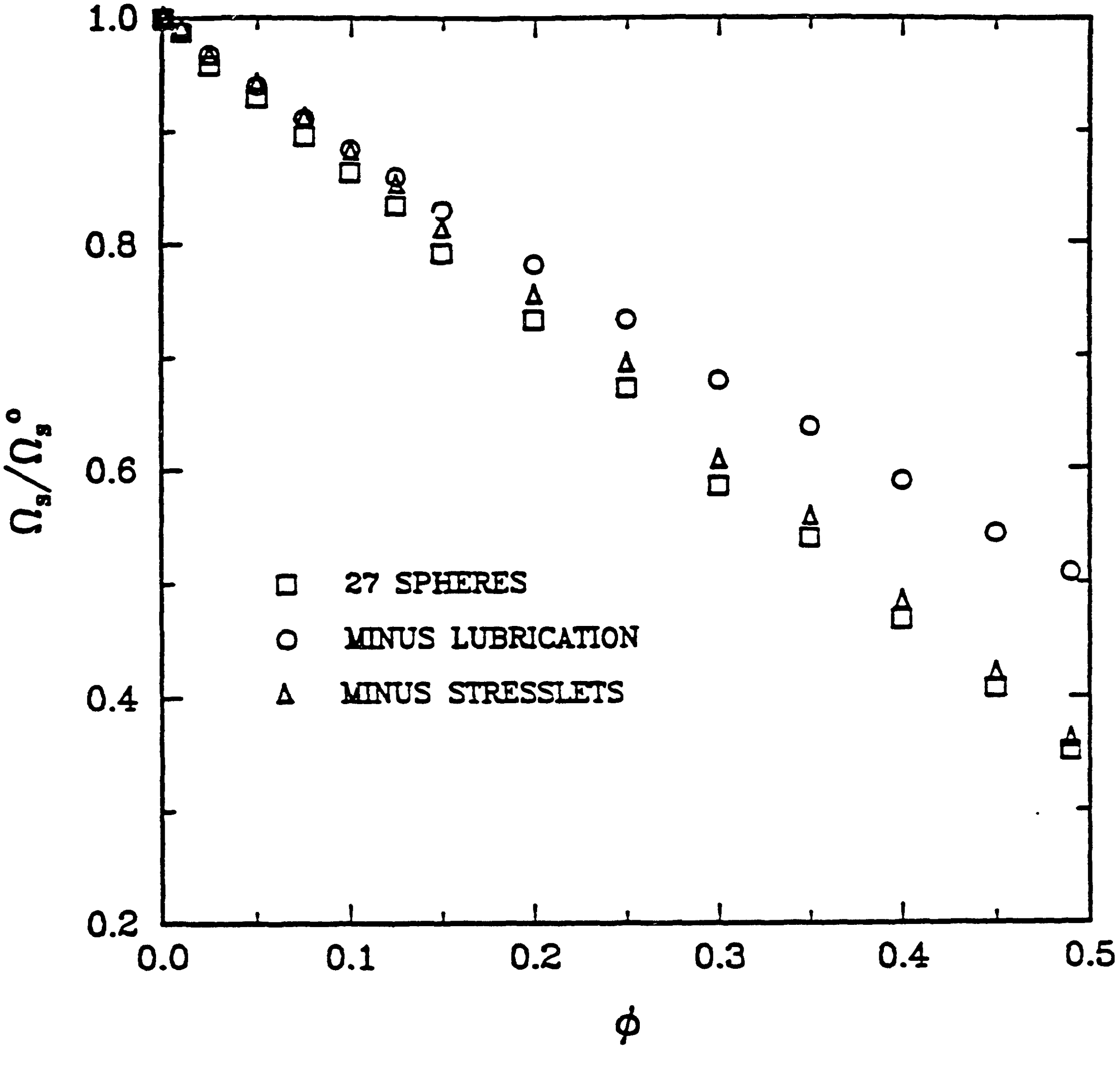

Figure 4.6 - Comparison of the effects of various levels of hydrodynamic approximation on the calculation of the rotational velocity. The open squares are the results for the full F-T-S method, including near-field interactions, for $N = 27$. The open triangles are the F-T method results (*i.e.*, no stresslets, but including near-field interactions), and show that the stresslets have no appreciable effect on the rotational velocity. The open circles are the F-T-S method without lubrication, and fall along the line given by (4.10).

cation fall precisely along the line given by (4.10), showing that the far-field interaction terms alone give rise to the dilute limit result. Finally, one also sees from Figure 4.6 that, in contrast to what was observed for the sedimentation velocity, lubrication does play an important role in the rotational velocity calculations. This is due to the fact that, for this case, there is relative motion between particle surfaces, and thus as spheres approach one another lubrication has a considerable effect.

In Figures 4.7 and 4.8 results are presented for D_r^s, the short-time rotational self-diffusion coefficient. The normalization parameter is the rotational diffusion coefficient for an isolated sphere, $D_0^r = kT/(8\pi\mu a^3)$. In Figure 4.7 one finds that, as was the case with the rotational velocity calculation, periodicity effects are negligible. An analysis similar to those discussed above will explain why this is the case. From (4.10) it is known that the rotating sphere's periodic reflections hinder its motion by ϕ/N, while it will be assumed that the effect of the neutrally buoyant spheres can be accounted for by an effective viscosity that grows like $(5/2)(1-1/N)\phi$ (Einstein's low ϕ viscosity result). Thus, the criterion for neglecting periodicity effects is

$$\frac{(\phi/N)}{(5/2)\phi(1 - 1/N)} \approx 0.4/N \ll 1 , \qquad (4.11)$$

an inequality that is satisfied in all of the simulations discussed here. Again, the finite size effects scale as N^{-1}.

Unlike the rotational velocity calculations, however, from Figure 4.8 one can see that the stresslets are important in this calculation. The

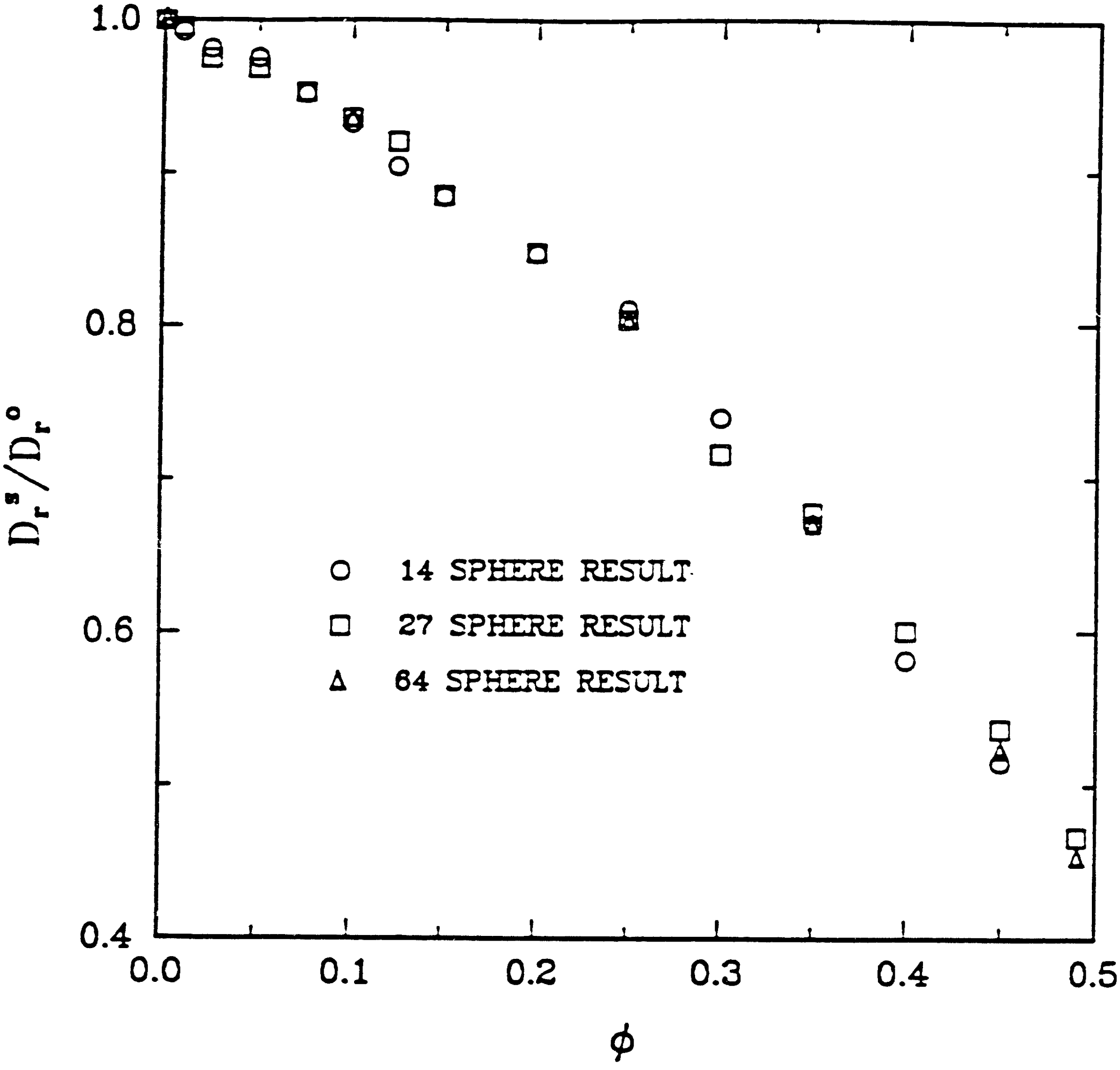

Figure 4.7 - The dimensionless short-time rotational diffusion coefficient D_r^s/D_r^o is plotted as a function of volume fraction ϕ for different numbers of spheres in the periodic unit cell. As in the rotational velocity case (*cf.* Figure 4.5), the effects of periodic boundary conditions are weak and almost imperceptible here.

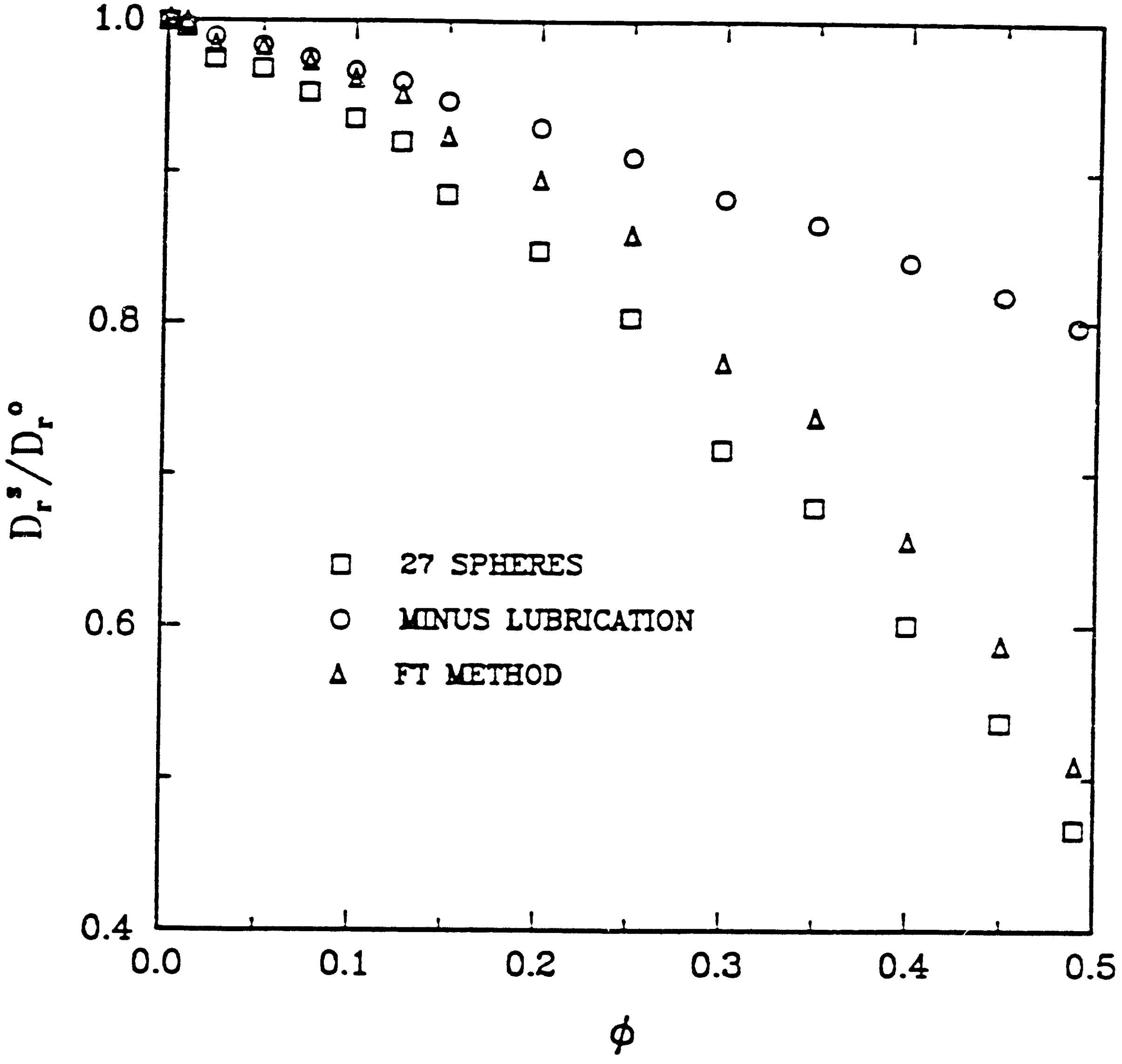

Figure 4.8 - Comparison of the effects of various levels of hydrodynamic approximation on calculation of the rotational diffusion coefficient. The open squares are the full F-T-S method results for $N = 27$, the open triangles are the F-T method results (*i.e.*, no stresslets, but including near-field interactions), and the open circles are the F-T-S method results without lubrication.

reason for this should be clear: in a suspension of spheres that have no applied forces or torques, the only far-field quantities left to interact with a single rotating sphere are the stresslets, in the absence of which it can only interact with its own periodic images. Indeed, although these data were left out for simplicity, if the F-T results that do not include lubrication effects were plotted, they would be identically reproduced by $(1-\phi/N)$, which is just the result given by (4.10) for an SC lattice of spheres in an otherwise pure fluid. This behavior underscores the importance of stresslets in determining the average properties of suspensions.

4.6 EFFECTIVE VISCOSITY

The final property that will be evaluated for suspensions is the shear, or effective, viscosity. This quantity is calculated exactly as described in (3.8), (3.9), and (3.10) of the previous chapter. However, for a disordered, isotropic suspension, one has in place of (3.10)

$$\langle A_{ijkl} \rangle = \frac{\beta}{2} \left(\delta_{ik}\delta_{jl} + \delta_{il}\delta_{jk} - \frac{2}{3} \delta_{ij}\delta_{kl} \right) , \qquad (4.12)$$

where β is a function of the volume fraction ϕ only. Substituting (4.12) and (3.7) into (2.12), one can calculate a relative viscosity μ_r, defined as the suspension viscosity divided by the fluid viscosity, as

$$\mu_r = 1 + \frac{n\beta}{2\mu} . \qquad (4.13)$$

As $\phi \to 0$. $\mathcal{S} - (20/3)\pi\mu a^3$ and the correction term in (4.13) becomes $\frac{5}{2}\phi$, yielding Einstein's result for the viscosity of a dilute suspension. The $O(\phi^2)$ correction has since been calculated by Batchelor and Green (1972) (see also Yoon and Kim, 1987), yielding

$$\mu_r = 1 + (5/2)\phi + 5.07\phi^2 \tag{4.14}$$

Note that the $O(\phi)$ correction term is independent of structure, and thus the finite size effects here are expected to be at most $O(N^{-1})$ as they were for the rotational velocity. The same scaling in the two cases might also be expected since both the torque and stresslet are first moments of the force distribution on the surface of a particle.

The weak dependence of μ_r on N is borne out in Figure 4.9, where the relative viscosity determined by the F-T-S method is plotted as a function of ϕ for N equal to 14, 27, and 64. Also shown in the figure are the low ϕ asymptotic result (4.14) and two correlations given by Krieger (1972). The upper curve of Krieger corresponds to the limit of low shear rate (low Peclet number), while the lower curve corresponds to the limit of high shear rate (high Peclet number). One should view these curves as simply providing an idea of where a representative sample of experimental data lies in relation to our simulation results.

In general, agreement between experiment, the simulation results and the low ϕ asymptotic result is quite good up to $\phi = 0.15$, which may be taken as a confirmation of Batchelor and Green's calculation. At higher ϕ, both

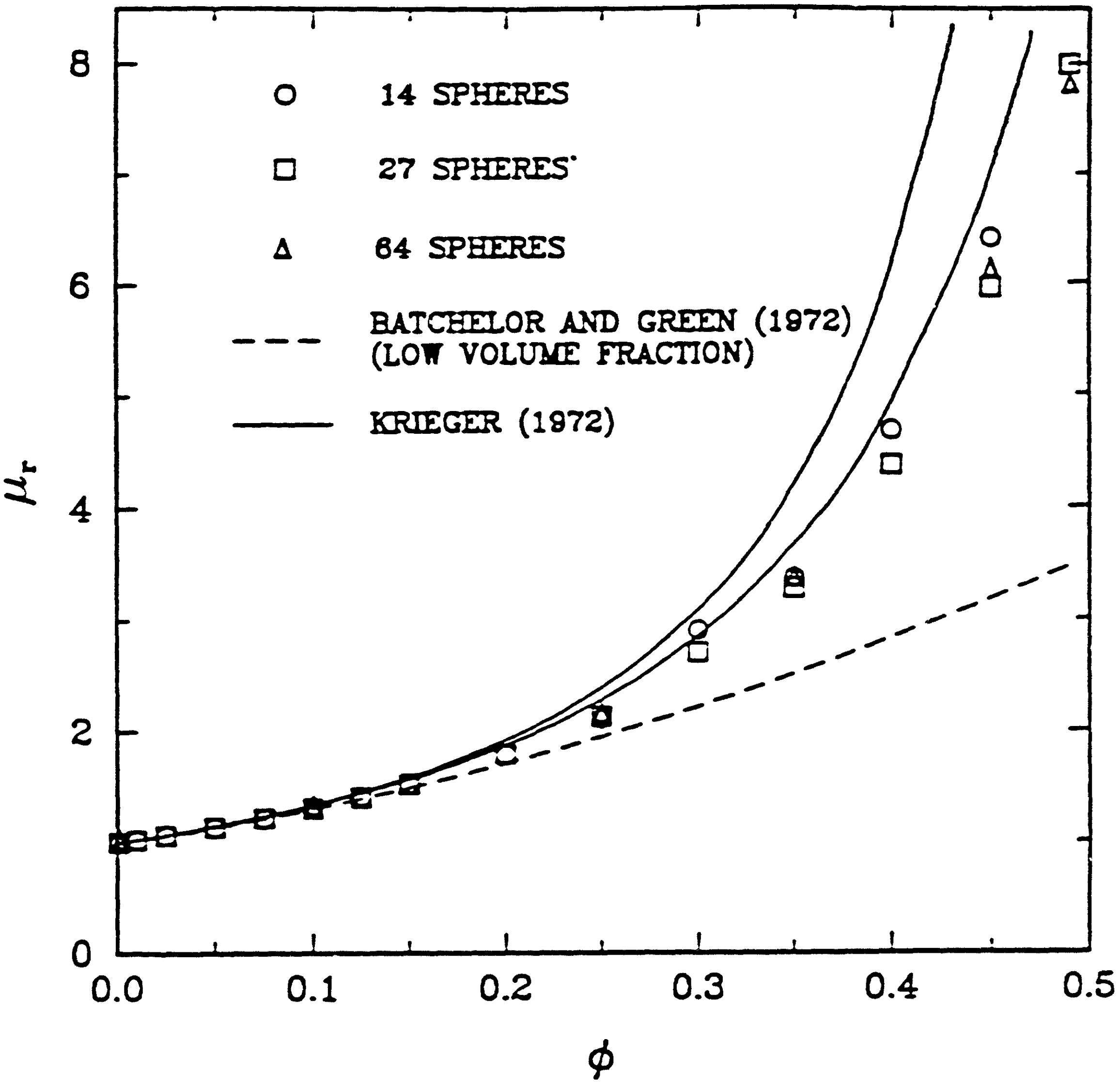

Figure 4.9 - The relative viscosity μ_r is plotted as a function of volume fraction ϕ for several cases. The open symbols are the Monte Carlo simulation results for 14, 27, and 64 spheres per periodic unit cell, showing the insensitivity of this calculation to changes in N. The dashed curve is the low ϕ result of Batchelor and Green (1972), and the solid curves are correlations of experimental data reported by Krieger (1972). The upper, solid curve corresponds to the low Peclet number limit, while the lower curve corresponds to the high Peclet number limit.

the simulation and the experimental results lie significantly above the low ϕ asymptote and increase rapidly with increasing ϕ.

Although the simulation results compare favorably with Krieger's high Peclet number asymptote, caution must be exercised in making a direct comparison between theory and experiment in this case. At low shear rates, Brownian motion has a strong randomizing effect, and the microstructure obtained through the Monte Carlo method (*i.e.*, the hard-sphere micro structure) is close to that of the slightly deformed, low-Peclet-number limit suspension corresponding to the upper curve of Krieger. (The Peclet number referred to here is $(e_{xy}a^2/D_o)$, where it has been assumed that the imposed velocity gradient is in the *y*-direction.) Hence, one may think that the simulation results should be compared with these data. However, as discussed by Batchelor (1977), there is an additional direct Brownian contribution to the bulk stress that can only be obtained by calculation of the deformed microstructure. Recent simulations (Bossis *et al.*, 1988) indicate that this contribution to μ_r is about equal in magnitude to the part calculated here. Thus, the simulation results are expected to fall well below the upper curve of Krieger, an expectation confirmed by Figure 4.9.

The Brownian contribution to the stress decreases with increasing shear rate (shear thinning), explaining the lowering of the curve for high shear rates. At high shear rates, however, the suspension microstructure is far from being a hard-sphere distribution. Dynamic simulations of monolayers of hard spheres performed under such conditions (Brady and Bossis, 1985; Bossis and Brady, 1987) indicate that the viscosity corresponding to the equilibrium, hard-sphere distribution (*i.e.*, the distribution used in the Monte

Carlo simulations) is lower than that corresponding to the actual microstructure that develops at high shear rates. This trend is evident in Figure 4.9, where the Monte Carlo results fall slightly below the high Peclet curve reported by Krieger. Hence, the reasonable agreement in magnitude and general trends suggests that the Stokesian dynamics method is capturing the proper physics.

There is an experimental situation which does correspond to the viscosity calculated in the Monte Carlo simulations. In high frequency, low amplitude shearing of Brownian suspensions, the microstructure is only slightly deformed from the equilibrium hard-sphere structure used here, and the direct Brownian contribution is out of phase with the applied oscillating shear field. (This situation also results in a shear modulus of elasticity, as discussed by Russel and Gast, 1986.) Thus, in the limit of small deformation, this "dynamic viscosity" corresponds to the Monte Carlo, hard-sphere viscosities In Figure 4.10, the simulation results are compared with the results of the high frequency experiments of van der Werff *et al.* (1988), in which the dynamic viscosity was measured for suspensions of silica particles. The agreement is quite satisfactory considering the sensitivity of the data to slight changes in ϕ. This therefore serves as an additional confirmation of the quantitative accuracy of the Stokesian dynamics method.

Because van der Werff *et al.* provide experimental data for systems with $\phi > 0.49$, included in Figure 4.10 are simulation results for $\phi = 0.55$ and $\phi = 0.60$. These results were obtained using a value of $N = 32$ because 27 spheres cannot be packed into a cubic unit cell at such high volume fractions. The error bars shown are the standard error, *i.e.*, the standard

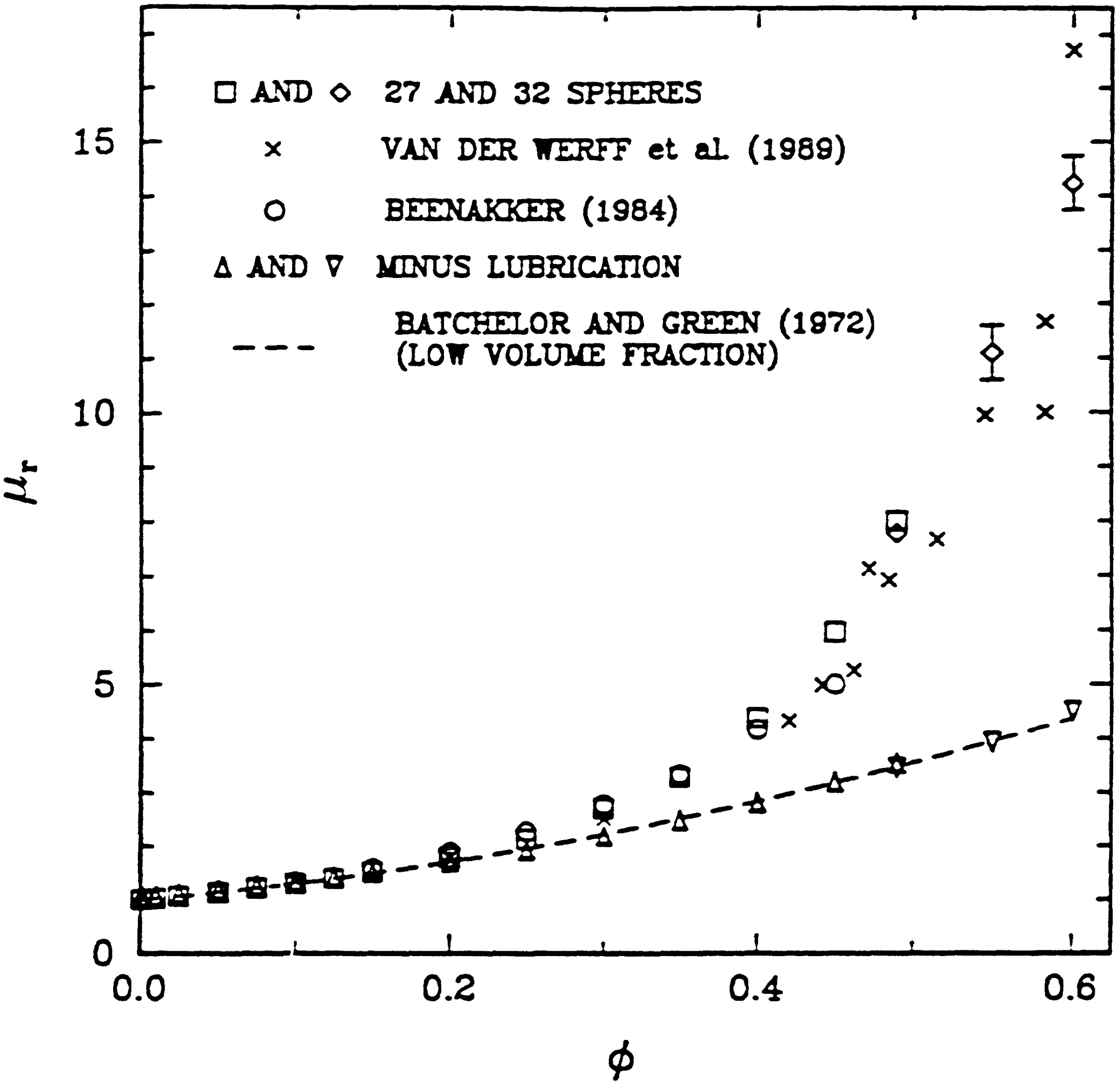

Figure 4.10 - Comparison of the simulation viscosities for 27 and 32 spheres per periodic unit cell with the high frequency, dynamic viscosities measured by van der Werff *et al.* (1989). The open circles are the theoretical predictions of Beenakker (1984). The open triangles are results for the F-T-S method without lubrication, and are described well by Batchelor and Green's low ϕ result over the entire range of ϕ studied.

deviation of the set of 50 results (5 values from each of the 10 samples used) divided by the square root of 50. The relatively large standard deviations associated with these points can be attributed to the presence of clusters of particles which vary in size from one sample to another, and hence cause large fluctuations in μ_r. A macroscopic system at these high values of ϕ would undoubtedly have clusters in some regions and freely mobile particles in others, a situation that is difficult to model with the number of particles considered here. More accurate results could undoubtedly be obtained by performing simulations with enough particles to model the complete structure. At present, however, computer time limitations make such an endeavor infeasible. Finally, it is noteworthy that the experimental results of van der Werff *et al*. show the proper hydrodynamic scaling with particle size and shear rate for all volume fractions studied, up to ϕ in excess of 0.7, even for particles as small as 28 nm. This indicates that the continuum mechanical description for smooth, hard spheres applies down to remarkably small particle surface-surface separations.

Also shown in Figure 4.10 are the effects of neglecting lubrication on the simulation calculations and the theoretical results of Beenakker (1984). Remarkably, the low ϕ result (4.14) agrees with the far-field, Stokesian dynamics results to volume fractions as high as $\phi = 0.60$. All the deviation from (4.14) and the rapid rise with increasing ϕ can therefore be attributed to the pairwise additive lubrication interactions. Thus, as with the self-diffusion coefficient calculations, the pairwise-additive method of accounting for near-field interactions is in quantitative agreement with experiment.

Beenakker has developed the most rigorous alternative theory available for the viscosity of a suspension with the hard-sphere microstructure (*i.e.*, the high frequency viscosity), and his results agree well with the simulation results and with the experimental data up to a volume fraction of $\phi \approx 0.4$. At higher volume fractions, Beenakker's theory underpredicts the relative viscosity, as it apparently does not incorporate enough of the near-field structure and interactions to obtain a high viscosity.

4.7 CONCLUSION

The primary purpose of this chapter was to present Stokesian dynamics predictions for the hydrodynamic transport properties of disordered hard-sphere suspensions. The hard-sphere distribution represents a convenient reference microstructure, and in many ways one could view these results as "experimental" data. It is hoped that they can play a role in developing theories and understanding of suspension properties much the same way conventional molecular dynamics has aided the development of liquid state theory. Indeed, one can use these results to begin to derive a "perturbation theory" of suspensions, similar to liquid state perturbation theory. This approach has actually been implemented for the low Peclet number limit (Russel and Gast, 1986), and recently dynamic simulations have been used to help test these perturbation theories (Bossis and Brady, 1988).

The comparisons made with experiment have been as complete as possible. It has been seen that the calculated sedimentation velocities do not agree particularly well with experiment, owing to the severe effects of periodicity at low volume fractions and the need for higher order, many-particle multipole moments at higher volume fractions (*cf.* Figure 4.1). These problems could be eliminated at increased computational cost.

Comparisons of experimental results with the effective viscosity and self-diffusion coefficients calculated using Stokesian dynamics have been much more favorable. The effective viscosity results lie near the experimental data corresponding to steady shear at high Peclet numbers. What discrepancies do exist could result from deviations from the hard-sphere microstructure that are expected in suspensions at high shear rates. Experimentally measured high frequency, dynamic viscosities and self-diffusion coefficients are in very good agreement with the simulation results (*cf.* Figures 4.4 and 4.10). Significantly, for these latter two cases the hard-sphere distribution is the microstructure actually present in the experimental systems, and thus these comparisons provide a rigorous test of the Stokesian dynamics method of calculating hydrodynamic interactions. Comparison between experimental data and the rotational properties (velocity and self-diffusion) must await experimental measurement.

An exhaustive comparison with all the available theories was not attempted. However, the results obtained here were compared with the dilute suspension theories of Batchelor (1972; 1976) and Batchelor and Green (1972), and it was found that the two sets of predictions were generally in excellent agreement, the notable exception being the low ϕ, limiting behavior of the sedimentation velocity. The other theories that are discussed are those of Beenakker (1984) and Beenakker and Mazur (1984), whose treatment of the self-diffusion coefficient and dynamic viscosity are the most complete and rigorous available. Their predictions are in excellent agreement with the simulations up to volume fractions of about 0.4. At higher ϕ, evidently more interactions need to be included in their analyses. Nevertheless, these theories represent a remarkable accomplishment.

In addition to the simulation results themselves, the rates of decay of the periodicity effects resulting from the use of periodic boundary conditions have been determined as a function of N, the number of particles per periodic unit cell. These effects are most severe for the sedimentation velocity and self-diffusion coefficient, where the decay with number of particles is an extremely slow $N^{-1/3}$. This behavior makes it possible, although somewhat difficult, to extract the $N \to \infty$ limiting results. On the other hand, for the rotational properties and the effective viscosity, the finite-size effects scale at most as N^{-1}. It is thus only the translational properties of free suspensions that are severely affected by the periodicity. There are, of course, other constraining effects of periodic boundary conditions, such as the necessity of fitting all important microstructure length scales within the periodic unit cell, but these constraints are not related to the long-range nature of the hydrodynamic interactions discussed here.

CHAPTER 5

TRANSPORT PROPERTIES OF DISORDERED POROUS MEDIA

In the previous chapter, it was shown how the Stokesian dynamics method for evaluating hydrodynamic interactions could be used to calculate bulk properties of disordered suspensions, such as sedimentation velocities, self-diffusion coefficients and effective viscosities. This approach can also be used to calculate transport properties of porous media, and thus in this chapter an analogous set of results will be presented for disordered porous media made up of hard spheres. The transport properties that are discussed consist of permeabilities, short-time hindered translational diffusion coefficients, rotational drag coefficients or spin viscosities, and short-time hindered rotational diffusion coefficients. As in Chapter 4, volume fractions (ϕ) ranging from infinite dilution to the fluid-solid transition at $\phi = 0.49$ are examined, and the effects of calculating the hydrodynamic interactions at three levels of approximation are compared. Finally, whenever possible the results are compared with experiment and with other theoretical results obtained from the literature, which thereby provide some criteria for assessing the accuracy of the method.

Several researchers have commented on the qualitative differences between the nature of hydrodynamic interactions in free suspensions and in porous media (Brinkman, 1947; Saffman, 1973; Hinch, 1977). Essentially these differences result from the fact that, in porous media, it is necessary to apply external forces (and torques) to particles in order to hold them immobile, whereas in suspensions of neutrally buoyant particles no such forces need be applied. The effect of these applied forces is to screen the hydrodynamic interactions between particles, causing them to decay as k/r^3 over long distances, where k is the permeability, rather than decaying as $1/r$, as is the case for Stokes flow in a suspension of freely mobile particles.

As stated in Chapter 1, it is common to incorporate this screening behavior directly into the method of calculation by considering interactions within an effective medium of particles and fluid. Brinkman (1947) pioneered this approach in his calculation of the hydraulic permeability of a disordered porous medium of hard spheres. The Stokesian dynamics method used here does *not* rely upon a similar effective medium assumption. It does, however, provide a method that allows one to calculate many-body interactions accurately in the far-field limit, and thus the screening behavior just discussed arises naturally for systems in which the sphere velocities are constrained to be zero. Indeed, Durlofsky and Brady (1987) have carefully studied such interactions in porous media and have shown that, using the Stokesian dynamics method, one can observe Brinkman screening. Thus, there is ample evidence to show that this method correctly captures the rather complicated nature of long-range hydrodynamic interactions in porous media.

As in Chapter 4, the results to be presented here were obtained using a Monte Carlo approach. The procedure consists of generating a series of samples, each modeling a portion of the microstructure of a porous medium, calculating the transport property of interest for each sample, and then averaging to obtain values describing the behavior of a macroscopic system. In the following section the averages used to calculate the relevant transport properties are derived. These are similar in nature to those used in Chapter 4. This discussion of methods is followed by a presentation of the simulation results, and then a conclusion in which some apparent differences between the results obtained here and in Chapter 4 will be discussed.

5.1 CALCULATIONAL PROCEDURES

The samples used for the calculations of Chapter 4 were also used for the calculations presented here. Indeed, once the resistance matrix (or its inverse, the mobility matrix) is formed, all of the information needed to calculate the suspension properties discussed in the previous chapter and the properties of porous media discussed here is available. It is merely necessary to perform the appropriate averaging procedures to obtain the transport property of interest.

Calculation of the drag coefficient K (and hence, from (3.3), the hydraulic permeability k) and the rotational drag coefficient K_r (or the spin viscosity) is discussed in Chapter 3 in the context of periodic systems (*cf.* equations (3.2), (3.4) and (3.11)). The procedures described there are general and can also be applied to disordered systems. However, the calculation of the mobilities, or hindered diffusion coefficients, of individual particles requires a somewhat different approach.

In order to calculate the hindered translational diffusion coefficient of a particle moving through a fixed array of like particles, one can set N-1 particle velocities equal to zero, and evaluate the relationship between the force and velocity of the one freely mobile particle. This relationship is governed by a 3×3 matrix that lies along the diagonal of R^*_{FU}, and thus the mobility of particle α is given by $(R_{FU}^{\alpha\alpha})^{-1}$. This mobility averaged over all the particles in the system, along with the Stokes-Einstein relations, defines the short-time hindered diffusion coefficient according to

$$D^{HD} = \frac{kT}{3} \operatorname{tr} \left(\frac{1}{N} \sum_{\alpha=1}^{N} (R_{FU}^{\alpha\alpha})^{-1} \right) , \tag{5.1}$$

where kT is the product of Boltzmann's constant and absolute temperature, and the term tr has the same meaning as in (3.4). The fact that D^{HD} is expressed as a scalar again reflects the isotropic nature of the porous medium.

Note the distinction between this diffusion coefficient and the short-time self-diffusion coefficient reported in Chapter 4: D^{HD} describes diffusion of a particle surrounded by other particles that are fixed in space (*i.e.*, a porous medium), whereas in Chapter 4 (*cf.* equation (4.3)) the surrounding particles were mobile and were required to be free of any applied forces or torques (*i.e.*, a free suspension). Just as in Chapter 4, however, the Monte Carlo method of simulation restricts the analysis to the calculation of short-time coefficients, which describe motion on a time scale so short that the mobile particle does not move a distance comparable either to its own radius or to the distance between particle surfaces. The importance of this restriction is readily apparent for the case of a mobile particle wandering randomly within a small "cage" in which the distance between the immobile particles is too small for the mobile particle to escape. Clearly the instantaneous mobility or hindered diffusion coefficient of the mobile particle will be finite, while its long-time hindered diffusivity will be zero. Finally, results are also presented here for the rotational hindered diffusion coefficient D_r^{HD}, analogous to D^{HD}, which is obtained by simply substituting $(R_{L\Omega}^{\alpha\alpha})^{-1}$ for $(R_{FU}^{\alpha\alpha})^{-1}$ in (5.1).

The calculations required to obtain the results presented in the next section were all performed on a CYBER 205 supercomputer, with the specifics of the time requirements being identical to those given in Chapter 4. Again, note that statistical errors are reduced by the fact that each sample produces three values for each of the transport properties described, a consequence of the independence of those quantities when calculated in each of the three coordinate directions. Thus, although only 10 samples are represented in each data point, that point is actually an average over 30 values.

5.2 RESULTS AND DISCUSSION

The results for the calculations described above can be examined in several ways. First, the effects of changing the size of the periodic unit cells that make up the infinite systems are studied by varying the number of particles per periodic unit cell N, and the accuracy of the F, F-T, and F-T-S methods will be compared as in Chapter 4. This latter information should be of interest to those who wish to perform similar calculations, but do not necessarily require the most accurate, and hence most computationally demanding, formulation available. Such comparisons also shed some light on the nature of the hydrodynamic interactions being studied. In addition, whenever possible comparisons will be made between the simulation results and those that have been reported previously in the literature. In making these comparisons one should bear in mind the flexibility of the Stokesian dynamics method, with which one can calculate all the transport properties of porous media that are reported here, the transport properties of suspensions reported in Chapter 4, and also perform dynamic simulations if so desired.

5.2.1 Hydraulic Permeability

As in Chapter 3, the permeability results will be presented in the form of the average drag coefficient K (*cf.* equation (3.3)). In Figure 5.1 values of K calculated for N equal to 14, 27, and 64 particles per periodic box are compared with the results of Kim and Russel (1985), the Carman correlation (Happel and Brenner, 1965), and the results of Zick and Homsy (1982) for a periodic simple cubic lattice of spheres. Note that, in general, the results for random systems lie below those for SC lattices, a fact which is no doubt related to the larger void spaces through which fluid can flow in disordered media. Also, the Stokesian dynamics results agree well with those of Kim and Russel and the Carman correlation up to volume fractions of about 0.35, while at higher volume fractions the simulation results tend to underestimate the correct value of K. This trend is consistent with the results obtained for periodic systems in Chapter 3 and for sedimenting suspensions in Chapter 4, and can again be explained by the fact that lubrication forces are not a dominant (or even significant) part of these calculations at any volume fraction.

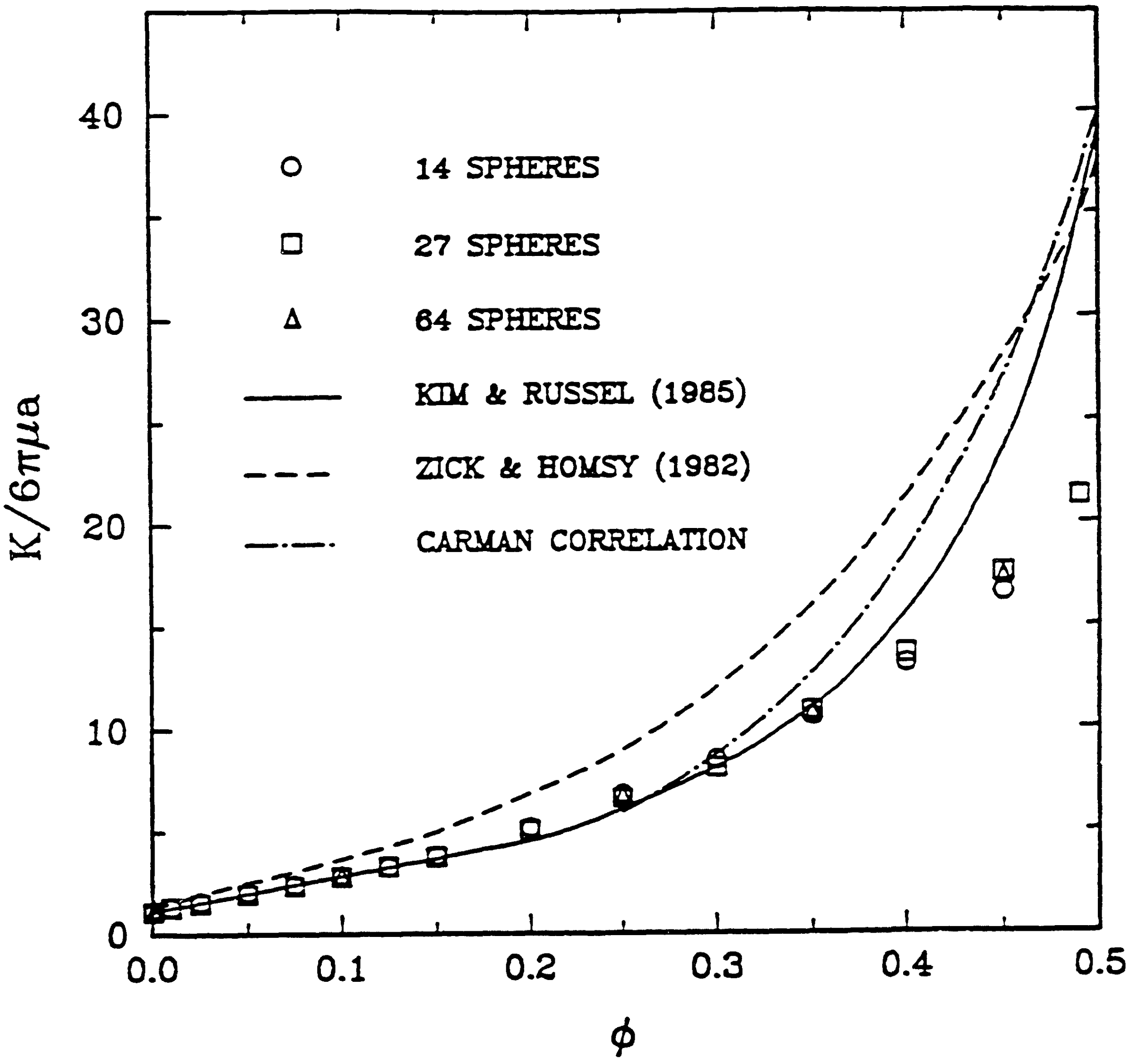

Figure 5.1 - Values of the dimensionless drag coefficient $K/6\pi\mu a$ are plotted as a function of ϕ for 14, 27, and 64 spheres per periodic unit cell. The Carman correlation, the results of Kim and Russel (1985) for random arrays, and those of Zick and Homsy (1982) for SC lattices are also shown.

One other significant observation that is evident from Figure 5.1 is the absence of periodicity effects, as evidenced by the roughly equivalent results obtained for the three values of N studied. As in Chapter 4, one can explain this result by comparing the effect on the permeability of a sphere's periodic reflections with the effect of all the other spheres in the system. The sphere's reflections are arranged in a simple cubic lattice with volume fraction ϕ/N, whereas the immobile spheres are assumed to behave as a random porous medium of volume fraction $\phi(1-1/N)$. The drag coefficient for a sphere in a dilute, simple cubic lattice is (Saffman, 1973)

$$\frac{K_{sc}}{6\pi\mu a} = 1 + 1.74\phi^{1/3} \quad , \tag{5.2}$$

while for a dilute, fixed, random array K_{ran} is given by (Brinkman, 1947)

$$\frac{K_{ran}}{6\pi\mu a} = 1 + (3/\sqrt{2})\phi^{1/2} \quad . \tag{5.3}$$

Therefore, for the effect of the periodic reflections to be negligible one requires that

$$\frac{1.74\ (\phi/N)^{1/3}}{(4.5)^{1/2}\ (1-1/N)^{1/2}\phi^{1/2}} << 1 \quad , \tag{5.4}$$

or, for large N,

$$N >> 0.55\ \phi^{-1/2}\ . \tag{5.5}$$

The inequality (5.5) is also the requirement that the Brinkman screening length $k^{1/2}$, given by $(\sqrt{2}/3)a\phi^{-1/2}$ for random arrays of spheres (for which $k = 2a^2/9\phi$), be small compared to the size of the periodic unit cell. As long as this condition is satisfied, the medium will appear disordered rather than ordered. Except for the most dilute systems studied, the inequality (5.5) was satisfied in these simulations.

The observation made above that lubrication forces do not significantly affect permeability calculations is clearly illustrated in Figure 5.2, where it is seen that results with and without the effects of near-field, lubrication interactions are virtually identical. In contrast, including the dipole interaction terms of the moment expansion (2.26) (i.e., moving from the F to the F-T-S method) does significantly improve the accuracy of the calculations. (Including torques only, as in the F-T formulation, did not significantly alter the F method results, and so for simplicity those data were not plotted.) The effect of the stresslet terms is indicative of what would be required to obtain more accurate values of K using the Stokesian dynamics method: the moment expansion used in determining the far-field interaction terms would have to be extended to include quadrupole, octupole, and several higher multipole moments (*cf.* Table 3.1), a procedure that would require excessive computer time.

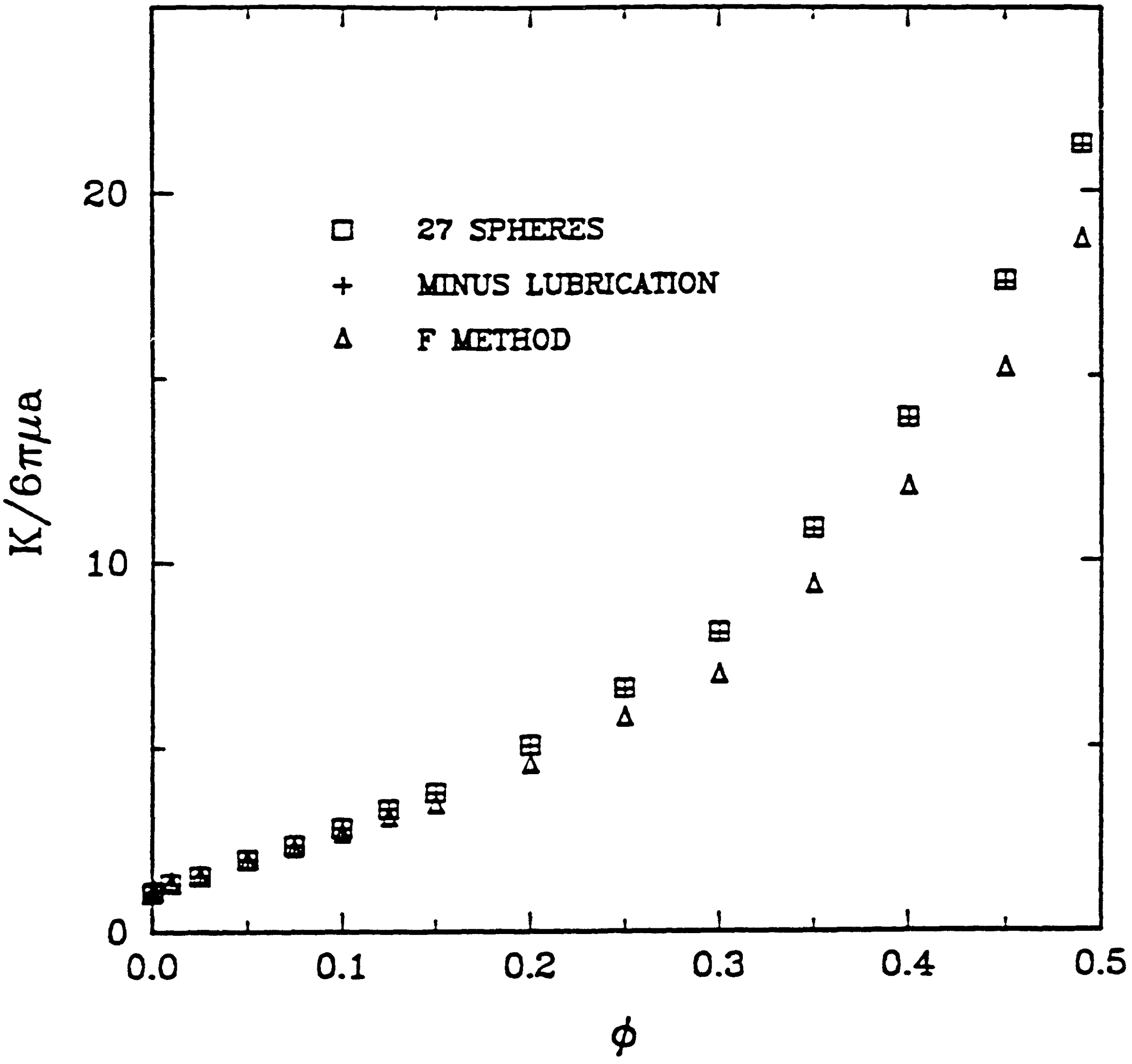

Figure 5.2 - Comparison of the effects of various levels of approximation in the formation of the resistance matrix on the calculation of the average drag coefficient K. The open squares are the complete, F-T-S calculation for $N = 27$ with near-field interactions included. The crosses (+) are results for the F-T-S calculation without near-field effects, and show that lubrication forces are not important in this calculation. The open triangles are the results for the F method with near-field interactions included.

5.2.2 Hindered Diffusion

As already stated, the calculation of short-time, hindered diffusion coefficients is accomplished by evaluating the mobility of a given sphere in a porous medium and applying the Stokes-Einstein equation. The mobility of a given sphere is evaluated by exerting a force on it and calculating the resulting velocity, given that the other spheres in the porous medium are held immobile. Note that restricting the surrounding spheres to be force- and torque-free rather than immobile yields the self-diffusion coefficient of a particle in a suspension, as discussed in Chapter 4.

For an unbounded porous medium with no periodicity, when the given test particle moves both the average velocity $\langle \mathbf{u} \rangle$ and the average force $\langle \mathbf{F} \rangle$ are zero. However, with the imposition of periodic boundary conditions it becomes impossible to insure that both of these conditions will hold. The disparity between the two situations results from the fact that, when periodic boundary conditions are used, any motion of the test particle is accompanied by motion of that particle's periodic reflections, which are arranged in an SC lattice. Since an infinite number of particles is moving rather than one, single particle, a "backflow" of fluid is necessary to insure that $\langle \mathbf{u} \rangle = 0$. This backflow is caused by a pressure gradient that arises to balance a non-zero average force (*cf.* section 2.1), and can reduce the calculated mobility if the periodic unit cells are not large enough. Fortunately, for the hindered diffusion coefficient calculation considered here, these periodicity effects decay rapidly, decreasing as N^{-1} as the number of particles per unit cell is increased (Durlofsky and Brady, 1987).

In Figure 5.3, the simulation results for 14, 27, and 64 particles per periodic unit cell are shown together with the asymptotic low ϕ result derived by Freed and Muthukumar (1978). Clearly the agreement between the two sets of results is excellent for the dilute systems where Freed and Muthukumar's result is valid. At higher ϕ, Freed and Muthukumar's calculations seem to underestimate the hindered diffusivity, although they do give the proper trend. Finally, periodicity effects are seen to be negligible, a result of the weak dependence on N discussed above.

In Figure 5.4, the complete F-T-S method results for $N = 27$ are shown and are compared with those obtained from the simpler F method and those from the F-T-S method without lubrication. As in Figures 5.1 and 5.2, the results for the F-T method deviate only slightly from those for the F method and so were left out for clarity. The data of Figure 5.4 can be interpreted as meaning that lubrication and stresslet interactions are of comparable importance up to volume fractions of about 0.25, while for higher volume fractions lubrication interactions begin to dominate the effects of all the higher-order moments.

Because stresslets do seem to be important here over such a wide range of volume fractions, it could be worthwhile to explore possible alternative methods of including them in the formulation. One such approach is to include torques and stresslets (*i.e.*, terms resulting from the dipole moment in (2.26)) in a pairwise fashion through the terms $(R_{2B}-R_{2B}^{\infty})$, thereby classifying torque and stresslet contributions as near-field rather than far-field interactions. This would increase the computational efficiency of the method by reducing the size of the mobility matrix that must be inverted in (2.48) from $11N\times11N$ to $3N\times3N$, resulting in a 50-fold savings in computation time.

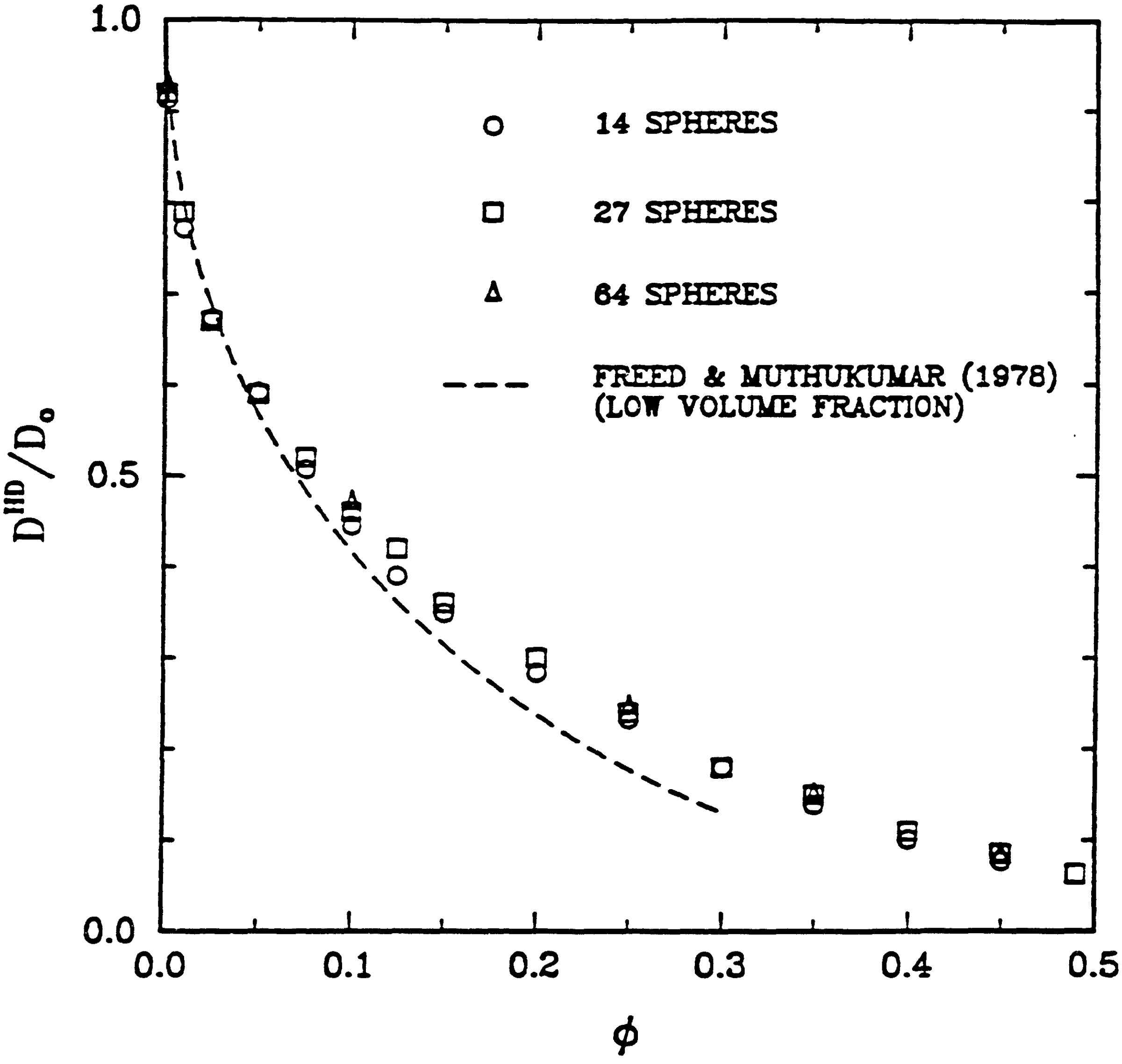

Figure 5.3 - Simulation results for the short-time hindered diffusion coefficient D^{HD} are plotted as a function of volume fraction ϕ for three values of N. The result reported by Freed and Muthukumar (1978), valid at low ϕ, is included for comparison.

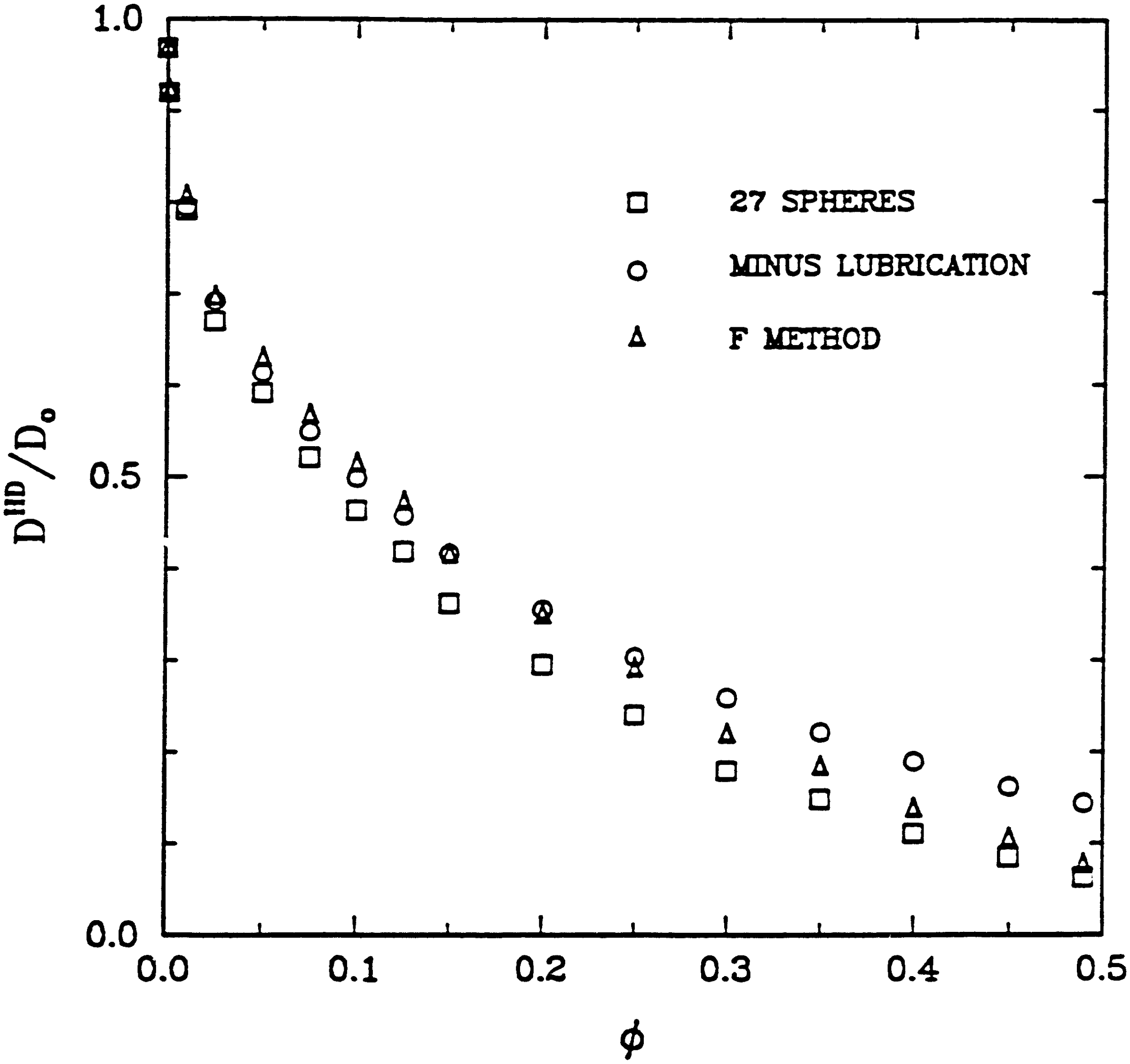

Figure 5.4 - Comparison of the effects of various levels of approximation in the formation of the resistance matrix on the calculation of the short-time hindered diffusion coefficient D^{HD}. The open squares are results for the complete F-T-S method for $N = 27$, including near-field interactions. The open circles are the results without near-field interactions, and the open triangles are the results for the F method with near-field interactions.

In Figure 5.5, results for such a variation of the F method are presented. These results were obtained for $N = 27$, and should be compared with the F-method results of Figure 5.4, in which the effects of stresslets and torques are left out entirely (*cf.* section 4.1). Clearly the agreement is excellent, showing that pairwise incorporation of torque and stresslet interactions results in essentially no loss in accuracy for this calculation. It should be noted, however, that from a rigorous mathematical point of view torque and stresslet interactions are not absolutely convergent, and therefore should be properly summed as described in Chapter 2. Thus, pairwise addition of these interactions, which seems to work extremely well in calculations of D^{HD}, should not be assumed to be equally valid for other calculations.

5.2.3 Rotational Drag and Rotational Hindered Diffusion

This discussion of transport properties of porous media is completed by presenting the results for the rotational analogs of the transport properties discussed above. Results for the rotational drag coefficient K_r are presented in Figures 5.6 and 5.7, while the rotational hindered diffusion coefficients are plotted in Figures 5.8 and 5.9. As was the case for the translational transport properties, neither set of rotational quantities calculated show any effects of periodicity, as the three values of N used all seem to yield essentially identical results. In addition, for both cases the lubrication terms appear to be much more important than the stresslet interaction terms, particularly at the higher volume fractions

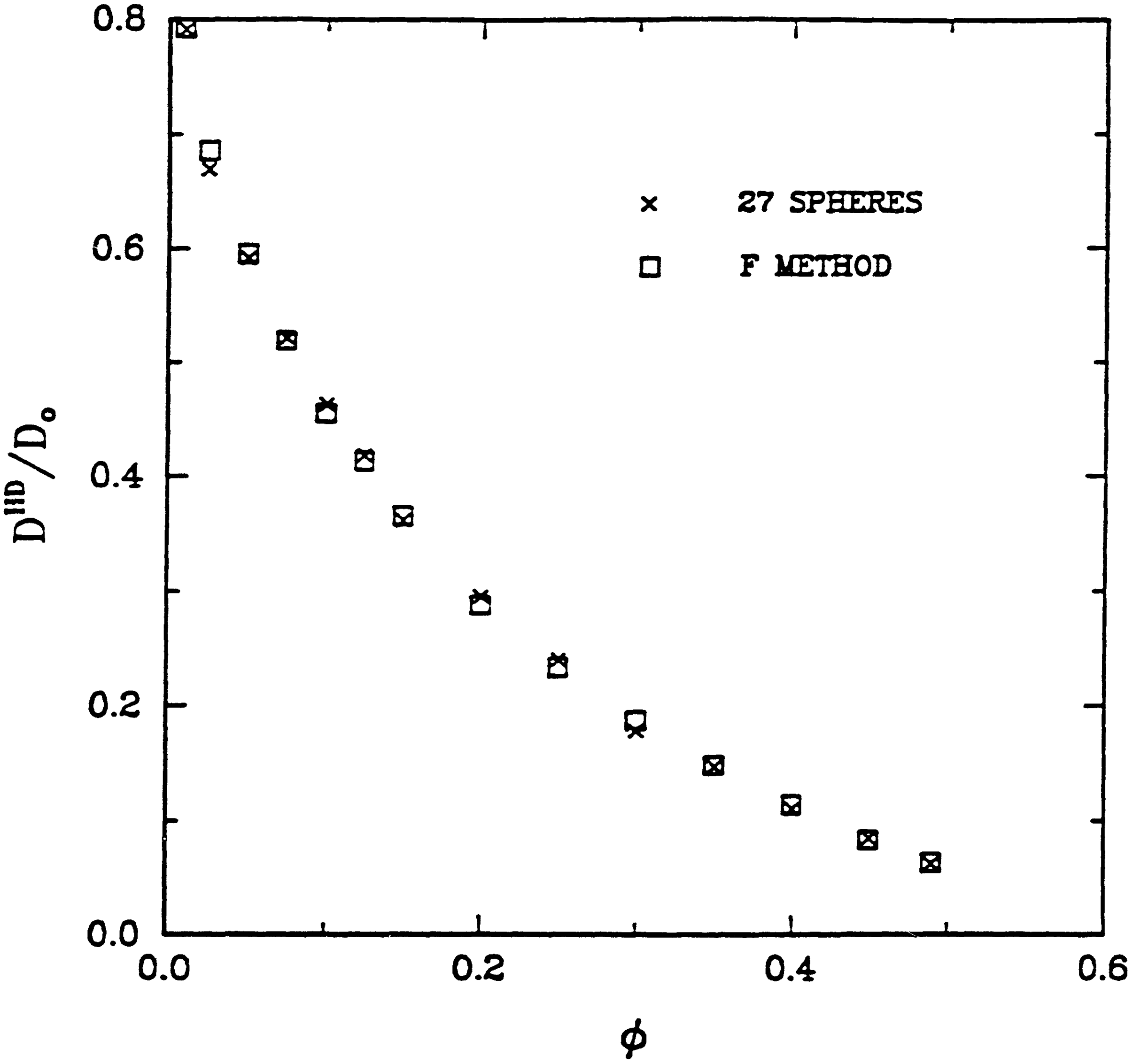

Figure 5.5 - Results for D^{BD} calculated using a variation of the F method in which torque and stresslet interactions are included in a pairwise fashion are compared with the complete F-T-S results (both sets of simulations were performed with $N = 27$).

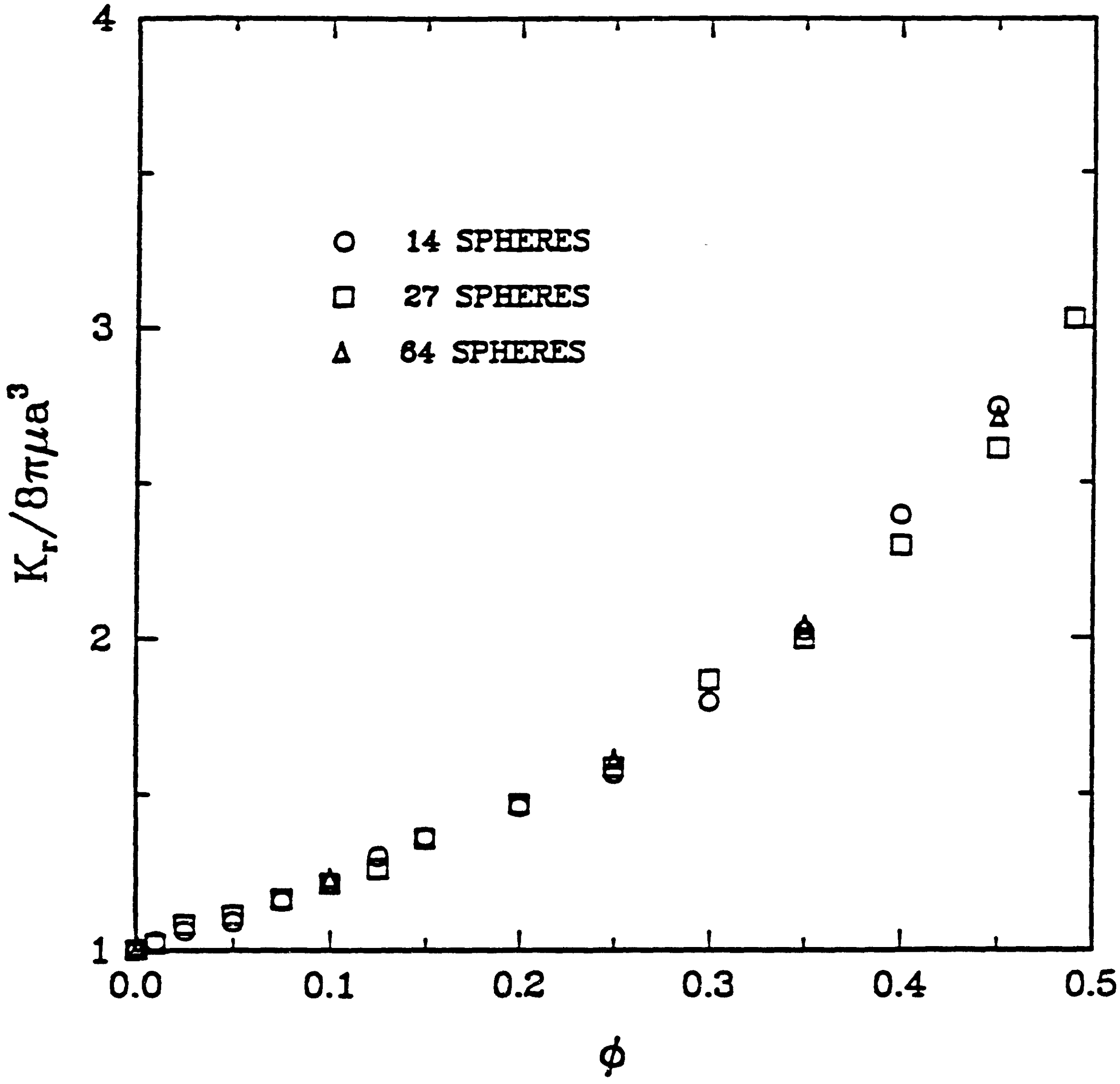

Figure 5.6 - The rotational drag coefficient K_r is plotted as a function of ϕ for different values of N, the number of spheres per periodic unit cell.

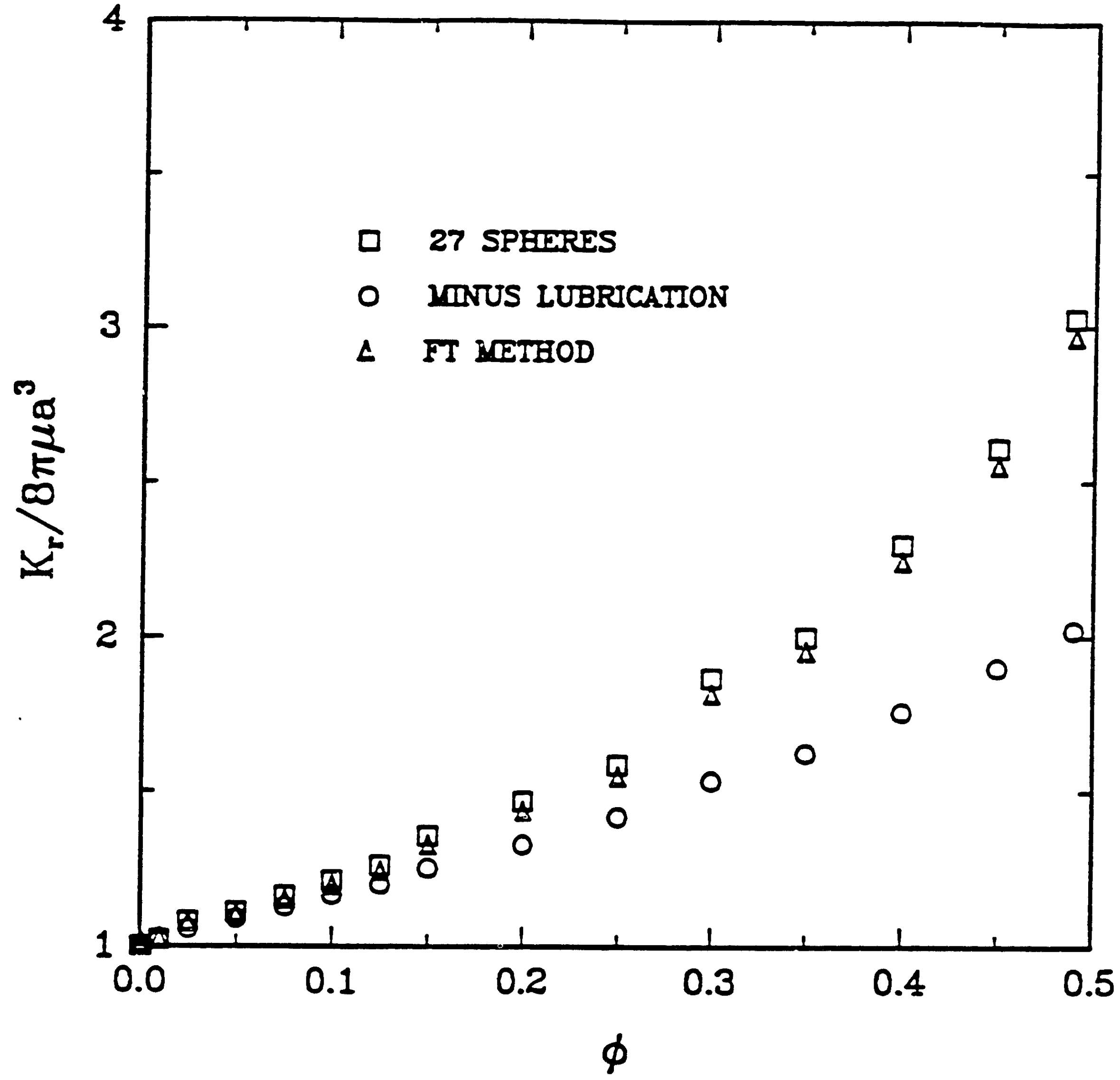

Figure 5.7 - Comparison of the effects of different levels of approximation in the formation of the resistance matrix on the calculation of the rotational drag coefficient K_r.

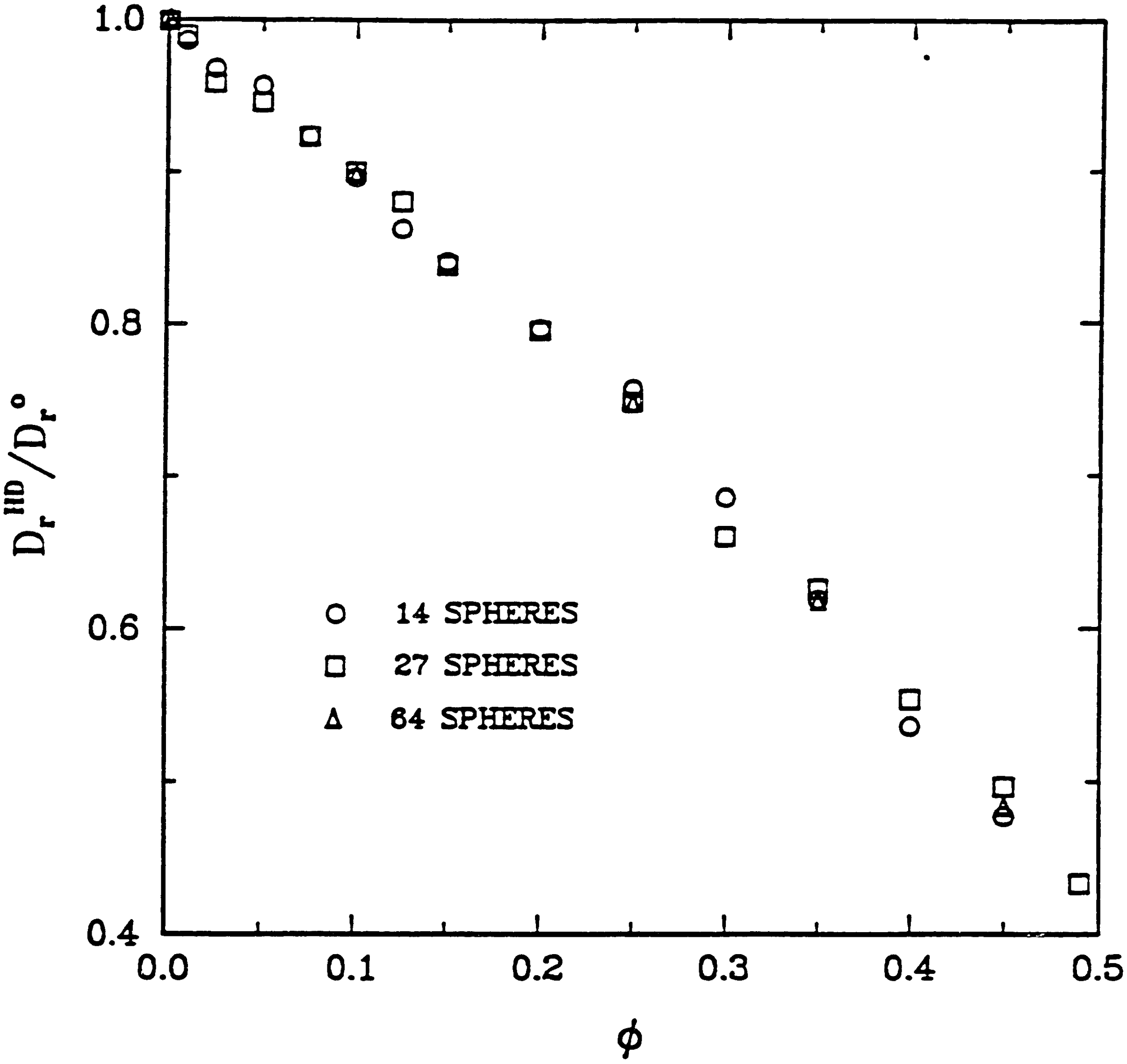

Figure 5.8 - The rotational hindered diffusion coefficient D_r^{HD} is plotted as a function of ϕ for different values of N, the number of spheres per periodic unit cell.

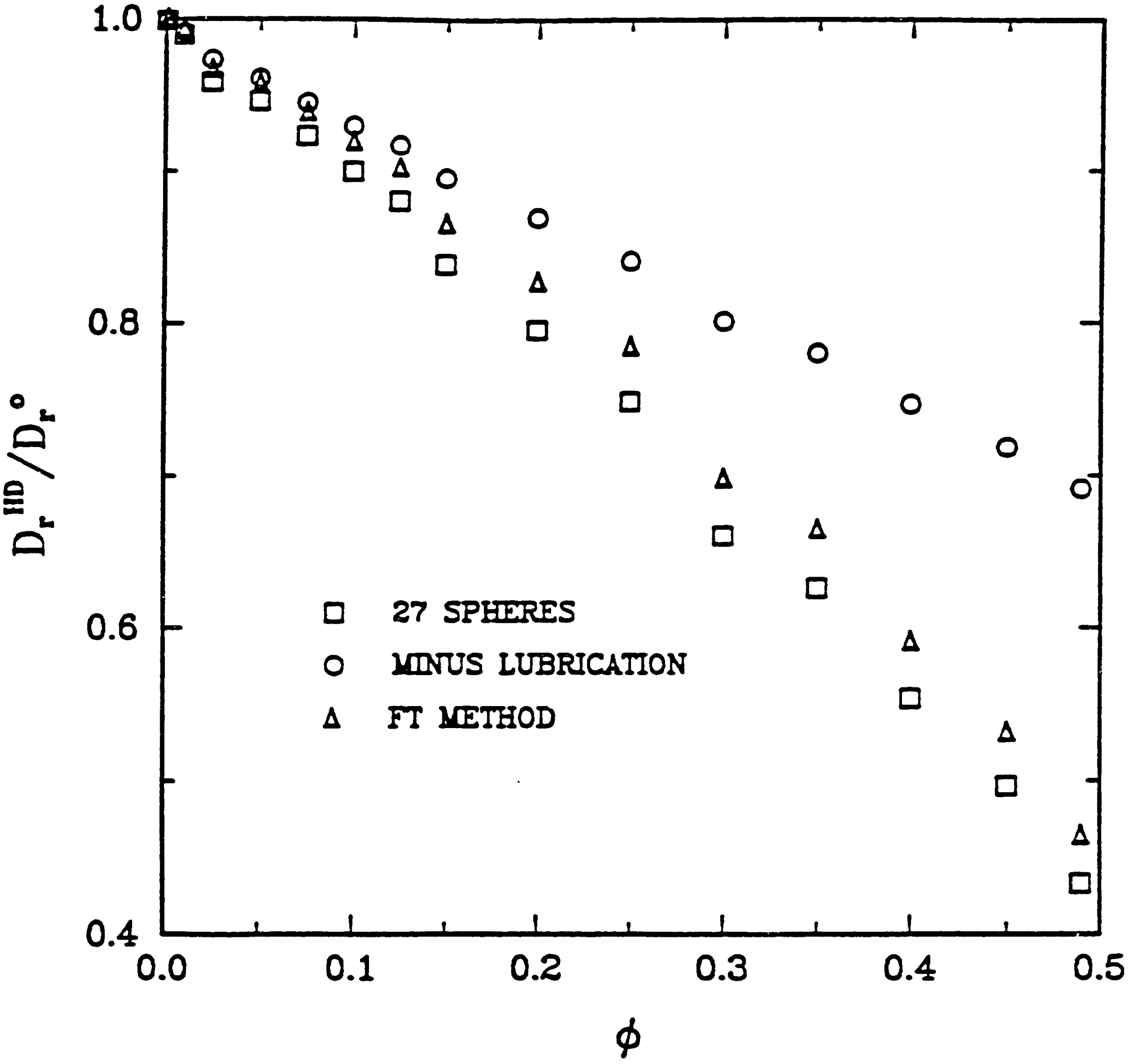

Figure 5.9 - Comparison of the effects of different levels of approximation in the formation of the resistance matrix on the calculation of the rotational hindered diffusion coefficient D_r^{HD}.

studied. Note also that, in contrast to the results for the drag coefficient *K*, lubrication is important for the rotational drag coefficient as there is now relative motion between particle surfaces. At present there are no theoretical or experimental results with which to compare these data. It may be remarked, however, that the calculations of Kim and Russel and those of Freed and Muthukumar could be extended to the rotational case.

5.3 CONCLUSION

The Stokesian dynamics method described in Chapter 2 has been successfully applied to a wide class of problems involving free suspensions and porous media. In Chapter 4 results for transport properties associated with suspensions of hard spheres, including sedimentation velocities, self-diffusion coefficients, and effective viscosities, were presented and analyzed. In this chapter a similar set of results were given for porous media, including calculations of permeabilities and short-time hindered diffusion coefficients. Among the more prominent differences between the results presented in these two chapters are the effects incurred by the imposition of periodic boundary conditions. While periodicity effects were clearly important in the translational properties (sedimentation and self-diffusion) of free suspensions, they are not at all apparent in the results presented in this chapter. The reasons for this difference lie in Brinkman screening effects, which cause interactions to decay more rapidly in porous media than in suspensions, thereby decreasing any effects of long-range order.

Finally, although the Stokesian dynamics method was originally applied to dynamic simulations of hard-sphere suspensions, the work presented in this and in the previous chapter has shown that it can be useful in other applications as well, a fact that will be made even more apparent in the chapters to follow.

CHAPTER 6

HINDERED TRANSPORT IN FIBROUS MEDIA

The problem of predicting rates of transport for globular proteins in fibrous membranes and gels has relevance to many important physiological and industrial processes. Ultrafiltration and size-exclusion chromatography serve as two examples. When the permeating macromolecules have dimensions comparable to the interfiber spacing, transport is hindered by steric as well as long-range interactions with the fibers. Steric interactions make some fraction of the fluid volume in the fiber matrix inaccessible to the center of a solute molecule. For fibers arranged in a spatially periodic fashion, this excluded volume can be calculated using elementary geometric principles. The corresponding calculation for random arrays of fibers is considerably more complicated, but has already been carried out for both the dilute (Ogston, 1958) and non-dilute case (Fanti and Glandt, 1989).

Unfortunately, there is much less information available on the effects of long-range interactions. Even in the absence of electrostatic effects, long-range hydrodynamic interactions between the solute macromolecule and the fibers will lead to an increase in the hydrodynamic drag. Previous studies on hindered transport in cylindrical or slit-like pores suggest that this increased drag can contribute significantly to the lowering of the apparent diffusivity (Deen, 1987). In the past, theories have been applied primarily to infinitesimally small solutes in fibrous media (Perrins *et al.*, 1979; Brenner and Adler, 1982; Carbonell and Whitaker, 1983; Koch and Brady, 1986). However, under these conditions neither steric nor hydrodynamic interactions play an important role. Thus, there is a great need for a better theoretical understanding of the effects of hydrodynamic interactions on the transport of finite-sized solutes in fibrous media.

In this chapter, two approaches for calculating transport coefficients for a spherical macromolecule in a matrix of fibers are described. The first method is an effective medium approach based on Brinkman's equation. In the second calculation, the Stokesian dynamics method is used to calculate *local* hydrodynamic coefficients at any position in a fibrous bed. These local coefficients describe transport over time scales so short that a mobile macromolecule does not move a distance comparable to its own radius, and are therefore not appropriate for calculating a macroscopic flux through a membrane or gel. However, local coefficients can be used in conjunction with dynamic simulations (Brady and Bossis, 1988) or with generalized Taylor dispersion theory (Brenner and Adler, 1982) to calculate *global* transport coefficients, that do describe diffusion and convection over macroscopic length scales.

Here the theory of Brenner and Adler is used to obtain numerical results for these global coefficients, and the predictions of the effective medium model and of generalized Taylor dispersion theory are compared for two different spatially periodic lattices of bead-and-string fibers. In addition, the effects of the size of the solute relative to that of the fibers is examined by varying the ratio of the solute radius to the fiber radius (λ) from 0.5 to 5. Finally, this comparison between two different theoretical results is complemented by a comparison between results obtained using the effective medium model and experimental data reported in the literature.

6.1 THEORY

6.1.1 Effective Medium Approach

The macroscopic flux $\mathbf{J}^*$ of probability density $\bar{P}$ through an effective medium can be described by the equation

$$\mathbf{J}^* = -\underset{\approx}{D}^* \cdot \nabla \bar{\mathrm{P}} + \mathbf{U}^* \bar{\mathrm{P}} \ . \tag{6.1}$$

Here the overbar on the probability density indicates that this is a macroscopic probability density. It is the volume average of the local probability density P over a length scale large enough to represent the microstructure of the porous medium. For a spatially periodic porous medium, the appropriate length scale for averaging is the dimension of a single unit cell. Thus, $\bar{P}$ varies over a length scale which is large compared to that of a unit cell. The dispersivity tensor $\underset{\approx}{D}^*$ in (6.1) can be thought of as the quantity that governs the flux resulting from a gradient in probability density, while the solute velocity $\mathbf{U}^*$ determines the flux resulting from an average velocity $\langle \mathbf{u} \rangle$. The time scale over which these flux terms are measured must be long enough to allow the Brownian solute to sample enough positions in the porous medium to obtain an adequate representation of its microstructure. For a spatially periodic medium with unit cells of dimension L', an order-of-magnitude estimate of the time t^* required for this to occur is $t^* \gg L'^2/D_o$.

The dispersion tensor for an isotropic porous medium can be expressed as the product of an effective dispersion coefficient D^* and the identity tensor $\underset{\approx}{I}$. A value for D^* can be obtained using the Stokes-Einstein equation, which states that $D^* = k_B T/f$, where $k_B T$ is the product of Boltzmann's constant and absolute temperature, and f is the friction coefficient, equal to $6\pi\mu a_s$ for a sphere of radius a_s in a pure fluid with viscosity μ. The friction coefficient for a sphere in a porous medium can be calculated by using Brinkman's equation (Brinkman, 1947) for flow in a porous medium:

$$\mu\nabla^2\mathbf{v} - \nabla\langle p\rangle = (\mu/k)\langle\mathbf{u}\rangle \, . \tag{6.2}$$

Here $\langle p\rangle$ is the pressure and $\langle\mathbf{u}\rangle$ is the velocity averaged over both the fluid and the fiber phases. Equation (6.2) can be seen as Stokes' equations with an additional term to account for the force exerted on the fluid by the fibers. This additional resistance term is proportional to $\langle\mathbf{u}\rangle$ and is distributed evenly throughout space. Alternatively, Brinkman's equation can be viewed as Darcy's law with an additional term that accounts for viscous stresses in the fluid phase. The only structural information included in this effective medium model is contained in k, the hydraulic permeability.

The value of f obtained by solving (6.2) subject to no-slip boundary conditions at the sphere surface and constant velocity far from the sphere center is (Brinkman, 1947; Howells, 1974)

$$\frac{f}{6\pi\mu a_s} = 1 + (a_s^2/k)^{1/2} + \frac{1}{3}\,(a_s^2/k) \, . \tag{6.3}$$

Thus, from the Stokes-Einstein equation, one would expect

$$\frac{D^*}{D_o} = \frac{1}{1 + (a_s^2/k)^{1/2} + \frac{1}{3}(a_s^2/k)} \qquad (6.4)$$

for the effective medium, where D_0 is the diffusivity in a pure fluid. For a force-free particle, Brinkman's equation would require that the particle velocity $\mathbf{U}^*$ be equal to the velocity $\langle \mathbf{u} \rangle$ averaged over both the fiber and fluid phases. However, for a particle that cannot access positions in the fiber phase, one expects that a better approximation can be obtained by equating $\mathbf{U}^*$ with the average velocity of the fluid phase only. Thus, for a medium with volume fraction ϕ, one has

$$\mathbf{U}^* = \frac{\langle \mathbf{u} \rangle}{1-\phi} , \qquad (6.5)$$

and both quantities required to evaluate the flux using (6.1) are known. The hydraulic permeability k can be measured directly in many cases. It can also be determined theoretically for certain fiber geometries (Hasimoto, 1959; Spielman and Goren, 1968), or can be evaluated using well-known, semi-empirical correlations (Jackson and James, 1986).

The result given by (6.3) can be derived rigorously for a medium consisting of a dilute, disordered array of hard spheres (Childress, 1972; Howells, 1974; Hinch, 1977; Freed and Muthukumar, 1978). Although one might expect that the details of a fibrous versus a hard-sphere microstructure might not be important for small enough volume fractions, it is not at all clear that this will be true for volume fractions of interest for hindered transport. Further examination of equations (6.4) and (6.5) (see below) is therefore required before passing judgement as to their value.

6.1.2 Calculation of Local Transport Coefficients

Following Brenner and Adler (1982), one can define a local flux J of probability density *P* at any point in the unit cell of a spatially periodic lattice by

$$\mathbf{J} = -\underset{\approx}{\mathrm{D}}^{HD} \cdot \nabla P + \mathbf{U}P \,, \tag{6.6}$$

where *P* is a function of position **X** and the time since the diffusing macromolecule was released at some particular position. The terms $\underset{\approx}{\mathrm{D}}^{HD}$ and **U** are the local dispersion coefficient and local velocity of the tracer macromolecule, respectively. The probability density *P* is normalized such that its integral over all space, including the fluid and solid phases of all unit cells, is unity.

The quantities $\underset{\approx}{\mathrm{D}}^{HD}$ and **U** in (6.6) can be calculated using the Stokesian dynamics method. Extension of this method to spheres of different radii was achieved by evaluating near-field interactions according to the method of Jeffrey and Onishi (1984) and far-field interactions using the equations given by Beenakker (1986). The local, or short-time hindered diffusion coefficient is obtained in exactly the same way as described in Chapter 5 (*cf.* Equation (5.1)), but with the immobile spheres aligned in rows to model fibers rather than randomly dispersed as in the Monte Carlo simulations. The velocity **U** can be found by solving for the velocity of the force- and torque-free spherical solute given that the translational and rotational velocities of the spheres in the bead-and-string fibers are zero. The result for a system with average velocity $\langle \mathbf{u} \rangle$ is

$$\mathbf{U}^{\alpha} = \left((\underset{\approx}{R}^{\alpha\alpha})^{-1} \cdot \sum_{\beta=1}^{N} \underset{\approx}{R}^{\alpha\beta} \right) \cdot \langle \mathbf{u} \rangle , \tag{6.7}$$

where $\underset{\approx}{R}^{\alpha\beta}$ is a 3×3 matrix relating the force on particle α to the velocity of particle β relative to the average velocity $\langle \mathbf{u} \rangle$. The quantity $\underset{\approx}{R}^{\alpha\beta}$ is a component of the resistance matrix formed by inverting the mobility matrix of (2.1).

The resistance matrices used to calculate $\underset{\approx}{D}^{HD}$ and U were obtained using a variation of the F method described in Chapters 4 and 5. This approach is discussed in section 5.2 (*cf*. Figure 5.5), and differs from the F method described in section 4.2 in that torque and stresslet interactions are included in a pairwise additive fashion rather than being neglected entirely. Results obtained using this variation of the F method were consistently within 2-3% of those calculated using the complete F-T-S method. This finding is in accordance with the excellent agreement observed between the results of Monte Carlo simulations performed using these two levels of approximation (*cf*. Figure 5.5).

In addition to errors associated with truncation of the moment expansion (2.26), there are errors associated with the periodic boundary conditions used in the Stokesian dynamics method. This error has the same origins as the periodicity effects discussed in Chapters 4 and 5, and is related to the fact that properties such as the average velocity $\langle \mathbf{u} \rangle$, which are specified for the infinite medium as a whole in equations such as (6.7), must actually be satisfied in each periodic unit cell if all of the unit cells are to be identical. This error alters the local coefficients by an amount that is O(1/N), and is discussed in some detail by Durlofsky and Brady (1987).

6.1.3 Calculation of Global Transport Coefficients

It now remains to relate the local coefficients of (6.1) to global coefficients, which describe transport on a macroscopic length scale (*i.e.*, over many periodic unit cells). The global transport coefficients D^* and U^* of (6.1), distinguished from the coefficients in (6.6) by the asterisk, can be evaluated using generalized Taylor dispersion theory. As this theory is quite involved and has been presented elsewhere (Brenner and Adler, 1982), only the relevant equations and definitions of the appropriate variables will be presented here.

If, as is the case here, one is studying a fibrous medium that is periodic on the length scale of a unit cell, then one can write the position vector $\mathbf{X}$ as the sum of global and local variables,

$$\mathbf{X} = \mathbf{X}_n + \mathbf{r} \ , \tag{6.8}$$

where $\mathbf{X}_n$ identifies a particular unit cell and $\mathbf{r}$ specifies a position within that unit cell. By summing the probability density in all of the unit cells, one can calculate P_0, where

$$P_o(\mathbf{r},t|\mathbf{r}') = \sum_n P(\mathbf{X}_n-\mathbf{X}_n',\mathbf{r},t|\mathbf{r}') \; . \tag{6.9}$$

Physically, $P_o(\mathbf{r},t|\mathbf{r}')$ is the probability of finding the diffusing macromolecule at a particular position **r** in *any* of the unit cells at some time t, given that it was at a position $\mathbf{r}'$ at time $t = 0$. The sum over n in (6.9) is a sum over all the unit cells in space. One can eliminate the time-dependence of P_o by restricting the analysis to long times and using as a probability density P_o^∞, where

$$P_o^\infty(\mathbf{r}) = \lim_{t\to\infty} P_o(\mathbf{r},t|\mathbf{r}') \; . \tag{6.10}$$

The probability density $P_o^\infty(\mathbf{r})$ represents the probability of finding the diffusing macromolecule at some local position **r** after it has had enough time to achieve steady state with respect to transport over the length scale of a unit cell, but not over the global, or macroscopic length scale. For a periodic unit cell of dimension L', an order-of-magnitude estimate of the time t^* required for this to occur is $t^* \gg L'^2/D_o$. It can be shown that the asymptotic approach to steady-state is exponentially rapid with time (Brenner and Adler, 1982).

The equation governing P_o^∞ is

$$\nabla\cdot(\mathbf{U}P_o^\infty) - \nabla\cdot\underset{\approx}{\mathbf{D}}\cdot\nabla P_o^\infty = 0 \; , \tag{6.11}$$

with the boundary conditions

$$\llbracket P_o^\infty \rrbracket = 0 \quad \text{and} \quad \llbracket \nabla P_o^\infty \rrbracket = 0 \qquad \text{on boundaries of the unit cell in the fluid phase} \tag{6.12}$$

and

$$\mathbf{n} \cdot (\mathbf{U} P_o^\infty - \underset{\approx}{\mathbf{D}} \cdot \nabla P_o^\infty) = 0 \qquad \text{on the solid surfaces} \tag{6.13}$$

and the normalization condition

$$\int_{\mathbf{r}_o} P_o^\infty \, d\mathbf{r} = 1 \, . \tag{6.14}$$

In (6.12) the symbol $\llbracket \quad \rrbracket$ denotes the difference between the values of the argument at geometrically equivalent positions on opposite faces of a unit cell, and $\mathbf{n}$ is a unit normal vector pointing into the unit cell. The velocity $\mathbf{U}^*$ is given by

$$\mathbf{U}^* = \int_{\mathbf{r}_o} (\mathbf{U} P_o^\infty - \underset{\approx}{\mathbf{D}} \cdot \nabla P_o^\infty) \, d\mathbf{r} \, . \tag{6.15}$$

The integral over $\mathbf{r}_o$ in (6.14) and (6.15) implies an integral over the volume of a unit cell in the periodic lattice. Note that setting P_o^∞ equal to a constant satisfies (6.11), (6.12), and (6.13) if the average velocity $\langle \mathbf{u} \rangle$ is zero, since if $\langle \mathbf{u} \rangle = 0$ then the local solute velocity $\mathbf{U}$ must also be zero. In this case, the value of P_o^∞ is determined by (6.14), and the value of $\mathbf{U}^*$ given by (6.15) is just a spatial average of the local coefficient $\mathbf{U}$.

The result for $\underset{\approx}{\mathbf{D}}^*$ is most conveniently expressed in terms of a vector field $\mathbf{B}$, defined by the solution to

$$\nabla \cdot (P_o^\infty \underset{\approx}{D} \cdot \nabla \mathbf{B}) - (\mathbf{U} P_o^\infty - \underset{\approx}{D} \cdot \nabla P_o^\infty) \cdot \nabla \mathbf{B} = P_o^\infty \mathbf{U}^* , \tag{6.16}$$

with boundary conditions

$$\llbracket \mathbf{B} \rrbracket = - \llbracket \mathbf{r} \rrbracket \quad \text{and} \quad \llbracket \nabla \mathbf{B} \rrbracket = \mathbf{0} \quad \text{on boundaries of the unit cell in the fluid phase} \tag{6.17}$$

and

$$\mathbf{n} \cdot \underset{\approx}{D} \cdot \nabla \mathbf{B} = \mathbf{0} \qquad \text{on the solid surfaces.} \tag{6.18}$$

The global dispersion coefficient, $\underset{\approx}{D}^*$, is then given by

$$\underset{\approx}{D}^* = \int_{\mathbf{r}_o} (P_o^\infty (\nabla \mathbf{B})^t \cdot \underset{\approx}{D} \cdot \nabla \mathbf{B}) \, d\mathbf{r} , \tag{6.19}$$

where $(\nabla \mathbf{B})^t$ denotes the transpose of the tensor $\nabla \mathbf{B}$. The vector field $\mathbf{B}$, which one must evaluate in order to make use of (6.19), arises as a matter of mathematical convenience in the development of Brenner and Adler (1982), and is related to physical quantities by Koch *et al.* (1989).

6.2 RESULTS

As stated previously, results have been obtained for two different periodic lattices of bead-and-string fibers, and for ratios of the solute radius to the fiber radius λ ranging from 0.5 to 5. The periodic lattices were chosen so as to provide a better understanding of the effects of inhomogeneity on transport through a fibrous bed, and also to allow one to examine the ability of the effective medium model to capture those effects. Similarly, the studies in which λ was varied provide new information on the influence of solute size on hindered transport in fibrous media. Finally, the ability of the effective medium model to predict hindered dispersion coefficients in fibrous media is investigated further by comparison with experimental data obtained from the literature.

6.2.1 Square Lattice of Fibers

Two cross-sections of a square lattice of bead-and-string fibers are shown in Figure 6.1. Parallel, bead-and-string fibers aligned along the z axis were arranged in a square lattice in the x-y plane, with fiber-to-fiber spacing L and a gap spacing d separating the spheres of a given fiber. The dimensions L and d are made dimensionless by the sphere radius a_s. This configuration was selected because it seemed the simplest geometry which could yield meaningful results for the hindered transport problem.

Transverse cross-sections of the square lattice of fibers were taken at the positions denoted by the lines AA′ and BB′ in Figure 6.1 (lower), and (6.11) and (6.16) were solved for each of these two cross-sections by neglecting the true three-dimensional nature of the bead-and-string fibers. In other words, once the local coefficients were obtained for the AA′ and BB′ cross-sections, (6.11) and (6.16) were solved assuming the fibers were cylinders of constant radius aligned in the z direction. The difference between these two cross-sections is that a diffusing macromolecule can sample a higher fraction of the total area in the cross-section taken at BB′ than in that taken at AA′. These differences can be minimized by choosing d to be a small fraction of the fiber radius. A value of $d = 0.05$ was used in this work. One would expect the actual result for a matrix of such fibers to lie between the two results obtained in this manner. Thus, when the transport properties calculated from the two cross-sections differed by more than about 2%, the average of the two results is reported and the range of results is given by the error bars shown.

Equations (6.11) and (6.16) were solved using a Galerkin finite element method with bilinear basis functions (Finlayson, 1980). The choice of a finite element method of solution is particularly convenient in this problem because of the form of the boundary conditions (6.13) and (6.18). For a finite-sized solute molecule, $\underset{\approx}{D}$ and $\mathbf{U}$ are identically zero on solid surfaces, and thus it is difficult to specify any properties of P and $\mathbf{B}$ other than that they and their gradients must be finite. The advantage of the finite element approach is that specific statements regarding the behavior of P and $\mathbf{B}$ are not required. Rather, one applies the conditions of no flux on the solid surfaces in precisely the form given in (6.13) and (6.18), and thus the proper physical requirement of no flux into the fibers is easily incorporated into the method of solution.

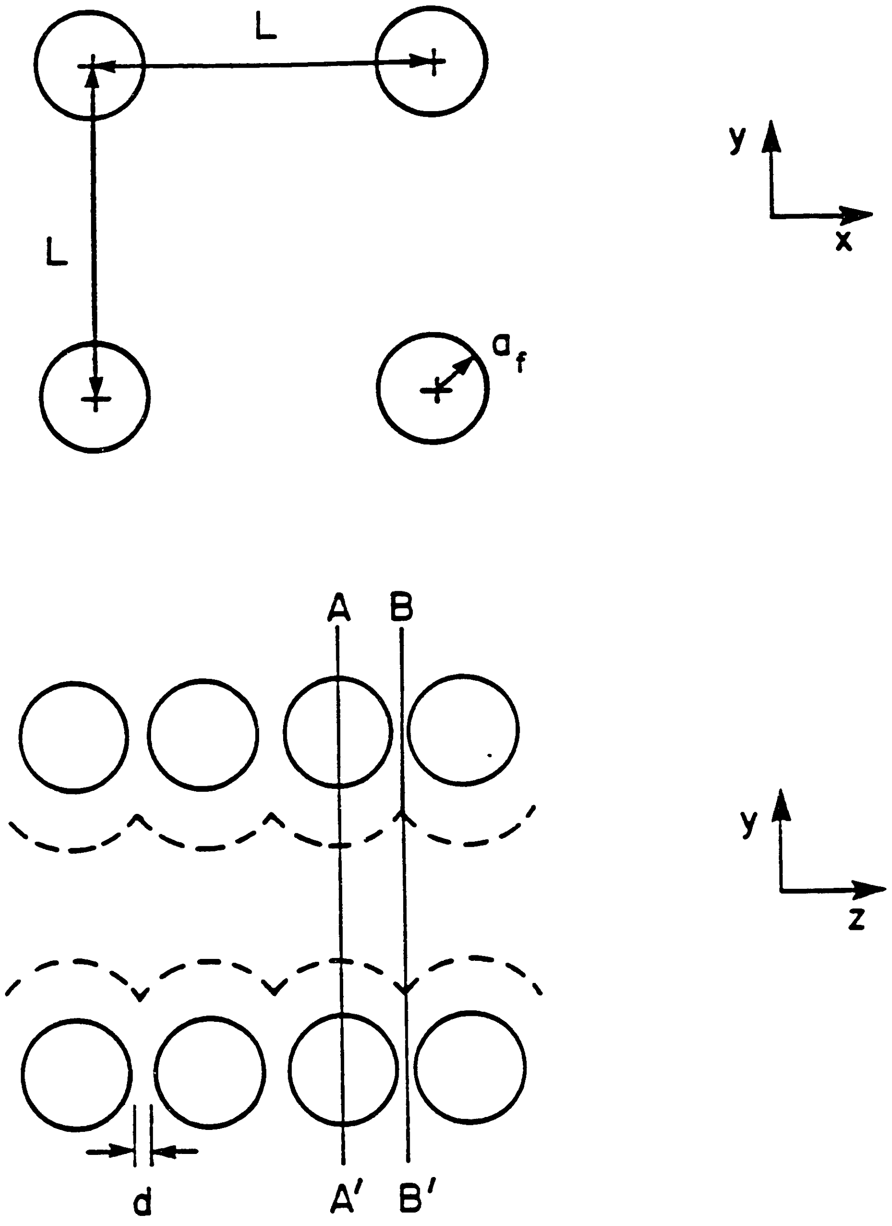

Figure 6.1 - *Upper:* Transverse cross-section of a periodic lattice of bead-and-string fibers. *Lower:* The cross-sections marked by the lines AA' and BB' were used in solving the equations of generalized Taylor dispersion theory (*i.e.*, (6.11) and (6.16)) Using either cross-section results in a two-dimensional lattice like that shown in Figure 1 (upper), but t gap between the fibers is larger for the BB' cross-section than for the AA' cross-section. The dashed curves bound the region accessible to a mobile sphere of radius a_s, where $a_s = a_f$.

The size of the periodic unit cell used to calculate the hydrodynamic interactions was not the same as the size of the periodic unit cell used in the Taylor dispersion calculations (*i.e.*, in solving (6.11) and (6.16)). For the latter, the smallest possible unit cell dimension L was employed. However, as discussed previously, there is an $O(1/N)$ error in the terms of the resistance matrix caused by the use of periodic boundary conditions in modeling the infinite system. It is therefore necessary to choose a large enough periodic unit cell (*i.e.*, a large enough value of N) to make this error in the calculation of the local coefficients negligible. In this work, $\underset{\approx}{D}$ and $\mathbf{U}$ were obtained using a unit cell of 9 fibers, each containing 10 spheres aligned in the z direction. The results were not changed by more than 2-3% when unit cells with 16 fibers or with 15 spheres per fiber were used, indicating that artifacts arising from periodic images were not important in these calculations. The calculations were done on a CYBER 205 supercomputer. A typical configuration required the evaluation of local coefficients at about 500 positions, which used about 30 minutes of CPU time. The computer time required to solve (6.11) and (6.16) was negligible compared to the time required to calculate the local coefficients.

6.2.2 Comparison of Theoretical Predictions

In Figure 6.2(a,b) drag coefficients and hydraulic permeabilities for flow in the x or y directions through a square lattice of fibers are plotted as a function of the interfiber spacing L for the two periodic fiber lattices of interest here. (See below for a description of the second periodic lattice.) The results for the drag coefficient K were obtained using (3.4), and are related to the hydraulic permeability by (3.3). Also plotted in Figure 6.2 are the theoretical results of Hasimoto (1959), who calculated the permeability of a square lattice of straight, cylindrical fibers in creeping flow. The good agreement between the two sets of results underscores both the validity of the Stokesian dynamics approximation for the resistance matrix and the hydrodynamic similarity of the bead-and-string and cylindrical rod models of fibers.

Although the parameter *L* used in Figure 6.2(a,b) is useful for describing square lattices of fibers, for other geometries it is often convenient to use the volume fraction of fibers ϕ. For a square lattice of bead-and-string fibers such as that shown in Figure 6.1, ϕ and *L* are related by

$$\phi = \frac{\frac{4}{3}\pi}{(2+d)L^2} \quad , \tag{6.20}$$

whereas for a square lattice of smooth, cylindrical fibers

$$\phi = \frac{\pi}{L^2} \quad . \tag{6.21}$$

Thus, a given value of ϕ will correspond to different values of *L* for the two types of fibers. Since the choice of whether to describe two fibrous systems using ϕ or *L* is somewhat arbitrary, the data of Figure 6.2(a,b) are replotted in Figure 6.3(a,b) as a function of ϕ. Clearly good agreement is obtained regardless of which of the two parameters is chosen to describe the square lattice. For most fibrous systems, the volume fraction is more readily obtained than the interfiber spacing, and thus the remaining results of this section will be presented as a function of ϕ rather than L.

In Figure 6.4, values of the dispersion coefficient are shown for a spherical macromolecule with the same radius as the fibers ($\lambda = 1$) diffusing in a medium with no flow ($\langle \mathbf{u} \rangle = 0$). The scalar coefficient D^*_{xx} is the component of $\underset{\approx}{\mathrm{D}}^*$ that governs dispersion in the x direction due to a probability density gradient in the x direction. For this periodic system, D^*_{yy} will equal D^*_{xx}, while D^*_{xy} and D^*_{yx} will be zero. The bulk solution diffusivity is denoted by D_o, and the volume fraction of fibers is given by ϕ. The calculations were done both with and without near-field interactions.

The solid curve in Figure 6.4 is the Brinkman, or effective medium result, obtained using (6.4) together with hydraulic permeabilities calculated from (3.3). The Brinkman results and the generalized Taylor dispersion results are in remarkably good agreement, especially when near-field interactions are neglected. This observation is consistent with the expectation that Brinkman's equation should become more accurate for dilute systems, where far-field interactions dominate. Indeed, Durlofsky and Brady (1987) demonstrated that the rate of decay of far-field hydrodynamic interactions evaluated using the Stokesian dynamics method corresponds closely to the prediction of Brinkman's equation. Including the near-field interactions caused a deviation of about 20% from the Brinkman results at the maximum volume fraction studied, $\phi = 10.1\%$, which corresponds to $L = 4.5$. (From Figure 6.1, macroscopic transport in the x and y directions ceases for $L < 4$, or $\phi > 12.8\%$, for the AA′ cross-section.) The close correspondence between the Brinkman results and those of the more detailed hydrodynamic model suggests that the hydraulic permeability k embodies the

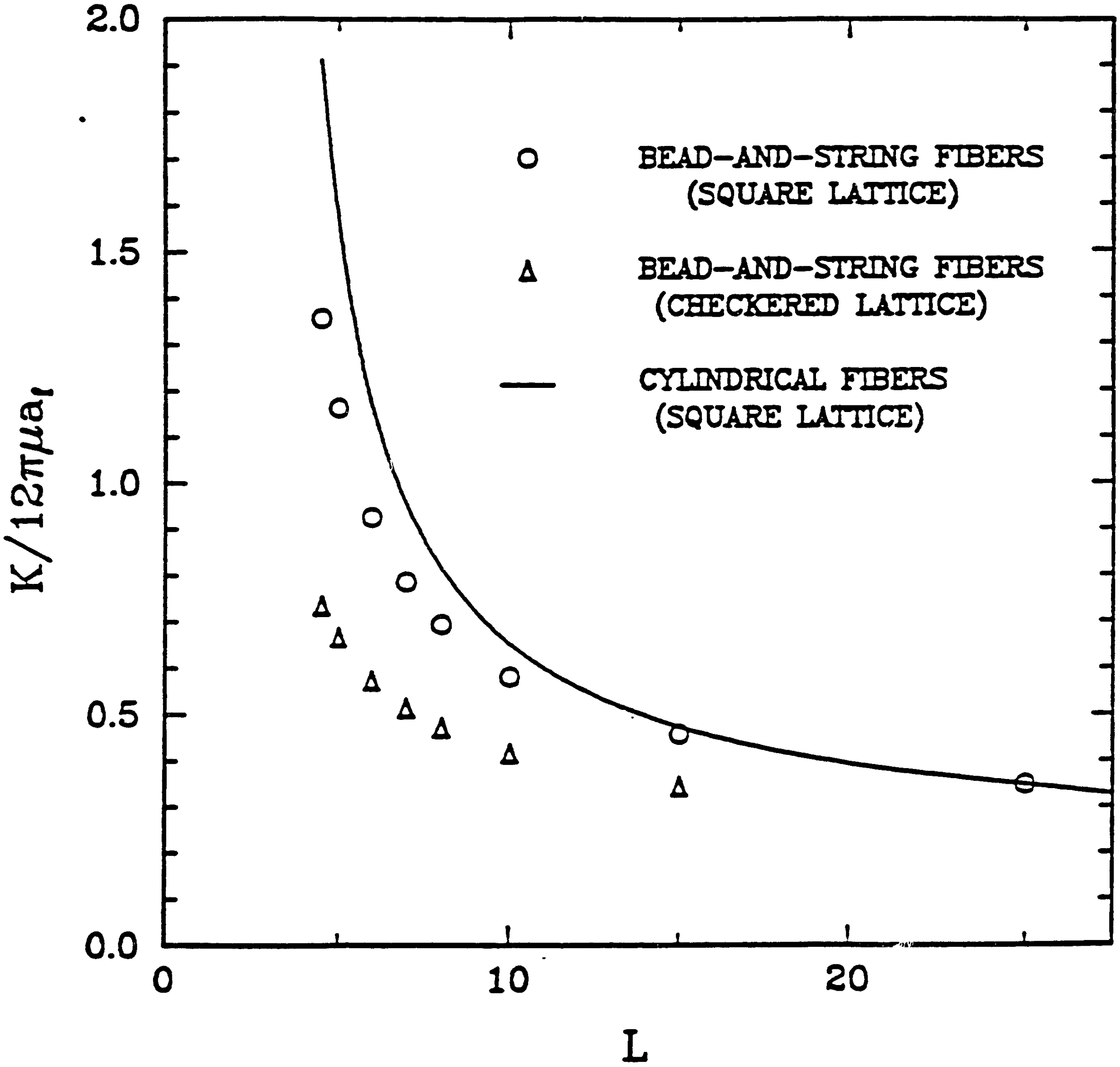

Figure 6.2a - The dimensionless drag coefficients $K/12\pi\mu a_f$ for square and checkered lattices of bead-and-string fibers are plotted as a function of the interfiber spacing L (*cf*. Figure 6.1). The result for a square lattice of cylindrical fibers (Hasimoto, 1959) is included for comparison.

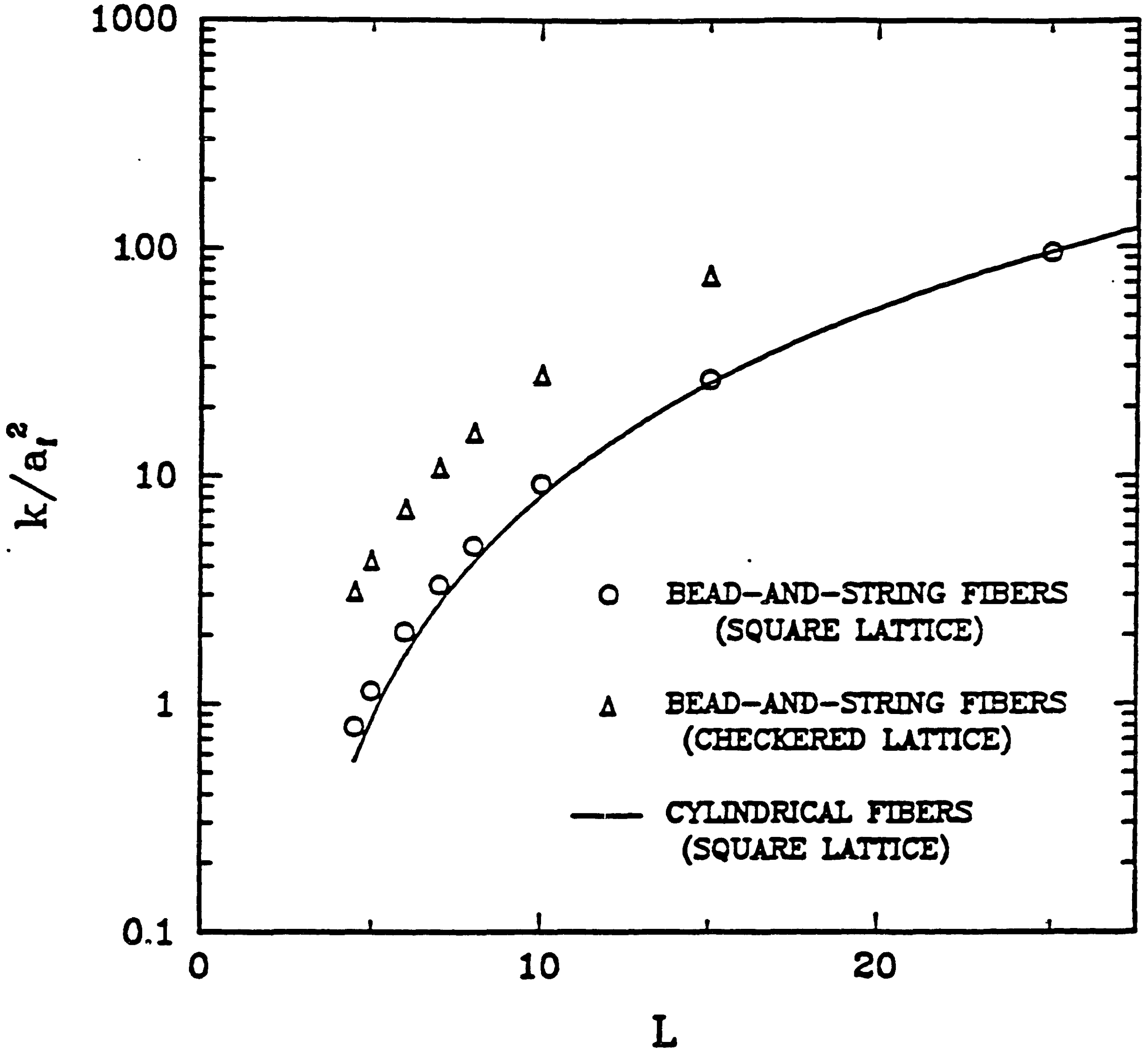

Figure 6.2b - The hydraulic permeability (calculated using (3.3)) is plotted as a function of *L* for a square lattice of bead-and-string fibers, a checkered lattice of bead-and-string fibers, and a square lattice of smooth, cylindrical fibers.

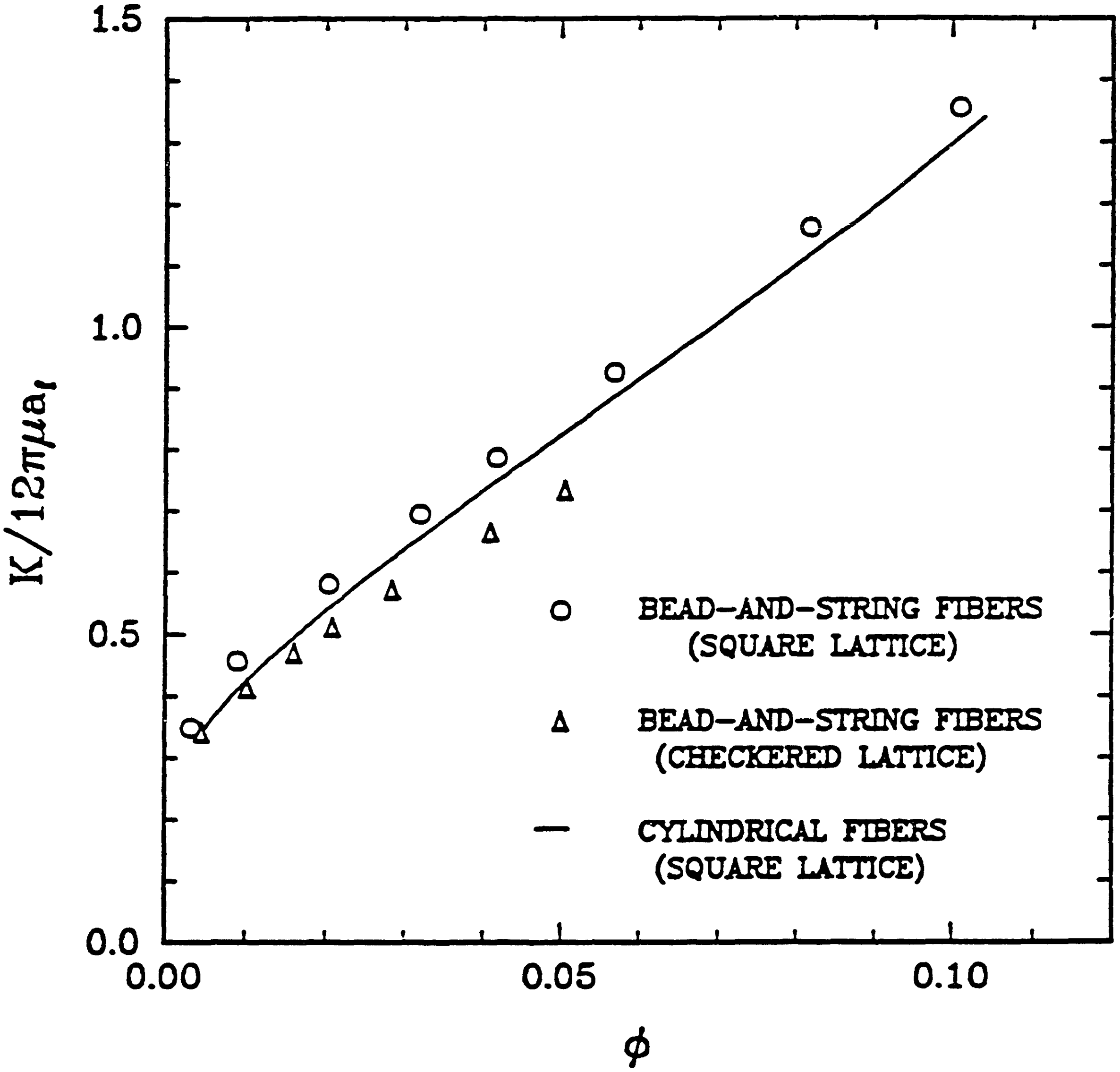

Figure 6.3a - The data of Figure 6.2a are replotted as a function of fiber volume fraction ϕ (*cf.* equations (6.20) and (6.21)).

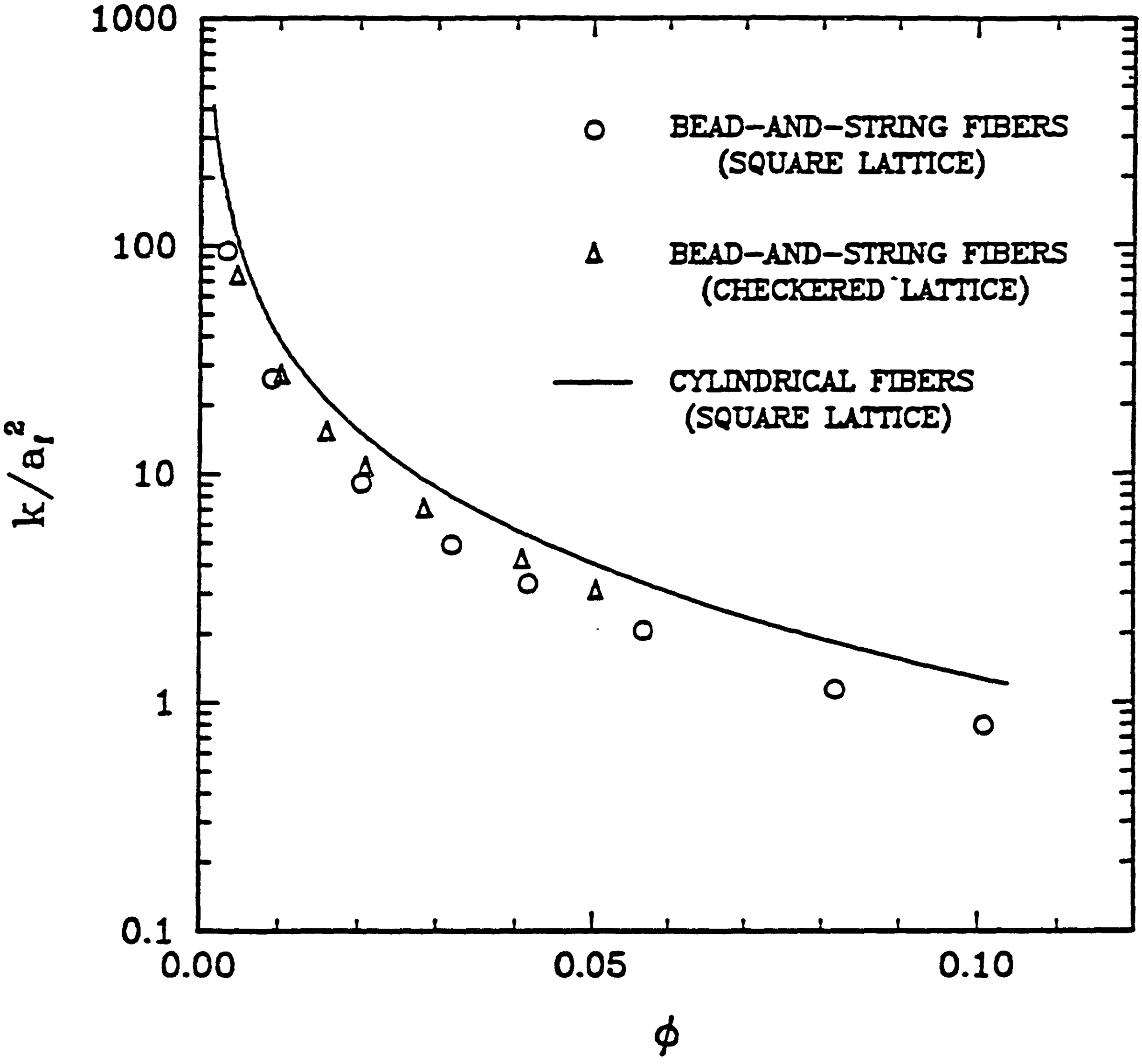

Figure 6.3b - The data of Figure 6.2b are replotted as a function of fiber volume fraction ϕ (*cf.* equations (6.20) and (6.21)).

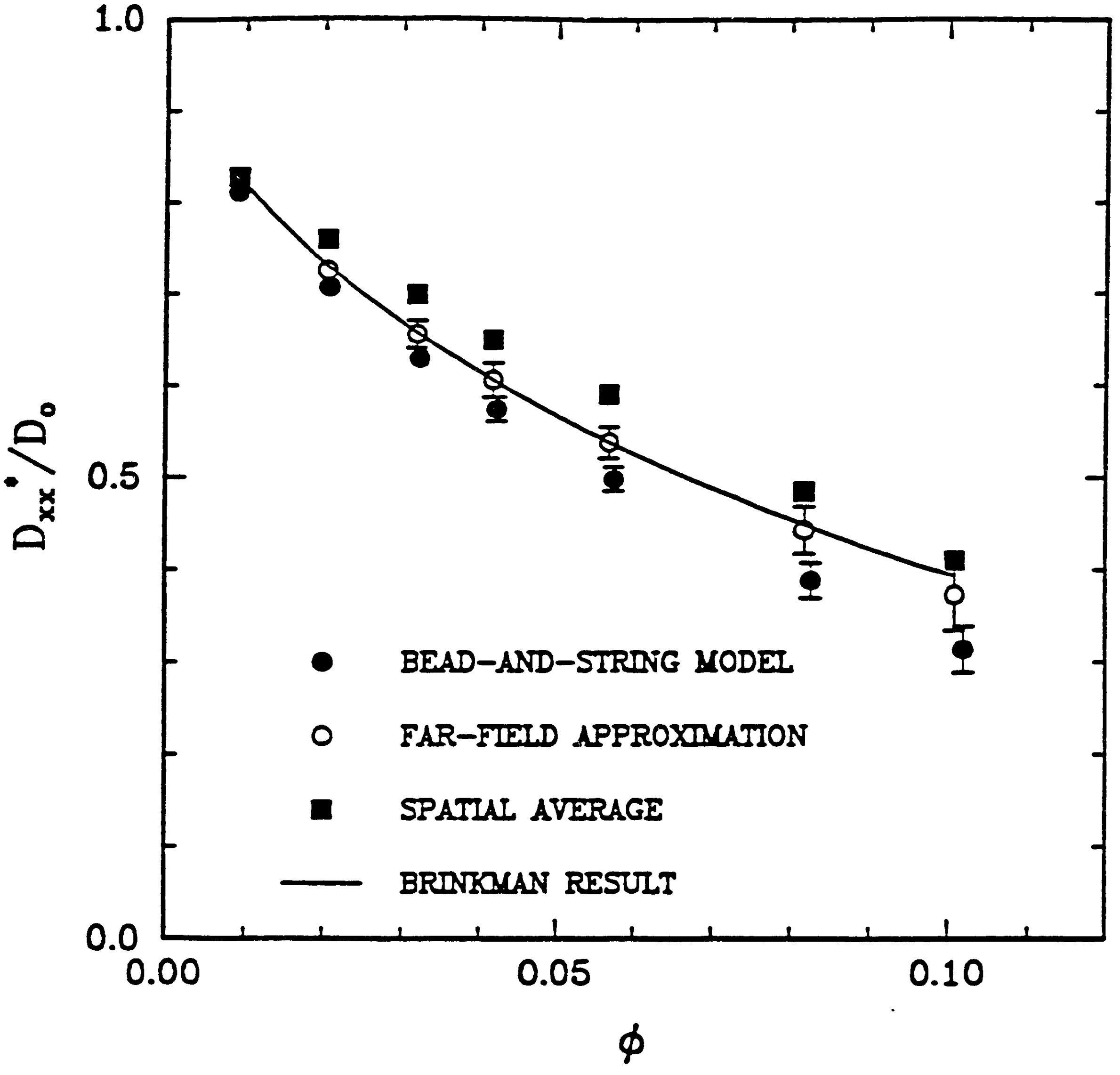

Figure 6.4 - The dimensionless, global dispersion coefficient D_{xx}^*/D_o is plotted as a function of volume fraction ϕ for the case where $\lambda = 1$. The solid circles denote the result obtained from (6.19) using local coefficients calculated from the complete (*i.e.*, including far- and near-field interactions) approximation to the resistance matrix. The open circles show results obtained if near-field interactions are neglected, while the solid squares represent the spatial average of local coefficients that do include near-field interactions. The solid curve is the result predicted by Brinkman's equation (see equation (6.4)) using the hydraulic permeabilities for square lattices of bead-and-string fibers shown in Figures 6.2 and 6.3.

principal effects of the fibers on diffusion, as well as their effect on solvent flow. In other words, the details of the shape and arrangement of the individual fibers appear to be only of secondary importance in determining hindrances to diffusive transport of a macromolecular solute.

The solid squares in Figure 6.4 are the results obtained by neglecting the effects predicted by generalized Taylor dispersion theory and simply spatially averaging the local coefficient $\underset{\approx}{D}^{HD}$. The values obtained in this manner differ significantly from the Brinkman prediction, and even more so from the more rigorous calculation involving (6.15) and (6.19). That one should not expect the spatial average of $\underset{\approx}{D}^{HD}$ to be the same as $\underset{\approx}{D}^{*}$ can be seen clearly by considering the case where a mobile solute is trapped inside a "cage" of surrounding fibers. For the periodic system under consideration here, such a condition could be achieved by setting $L = 4$ using the AA′ cross-section of Figure 6.1. Because the solute is not able to escape from its "cage," the global dispersion coefficient $\underset{\approx}{D}^{*}$ must be zero. However, the local dispersion coefficient $\underset{\approx}{D}^{HD}$ is still finite everywhere except on the lines connecting the fiber centers, and thus the spatial average of $\underset{\approx}{D}^{HD}$ is non-zero. Only by properly solving (6.11) and (6.16) can the correct global coefficients be obtained. This simple example illustrates the important distinction between local and global coefficients.

In Figure 6.5, results for the dispersion coefficient D^{*}_{xx} are shown for values of the ratio of solute radius to fiber radius λ varying from 0.0 to 5.0. The result for $\lambda = 0.0$ was obtained from the work of Perrins *et al.* (1979), and was derived for a square lattice of smooth, cylindrical fibers:

$$\frac{D^*}{D_o} = 1 - \frac{2\phi}{1 + \phi - \dfrac{0.305827\phi^4}{1 - 1.402958\phi^4} - 0.013362\phi^8} . \tag{6.22}$$

Equation (6.22) is valid only for an infinitesimally small solute that does not interact with the fibers. The dashed lines in Figure 6.5 represent a curve-fit to the data shown. The exponential expression used was

$$\frac{D^*_{xx}}{D_o} = \exp(-\alpha\phi^{3/4}) \quad , \tag{6.23}$$

where values of the adjustable parameter α are given by

$$\alpha = 5.1768 - 4.0075\lambda + 5.4388\lambda^2 - 0.6081\lambda^3 \quad , \tag{6.24}$$

and ϕ is the volume fraction of fibers. The expressions (6.23) and (6.24) are presented as an aid to interpolating between results presented for $\lambda = 0.5$ and $\lambda = 5.0$. Thus, no special significance should be attached to the power of ϕ in (6.23), and care should be taken in extrapolating beyond the results shown. No attempt was made to include the result of Perrins *et al.* in the curve-fit. As in Figure 6.4, the solid lines of Figure 6.5 are the Brinkman result given by (6.4) using the values of k shown in Figure 6.3.

For any given ratio of sphere radius to fiber radius, the dispersion coefficient decreases as the volume fraction of fibers increases, as shown in Figure 6.5. Moreover, at a fixed value of ϕ, D^*_{xx}/D_o decreases as λ is increased, due to the more restricted motion of the larger spheres. The trends exhibited by the more rigorous, generalized Taylor dispersion calcu-

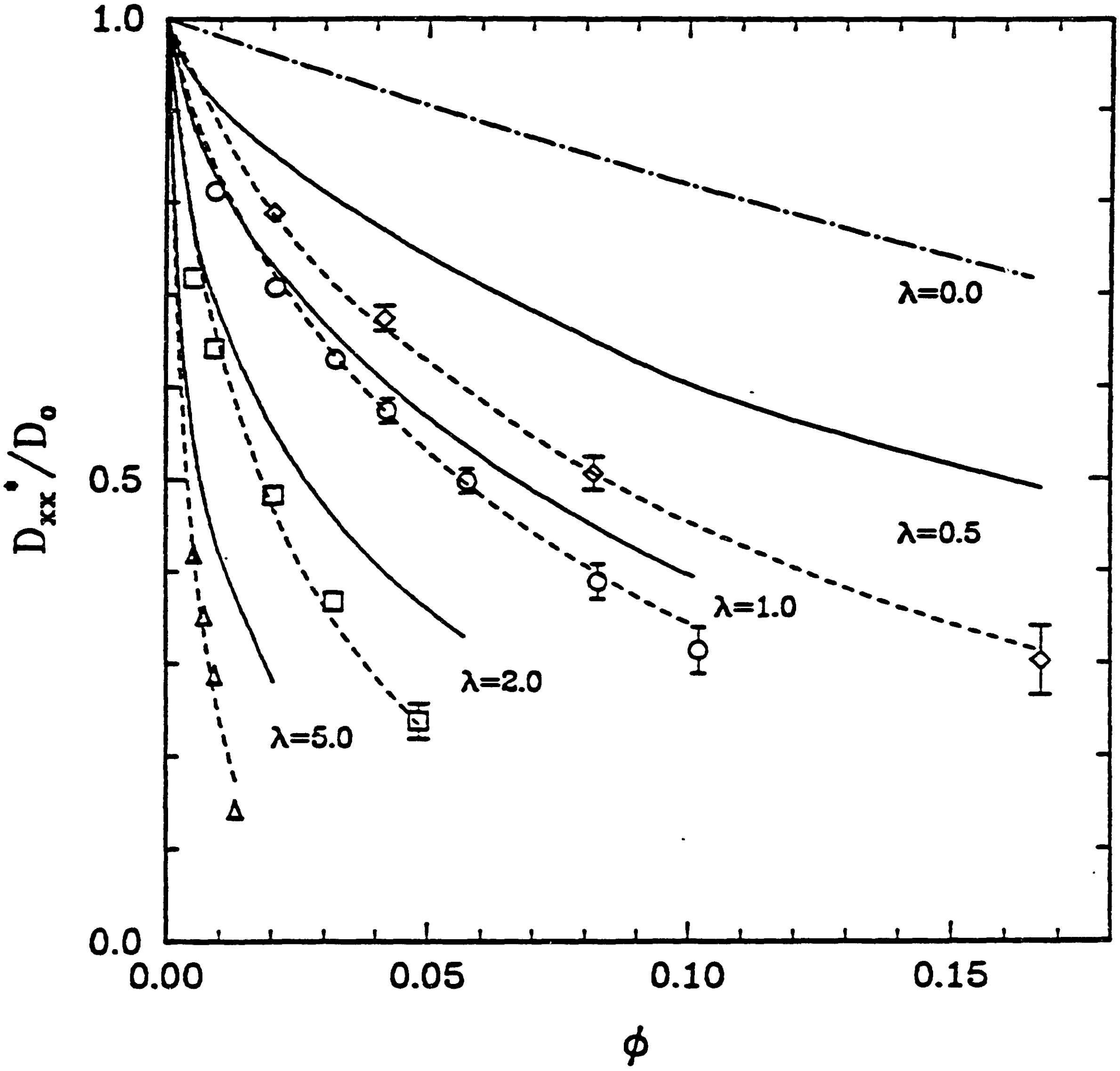

Figure 6.5 - The dimensionless dispersion coefficient D_{xx}^{*}/D_o is plotted as a function of volume fraction ϕ for square lattices of bead-and-string fibers. The points for λ = 0.5 - 5.0 are the Taylor dispersion results, the solid curves are the results of the Brinkman prediction (6.4), and the dashed curves are results of the correlation (6.23). The curve for λ = 0.0 was obtained from the work of Perrins *et al.* (1979).

lations are consistently reproduced by the effective medium results. Quantitative agreement appears to be best for $\lambda = 1.0$ and when the value of D^*_{xx}/D_0 approaches unity. The fact that the Brinkman prediction becomes worse in each case as transport becomes more hindered is consistent with the fact that individual solute-fiber interactions are not accounted for in an effective medium model. Instead, the influence of the fibers is present only in an average sense, and so the more severe hindrances that occur when the solute moves directly between two fibers are not fully taken into account.

In Figure 6.6, values of $U^*_x/\langle u_x \rangle$ are plotted as a function of volume fraction for $\lambda = 1$ in the limiting case where $\langle u_x \rangle \to 0$. As in Figure 6.4, both the far-field and the complete results are plotted. The solid curve is the average fluid velocity given by (6.5). Note that the particle velocity should not be expected to equal the average fluid velocity, even for small ϕ. This is because the finite size of the particle prevents it from sampling regions near solid boundaries, where the fluid velocity is lowest. The far-field approximation tends to overestimate U^*_x by a significant amount. The result obtained from (6.5) underestimates it up to volume fractions of about $\phi = 5\%$, after which point the hindering effect of the fibers causes the particle velocity to fall below the average fluid velocity. Note that this qualitative behavior must be obtained in order for macroscopic transport to cease at $\phi = 0.13$, which corresponds to $L = 4$. The overall effects of the fibers on convective solute transport for $\lambda = 1.0$ are seen to be relatively small over the volume fractions studied, the values of $U^*_x/\langle u_x \rangle$ from (6.15) never deviating more than 10% from unity.

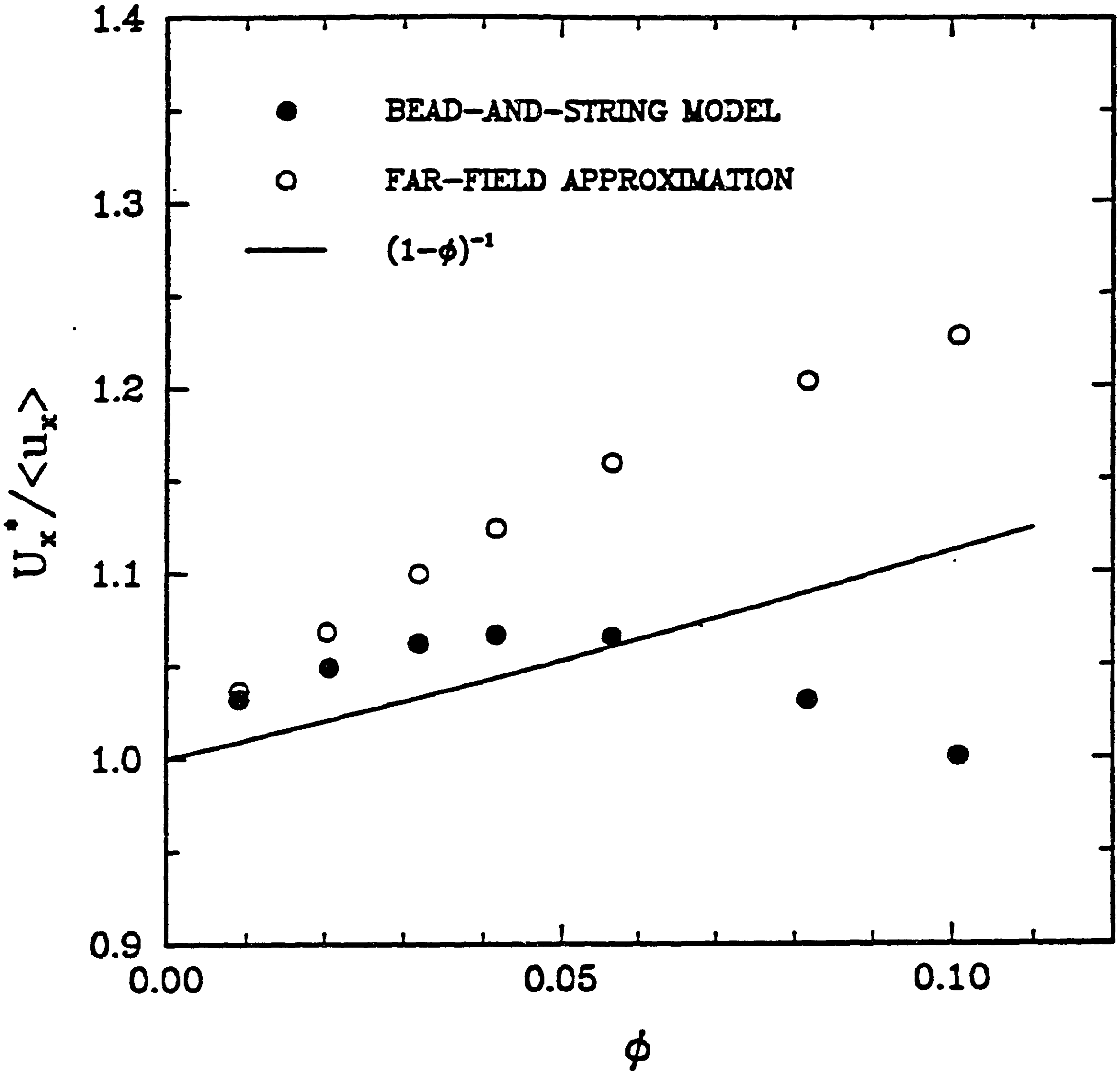

Figure 6.6 - The dimensionless solute velocity $U_x^*/\langle u_x \rangle$ is plotted as a function of volume fraction ϕ for the case where $\lambda = 1$. The solid circles and open circles are analogous to those in Figure 6.4, and show the results obtained from (6.15) using the complete and far-field approximation to the resistance matrix, respectively. The solid line is the average fluid velocity given by (6.5).

In Figure 6.7, values for $U_x^*/\langle u_x \rangle$ are shown for values of λ varying from 0.5 to 5.0. In this case, the value of $U_x^*/\langle u_x \rangle$ corresponding to $\lambda = 0$ is given by (6.5), the average fluid velocity. The parabolic shape of the curves in Figure 6.7 can be understood in the context of the competing effects felt by the spherical solute when exposed to fluid flow. One effect is that the finite size of the solute prevents it from sampling positions closest to solid boundaries, where the fluid velocity is slowest. On this basis, one expects finite-sized solutes to move through the fibrous medium faster on average than does the fluid. This trend has been found theoretically for both cylindrical pores (Brenner and Gaydos, 1977) and for periodic porous media in general (Brenner and Adler, 1982), and has been observed experimentally for colloidal particles moving through porous beds (Small, 1974; Silebi and McHugh, 1979). However, as the radius of the solute is increased and grows closer to the gap spacing between adjacent fibers, at some point its motion begins to be hindered by hydrodynamic interactions with those fibers. This hindrance will eventually dominate to the point where $U_x^* = 0$ for all $\langle u_x \rangle$ when $L = 2 + 2\lambda$ (using the AA′ cross section).

The two curves in Figure 6.7 which lack significant maxima do so for different reasons. For $\lambda = 0.5$, the solute is able to sample a relatively high fraction of the fluid volume. Thus, at this low value of λ the average solute velocity will most closely approximate the average fluid velocity, and even weak interactions with the fibers will cause it to fall below the line given by (6.5). In contrast, for $\lambda = 5.0$ the particle is restricted to sampling the portion of fluid moving most quickly. However, even at values of ϕ as low as 0.01, such a large solute will be significantly hindered by

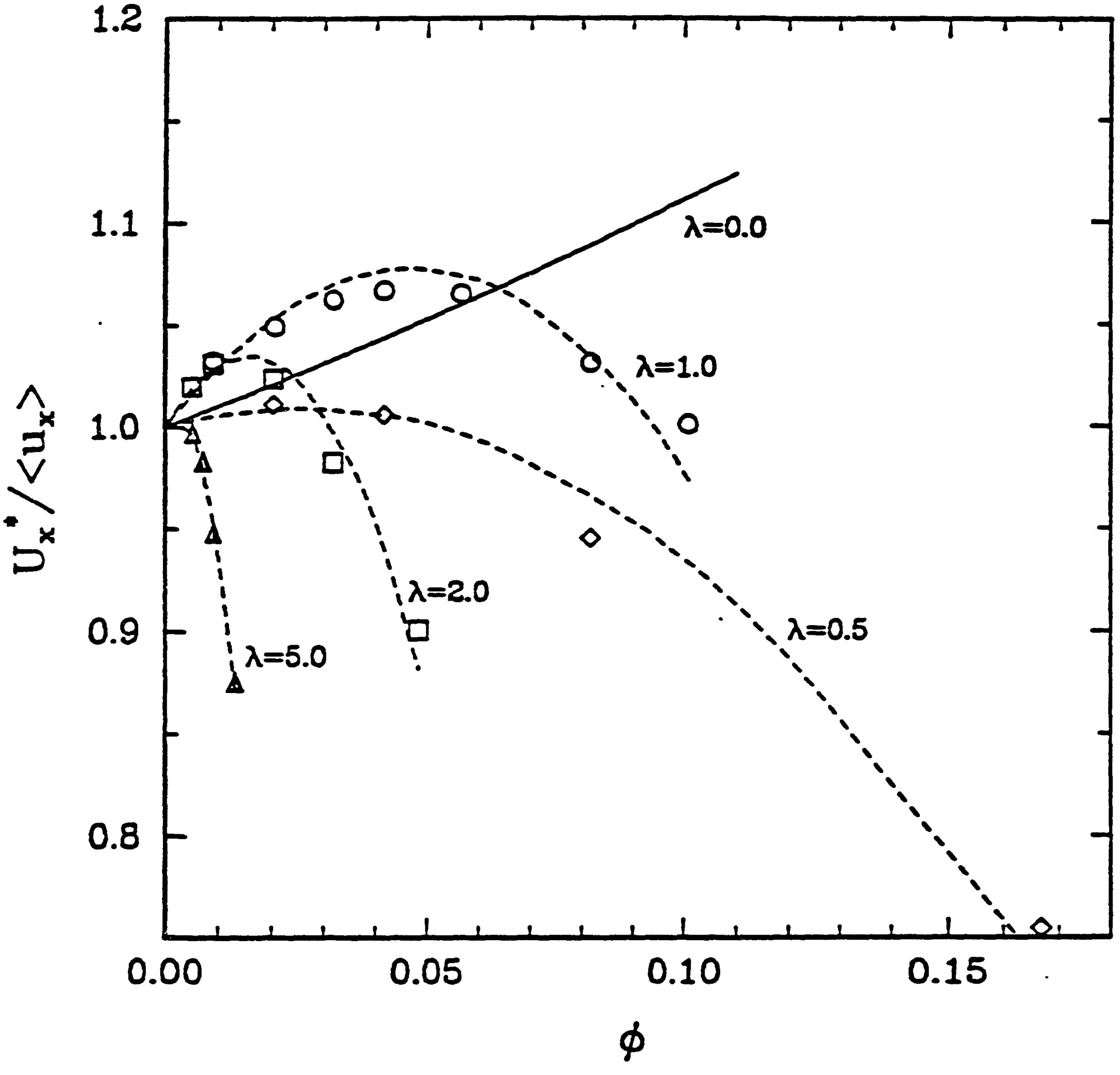

Figure 6.7 - The dimensionless solute velocity $U_x^*/\langle u_x \rangle$ is plotted as a function of volume fraction ϕ for square lattices of fibers. The points for $\lambda = 0.5 - 5.0$ are the Taylor dispersion results, and the dashed lines show the results of the correlation (6.25). The solid line is the average fluid velocity given by (6.5).

interactions with the immobile fibers and thus the curve descends very quickly. The other two curves, corresponding to $\lambda = 1.0$ and $\lambda = 2.0$, each show a definite maximum before the effects of solute-fiber hydrodynamic interactions become dominant.

As with the results shown in Figure 6.5, the curves in Figure 6.7 have been fitted to an analytical expression to aid in interpolation. The polynomial expression used, shown as dashed curves in Figure 6.7, is

$$\frac{U_x^*}{\langle u_x \rangle} = 1 + \beta\phi + \gamma\phi^2 \tag{6.25}$$

where

$$\beta = 5.1712 - 0.9724(1/\lambda) - 1.1355(1/\lambda)^2 + 0.2511(1/\lambda)^3 \tag{6.26a}$$

and

$$\gamma = -9.97883 + 8.9787\lambda - 31.6717\lambda^2 - 2.9586\lambda^3 \quad . \tag{6.26b}$$

Again, caution should be used in applying (6.25) and (6.26) outside the range of parameters studied here ($0.5 < \lambda < 5.0$).

The results shown in Figures 6.4-7 are valid in the limit of low Peclet number, $Pe = \langle u_x \rangle a_f/D_o \rightarrow 0$. For nonzero Pe, the probability distribution P_o^∞ in (6.15) changes, and thus, in principle, both D^*/D_o and $U_x^*/\langle u_x \rangle$ can change also. In Figure 6.8, D^*/D_o is plotted versus Pe for $\lambda = 1$ and various values of ϕ. As seen in many other systems (Taylor, 1953; Brenner and Gaydos, 1977; Brenner and Adler, 1982), the dispersion coefficient increases with increasing Peclet number. In interpreting Figure 6.8 it is important to note that the length scale used in the Peclet number is the fiber radius. In most applications, even where convection contributes appreciably to the macroscopically observable transport, this "microscopic" Peclet number will

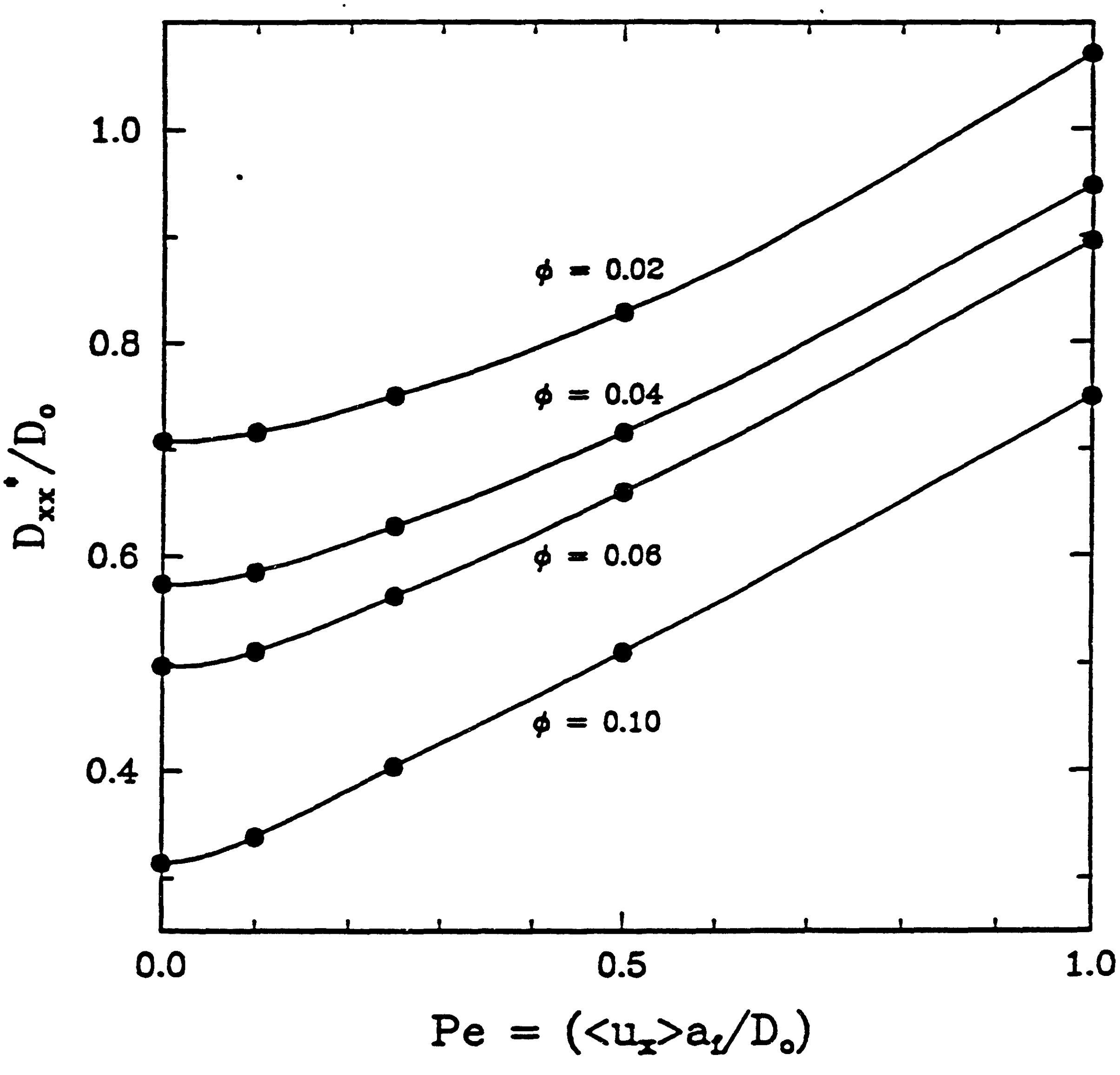

Figure 6.8 - The dimensionless, global dispersion coefficient D_{xx}^{*}/D_o is plotted as a function of Peclet number *Pe* for $\lambda = 1$ and volume fractions ranging from $\phi = 0.02$ (L = 10.0) to $\phi = 0.10$ (L = 4.5). Although the error bars have been left off for clarity, they are comparable in size or smaller than those shown in Figure 6.4 for the corresponding volume fraction.

be exceedingly small. Thus, in general, the effect of *Pe* on D^*_{xx} will be negligible, as has been shown for hindered transport in cylindrical pores (Deen, 1987). The dependence of $U^*_x/\langle u_x \rangle$ on *Pe* did not significantly alter the results shown in Figures 6.6 over the range of *Pe* considered ($Pe \leq 1$).

6.2.3 Inhomogeneous Fiber Matrix

A variation of the spatially periodic lattice was studied in order to examine the impact of spatial heterogeneity on dispersive behavior, as well as to see how such a change would affect the agreement between the two theoretical approaches used. The "checkered" lattice used for this purpose is shown in Figure 6.9. To relate this pattern to the previous geometry, consider grouping the fibers of a square lattice such as that in Figure 6.1 into cells of 4 fibers each, and then removing alternating cells in both the *x* and *y* directions. The resulting lattice provides a model system containing significant variations in fiber density. As with the square lattice, AA′ and BB′ cross-sections can be used for calculations on the checkered lattice. Thus, where local coefficients from the two cross-sections yield different results, error bars will again be used to mark the range of the two values. It was found that a periodic cell containing 81 spheres (8 fibers of 10 spheres each and one mobile sphere) was sufficient to limit errors related to the cell size to about 2%.

In Figure 6.10, values of the dispersion coefficient for the checkered lattice are plotted versus *1/L*. Values for the square lattice are also shown, as are the Brinkman predictions for the two cases. Hydraulic

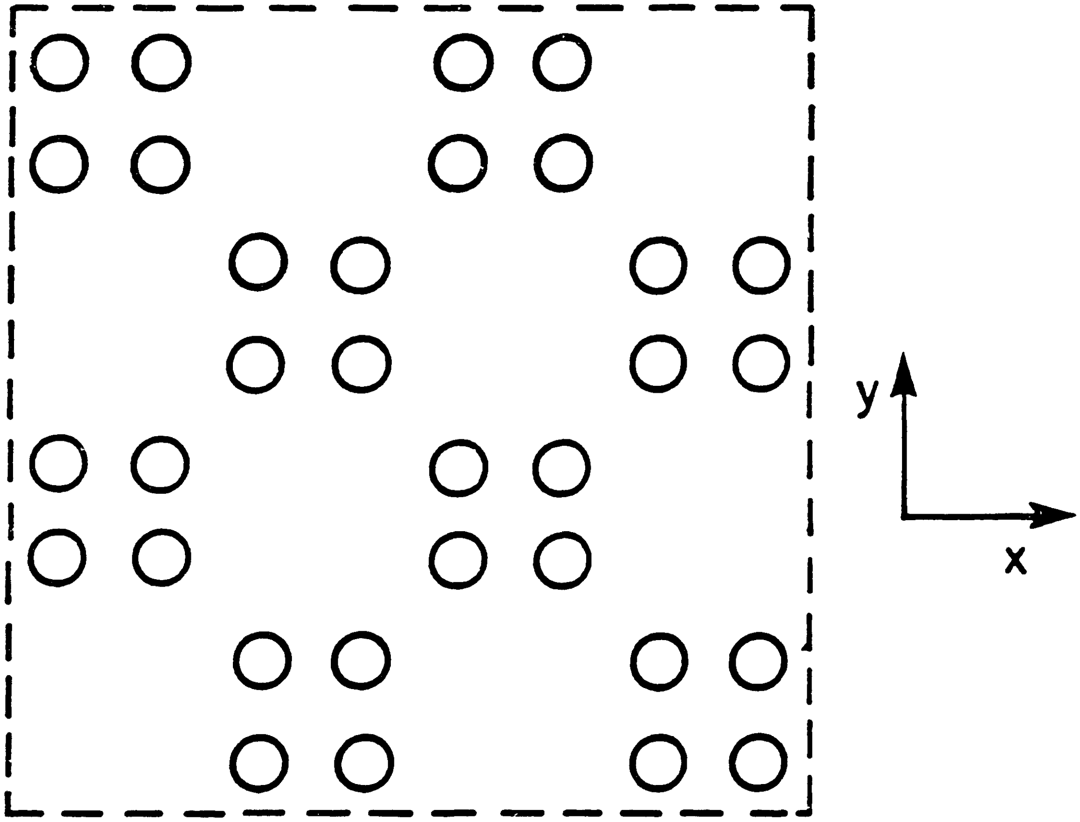

Figure 6.9 - Transverse section of a spatially periodic, checkered lattice of bead-and-string fibers.

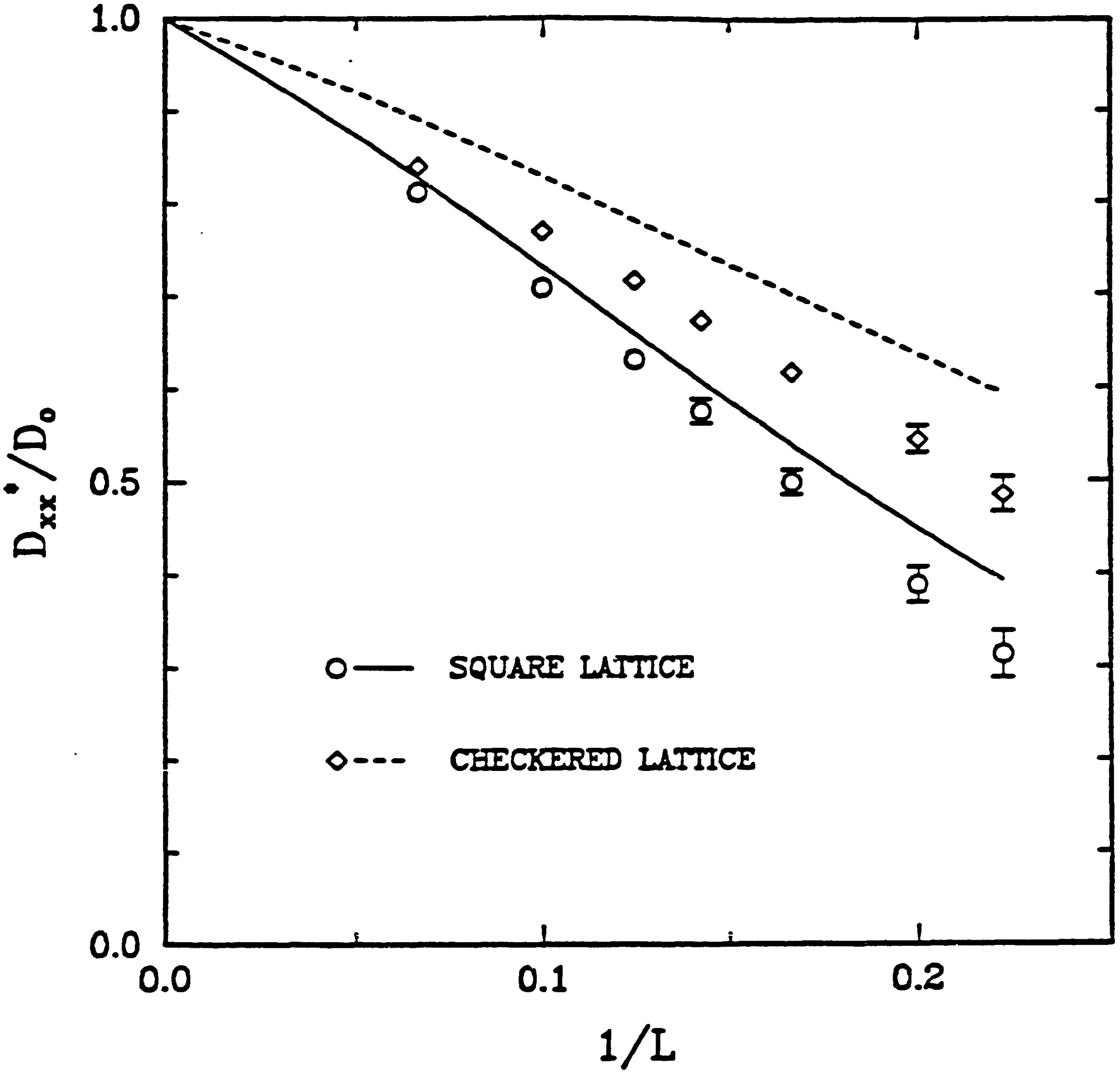

Figure 6.10 - The dimensionless dispersion coefficient D_{xx}^*/D_0 is plotted as a function of $1/L$ for a checkered lattice of bead-and-string fibers. Results for a square lattice of fibers (*cf.* Figure 6.4) are included for comparison. All results shown are for $\lambda = 1$. The two curves shown were calculated using the Brinkman prediction (6.4).

permeabilities used for the checkered lattice were obtained using the Stokesian dynamics method (*cf.* Equation (3.3)) and are shown in Figure 6.3. As one would expect, removing alternate groups of fibers while keeping L the same results in an increase in the dispersion coefficient. In addition, one sees that once again there is qualitative agreement between the more rigorous results and the Brinkman prediction (6.4). However, the effective medium approach seems to lose accuracy for the less homogeneous matrix.

The dispersion data of Figure 6.10 are plotted versus the volume fraction of fibers in Figure 6.11. In interpreting this graph one should note that, for a given value of ϕ, the checkered lattice will have a much lower value of L than will the square lattice. In other words, the checkered lattice, which has large regions in which there are no fibers, must have much smaller gaps between those fibers that do remain in order to have the same volume fraction as the homogeneous, square lattice. This results in the dispersion coefficients for the inhomogeneous fibrous medium actually being lower than those for the homogeneous medium at the same volume fraction. Significantly, the effective medium approach misses this effect of inhomogeneity entirely, and predicts that the inhomogeneous medium, which has a slightly higher permeability, will also have a higher dispersion coefficient.

One should also note the fact that both theories predict only a slight change in the dispersion coefficient when plotted versus ϕ. This suggests that contributions from those regions in the inhomogeneous medium that do not contain fibers, where local dispersion coefficients are relatively high, roughly cancel those from the regions of tightly packed fibers, where

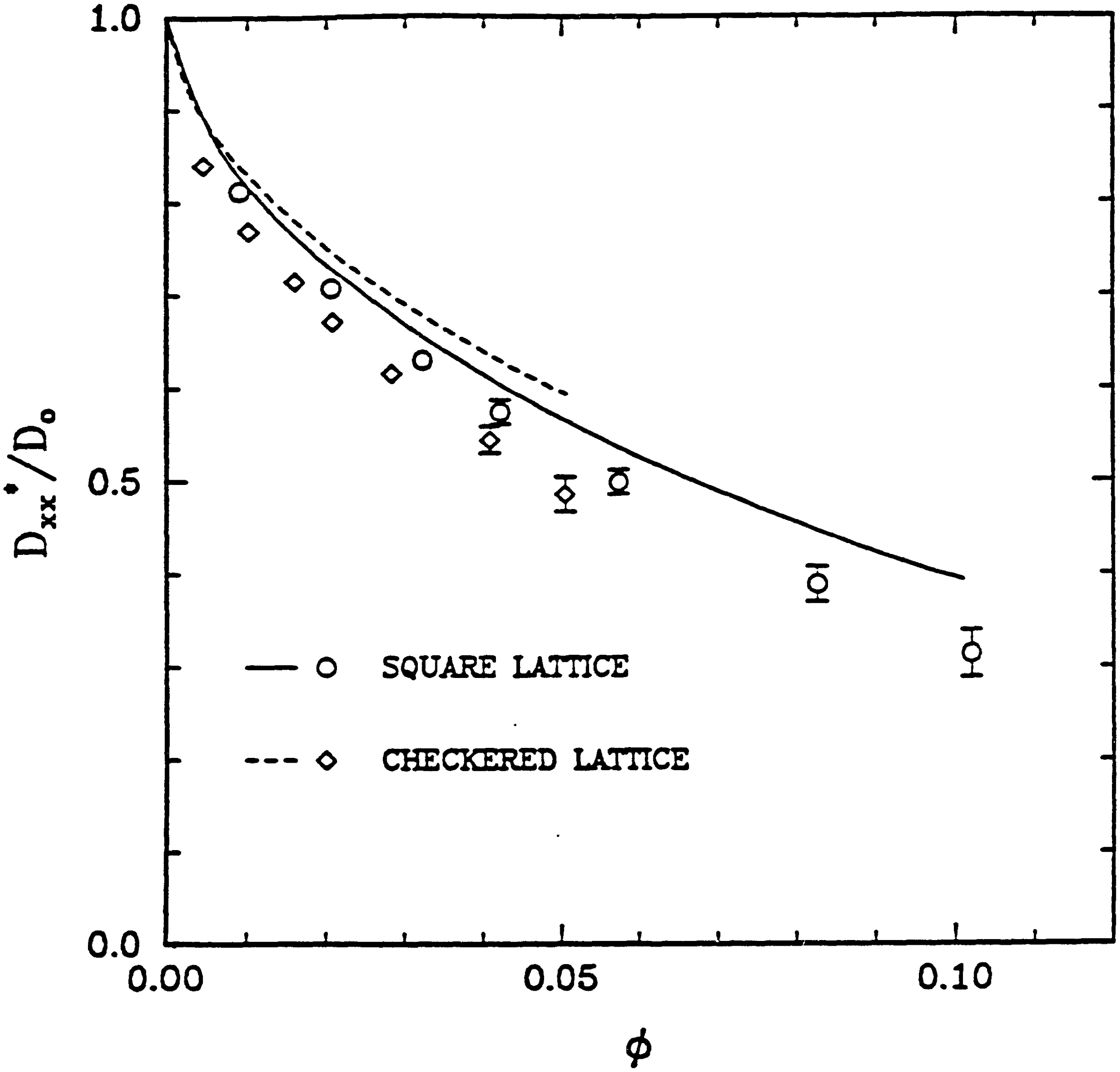

Figure 6.11 - The results of Figure 6.10 are replotted as a function of the volume fraction of fibers ϕ.

local dispersion coefficients are relatively low. Thus, the most important parameter in describing transport is simply the volume fraction. This fact is particularly significant since it is often easier to measure the volume fraction of fibers than it is to describe other, more subtle features of the microstructure.

Values of $U_x^*/\langle u_x \rangle$ for the square and checkered lattices are shown in Figure 6.12. The two sets of results are similar, except that at the higher values of $1/L$ the fibers hinder the solute somewhat less for the "checkered" lattice since there are large gaps where no fibers are present. For both systems the overall effect is small, $U_x^*/\langle u_x \rangle$ never deviating from unity by more than about 10%.

6.2.4 Comparison With Experiment

Calculations involving the more rigorous bead-and-string model are rather involved, and therefore have only been carried out for periodic lattices of fibers. However, the results predicted by Brinkman's equation, which agree closely with the more rigorous theory, can be readily applied to any fibrous system for which the hydraulic permeability is known. Indeed, the good agreement between these two approaches suggests that the effective medium model may be a very useful one for fibrous systems in general. It is therefore of interest to compare the predictions of (6.4) with experimental data taken from the literature.

Laurent and Pietruszkiewicz (1961) and Laurent *et al.* (1963) measured the sedimentation rates, and hence friction coefficients, of several proteins in hyaluronic acid solutions. Hydraulic permeabilities for

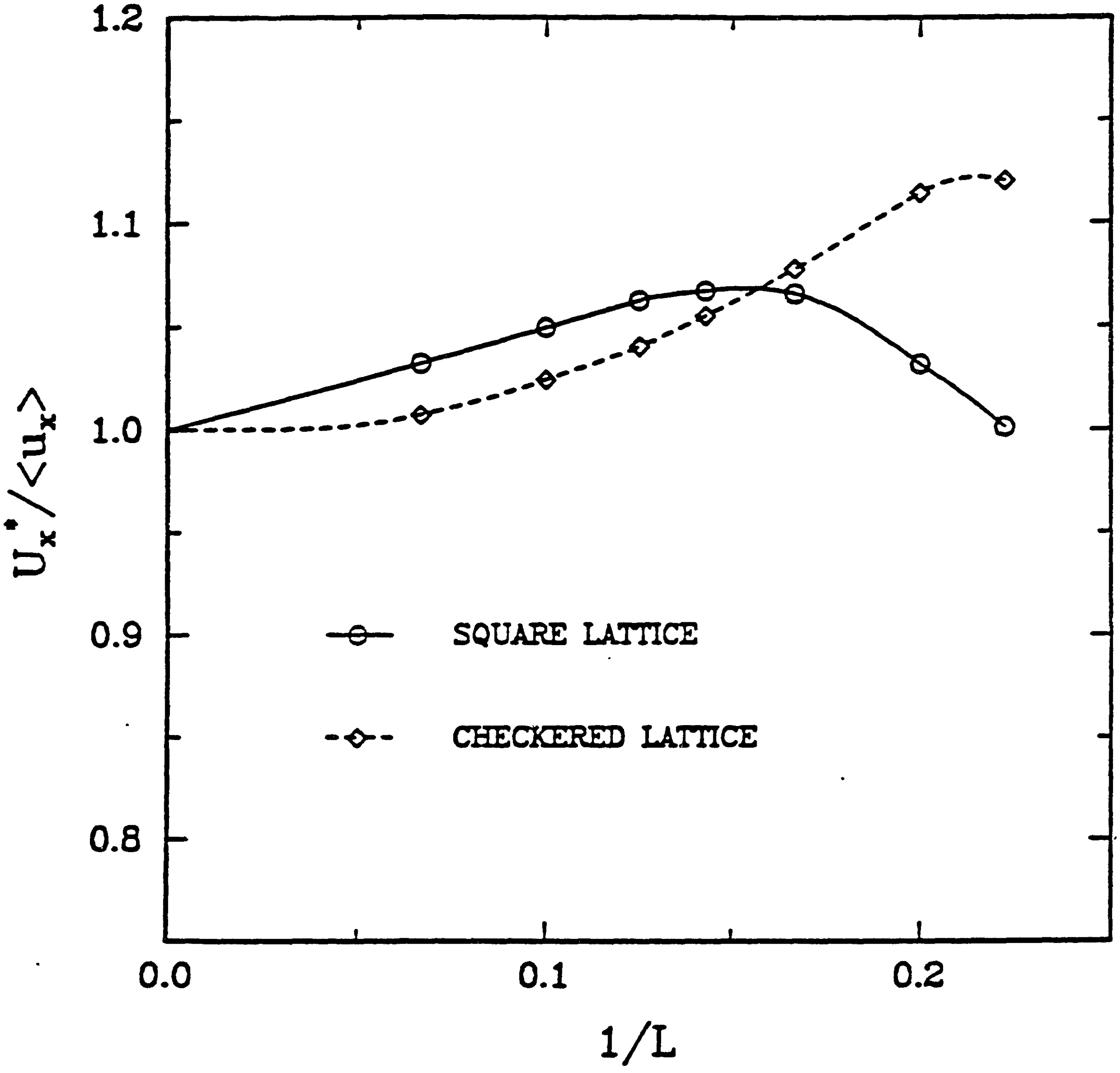

Figure 6.12 - The dimensionless solute velocity $U_x/\langle u_x \rangle$ is plotted as a function of *1/L* for a checkered lattice of bead-and-string fibers, for the case where $\lambda = 1$. Results for a square lattice of fibers are included for comparison (*cf.* Figure 6.6). The curves were fitted to the data shown.

hyaluronic·acid solutions have been measured by several research groups, and the results are critically summarized by Ethier (1986). In Figure 6.13, the results predicted using (6.4) together with the experimentally measured hydraulic permeability data are compared with the experimental results for D^*/D_o. In generating the solid curves shown, the sphere radius a_s in (6.4) was assumed to be equal to the Stokes-Einstein radii r_s of the proteins. As shown, theory and experiment agree to within about 2-3% for the γ-crystallin and bovine serum albumin measurements, and to within 10% for the human γ-globulin, α-crystallin, and turnip yellow mosaic virus measurements. Note that these solutes represent more than a 5 fold variation in the Stokes-Einstein radius. Remarkably, no adjustable parameters were needed to obtain this excellent agreement between theory and experiment. In addition, the only structural information required was the Stokes-Einstein radius of the diffusing macromolecules and the hydraulic permeability of the hyaluronic acid medium. Such information is readily available for many systems of interest. Thus, the simplicity and accuracy of the effective medium model suggest that it could be of great use in predicting rates of hindered transport through fibrous membranes and gels used in both physiological and industrial processes.

6.3 DISCUSSION

Two methods of calculating hindered transport coefficients in fibrous media have been discussed and compared. The first was an effective medium theory based on Brinkman's equation. The fact that the Brinkman prediction given by (6.4) requires very little information on the details of the

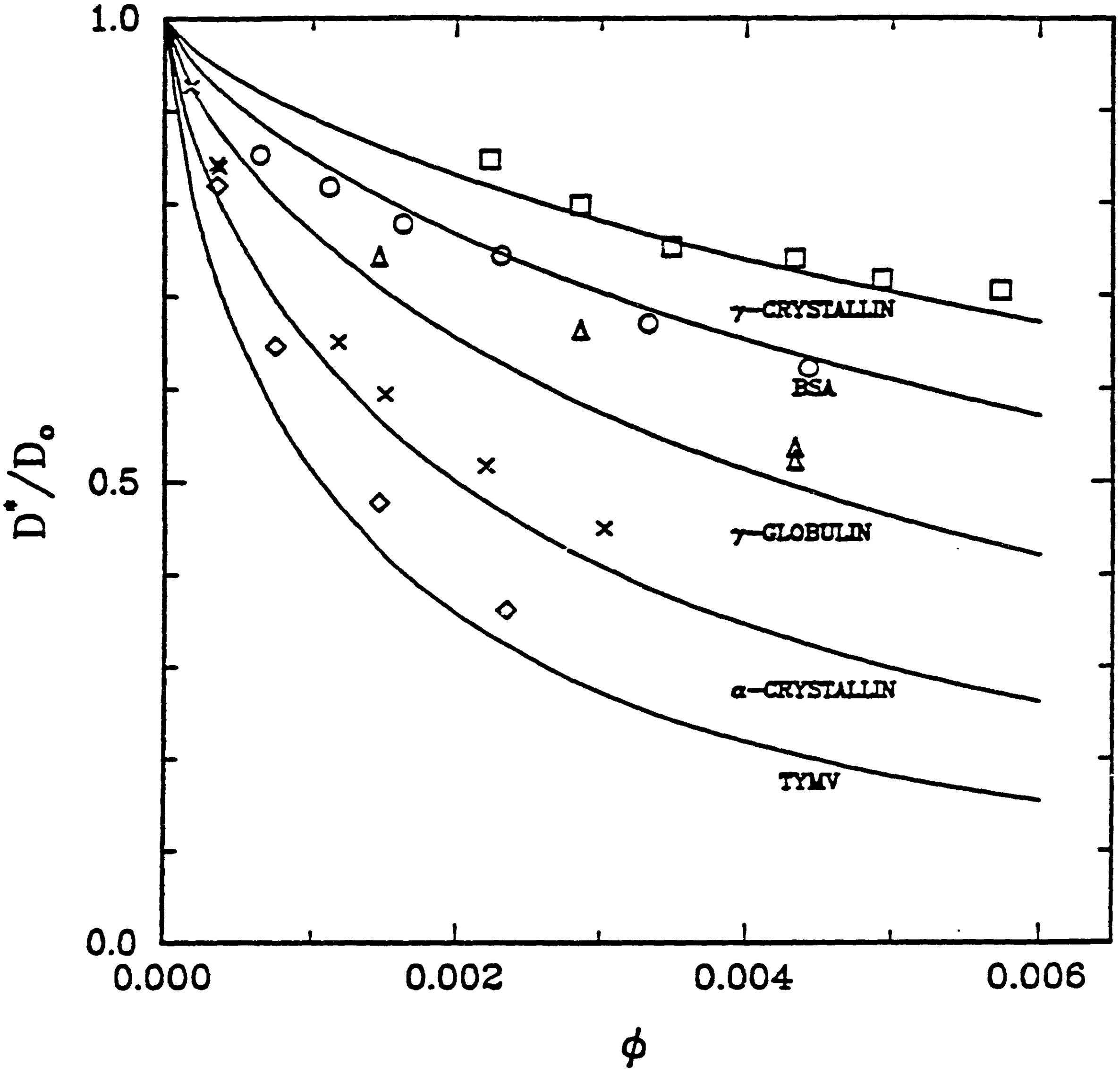

Figure 6.13 - Dispersion coefficients that were measured experimentally for proteins in hyaluronic acid solution (Laurent and Pietruszkiewicz, 1961; Laurent *et al.*, 1963) are compared with values predicted by (6.4). The macromolecules used and their Stokes-Einstein radii r_s are γ-crystallin (r_s = 23.5Å), bovine serum albumin (r_s = 34Å), human and bovine γ-globulin (r_s = 56Å), α-crystallin (r_s = 97Å), and turnip yellow mosaic virus (r_s = 155Å). Experimental data reported in Ethier (1986) were used in (6.4) to obtain the values predicted by Brinkman's equation (solid curves).

fibrous microstructure could make it very useful in a variety of practical situations. However, it suffers the drawback that it is not able to account for local solute-fiber interactions which, under certain conditions, can be very important. The second method, which involves deriving global transport coefficients from local coefficients using generalized Taylor dispersion theory, is by far the more rigorous of the two theories. However, it requires the assumption of a particular arrangement of fibers in order to obtain results. Since this information is not available in many practical situations, it is worthwhile to gain some idea of how accurate the first method is as well as how important a role the fibrous microstructure might play.

To begin to ascertain this information, a series of calculations were performed in which the predictions of the two theories were compared for a square lattice of bead-and-string fibers. For a given volume fraction of fibers, the dispersion results obtained showed a strong dependence on λ, the ratio of the solute radius to the fiber radius, with the value of D^*_{xx} decreasing significantly as λ was increased from 0.5 to 5.0. The solute velocities showed evidence of competing effects with changes in either ϕ or λ, as larger solutes are restricted from sampling regions where the fluid velocity is lowest, but are also more severely hindered by hydrodynamic interactions than are smaller solutes. The effective medium approach consistently predicted the trends in the dispersion coefficients calculated by the more rigorous method. However, quantitative agreement varied depending on the fiber volume fraction and the value of λ.

In addition, the homogeneous, square lattice was modified to the less homogeneous "checkered" lattice of fibers, in which alternate groups of four fibers were removed. Interestingly, when plotted versus the volume fraction ϕ, values of the dispersion coefficient for the two systems were very similar. This suggests that the details of the microstructure of the inhomogeneous system were much less important than the overall volume fraction. Again, the effective medium result correctly predicted that removal of some fibers would lead to an increase in the dispersion coefficient, but it seemed less accurate for the inhomogeneous medium than it was for the homogeneous, square lattice.

One might wonder to what extent the approximations made in the Stokesian dynamics method affect the comparisons between the Brinkman prediction (6.4) and the Taylor dispersion results. In Chapters 3 and 5 it was shown that Stokesian dynamics tends to underestimate the drag coefficients of particles in porous media (*cf*. Figures 3.1(a,b,c) and 5.1). One would therefore expect hydraulic permeabilities calculated using Stokesian dynamics to be higher than the actual value, making the agreement shown in Figures 6.4 and 6.5 appear less favorable than it would if the true value of k were used in (6.4). It is assumed here that the local dispersion coefficients used in the Taylor dispersion calculations were close approximations to the actual values since, for every case considered in Chapters 3-5 where there was relative motion between sphere surfaces, Stokesian dynamics was shown to yield highly accurate results (*cf*. Figures 3.2, 3.3, 4.4, 4.10, and 5.3). Thus, if the approximations used in Stokesian dynamics did affect the results presented here, then the error incurred would tend to make the agreement between the Brinkman prediction and the Taylor dispersion results appear worse than is actually the case. However, one should bear in mind that, at the volume fractions considered in the fibrous media calculations ($\phi < 0.17$), the permeabilities reported in Chapters 3 and 5 were always in excellent agreement with other theoretical and experimental results (*cf*. Figures 3.1(a,b,c) and 5.1).

Although remarkably accurate in many of its predictions, the inability of the effective medium model to capture local interactions can lead to highly inaccurate results under certain conditions. As an example, consider transport of a spherical solute in a square lattice of cylindrical fibers. In the limit where the interfiber spacing L grows very large (or $\phi \rightarrow 0$), Hasimoto (1959) calculated the permeability as

$$\frac{k}{a_f^2} = \frac{-\ln\phi}{8\phi} \quad , \tag{6.27}$$

and thus

$$\frac{k}{a_s^2} = \frac{-\ln\phi}{8\lambda^2\phi} \quad . \tag{6.28}$$

If one additionally considers the case where $\lambda = L-2$, so that transport is severely hindered, then one obtains for $L >> 2$

$$\phi = \frac{\pi}{L^2} \approx \frac{\pi}{\lambda^2} \quad . \tag{6.29}$$

Substituting (6.28) and (6.29) into (6.4) and considering the limit where $\phi \rightarrow 0$ and $\lambda \rightarrow \infty$ gives

$$\frac{D^*}{D_o} = 1 \quad . \tag{6.30}$$

In actuality, one clearly expects the dispersion coefficient to be zero when $\lambda = L-2$, which corresponds to the diameter of the solute equaling the spacing between two adjacent fibers. The effective medium model fails to capture the interactions that hinder a large solute in an extremely dilute fibrous medium, since these interactions originate more from the two nearest fibers than from the fibrous bed as a whole. This example should serve as a caution against applying an effective medium approach in cases where transport is severely hindered, since these types of local interactions are expected to be most significant under such conditions. Choosing a specific value of D^*/D_0 that constitutes "severe hindrance" is somewhat arbitrary, but based on Figure 6.5 a choice of about 0.5 would seem reasonable.

In spite of its inaccuracy under certain conditions, one should note that the only information required to obtain the results from (6.4) is the hydraulic permeability of the fibrous medium and the solute radius. Each of these parameters is easily obtained for many physical situations, and thus the effective medium approach provides a means for making at least reasonable estimates for D^*/D_0 based on very little information.

For many applications it is desirable to write the solute flux in (6.1) in terms of a concentration C instead of $\overline{P}$. The use of concentration in conjunction with finite-sized solutes can pose conceptual difficulties since, because of steric interactions, no more than one solute macromolecule can be located in a finite region at a given time. However, these difficulties do not give rise to inconsistencies so long as C is recognized as representing a time average at a particular point (for a macroscopically steady process) or, alternatively, a spatial average covering many equivalent positions in the fibrous matrix. For transport which is macroscopically one-dimensional in the x direction, "equivalent" positions are those having the same value of x.

In computing fluxes across phase boundaries, it is important to note that the volume occupied by the fibers, and the solute-fiber steric interactions, will result in discontinuities in both the fluid-phase and volume-average concentrations. Thus, appropriate boundary conditions under these circumstances will require the use of partition coefficients. Because the probability density $\bar{P}$ used in (6.1) represents an average over the total volume, including fluid and fibers, the partition coefficient Φ describing the discontinuity in concentration must be based on the total volume also. For systems involving only steric interactions, values of Φ can therefore be computed by dividing the volume accessible to the solute center by the total volume of the medium. For the square lattice of bead-and-string fibers shown in Figure 6.1, the resulting expression for Φ is

$$\Phi = 1 - [(\lambda+1)^3 - \frac{1}{2}(\lambda-d/2)^2(2\lambda+3+d/2)] \tag{6.31}$$

Note that the form of (6.31) will vary depending on the geometry of the fibrous medium of interest. For example, the partition coefficient for a sphere in a random array of fibers has been shown to have an exponential dependence on ϕ (Ogston, 1958; Fanti and Glandt, 1989).

By comparing Φ and D^*_{xx}/D_0, one can get an estimate of the relative importance of partitioning and hydrodynamic interactions in hindered transport through a fibrous membrane composed of a square lattice of fibers. Such a comparison is made in Table 6.1. It would appear that, for this particular geometric configuration and for the range of λ considered here, partitioning and hydrodynamic effects are of comparable importance. Although the values given in Table 6.1 could vary greatly for other fiber configurations and other values of λ, they do suggest that hydrodynamic interactions can play a very significant role in the transport of spherical macromolecules across fibrous membranes and gels.

TABLE 6.1

Comparison of Values of Dispersion and Partition Coefficients[a]

	$\lambda = 0.5$		$\lambda = 1.0$		$\lambda = 5.0$	
ϕ	Φ	D^*_{xx}/D_o	Φ	D^*_{xx}/D_o	Φ	D^*_{xx}/D_o
0.003	0.9902	0.9445	0.9832	0.9260	0.8356	0.5610
0.006	0.9804	0.9084	0.9663	0.8787	0.6711	0.3782
0.010	0.9674	0.8685	0.9439	0.8272	0.4519	0.2402
0.050	0.8370	0.6242	0.7194	0.5302	-	-
0.100	0.6741	0.4527	0.4388	0.3441	-	-
0.170	0.4459	0.3073	-	-	-	-

[a] Values shown are for a square lattice of bead-and-string fibers with $\lambda = 1$.

CHAPTER 7

CONCLUSION

The Stokesian dynamics method of calculating hydrodynamic interactions in unbounded systems of spheres is a powerful new approach to studying suspensions and porous media. Because this method does not require that any restrictions be placed on the locations of the spherical particles within a unit cell, it is well suited for use in studying systems with different microstructures. In this thesis it has been applied to calculating such parameters as diffusion coefficients, drag coefficients, and viscosities for both spatially periodic and disordered hard-sphere dispersions. In addition, fibrous systems were studied using "bead-and-string" fibers formed by aligning spheres in rows. This method is also adaptable for use in dynamic simulations, or "computer experiments" in which particle trajectories are calculated and followed over time, although none were reported here. Indeed, Stokesian dynamics was originally developed for this purpose, and modified versions of the method described in Chapter 2 have already been of use in gaining a better understanding of the properties of suspensions (Brady and Bossis, 1988).

Stokesian dynamics is an approximate method, and relies upon the assumption that hydrodynamic interactions can be separated into two categories. Far-field interactions are accounted for in terms of a moment expansion of the force density on the particle surfaces about their centers. In principle this expansion could be carried out to any level of accuracy desired, but in the development provided in this thesis it is truncated at the level of quadrupole moments, which are themselves calculated using a mean-field approximation. Near-field, or lubrication interactions are calculated in a pairwise additive fashion and are added to the far-field interactions in exactly the same manner as was done for finite systems of spheres by Durlofsky *et al.* (1987).

Calculations of far-field interactions become complicated for unbounded systems, as care must be taken to properly account for the qualitative differences between interactions in infinite and finite media. Failure to account for these differences using an appropriate "renormalization" process will often result in sums over those interactions being divergent. The method of O'Brien, as adapted for use in hydrodynamic calculations in Chapter 2, provides one method of renormalization that does not require any preaveraging of hydrodynamic interactions, thereby allowing one to perform calculations for specific configurations of particles. The resulting expressions for the renormalized interactions are absolutely convergent, but are still difficult to handle computationally. As a result, periodic boundary conditions are applied, thereby allowing one to model an infinite system with a relatively small number of particles. This choice of boundary conditions also allows the convergence of the sums over hydrodynamic interactions to be accelerated through use of the Ewald summation technique.

Because of the relatively complete set of information available for spatially periodic media, one convenient way to examine the accuracy of the Stokesian dynamics method is to calculate transport coefficients for cubic lattices of spheres and compare with other theoretical results available in the literature. Such calculations and comparisons are described in Chapter 3. Excellent agreement was obtained for rotational drag coefficients and shear viscosities of the cubic arrays over the full range of volume fractions possible, and similarly good agreement was obtained for the translational drag coefficients for volume fractions up to about 30%. The drag coefficient calculations differ from the others in that, during flow through a stationary porous medium, there is no relative motion between spheres, and near-field interactions between neighboring spheres never become singular. As a result, these near-field or lubrication interactions never dominate other interactions. Thus, the higher moments that are lost through truncation of the aforementioned moment expansion are not negligible in this case, and must be included to obtain an accurate result at high volume fractions. A complete accounting for these higher moments is not computationally feasible at this time.

Although the calculations performed for ordered arrays of spheres provide a useful means for assessing the accuracy of Stokesian dynamics, the method is also general enough to be applied to disordered systems. Transport properties of such systems have been evaluated by Monte Carlo simulation, as described in Chapters 4 and 5. In general the properties calculated in this manner showed excellent agreement with the existing body of theoretical and experimental results. The results for the short-time self-diffusion coefficients and shear viscosities of suspensions showed particularly good agreement with experiment. This good agreement demonstrates the remarkable extent to which these two properties can depend upon hydrodynamic interactions. In addition, these simulation results can serve as a starting point for future research on how other types of interactions, such as electrostatic or DLVO interactions, might affect transport properties in suspensions and porous media.

Fibrous media represent a particularly interesting class of porous media in that they constitute materials such as fibrous membranes and gels, which are commonly used in both physiological and industrial separations processes. The Stokesian dynamics method can be easily adapted to calculating local, or short-time hindered diffusion coefficients of spherical solutes in systems of bead-and-string fibers. These local coefficients can be used in conjunction with generalized Taylor dispersion theory to evaluate global coefficients, which describe transport over experimentally observable length scales. Global coefficients for two different spatially periodic lattices of bead-and-string fibers have been calculated in this manner, and were used in Chapter 6 to determine the accuracy of predictions of an effective medium model based on Brinkman's equation. Comparisons between the two models were made for ratios of the solute radius to fiber radius varying over a factor of ten. In every case, the effective medium model qualitatively reproduced the trends of the more accurate generalized Taylor dispersion theory calculations. In addition, quantitative agreement was obtained for volume fractions at which hindrance due to the presence of the fibers was not too severe (*i.e.*, for D^*/D_0 less than about 0.5). The success of the effective medium approach is somewhat surprising in light of the fact that so little of the microstructure of the periodic media is incorporated into Brinkman's equation.

Although the Brinkman prediction is not as accurate as the generalized Taylor dispersion theory calculation for the full range of volume fractions studied, it does have the advantage of being readily applicable to systems with highly complex or unknown microstructure. Indeed, this approach can be used to predict dispersion coefficients for any system provided that the hydraulic permeability of the medium and the radius of the solute are known or can be determined. A comparison of the effective medium model's predictions with experimental measurements of protein dispersion in hyaluronic acid solution showed remarkably good agreement. This agreement suggests that hydrodynamic interactions can play a dominant role in hindering the motion of macromolecules in fibrous media. This hindrance was found to be significant even for fiber volume fractions less than 1%. In addition, it appears that accounting for the detailed microstructure of the fibrous medium is less important than accounting for its presence in an average sense, as in Brinkman's equation. This finding could be of great use in future experimental and theoretical research on hindered transport in fibrous media of unknown or highly complex microstructure.

CHAPTER 8

REFERENCES

Barker, J.A. and D. Henderson, "Monte Carlo Values for the Radial Distribution Function of a System of Fluid Hard Spheres," *Molec. Phys.*, 21, 187 (1971).

Batchelor, G.K., "The Stress System in a Suspension of Force-Free Particles," *J. Fluid Mech.*, 41, 545 (1970).

Batchelor, G.K., "Sedimentation in a Dilute Dispersion of Spheres," *J. Fluid Mech.*, 52, 245 (1972).

Batchelor, G.K., "Brownian Diffusion of Particles with Hydrodynamic Interaction," *J. Fluid Mech.*, 74, 1 (1976).

Batchelor, G.K., "The Effect of Brownian Motion on the Bulk Stress in a Suspension of Spherical Particles," *J. Fluid Mech.*, 83, 97, (1977).

Batchelor, G.K. and J.T. Green, "The Determination of The Bulk Stress in a Suspension of Spherical Particles to Order c^2," *J. Fluid Mech.*, 56, 401 (1972).

Beenakker, C.W.J., "The Effective Viscosity of a Concentrated Suspension of Spheres (and its Relation to Diffusion)," *Physica*, 128A, 48 (1984).

Beenakker, C.W.J., "Ewald Sum of the Rotne-Prager Tensor," *J. Chem. Phys.*, 85, 1581 (1986).

Beenakker, C.W.J. and P. Mazur, "Diffusion of Spheres in a Concentrated Suspension II," *Physica*, 126A, 349 (1984).

Berne, B.J. and R. Pecora, *Dynamic Light Scattering*, Wiley (1976).

Binder, K., "Introduction: Theory and 'Technical' Aspects of Monte Carlo Simulations," in *Monte Carlo Methods in Statistical Physics*, ed. K. Binder, Springer (1986).

Bossis, G. and J.F. Brady, "Dynamic Simulation of Sheared Suspensions. I. General Method," *J. Chem. Phys.*, 80, 5141 (1984).

Bossis, G. and J.F. Brady, "Self-Diffusion of Brownian Particles in Concentrated Suspensions under Shear," *J. Chem. Phys.*, 87, 5437 (1987).

Bossis, G., J.F. Brady and C. Mathis, "Shear-Induced Structure in Colloidal Suspensions. I. Numerical Simulation," *J. Colloid Interface Sci.*, 126, 1 (1988).

Brady, J.F. and G. Bossis, "The Rheology of Concentrated Suspensions of Spheres in Simple Shear Flow by Numerical Simulation," *J. Fluid Mech.*, 155, 105 (1985).

Brady, J.F. and G. Bossis, "Stokesian Dynamics," *Ann. Rev. Fluid Mech.*, 20, 111 (1988).

Brady, J.F. and L.J. Durlofsky, "The Sedimentation Rate of Disordered Suspensions," *Phys. Fluids*, 31, 717 (1988).

Brady, J.F., R.J. Phillips, J.C. Lester, and G. Bossis, "Dynamic Simulation of Hydrodynamically Interacting Suspensions," *J. Fluid Mech.*, 195, 257 (1988).

Brenner, H. and P.M. Adler, "Dispersion Resulting from Flow through Spatially Periodic Media. II. Surface and Intraparticle Transport," *Phil. Trans. R. Soc. Lond. A*, 307, 149 (1982).

Brenner, H. and L.J. Gaydos, "The Constrained Brownian Movement of Spherical Particles in Cylindrical Pores of Comparable Radius: Models of Diffusive and Convective Transport of Solute Molecules in Membranes and Porous Media," *J. Colloid Interface Sci.*, 58, 312 (1977).

Brinkman, H.C., "A Calculation of the Viscous Force Exerted by a Flowing Fluid in a Dense Swarm of Particles," *Appl. Sci. Res. A*, 1, 27 (1947).

Buscall, R., J.W. Goodwin and R.H. Ottewill, "The Settling of Particles through Newtonian and Non-Newtonian Media," *J. Colloid Interface Sci.*, *85, 78 (1982).*

Carbonell, R.G. and S. Whitaker, "Dispersion in Pulsed Systems. II. Theoretical Developments for Passive Dispersion in Porous Media," *Chem. Eng. Sci.*, 38, 1795 (1983).

Cheng, P.Y. and H.K. Schachman, "Studies on the Validity of the Einstein Viscosity Law and Stokes' Law of Sedimentation," *J. Polym. Sci.*, 16, 19 (1955).

Childress, S., "Viscous Flow Past a Random Array of Spheres," *J. Chem. Phys.*, 56, 2527 (1972).

Curry, F.E. and C.C. Michel, "A Fiber Matrix Model of Capillary Permeability," *Microvasc. Res.*, 20, 96 (1980).

Deen, W.M., "Hindered Transport of Large Molecules in Liquid-Filled Pores," *AIChE J.*, 33, 1409 (1987).

Dickinson, E., "Brownian Dynamics with Hydrodynamic Interactions: The Application to Protein Diffusional Problems," *Chem. Soc. Rev.*, 14, 421 (1985).

Durlofsky, L.J. and J.F. Brady, "Analysis of the Brinkman Equation as a Model for Flow in Porous Media," *Phys. Fluids*, **30**, 3329 (1987).

Durlofsky, L.J., J.F. Brady and G. Bossis, "Dynamic Simulation of Hydrodynamically Interacting Particles," *J. Fluid Mech.*, **180**, 21 (1987).

Ethier, C.R., "The Hydrodynamic Resistance of Hyaluronic Acid: Estimates from Sedimentation Studies," *Biorheology*, **23**, 99 (1986).

Ewald, P.P., "Die Berechnung Optischa und Elektostatischer Gitterpotentiale," *Ann. Phys.*, **64**, 253 (1921).

Fanti, L. and Glandt, E., "Partitioning of Spherical Particles into Fibrous Matrices I," *J. Colloid Inter. Sci.* (in press).

Fanti, L. and Glandt, E., "Partitioning of Spherical Particles into Fibrous Matrices. II. Monte Carlo Simulation," *J. Colloid Interface Sci.* (in press).

Faxen, H., "Simplified Representation of the Generalized Green's Equations for the Constant Motion of Translation of a Rigid Body in a Viscous Fluid," *Arkiv. Mat. Astron. Fysik.*, **20**:8 (1927).

Finlayson, B.A., *Nonlinear Analysis in Chemical Engineering*, McGraw-Hill (1980).

Freed, K.F. and M. Muthukumar, "On the Stokes Problem for a Suspension of Spheres at Finite Concentrations," *J. Chem. Phys.*, **68**, 2088 (1978).

Gladden, J.K., and M. Dole, "Diffusion in Supersaturated Solutions. II. Glucose Solutions," *J. Am. Chem. Soc.*, **75**, 3900 (1953).

Glendinning, A.B. and W.B. Russel, "A Pairwise Additive Description of Sedimentation and Diffusion in Concentrated Suspensions of Hard Spheres," *J. Colloid Interface Sci.*, **89**, 124 (1982).

Happel, J. and H. Brenner, *Low Reynolds Number Hydrodynamics*, Prentice-Hall (1965).

Hasimoto, H., "On the Periodic Fundamental Solutions of the Stokes Equations and their Application to Viscous Flow Past a Cubic Array of Spheres," *J. Fluid Mech.*, **5**, 317 (1959).

Hinch, E.J., "An Averaged-Equation Approach to Particle Interactions in a Fluid Suspension," *J. Fluid Mech.*, **83**, 695 (1977).

Hoover, W.G. and F.H. Ree, "Melting Transition and Communal Entropy for Hard Spheres," *J. Chem. Phys.*, **49**, 3609 (1968).

Howells, I.D., "Drag Due to the Motion of a Newtonian Fluid through a Sparse Random Array of Small Fixed Rigid Objects," *J. Fluid Mech.*, **64**, 449 (1974).

Jackson, G.W. and D.F. James, "The Permeability of Fibrous Porous Media," *Can. J. Chem. Eng.*, **64**, 364 (1986).

Jeffrey, D.J. and Y. Onishi, "Calculation of the Resistance and Mobility Functions for Two Unequal Rigid Spheres in Low-Reynolds-Number Flow," *J. Fluid Mech.*, **139**, 261 (1984).

Kim, S. and R.T. Mifflin, "The Resistance and Mobility Functions of Two Equal Spheres in Low-Reynolds-Number Flow," *Phys. Fluids*, **28**, 2033 (1985).

Kim, S. and W.B. Russel, "Modelling of Porous Media by Renormalization of the Stokes Equations," *J. Fluid Mech.*, **154**, 269 (1985).

Kittel, C., *Introduction to Solid State Physics*, Wiley (1976).

Koch, D.L. and J.F. Brady, "The Effective Diffusivity of Fibrous Media," *AIChE J.*, **32**, 575 (1986).

Koch, D.L., R.G. Cox, H. Brenner, and J.F. Brady, "The Effect of Order on Dispersion in Porous Media," *J. Fluid Mech.*, **200**, 173 (1989).

Krieger, I.M., "Rheology of Monodisperse Latices," *Advan. Colloid Interface Sci.*, **3**, 111 (1972).

Ladyzhenskaya, O.A., *The Mathematical Theory of Viscous Incompressible Flow*, Gordon & Breach (1963).

Landau, L.D. and E.M. Lifshitz, *Fluid Mechanics*, Pergamon (1959).

Laurent, T.C., I. Bjork, A. Pietruszkiewicz, and H. Persson, "On the Interaction between Polysaccharides and Other Macromolecules. II. The Transport of Globular Particles through Hyaluronic Acid Solutions," *Biochimica et Biophysica Acta*, **78**, 351 (1963).

Laurent, T.C. and A. Pietruszkiewicz, "The Effect of Hyaluronic Acid on the Sedimentation Rate of Other Substances," *Biochimica et Biophysica Acta*, **49**, 258 (1961).

Levesque, D., J. Weis and J. Hansen, "Simulation of Classical Fluids," in *Monte Carlo Methods in Statistical Physics*, ed. K. Binder, Springer (1986).

Maude, A.D. and R.L. Whitmore, "A Generalized Theory of Sedimentation," *Brit. J. Appl. Phys.*, **9**, 477 (1958).

Nijboer, B.R.A. and F.W. de Wette, "On the Calculation of Lattice Sums," *Physica*, **23**, 309 (1957).

Nunan, K.C. and J.B. Keller, "Effective Viscosity of a Periodic Suspension," *J. Fluid Mech.*, **142**, 269 (1984).

O'Brien, R.W., "A Method for the Calculation of the Effective Transport Properties of Interacting Particles," *J. Fluid Mech.*, **91**, 17 (1979).

Ogston, A.G., "The Spaces in a Uniform Random Suspension of Fibres," *Trans. Faraday Soc.*, **54**, 1754 (1958).

Ogston, A.G., B.N. Preston, and J.D. Wells, "On the Transport of Compact Particles through Solutions of Chain-Polymers," *Proc. R. Soc. Lond. A*, **333**, 297 (1973).

Ottewill, R.H. and N.St.J. Williams, "Study of Particle Motion in Concentrated Dispersions by Tracer Diffusion," *Nature*, **325**, 232 (1987).

Peppas, N.A. and C.T. Reinhart, "Solute Diffusion in Swollen Membranes. I. A New Theory," *J. Membrane Sci.*, **15**, 275 (1983).

Perrins, W.T., D.R. McKenzie and R.C. McPhedran, "Transport Properties of Regular Arrays of Cylinders," *Proc. R. Soc. Lond. A*, **369**, 207 (1979).

Phillips, R.J., J.F. Brady, and G. Bossis, "Hydrodynamic Transport Prop erties of Hard-Sphere Dispersions. I. Suspensions of Freely Mobile Particles," *Phys. Fluids*, 31, 3462 (1988a).

Phillips, R.J., J.F. Brady, and G. Bossis, "Hydrodynamic Transport Properties of Hard-Sphere Dispersions. II. Porous Media," *Phys. Fluids*, 31, 3473 (1988b).

Phillips, R.J., W.M. Deen and J.F. Brady, "Hindered Transport of Spherical Macromolecules in Fibrous Membranes and Gels," *AIChE J.* (in press).

Phillips, R.J., W.M. Deen and J.F. Brady, "Hindered Transport in Fibrous Membranes and Gels," *J. Colloid Interface Sci.* (submitted).

Pusey, P.N. and W. van Megen, "Measurement of the Short-Time Self-Mobility of Particles in Concentrated Suspension. Evidence for Many-Particle Hydrodynamic Interactions," *J. Physique*, **44**, 285 (1983).

Rallison, J.M. and E.J. Hinch, "The Effect of Particle Interactions on Dynamic Light Scattering from a Dilute Suspension," *J. Fluid Mech.*, **167**, 131 (1986).

Reid, R.C., J.M. Prausnitz and B.E. Poling, *The Properties of Liquids and Gases*, McGraw-Hill (1987).

Rosensweig, R.E., *Ferrohydrodynamics*, Cambridge University Press (1987).

Russel, W.B. and A. Gast, "Nonequilibrium Statistical Mechanics of Concentrated Colloidal Dispersions: Hard Spheres in Weak Flows," *J. Chem. Phys.*, **84**, 1815 (1986).

Saffman, P.G., "On the Settling Speed of Free and Fixed Suspensions," *Stud. Appl. Maths.*, 52, 115 (1973).

Silebi, C.A. and A.J. McHugh, "The Determination of Particle Size Distributions by Hydrodynamic Chromatography: An Analysis of Dispersion Methods for Improved Signal Resolution," *J. Appl. Polymer Sci.*, **23**, 1699 (1979).

Small, H., "Hydrodynamic Chromatography, A Technique for Size Analysis of Colloidal Particles," *J. Colloid Interface Sci.*, **48**, 147 (1974).

Spielman, L. and S.L. Goren, "Model for Predicting Pressure Drop and Filtration Efficiency in Fibrous Media," *Envir. Sci. Tech.*, 2, 279 (1968).

Stokes, G.G., *Trans. Camb. Phil. Soc.*, **9**, 8 (1851).

Taylor, G.I., "Dispersion of Soluble Matter in Solvent Flowing Slowly through a Tube," *Proc. Roy. Soc.*, **A219**, 186 (1953).

van der Werff, J.C., C.G. de Kruif, C. Blom and J. Mellema, in *Proceedings of the Fourth EPS Liquid State Conference*, Arcachon, France, M. Mijhoff, Amsterdam (1989).

Whitaker, S., *Introduction to Fluid Mechanics*, Krieger (1981).

Yoon, B.J. and S. Kim, "Note on the Direct Calculation of Mobility Functions for Two Equal-Sized Spheres in Stokes Flow," *J. Fluid Mech.*, **185**, 437 (1987).

Zick, A. and G.M. Homsy, "Stokes Flow through Periodic Arrays of Spheres," *J. Fluid Mech.*, **115**, 13 (1982).

Zuzovsky, M., P.M. Adler and H. Brenner, "Spatially Periodic Suspensions of Convex Particles in Linear Shear Flows. III. Dilute Arrays of Spheres Suspended in Newtonian Fluids," *Phys. Fluids*, **26**, 1714 (1983).

APPENDIX A

The following are the real and reciprocal space parts of the far-field mobility interactions for use in conjunction with the Ewald summation method. The terms coupling translational velocities and forces were first derived by Beenakker (1986). The remaining terms can be derived as explained in Chapter 2. The parameter ξ has units of inverse length and governs the speed of convergence of the two sums. Beenakker recommends using a value of $\xi = V^{-1/3}$, where V is the volume of a unit cell. The vector **e** is a unit vector along the line connecting the particle centers, *r* is the interparticle separation distance, and $\hat{\mathbf{k}}$ is a unit vector in the reciprocal lattice. All lengths have been nondimensionalized by the particle radius *a* (see Beenakker's derivation for an explanation of how to include spheres with different radii), and a common normalization of $6\pi\mu a^n$ has been used for the mobility functions, where n = 1,2, or 3 depending on the mobility coupling.

(a) Translational velocity/force, or U-F coupling:

$$\begin{aligned} M_{ij}^{(1)}(\mathbf{r}) = \delta_{ij}\Big\{ & \Big(\frac{3}{4}\frac{1}{r} + \frac{1}{2}\frac{1}{r^3} \Big) \operatorname{erfc}(\xi r) + \frac{1}{\sqrt{\pi}} \Big(4\xi^7 r^4 + 3\xi^3 r^2 \\ & - 20\xi^5 r^2 - \frac{9}{2}\xi + 14\xi^3 + \frac{\xi}{r^2} \Big) e^{-\xi^2 r^2} \Big\} \\ & + e_i e_j \Big\{ \Big(\frac{3}{4}\frac{1}{r} - \frac{3}{2}\frac{1}{r^3} \Big) \operatorname{erfc}(\xi r) + \frac{1}{\sqrt{\pi}} \Big(-4\xi^7 r^4 - 3\xi^3 r^2 \\ & + 16\xi^5 r^2 + \frac{3}{2}\xi - 2\xi^3 - \frac{3\xi}{r^2} \Big) e^{-\xi^2 r^2} \Big\} \end{aligned}$$

$$M_{ij}^{(2)}(\mathbf{k}) = (\delta_{ij} - \hat{k}_i \hat{k}_j)(1 - k^2/3) \Big(1 + \frac{1}{4}\frac{k^2}{\xi^2} + \frac{1}{8}\frac{k^4}{\xi^4} \Big) 6\pi k^{-2} \exp\Big(- \frac{k^2}{4\xi^2} \Big)$$

$$M_{ij}^{(2)}(r=0) = \frac{1}{\sqrt{\pi}} \left(6\xi - \frac{40}{3}\xi^3 \right)$$

(b) Translational velocity/torque, or U-L coupling:

$$M_{ij}^{(1)}(r) = -\frac{3}{8}\epsilon_{lkj}\{ \left(-\frac{1}{r^3}\mathrm{erfc}(\xi r) + \frac{2}{\sqrt{\pi}}\xi \left(-\frac{1}{r^2} + 10\xi^2 - 4\xi^4 r^2 \right) e^{-\xi^2 r^2} \right) e_k \delta_{il}$$
$$+ \left(\frac{1}{r^3}\mathrm{erfc}(\xi r) + \frac{2}{\sqrt{\pi}}\xi \left(\frac{1}{r^2} - 2\xi^2 \right) e^{-\xi^2 r^2} \right) e_l \delta_{ik}$$

$$M_{ij}^{(2)}(\mathbf{k}) = 3\pi(\epsilon_{ikj}\hat{k}_k) \left(\frac{1}{k} + \frac{1}{4}\frac{k}{\xi^2} + \frac{1}{8}\frac{k^3}{\xi^4} \right) \exp(-\frac{k^2}{4\xi^2})$$

$$M_{ij}^{(2)}(r=0) = 0$$

(c) Rotational velocity/torque, or Ω-L coupling:

$$M_{ij}^{(1)}(r) = \delta_{ij} \left(-\frac{3}{8r^3}\mathrm{erfc}(\xi r) - \frac{3}{\sqrt{\pi}}(\xi/r^2 + 14\xi^3 - 20\xi^5 r^2 + 4\xi^7 r^4) e^{-\xi^2 r^2} \right)$$
$$- \frac{3}{4} e_i e_j \left(-\frac{3}{2r^3}\mathrm{erfc}(\xi r) + \frac{1}{\sqrt{\pi}}(-3\xi/r^2 - 2\xi^3 + 16\xi^5 r^2 - 4\xi^7 r^4) e^{-\xi^2 r^2} \right)$$

$$M_{ij}^{(2)}(\mathbf{k}) = \frac{3\pi}{2}(\delta_{ij} - \hat{k}_i\hat{k}_j)(1 + \frac{k^2}{4\xi^2} + \frac{k^4}{8\xi^4}) \exp(-\frac{k^2}{4\xi^2})$$

$$M_{ij}^{(2)}(r = 0) = \frac{10}{\sqrt{\pi}}\xi^3$$

(d) Translational velocity/stresslet, or U-S coupling:

$$M_{ijk}^{(1)}(r) = \frac{3}{8} \left((x_4 + x_5)(e_k\delta_{ij} + e_j\delta_{ik}) + 2x_5(e_i\delta_{jk}) + 2x_6(e_i e_j e_k) \right.$$
$$\left. + \frac{4}{15}\left((x_1 + x_2)(e_k\delta_{ij} + e_j\delta_{ik}) + 2x_2(e_i\delta_{jk}) + 2x_3(e_i e_j e_k) \right) \right)$$

$$M^{(2)}_{ijk}(\mathbf{k}) = -3\pi(1 - \frac{4}{15}k^2)\,[\hat{k}_k(\delta_{ij} - \hat{k}_i\hat{k}_j) + \hat{k}_j(\delta_{ik} - \hat{k}_i\hat{k}_k)]$$
$$\times \left(\frac{1}{k} + \frac{k}{4\xi^2} + \frac{k^3}{8\xi^4} \right) \exp(-\frac{k^2}{4\xi^2})$$

$$M^{(2)}_{ijk}(r = 0) = 0$$

where

$$x_1 = -(6/r^4)\mathrm{erfc}(\xi r) + \frac{4}{\sqrt{\pi}}(-3\xi/r^3 - 2\xi^3/r - 68\xi^5 r + 56\xi^7 r^3 - 8\xi^9 r^5)e^{-\xi^2 r^2}$$

$$x_2 = 4\left(-\frac{3}{2r^4}\mathrm{erfc}(\xi r) + \frac{1}{\sqrt{\pi}}(-3\xi/r^3 - 2\xi^3/r + 16\xi^5 r - 4\xi^7 r^3)\,e^{-\xi^2 r^2} \right)$$

$$x_3 = 4\left(\frac{15}{2r^4}\mathrm{erfc}(\xi r) + \frac{1}{\sqrt{\pi}}(15\xi/r^3 + 10\xi^3/r + 4\xi^5 r - 40\xi^7 r^3 + 8\xi^9 r^5)e^{-\xi^2 r^2} \right)$$

$$x_4 = -\frac{1}{r^2}\mathrm{erfc}(\xi r) + \frac{2}{\sqrt{\pi}}\xi\,(-1/r + 10\xi^2 r - 4\xi^4 r^3)\,e^{-\xi^2 r^2}$$

$$x_5 = \frac{1}{r^2}\mathrm{erfc}(\xi r) + \frac{2}{\sqrt{\pi}}\xi(1/r - 2\xi^2 r)\,e^{-\xi^2 r^2}$$

$$x_6 = -\frac{3}{r^2}\mathrm{erfc}(\xi r) + \frac{2}{\sqrt{\pi}}\xi\,(-3/r - 2\xi^2 r + 4\xi^4 r^3)\,e^{-\xi^2 r^2}$$

(e) Rotational velocity/stresslet, or Ω-S coupling:

$$M^{(1)}_{ijk}(r) = -\frac{3}{16}(y_2 - y_1)[\hat{k}_k(\hat{k}_l\epsilon_{lij}) + \hat{k}_j(\hat{k}_l\epsilon_{lik})]$$

$$M^{(2)}_{ijk}(\mathbf{k}) = -\frac{3\pi}{2}[\hat{k}_k(\hat{k}_l\epsilon_{lij})] + \hat{k}_j(\hat{k}\epsilon_{lik})](1 + \frac{k^2}{4\xi^2} + \frac{k^4}{8\xi^4})$$
$$\times \exp(-\frac{k^2}{4\xi^2})$$

$$M^{(2)}_{ijk}(r{=}0) = 0$$

where

$$y_1 = \frac{3}{r^3}\,\mathrm{erfc}(\xi r) + \frac{2}{\sqrt{\pi}}\,\xi\,(3/r^2 + 2\xi^2 - 28\xi^4 r^2 + 8\xi^6 r^4)\; e^{-\xi^2 r^2}$$

$$y_2 = -\frac{3}{r^3}\,\mathrm{erfc}(\xi r) + \frac{2}{\sqrt{\pi}}\,\xi\,(3/r^2 - 2\xi^2 + 4\xi^4 r^2)\; e^{-\xi^2 r^2}$$

(f) Rate of strain/stresslet, or E-S coupling:

$$M^{(1)}_{iljk}(r) = -\frac{3}{16}\,r^2\,M^{(1A)}_{iljk}(r) - \frac{3}{80}\,M^{(1B)}_{iljk}(r)$$

$$\begin{aligned} M^{(2)}_{iljk}(\mathbf{k}) = \frac{3\pi}{2}\,(1 - \tfrac{1}{5}\,k^2)[&\hat{k}_l\hat{k}_k(\delta_{ij} - \hat{k}_i\hat{k}_j) + \hat{k}_l\hat{k}_j(\delta_{ik} - \hat{k}_i\hat{k}_k) \\ &+ \hat{k}_i\hat{k}_k(\delta_{lj} - \hat{k}_l\hat{k}_j) + \hat{k}_i\hat{k}_j(\delta_{lk} - \hat{k}_l\hat{k}_k)](1 + \frac{k^2}{4\xi^2} \\ &+ \frac{k^4}{8\xi^4})\,\exp(-\frac{k^2}{4\xi^2}) \end{aligned}$$

$$M^{(2)}_{iljk}(r = 0) = \frac{3}{\sqrt{\pi}}\,(2\xi^3 - \frac{126}{25}\,\xi^5)(\delta_{ij}\delta_{lk} + \delta_{ik}\delta_{lj} - \frac{2}{3}\,\delta_{il}\delta_{jk})$$

where

$$\begin{aligned} M^{(1A)}_{iljk}(r) = {} & 2(z_3 + z_1)(\delta_{lk}\delta_{ij} + \delta_{jl}\delta_{ik}) + 4z_3\delta_{jk}\delta_{il} \\ & + (z_2 + 3z_4)(\delta_{ij}e_l e_k + \delta_{jl}e_i e_k + \delta_{lk}e_i e_j + \delta_{ik}e_j e_l) \\ & + 4z_4(\delta_{il}e_j e_k + \delta_{jk}e_i e_l) + 4z_5 e_i e_j e_k e_l \end{aligned}$$

$$\begin{aligned} M^{(1B)}_{iljk}(r) = {} & 2(D2z_1 + 2z_2 + 6z_4 + D2z_3)(\delta_{jl}\delta_{ki} + \delta_{kl}\delta_{ij}) \\ & + 4(D2z_3 + 4z_4)\delta_{jk}\delta_{il} + 4(D2z_4 + 2z_5 + 4Dz_4) \\ & \qquad\qquad \times (\delta_{il}e_k e_j + \delta_{jk}e_i e_l) \\ & + [3(D2z_4 + 2z_5 + 4Dz_4) + 4Dz_2 + D2z_2 + 2z_5](\delta_{ik}e_j e_l \\ & + \delta_{kl}e_i e_j + \delta_{jl}e_i e_k + \delta_{ij}e_k e_l) + 4(8Dz_5 + D2z_5)e_i e_j e_k e_l \end{aligned}$$

and

$$z_1 = -(1/r^5)\mathrm{erfc}(\xi r) + \frac{2}{\sqrt{\pi}}\,\xi\,(-1/r^4 + 10\xi^2/r^2 - 4\xi^4)e^{-\xi^2 r^2}$$

$$z_2 = (3/r^5)\mathrm{erfc}(\xi r) + \frac{2}{\sqrt{\pi}}\,\xi\,(3/r^4 - 28\xi^4 + 2\xi^2/r^2 + 8\xi^6 r^2)e^{-\xi^2 r^2}$$

$$z_3 = (1/r^5)\mathrm{erfc}(\xi r) + \frac{2}{\sqrt{\pi}}\,\xi\,(1/r^4 - 2\xi^2/r^2)e^{-\xi^2 r^2}$$

$$z_4 = -(3/r^5)\mathrm{erfc}(\xi r) + \frac{2}{\sqrt{\pi}}\,\xi\,(-3/r^4 - 2\xi^2/r^2 + 4\xi^4)\, e^{-\xi^2 r^2}$$

$$z_5 = (15/r^5)\mathrm{erfc}(\xi r) + \frac{2}{\sqrt{\pi}}\,\xi\,(15/r^4 + 10\xi^2/r^2 + 4\xi^4 - 8\xi^6 r^2)e^{-\xi^2 r^2}$$

$$Dz_1 = (3/r^5)\mathrm{erfc}(\xi r) + \frac{2}{\sqrt{\pi}}\,\xi\,(3/r^4 - 8\xi^4 + 2\xi^2/r^2 - 20\xi^4 + 8\xi^6 r^2)e^{-\xi^2 r^2}$$

$$\begin{aligned} Dz_2 = -(15/r^5)\mathrm{erfc}(\xi r) + \frac{2}{\sqrt{\pi}}\,\xi\,(&-15/r^4 - 10\xi^2/r^2 + 72\xi^6 r^2 - 4\xi^4 \\ &-16\xi^8 r^4)e^{-\xi^2 r^2} \end{aligned}$$

$$Dz_3 = -(3/r^5)\mathrm{erfc}(\xi r) + \frac{2}{\sqrt{\pi}}\,\xi\,(-3/r^4 - 2\xi^2/r^2 + 4\xi^4)e^{-\xi^2 r^2}$$

$$Dz_4 = (15/r^5)\mathrm{erfc}(\xi r) + \frac{2}{\sqrt{\pi}}\,\xi\,(15/r^4 + 10\xi^2/r^2 + 4\xi^4 - 8\xi^6 r^2)e^{-\xi^2 r^2}$$

$$\begin{aligned} Dz_5 = -(105/r^5)\mathrm{erfc}(\xi r) + \frac{2}{\sqrt{\pi}}\,\xi\,(&-105/r^4 - 70\xi^2/r^2 - 28\xi^4 - 8\xi^6 r^2 \\ &+ 16\xi^8 r^4)e^{-\xi^2 r^2} \end{aligned}$$

$$\begin{aligned} D2z_1 = -(6/r^5)\mathrm{erfc}(\xi r) + \frac{2}{\sqrt{\pi}}\,\xi\,&(-6/r^4 - 88\xi^4 - 4\xi^2/r^2 + 96\xi^6 r^2 - 16\xi^8 r^4) \\ &\times e^{-\xi^2 r^2} \end{aligned}$$

$$\begin{aligned} D2z_2 = (60/r^5)\,\mathrm{erfc}(\xi r) + \frac{2}{\sqrt{\pi}}\,\xi\,(&60/r^4 + 40\xi^2/r^2 + 224\xi^6 r^2 + 16\xi^4 - 224\xi^8 r^4 \\ &+32\xi^{10} r^6)e^{-\xi^2 r^2} \end{aligned}$$

$$D2z_3 = (6/r^5)\mathrm{erfc}(\xi r) + \frac{2}{\sqrt{\pi}}\,\xi\,(6/r^4 + 4\xi^2/r^2 + 16\xi^4 - 8\xi^6 r^2)e^{-\xi^2 r^2}$$

$$\begin{aligned} D2z_4 = -(60/r^5)\mathrm{erfc}(\xi r) + \frac{2}{\sqrt{\pi}}\,\xi\,(&-60/r^4 - 40\xi^2/r^2 - 16\xi^4 - 32\xi^6 r^2 \\ &+ 16\xi^8 r^4)e^{-\xi^2 r^2} \end{aligned}$$

$$\begin{aligned} D2z_5 = (630/r^5)\mathrm{erfc}(\xi r) + \frac{2}{\sqrt{\pi}}\,\xi\,(&630/r^4 + 420\xi^2/r^2 + 168\xi^4 + 48\xi^6 r^2 \\ &+ 649\xi^8 r^4 - 32\xi^{10} r^6)e^{-\xi^2 r^2} \end{aligned}$$

APPENDIX B

The following FORTRAN 77 computer program, entitled SIM1, evaluates the complete, F-T-S resistance matrix *R* for *N* particles in a periodic unit cell that is periodically replicated throughout space. The far-field interactions are calculated and renormalized using the moment expansion process described in Chapter 2, and are summed using the Ewald summation technique. Near-field, or lubrication interactions are included in a pairwise fashion according to (2.48). Once formed, the 11N×11N resistance matrix can be used to calculate any of the transport properties described in Chapters 3-6. In the case considered here, it is assumed that one sphere is force- and torque-free, thereby modeling a spherical solute. The remaining *N-1* spheres are fixed in place, and are arranged so as to form a square lattice of bead-and-string fibers. The program output file VEL.DAT gives the local hindered diffusion coefficient $\underset{\approx}{D}^{HD}$ and the local velocity **U** of the mobile sphere.

The input parameters required by SIM1 are as follows:

1) NSPH - Number of spheres per periodic unit cell (*i.e.*, NSPH in SIM1 is the same as *N*).
2) NROW - Number of rows of fibers in the square lattice.
3) PHI - Volume fraction of spheres.
4) DIM - L/2, where *L* is defined as in Figure 6.1.
5) SHR1, SHR2, and SHR3 - Relative lengths of the periodic unit cell in the *x*, *y*, and *z* directions, normalized so that the product (SHR1)(SHR2)(SHR3) = 1.

In addition, the data files with numbers 29-36 provide tabulated, two-sphere interactions that are needed for the calculation of near-field interactions. These are not calculated or listed here, but can be evaluated using the methods of Jeffrey and Onishi (1984) or Kim and Mifflin (1985).

The subroutines called by SIM1 and their roles in the calculation of R are as follows:

1) FIBPOS - Sets the positions of the spheres.

2) STOKES1 - Calculates the resistance matrix given the sphere positions and the dimensions of the periodic unit cell. Except for CHINVTR, all of the subroutines to follow are called from STOKES1.

3) EWMOBA - Calculates the mobility interactions that couple forces and translational velocities for use in conjunction with the Ewald summation technique.

4) EWMOBB - Calculates the mobility interactions that couple forces and rotational velocities (or torques and translational velocities) for use in conjunction with the Ewald summation technique.

5) EWMOBC - Calculates the mobility interactions coupling torques and rotational velocities for use in conjunction with the Ewald summation technique.

6) EWFTS - Calculates the mobility interactions coupling forces and torques with the suspension average rate-of-strain for use in conjunction with the Ewald summation technique.

7) EWMOBES - Calculates the mobility interactions coupling stresslets and the suspension average rate-of-strain for use in conjunction with the Ewald summation technique.

8) ASSLE1 - Expresses 3rd and 4th order tensors as two-dimensional arrays, a more convenient form for matrix manipulations (*i.e.*, matrix inversion).

9) ASSLE2 - Assembles the submatrices coupling forces and velocities, torques and velocities, etc. into larger matrices for later use.

10) SSI1 - Calculates near-field interactions in the form of a temporary matrix (TEMP), which is used to form the lubrication matrix (RL) in ASSLE2.

In addition to these subroutines, a function DERFC is called in EWMOBA. This function calculates the complementary error function of a given argument, and can be obtained in the IMSL routine MERRCD.

```
      PROGRAM SIM1
      IMPLICIT INTEGER (I-N)
      COMMON/BLK 1/X(21),Y(21),Z(21),NSPH,NROW
      COMMON/BLK 2/A1(231,231),YUP(231,3),A3(231,231),YUP1(231,3),
C             YUP2(231,5)
      COMMON/BLK 3/TEMP(12,12),DS
      COMMON/BLK 4/  E(3),EP(3,3,3),D(3,3)
      COMMON/BLK 5/A(231,231)
      COMMON/BLK 6/RSS(50),X11AS(50),X12AS(50),Y11AS(50),Y12AS(50),
C          Y11BS(50),Y12BS(50),X11CS(50),X12CS(50),Y11CS(50),
C                 Y12CS(50)
      COMMON/BLK 7/X11ASINF(50),X12ASINF(50),Y11ASINF(50),
C             Y12ASINF(50),Y11BSINF(50),Y12BSINF(50),
C     Y11CSINF(50),Y12CSINF(50),X11CSINF(50),X12CSINF(50)
      COMMON/BLK 8/XM11(5,5),H11(3,5),G11(3,5),XM12(5,5),H12(3,5),
C             G12(3,5),H12T(3,3,3),G12T(3,3,3),XM12T(3,3,3,3)
      COMMON/BLK 9/XMES(105,105),XMUS(126,105),XMOBMATA(63,63),
C             XMOBMATB(63,63),XMOBMATC(63,63),RL(126,126),I,J
      COMMON/BLK 11/V,DX,DY,DZ,DRS,ES(3),A1N(3,3),DK,EK(3),
C                     B1N(3,3),C1N(3,3),PHI
      COMMON/BLK 12/R2,R3,R4,R5,R6,C,C2,C3,C4,C5,C6,C7,C8,C9,C10,
C             RN1,RN2,RN3,RN4,RN5,W,PI,PIP5,CR,CR2,ERFCO,EXPO,
C             XKC,XKC2,DK2
      COMMON/BLK 13/RSS1(60),XG1INFS(60),
C             XG2INFS(60),YG1INFS(60),YG2INFS(60),YH1INFS(60),
C             YH2INFS(60),XMINFS(60),YMINFS(60),ZMINFS(60)
      COMMON/BLK 14/S1,S2,S3,S4,S5,S6,S7,S8,S9,S10,X11AR,Y11AR,
C             Y11BR,X11CR,Y11CR
      COMMON/BLK 15/DAM111(3,3,3),DBM111(3,3,3),DCM111(3,3,3),
C             GRADR(6,6,3)
      COMMON/BLK 16/DRSS(55),DX11AS(55),DY11AS(55),DY11BS(55),
C             DX11CS(55),DY11CS(55)
      DIMENSION AVGU(3),U(3),PMOB(6,6),RAB(3,3),CONV(3,3)
      DIMENSION DX12AS(55),DY12AS(55),DY12BS(55),DX12CS(55),
C             DY12CS(55),DIVRINV(3),SIGMA(3,3),RX(3),RSTEP(3)
      OPEN (23,FILE = 'DATAIN1.DAT',STATUS = 'OLD', RECFM = 'DS')
      OPEN (24, FILE='IPOS.DAT')
      OPEN (25, FILE = 'VEL.DAT')
      OPEN (29, FILE = 'SLOPE1')
      OPEN (30, FILE = 'SSFCNS.DAT', STATUS = 'OLD', RECFM = 'DS')
      OPEN (31, FILE = 'SSFI.DAT', STATUS = 'OLD', RECFM = 'DS')
      OPEN (32, FILE = 'SSFIXC.DAT', STATUS = 'OLD', RECFM = 'DS')
      OPEN (35, FILE = 'SSFI2.DAT')
      OPEN (36, FILE = 'SSMI.DAT')
      READ (30,2800)
      READ (31,2900)
      READ (32,3000)
      READ (35,2900)
      READ (36,3000)
      DO 40 I = 1,56
        READ (35,3075) RSS1(I),XG1INFS(I),XG2INFS(I),YG1INFS(I),
C             YG2INFS(I),YH1INFS(I),YH2INFS(I)
```

```
        READ (36,3050) RSS1(I),XMINFS(I),YMINFS(I),ZMINFS(I)
40    CONTINUE
      DO 50 I = 1,47
        READ (30,2800) RSS(I),X11AS(I),X12AS(I),Y11AS(I),Y12AS(I),
     C                 Y11BS(I),Y12BS(I),X11CS(I),X12CS(I),Y11CS(I),
     C                 Y12CS(I)
C
        READ (31,2900) RSS(I),X11ASINF(I),X12ASINF(I),Y11ASINF(I),
     C                Y12ASINF(I),Y11BSINF(I),Y12BSINF(I),
     C                Y11CSINF(I),Y12CSINF(I)
C
        READ (32,3000) RSS(I),X11CSINF(I),X12CSINF(I)
50    CONTINUE
      READ (29,2800)
      DO 80 I = 1,54
        READ (29,2800) DRSS(I),DX11AS(I),DX12AS(I),DY11AS(I),
     C         DY12AS(I),DY11BS(I),DY12BS(I),DX11CS(I),DX12CS(I),
     C         DY11CS(I),DY12CS(I)
80    CONTINUE
C
C     READ IN PARAMETERS
C
      READ (23,*) NSPH,NROW,NLAY,PHI
      READ (23,*) DIM,SHR1,SHR2,SHR3
      PI = 3.14159265400
      XSP = ((4.00/3.00)*PI/PHI)**0.3333333333300
      N = 3*NSPH
      NX5 = 5*NSPH
      NDIM = 2*N
      XNR = FLOAT(NROW-1)
      XN = FLOAT(NSPH)
      W = (XN*(4.0/3.0)*PI/PHI)**0.33333333333
      V = W/2.00
      DSEED = 21474.D0
      PIP5 = 1.00/(PI**0.500)
      C = (PI**0.500)/W
      C2 = C*C
      C3 = C2*C
      C4 = C2*C2
      C5 = C3*C2
      C6 = C3*C3
      C7 = C4*C3
      C8 = C4*C4
      C9 = C5*C4
      C10 = C5*C5
C
C     CREATE KROENECKER DELTA AND PERMUTAION SYMBOLS
C
      DO 112 I = 1,3
        DO 111 J = 1,3
          D(I,J) = 0.00
111     CONTINUE
```

```
112     CONTINUE
        DO 113 I = 1,3
          D(I,I) = 1.00
113     CONTINUE
        DO 120 I = 1,3
          DO 118 J = 1,3
            DO 115 K = 1,3
              EP (I,J,K) = 0.00
115         CONTINUE
118       CONTINUE
120     CONTINUE
        EP(1,2,3) = 1.00
        EP(1,3,2) = -1.00
        EP(2,1,3) = -1.00
        EP(2,3,1) = 1.00
        EP(3,1,2) = 1.00
        EP(3,2,1) = -1.00
C
C       SET SPHERE POSITIONS
C
        CALL FIBPOS(DIM)
C
C       WRITE POSITIONS IN IPOS
C
        DO 140 I = 1,NSPH
          WRITE(24,1500) X(I),Y(I),Z(I)
140     CONTINUE
         WRITE(24,1500)
        WRITE(24,1500)
        XCT = 0.00
142     CONTINUE
        XCT = XCT + 1.00
C
C       CALL STOKES TO GET RESISTANCE MATRIX FOR
C       ENTIRE SYSTEM, THEN ABSTRACT HINDERED DIFFUSION
C       COEFFICIENT.
C
        DO 145 I = 1,3
          DO 144 J = 1,3
            RAB(I,J) = 0.00
            CONV(I,J) = 0.00
144       CONTINUE
145     CONTINUE
        DO 150 I = 1,6
          DO 149 J = 1,6
            PMOB(I,J) = 0.00
149       CONTINUE
150     CONTINUE
C
        CALL STOKES1(SHR1,SHR2,SHR3)
C
C       CALL PERM2(NDIM,NSPH)
```

```
        ICT - ICT + 1
C
C       THE RESISTANCE MATRIX IS NOW IN "A."  ABSTRACT PORTION
C       CORRESPONDING TO THE HINDERED RESISTIVITY OF THE ONE
C       MOBILE SPHERE (SPHERE ONE).
C
        DO 160 I - 1,3
          DO 155 J - 1,3
            PMOB(I,J) - A(I,J)
            PMOB(I,J+3) - A(I,N+J)
            PMOB(I+3,J+3) - A(I+N,J+N)
            PMOB(I+3,J) - A(I+N,J)
155       CONTINUE
160     CONTINUE
C
C       WRITE OUT THE HINDERED RESISTIVITY
C
        DO 165 I - 1,6
                WRITE(25,8000) (PMOB(I,J), J- 1,6)
165     CONTINUE
        WRITE(25,8000)
        WRITE(25,8000)
C
        CALL CHINVTR(PMOB)
C
C
C       WRITE OUT THE HINDERED MOBILITY
C
        DO 167 I - 1,6
          DO 166 J - 1,6
            WRITE(25,8000) (PMOB(I,J), J - 1,6)
166       CONTINUE
167     CONTINUE
        WRITE(25,8000)
        WRITE(25,8000)
C
C       EVALUATE THE VELOCITY
C
        NL - 3*NSPH-2
        DO 200 NUM - 1,NL,3
          NUM1 - NUM - 1
          DO 190 I - 1,3
            DO 180 J - 1,3
                RAB(I,J) - RAB(I,J) + A(I+NUM1,J)
180         CONTINUE
190       CONTINUE
200     CONTINUE
        WRITE(25,8000)
        WRITE(25,8000)
        DO 220 I - 1,3
          DO 210 J - 1,3
            SUM - 0.00
```

```
            DO 205 K = 1,3
                SUM = SUM + PMOB(I,K)*RAB(K,J)
205         CONTINUE
            CONV(I,J) = SUM
210       CONTINUE
220     CONTINUE
C
C       WRITE OUT THE VELOCITY (THIS 3X3 MATRIX CAN BE DOTTED
C       WITH THE SUSPENSION AVERAGE VELOCITY TO YIELD THE
C       PARTICLE VELOCITY).
C
        DO 229 I = 1,3
          WRITE(25,1500) (CONV(I,J),J = 1,3)
229     CONTINUE
        WRITE(25,1500)
        WRITE(25,1500)
1500    FORMAT (3(F12.4,1X))
2800    FORMAT (1X,F5.3,10E12.6)
2900    FORMAT (1X,F5.3,8E15.6)
3000    FORMAT (1X,F5.3,2E15.6)
3050    FORMAT (1X,F5.3,3E15.6)
3075    FORMAT (1X,F5.3,6E15.6)
3200    FORMAT (6(1X,E12.6))
8000    FORMAT (6(1X,E12.6))
9000    FORMAT (3(1X,E12.6))
        END
```

```
      SUBROUTINE FIBPOS(DIM)
      IMPLICIT INTEGER (I-N)
      COMMON/BLK 1/X(21),Y(21),Z(21),NSPH,NROW
C
C     POSITION FIBERS
C
      DO 100 I = 2,6
        X(I) = 0.00
        X(I+5) = 2.0*DIM
        X(I+10) = 0.00
        X(I+15) = 2.0*DIM
C
        Y(I) = 0.00
        Y(I+5) = 0.00
        Y(I+10) = 2.0*DIM
        Y(I+15) = 2.0*DIM
100   CONTINUE
      DO 200 I = 2,21,5
        Z(I) =   0.0
        Z(I+1) = 2.05
        Z(I+2) = 4.10
        Z(I+3) = 6.15
        Z(I+4) = 8.20
200   CONTINUE
      X(1) = 2.50000
      Y(1) = 0.00
      Z(1) = 0.000
      RETURN
      END
```

```
      SUBROUTINE STOKES1(SHR1,SHR2,SHR3)
      IMPLICIT INTEGER (I-N)
      COMMON/BLK 1/X(21),Y(21),Z(21),NSPH,NROW
      COMMON/BLK 2/A1(231,231),YUP(231,3),A3(231,231),
   C          YUP1(231,3),YUP2(231,5)
      COMMON/BLK 3/TEMP(12,12),DS
      COMMON/BLK 4/  E(3),EP(3,3,3),D(3,3)
      COMMON/BLK 5/A(231,231)
      COMMON/BLK 6/RSS(50),X11AS(50),X12AS(50),Y11AS(50),Y12AS(50),
   C         Y11BS(50),Y12BS(50),X11CS(50),X12CS(50),Y11CS(50),
   C              Y12CS(50)
      COMMON/BLK 7/X11ASINF(50),X12ASINF(50),Y11ASINF(50),
   C          Y12ASINF(50),Y11BSINF(50),Y12BSINF(50),
   C  Y11CSINF(50),Y12CSINF(50),X11CSINF(50),X12CSINF(50)
      COMMON/BLK 8/XM11(5,5),H11(3,5),G11(3,5),XM12(5,5),H12(3,5),
   C          G12(3,5),H12T(3,3,3),G12T(3,3,3),XM12T(3,3,3,3)
      COMMON/BLK 9/XMES(105,105),XMUS(126,105),XMOBMATA(63,63),
   C          XMOBMATB(63,63),XMOBMATC(63,63),RL(126,126),I,J
      COMMON/BLK 11/V,DX,DY,DZ,DRS,ES(3),A1N(3,3),DK,EK(3),
   C                B1N(3,3),C1N(3,3),PHI
      COMMON/BLK 12/R2,R3,R4,R5,R6,C,C2,C3,C4,C5,C6,C7,C8,C9,C10,
   C          RN1,RN2,RN3,RN4,RN5,W,PI,PIP5,CR,CR2,ERFCO,EXPO,
   C          XKC,XKC2,DK2
      COMMON/BLK 13/RSS1(60),XG1INFS(60),
   C          XG2INFS(60),YG1INFS(60),YG2INFS(60),YH1INFS(60),
   C          YH2INFS(60),XMINFS(60),YMINFS(60),ZMINFS(60)
      COMMON/BLK 14/S1,S2,S3,S4,S5,S6,S7,S8,S9,S10,X11AR,Y11AR,
   C          Y11BR,X11CR,Y11CR
      COMMON/BLK 15/DA111(3,3,3),DB111(3,3,3),DC111(3,3,3),
   C          GRADR(6,6,3)
      COMMON/BLK 16/DRSS(55),DX11AS(55),DY11AS(55),DY11BS(55),
   C          DX11CS(55),DY11CS(55)
      DIMENSION F(42),U(42),R(126,126),SAV(105,126),DZP(21)
      DIMENSION RAVG(6,6),CORM(126,126),A2(231,231),DXP(21),DYP(21)
      XSP = ((4.00/3.00)*PI/PHI)**0.3333333333300
      N = 3*NSPH
      NX5 = 5*NSPH
      NDIM = 2*N
      N11 = 11*NSPH
      V = W/2.00
C
C     SET DIMENSIONS OF PERIODIC BOX
C
      WX = SHR1*W
      WY = SHR2*W
      WZ = SHR3*W
      NLAY = 2
C
C     INITIALIZE ARRAYS TO ZERO
C
      DO 143 I = 1,6
        DO 142 J = 1,6
```

```
              DO 141 K = 1,3
                GRADR(I,J,K) = 0.00
141           CONTINUE
142         CONTINUE
143       CONTINUE
          DO 156 I = 1,NDIM
            DO 155 J = 1,NDIM
              RL(I,J) = 0.00
155         CONTINUE
156       CONTINUE
C
C         LOOP OVER SPHERES IN SYSTEM TO CALCULATE INTERACTIONS.  THE
C         LOOP OVER J GOES FROM I+1 TO NSPH TO MAKE USE OF THE SYMMETRY
C         IN THE INTERACTIONS - THAT IS, IF THE INTERACTION BETWEEN
C         SPHERES 1 AND 2 HAS BEEN CALCULATED, THEN ONE NEED NOT CALCU-
C         LATE THE INTERACTION BETWEEN 2 AND 1, ETC.
C
          DO 400 I = 1,NSPH-1
            DO 350 J = I+1,NSPH
            DX = X(J) - X(I)
            DY = Y(J) - Y(I)
            DZ = Z(J) - Z(I
C
C         APPLY PERIODIC BOUNDARY CONDITIONS
C
            DX1 = DX - WX
            DX2 = DX + WX
            DY1 = DY - WY
            DY2 = DY + WY
            DZ1 = DZ - WZ
            DZ2 = DZ + WZ
            IF (ABS(DX1).LT.ABS(DX)) DX = DX1
            IF (ABS(DX2).LT.ABS(DX)) DX = DX2
            IF (ABS(DY1).LT.ABS(DY)) DY = DY1
            IF (ABS(DY2).LT.ABS(DY)) DY = DY2
            IF (ABS(DZ1).LT.ABS(DZ)) DZ = DZ1
            IF (ABS(DZ2).LT.ABS(DZ)) DZ = DZ2
154         CONTINUE
            DS = (DX*DX + DY*DY + DZ*DZ)**0.500
            DR = DS
            E(1) = DX/DS
            E(2) = DY/DS
            E(3) = DZ/DS
177       CONTINUE
C
C
          DO 160 K = 1,3
            DO 159 L = 1,3
              A1N(K,L) = 0.00
              B1N(K,L) = 0.00
              C1N(K,L) = 0.00
              DO 158 K1 = 1,3
```

```
              H12T(K,L,K1) = 0.00
              G12T(K,L,K1) = 0.00
              DO 157 L1 = 1,3
                XM12T(K,L,K1,L1) = 0.00
157           CONTINUE
158          CONTINUE
159       CONTINUE
160     CONTINUE
        DO 175 L = -NLAY,NLAY
          DO 170 K = -NLAY,NLAY
            DO 165 M = -NLAY,NLAY
                DL = FLOAT(L)
                DN = FLOAT(K)
                DM = FLOAT(M)
                DN1 = DX + DN*WX
                DL1 = DY + DL*WY
                DM1 = DZ + DM*WZ
           DRS = (DN1*DN1+DL1*DL1+DM1*DM1)**0.500
                ES(1) = (DX+DN*WX)/DRS
                ES(2) = (DY+DL*WY)/DRS
                ES(3) = (DZ+DM*WZ)/DRS
           DK =(((DN/WX)*(DN/WX)+(DL/WY)*(DL/WY)+(DM/WZ)*(DM/WZ))**0.5)
     C                  *2.00*PI
                IF (DK.EQ.0.00) GO TO 164
                  EK(1) = 2.00*PI*(DN/WX)/DK
                  EK(2) = 2.00*PI*(DL/WY)/DK
                  EK(3) = 2.00*PI*(DM/WZ)/DK
164             CONTINUE
                CALL EWMOBA
                IF (L.GT.1) GO TO 165
                IF (L.LT.-1) GO TO 165
                IF (K.GT.1) GO TO 165
                IF (K.LT.-1) GO TO 165
                IF (M.GT.1) GO TO 165
                IF (M.LT.-1) GO TO 165
                CALL EWMOBB
                CALL EWMOBC
                CALL EWFTS
                CALL EWMOBES
165         CONTINUE
170       CONTINUE
175     CONTINUE
        CALL ASSLE1
176     CONTINUE
C
          CALL SSI
          CALL ASSLE2(N)
350      CONTINUE
400     CONTINUE
C
C       COMPUTE INTERACTIONS WITH SELF REFLECTIONS
C
```

```
        DO 442 L = 1,3
          DO 441 K = 1,3
            A1N(L,K) = 0.00
            C1N(L,K) = 0.00
441       CONTINUE
442     CONTINUE
        DO 444 L = 1,3
          DO 443 K = 1,3
            DO 439 L1 = 1,3
              DO 438 K1 = 1,3
                XM12T(L,K,L1,K1) = 0.00
438           CONTINUE
439         CONTINUE
443       CONTINUE
444     CONTINUE
        DO 455 L = -NLAY,NLAY
          DO 450 K = -NLAY,NLAY
            DO 445 M = -NLAY,NLAY
                DL = FLOAT(L)
                DN = FLOAT(K)
                DM = FLOAT(M)
           DL1 = DL*WY
           DN1 = DN*WX
           DM1 = DM*WZ
           DRS = (DN1*DN1 + DL1*DL1 + DM1*DM1)**0.500
                IF (DRS.EQ.0.00) GO TO 445
                  DK = 2.00*PI*(((DN/WX)*(DN/WX)+(DL/WY)*(DL/WY)
     C                          +(DM/WZ)*(DM/WZ))**0.5)
                  ES(1) = (DN*WX)/DRS
                  ES(2) = (DL*WY)/DRS
                  ES(3) = (DM*WZ)/DRS
                  EK(1) = 2.00*PI*DN/(WX*DK)
                  EK(2) = 2.00*PI*DL/(WY*DK)
                  EK(3) = 2.00*PI*DM/(WZ*DK)
                  DX = 0.00
                  DY = 0.00
                  DZ = 0.00
                  CALL EWMOBA
                  IF (L.GT.1) GO TO 445
                  IF (L.LT.-1) GO TO 445
                  IF (K.GT.1) GO TO 445
                  IF (K.LT.-1) GO TO 445
                  IF (M.GT.1) GO TO 445
                  IF (M.LT.-1) GO TO 445
                  CALL EWMOBC
                  CALL EWMOBES
445         CONTINUE
450       CONTINUE
455     CONTINUE
        CALL ASSLE1
        DO 500 I = 1,N
          XMOBMATA(I,I) = A1N(1,1)-6.00*PIP5*C+(40.00/3.00)*PIP5
```

```
   C    *(C**3)*(1.00-0.200*PHI)+1.00
     XMOBMATC(I,I) = 0.7500+C1N(1,1)-10.00*PIP5*(C**3)
500 CONTINUE
    DO 510 I = 1,NX5,5
     J = 4
     XMES(I,I) = 0.900*(2.00/1.00)+(3.00/16.00)*PIP5*(-128.00
   C    *(C**3)+(8064.00/25.00)*(C**5))+XM12(1,1)
     XMES(I+J,I+J) = XMES(I,I)
C
     XMES(I+1,I+1) = 1.8000+(3.00/16.00)*PIP5*(-128.00*
   C    (C**3)+(8064.00/25.00)*(C**5))+XM12(2,2)
     XMES(I+2,I+2) = XMES(I+1,I+1)
     XMES(I+3,I+3) = XMES(I+1,I+1)
C
     XMES(I,I+J) = 0.500*XMES(I,I)
     XMES(I+J,I) = 0.500*XMES(I,I)
510 CONTINUE
C
C   USE SYMMETRY TO FILL IN XMOBMATS
C
    DO 550 I = 1,N
     DO 525 J = 1,I
      XMOBMATA(I,J) = XMOBMATA(J,I)
      XMOBMATC(I,J) = XMOBMATC(J,I)
525  CONTINUE
550 CONTINUE
551 CONTINUE
C
C   USE SYMMETRY TO FILL IN RL AND XMES
C
    DO 558 I = 1,NDIM
     DO 555 J = 1,I
      RL(I,J) = RL(J,I)
555  CONTINUE
558 CONTINUE
    DO 408 I = 1,NX5
     DO 405 J = I,NX5
      XMES(J,I) = XMES(I,J)
405  CONTINUE
408 CONTINUE
C
C   INVERT MOBMATS USING CHOLESKI'S METHOD
C
    DO 560 I = 1,N11
     DO 559 J = 1,N11
      A2(I,J) = A3(I,J)
559  CONTINUE
560 CONTINUE
C
C   FILL IN 11NX11N MATRIX FOR INVERSION
C
    DO 580 I = 1,N
```

```
          DO 570 J = 1,N
            A(I,J) = XMOBMATA(I,J)
            A(I,J+N) = XMOBMATB(I,J)
            A(I+N,J+N) = XMOBMATC(I,J)
            A(J+N,I) = A(I,J+N)
570       CONTINUE
580     CONTINUE
        DO 582 I = 1,NDIM
          DO 581 J = 1,NX5
            A(I,J+NDIM) = XMUS(I,J)
581       CONTINUE
582     CONTINUE
        DO 584 I = 1,NX5
          DO 583 J = 1,NX5
            A(I+NDIM,J+NDIM) = XMES(I,J)
583       CONTINUE
584     CONTINUE
        DO 586 I = 1,N11
          DO 585 J = 1,N11
            A(J,I) = A(I,J)
            A3(I,J) = A(I,J)
585       CONTINUE
586     CONTINUE
C
C       INVERT FAR-FIELD MOBILITY
C
          CALL CHINV(N11)
          DO 588 I = 1,N11
            DO 587 J = 1,N11
              A1(I,J) = A(I,J)
587         CONTINUE
588       CONTINUE
596     CONTINUE
600     CONTINUE
C
C       CREATE COMPLETE R BY ADDING MINV TO RL
C
        DO 650 I = 1,NDIM
          DO 625 J = 1,NDIM
            A(I,J) = A1(I,J) + RL(I,J)
625       CONTINUE
650     CONTINUE
        RETURN
        END
```

```
           SUBROUTINE EWMOBA
           IMPLICIT INTEGER (I-N)
           COMMON/BLK 4/E(3),EP(3,3,3),D(3,3)
           COMMON/BLK 11/V,DX,DY,DZ,DRS,ES(3),A1N(3,3),DK,EK(3)
      C                   ,B1N(3,3),C1N(3,3),PHI
           COMMON/BLK 12/R2,R3,R4,R5,R6,C,C2,C3,C4,C5,C6,C7,C8,C9,C10,
      C           RN1,RN2,RN3,RN4,RN5,W,PI,PIP5,CR,CR2,ERFCO,
      C           EXPO,XKC,XKC2,DK2
           DIMENSION XM1A(3,3),XM1B(3,3),XM2(3,3)
           DO 4 I = 1,3
             DO 3 J = 1,3
                   XM1A(I,J) = 0.00
                   XM1B(I,J) = 0.00
                   XM2(I,J) = 0.00
 3           CONTINUE
 4         CONTINUE
           RN1 = 1.00/DRS
           RN2 = RN1*RN1
           RN3 = RN1*RN2
           RN4 = RN3*RN1
           RN5 = RN4*RN1
           R2 = DRS*DRS
           R3 = R2*DRS
           R4 = R2*R2
           R5 = R3*R2
           R6 = R3*R3
           CR = C*DRS
           CR2 = CR*CR
           ERFCO = DERFC(CR)
           EXPO = 2.00*PIP5*C*EXP(-CR2)
           DK2 = DK*DK
           XKC = DK/C
           XKC2 = XKC*XKC
           PHIX = 1.00 - 0.200*PHI
           DO 20 I = 1,3
             DO 10 J = 1,3
               XM1A(I,J) = D(I,J)*((0.7500*RN1+0.500*RN3*PHIX)*ERFCO+
      C           ((4.00*(C7)*R4+C*RN2
      C           -20.00*(C5)*R2+14.00*(C3))*PHIX
      C           +3.00*(C3)*R2-4.500*C)*PIP5*EXP(-CR2))
 C
               XM1B(I,J) = ES(I)*ES(J)*((0.7500*RN1-1.500*RN3*PHIX)*ERFCO
      C           +(-4.00*(C7)*R4*PHIX-3.00*(C3)*R2
      C           +16.00*(C5)*R2*PHIX+1.500*C-2.00*(C3)*PHIX
      C           -3.00*C*RN2*PHIX)*PIP5*EXP(-CR2))
 C
             IF (DK.EQ.0.00) GO TO 5
             XM2(I,J) = (D(I,J)-EK(I)*EK(J))*(1.00-(DK2*PHIX)/3.00)
      C           *(1.00+0.2500*(XKC**2)+0.12500*(XKC**4))
      C           *6.00*PI*EXP(-0.2500*XKC2)/DK2
 5           CONTINUE
 10          CONTINUE
```

```
 20       CONTINUE
          DO 40 I = 1,3
            DO 30 J = 1,3
              A1N(I,J) = A1N(I,J) + XM1A(I,J)+XM1B(I,J)
     C    +XM2(I,J)*COS(DK*(EK(1)*DX+EK(2)*DY+EK(3)*DZ))/(W**3)
 30         CONTINUE
 40       CONTINUE
          RETURN
          END
```

```
      SUBROUTINE EWMOBB
      IMPLICIT INTEGER (I-N)
      COMMON/BLK 4/E(3),EP(3,3,3),D(3,3)
      COMMON/BLK 11/V,DX,DY,DZ,DRS,ES(3),A1N(3,3),DK,EK(3),
    C             B1N(3,3),C1N(3,3),PHI
      COMMON/BLK 12/R2,R3,R4,R5,R6,C,C2,C3,C4,C5,C6,C7,C8,C9,C10,
    C         RN1,RN2,RN3,RN4,RN5,W,PI,PIP5,CR,CR2,ERFCO,
    C         EXPO,XKC,XKC2,DK2
      DIMENSION XM1A(3,3),XM2(3,3),DOT(3,3),DOTK(3,3),DDOT(3)
      DO 2 I = 1,3
        DDOT(I) = 0.0
2     CONTINUE
      DO 4 I = 1,3
        DO 3 J = 1,3
          XM1A(I,J) = 0.00
          XM2(I,J) = 0.00
          DOT(I,J) = 0.0
          DOTK(I,J) = 0.0
3       CONTINUE
4     CONTINUE
C
      DO 20 I = 1,3
        DO 10 J = 1,3
          DO 5 K = 1,3
              DOT(J,I) = DOT(J,I) + ES(K)*EP(K,J,I)
              DOTK(J,I) = DOTK(J,I) + EK(K)*EP(K,J,I)
5         CONTINUE
10      CONTINUE
20    CONTINUE
      DO 40 I = 1,3
        DO 30 L = 1,3
          XM1A(I,L) = (3.00/8.00)*DOT(I,L)*(-RN2*ERFCO
    C         +(-RN1+10.00*DRS*C2-4.00*C4*R3)*EXPO-RN2*ERFCO
    C         -(RN1-2.00*DRS*C2)*EXPO)
C
      IF (DK.NE.0.00) THEN
        XM2(I,L) = (-3.00*PI)*(-DOTK(I,L)-EK(I)*DDOT(L))
    C         *(1.00/DK+DK/(4.00*C2)+(DK**3)/(8.00*C4))
    C         *EXP(-XKC2/4.00)
      ENDIF
30    CONTINUE
40    CONTINUE
      DO 60 I = 1,3
        DO 50 J = 1,3
          B1N(I,J) = B1N(I,J) + XM1A(I,J) - XM2(I,J)*
    C         SIN(DK*(EK(1)*DX+EK(2)*DY+EK(3)*DZ))/(W**3)
50      CONTINUE
60    CONTINUE
      RETURN
      END
```

```
        SUBROUTINE EWMOBC
        IMPLICIT INTEGER (I-N)
        COMMON/BLK 4/E(3),EP(3,3,3),D(3,3)
        COMMON/BLK 11/V,DX,DY,DZ,DRS,ES(3),A1N(3,3),DK,EK(3),
     C               B1N(3,3),C1N(3,3),PHI
        COMMON/BLK 12/R2,R3,R4,R5,R6,C,C2,C3,C4,C5,C6,C7,C8,C9,C10,
     C          RN1,RN2,RN3,RN4,RN5,W,PI,PIP5,CR,CR2,ERFCO,
     C          EXPO,XKC,XKC2,DK2
        DIMENSION XM1A(3,3),XM2(3,3),DOT(3,3),DOTK(3,3),DDOT(3)
     C          ,XM1B(3,3)
        DO 4 I = 1,3
          DO 3 J = 1,3
            XM1A(I,J) = 0.00
            XM1B(I,J) = 0.00
            XM2(I,J) = 0.00
3         CONTINUE
4       CONTINUE
        EXP1 = EXPO
        EXPO = EXPO/(2.00*PIP5*C)
C
        DO 20 I = 1,3
          DO 10 J = 1,3
            XM1A(I,J) = D(I,J)*((3.00/8.00)*RN3*ERFCO+0.7500*
     C          PIP5*(C*RN2+14.00*C3-20.00*R2*C5+4.00*R4*C7)*EXPO)
C
C
            XM1B(I,J) = 0.7500*ES(I)*ES(J)*(-1.500*RN3*ERFCO
     C          +PIP5*(-3.00*C*RN2-2.00*C3+16.00*R2*C5-
     C          4.00*R4*C7)*EXPO)
C
        IF (DK.EQ.0.00) GO TO 5
            XM2(I,J) = -1.500*PI*(D(I,J)-EK(I)*EK(J))
     C          *(1.00+0.2500*XKC2+0.12500*(XKC2**2))
     C          *EXP(-XKC2/4.00)
5       CONTINUE
10      CONTINUE
20      CONTINUE
        DO 40 I = 1,3
          DO 30 J = 1,3
            C1N(I,J) = C1N(I,J) - XM1A(I,J)-XM1B(I,J)-
     C          XM2(I,J)*COS(DK*(EK(1)*DX+EK(2)*DY+EK(3)*DZ))/
     C          (W**3)
30        CONTINUE
40      CONTINUE
        EXPO = EXP1
        RETURN
        END
```

```
      SUBROUTINE EWFTS
      IMPLICIT INTEGER (I-N)
      COMMON/BLK 3/TEMP(12,12),DS
      COMMON/BLK 4/E(3),EP(3,3,3),D(3,3)
      COMMON/BLK 8/XM11(5,5),H11(3,5),G11(3,5),XM12(5,5),H12(3,5),
     C                G12(3,5),H12T(3,3,3),G12T(3,3,3),XM12T(3,3,3,3)
      COMMON/BLK 11/V,DX,DY,DZ,DRS,ES(3),A1N(3,3),DK,EK(3),
     C        B1N(3,3),C1N(3,3),PHI
      COMMON/BLK 12/R2,R3,R4,R5,R6,C,C2,C3,C4,C5,C6,C7,C8,C9,C10,
     C        RN1,RN2,RN3,RN4,RN5,W,PI,PIP5,CR,CR2,ERFCO,EXPO,
     C        XKC,XKC2,DK2
      DIMENSION H12AT(3,3,3),H12BT(3,3,3),G12AT(3,3,3),
     C        G12BT(3,3,3),DOT(3,3),DOTK(3,3),DDOT(3)
C
C     FILL IN XM11(5,5)
C
      DO 20 I = 1,5
        DO 10 J = 1,5
          XM11(I,J) = 0.00
10      CONTINUE
20    CONTINUE
      DO 25 I = 1,5
        XM11(I,I) = 9.00/5.00
25    CONTINUE
      XM11(5,1) = 9.00/10.00
      XM11(1,5) = 9.00/10.00
      DO 33 I = 1,3
        SUM2 = 0.00
        DO 30 J = 1,3
          SUM = 0.00
          SUM1 = 0.00
          DO 28 K = 1,3
              SUM = SUM+ES(K)*EP(K,J,I)
              SUM1 = SUM1+EK(K)*EP(K,J,I)
              SUM2 = SUM2 + EK(K)*EK(J)*EP(K,J,I)
28        CONTINUE
          DOT(J,I) = SUM
          DOTK(J,I) = SUM1
30      CONTINUE
        DDOT(I) = SUM2
33    CONTINUE
C
C     TO CREATE OTHER 2D ARRAYS, FIRST FILL IN 3D AND 4D ARRAYS
C
C
      DO 50 I = 1,3
        DO 45 J = 1,3
          DO 40 K = 1,3
              H12AT(I,J,K) = 0.00
              H12BT(I,J,K) = 0.00
              G12AT(I,J,K) = 0.00
              G12BT(I,J,K) = 0.00
```

```
40          CONTINUE
45        CONTINUE
50      CONTINUE
        EXP1 = EXPO
        EXPO = EXPO/(2.00*PIP5*C)
C
        X1 = (-6.00/R4)*ERFCO+4.00*PIP5*(-3.00*C*RN3-68.00*C5*DRS
     C         +56.00*R3*C7-2.00*C3*RN1-8.00*C9*R5)*EXPO
        X2 = 4.00*((-1.500/R4)*ERFCO+(-3.00*C*RN3-2.00*C3*RN1
     C         +16.00*C5*DRS-4.00*R3*C7)*PIP5*EXPO)
        X3 = 4.00*((7.500/R4)*ERFCO+(15.00*C*RN3+10.00*C3*RN1
     C         -40.00*C7*R3+4.00*C5*DRS+8.00*C9*R5)*PIP5*EXPO)
        X4 = (-RN2*ERFCO)+(-RN1+10.00*C2*DRS-4.00*C4*R3)*2.00*C
     C         *PIP5*EXPO
        X5 = RN2*ERFCO+(RN1-2.00*C2*DRS)*2.00*C*PIP5*EXPO
        X6 = -3.00*RN2*ERFCO+(-3.00*RN1-2.00*C2*DRS+4.00*C4*R3)
     C         *2.00*C*PIP5*EXPO
C
        X7 = 3.00*RN3*ERFCO+(3.00*RN2-28.00*C4*R2+2.00*C2+8.00
     C         *C6*R4)*2.00*PIP5*C*EXPO
        X8 = -3.00*RN3*ERFCO+(-3.00*RN2-2.00*C2+4.00*C4*R2
     C         )*2.00*C*PIP5*EXPO
        X9 = 15.00*RN3*ERFCO+(15.00*RN2+10.00*C2+4.00*C4*R2-
     C         8.00*C6*R4)*2.00*C*PIP5*EXPO
C
        DO 100 K = 1,3
          DO 90 J = K,3
            DO 80 I = 1,3
                G12AT(K,J,I) = (3.00/8.00)*((X4+X5)*(ES(K)*D(I,J)
     C            +ES(J)*D(I,K))+2.00*X5*ES(I)*D(J,K)+2.00*X6*
     C            ES(K)*ES(I)*ES(J)+(4.00/15.00)*((X1+X2)*(ES(K)
     C            *D(I,J)+ES(J)*D(I,K))+2.00*X2*E(I)*D(J,K)
     C            +2.00*X3*ES(I)*ES(J)*ES(K)))
C
                H12AT(K,J,I) = (-3.00/16.00)*(X8-X7)*(ES(K)*DOT(I,J)
     C            +ES(J)*DOT(I,K))
        IF (DK.EQ.0.00) GO TO 80
                G12BT(K,J,I) = 0.7500*0.500*(-1.00+(4.00/15.00)
     C            *DK2)*(EK(K)*(D(I,J)-EK(I)*EK(J))+EK(J)*
     C            (D(I,K)-EK(I)*EK(K)))*8.00*PI*(1.00/DK+
     C            DK/(4.00*C2)+(DK**3)/(8.00*C4))*EXP(-XKC2
     C            /4.00)
C
                H12BT(K,J,I) = (3.00/16.00)*(-DOT(I,J)*EK(K)
     C            -DOT(I,K)*EK(J))
     C            *(8.00*PI)*(1.00+XKC2/4.00+(XKC2**2)/8.00)
     C            *EXP(-XKC2/4.00)
80          CONTINUE
90        CONTINUE
100     CONTINUE
C
        DO 120 I = 1,3
```

```
          DO 110 J = I,3
            DO 105 K = 1,3
                G12T(I,J,K) = G12T(I,J,K)+G12AT(I,J,K)+
     C            G12BT(I,J,K)*SIN(DK*(EK(1)*DX+EK(2)*DY+EK(3)*DZ))
     C            /(W**3)
C
                H12T(I,J,K) = H12T(I,J,K)+H12AT(I,J,K)+
     C            H12BT(I,J,K)*COS(DK*(EK(1)*DX+EK(2)*DY+EK(3)*DZ))
     C            /(W**3)
105         CONTINUE
110       CONTINUE
120     CONTINUE
        EXPO = EXP1
        RETURN
        END
```

```
        SUBROUTINE EWMOBES
        IMPLICIT INTEGER (I-N)
        COMMON/BLK 4/E(3),EP(3,3,3),D(3,3)
        COMMON/BLK 8/XM11(5,5),H11(3,5),G11(3,5),XM12(5,5),
     C          H12(3.5),G12(3,5),H12T(3,3,3),G12T(3,3,3),
     C          XM12T(3,3,3,3)
        COMMON/BLK 11/V,DX,DY,DZ,DRS,ES(3),A1N(3,3),DK,EK(3),
     C          B1N(3,3),C1N(3,3),PHI
        COMMON/BLK 12/R2,R3,R4,R5,R6,C,C2,C3,C4,C5,C6,C7,C8,C9,C10,
     C          RN1,RN2,RN3,RN4,RN5,W,PI,PIP5,CR,CR2,ERFCO,
     C          EXPO,XKC,XKC2,DK2
        DIMENSION XM1A(3,3,3,3),XM1B(3,3,3,3),XM2(3,3,3,3)
C
C
        DO 50 I = 1,3
          DO 45 J = 1,3
            DO 40 K = 1,3
              DO 35 L = 1,3
                XM1A(I,J,K,L) = 0.00
                XM1B(I,J,K,L) = 0.00
                XM2(I,J,K,L) = 0.00
35            CONTINUE
40          CONTINUE
45        CONTINUE
50      CONTINUE
C
C
        X1 =(-RN3*ERFCO+(-RN2+10.00*C2-4.00*C4*R2)*EXPO)*RN2
        X2 =(3.00*RN3*ERFCO+(3.00*RN2-28.00*C4*R2+2.00*C2
     C          +8.00*C6*R4)*EXPO)*RN2
        X3 =(RN3*ERFCO+(RN2-2.00*C2)*EXPO)*RN2
        X4 =(-3.00*RN3*ERFCO+(-3.00*RN2-2.00*C2+4.00*C4*R2)*EXPO)*RN2
        X5 =(15.00*RN3*ERFCO+(15.00*RN2+10.00*C2+4.00*C4*R2
     C          -8.00*C6*R4)*EXPO)*RN2
C
C
        DX1 = 3.00*RN5*ERFCO+(3.00*RN4-8.00*C4+2.00*C2*RN2
     C          -20.00*C4+8.00*C6*R2)*EXPO
        DX2 = -15.00*RN5*ERFCO+(-15.00*RN4-10.00*C2*RN2
     C          +72.00*C6*R2-4.00*C4-16.00*C8*R4)*EXPO
        DX3 = -3.00*RN5*ERFCO+(-3.00*RN4-2.00*C2*RN2+4.00*C4)*EXPO
        DX4 = 15.00*RN5*ERFCO+(15.00*RN4+10.00*C2*RN2+4.00*C4
     C          -8.00*C6*R2)*EXPO
        DX5 = -105.00*RN5*ERFCO+(-105.00*RN4-70.00*C2*RN2-28.00*C4
     C          -8.00*C6*R2+16.00*C8*R4)*EXPO
C
C
        D2X1 = -6.00*RN5*ERFCO+(-6.00*RN4-88.00*C4-4.00*C2*RN2
     C          +96.00*C6*R2-16.00*C8*R4)*EXPO
        D2X2 = 60.00*RN5*ERFCO+(60.00*RN4+40.00*C2*RN2+224.00
     C          *C6*R2+16.00*C4-224.00*C8*R4+32.00*C10*R6)*EXPO
        D2X3 = 6.00*RN5*ERFCO+(6.00*RN4+4.00*C2*RN2+16.00*C4
```

```
     C          -8.00*C6*R2)*EXPO
        D2X4 = -60.00*RN5*ERFCO+(-60.00*RN4-40.00*C2*RN2
     C          -16.00*C4-32.00*C6*R2+16.00*C8*R4)*EXPO
        D2X5 = 630.00*RN5*ERFCO+(630.00*RN4+420.00*C2*RN2
     C          +168.00*C4+48.00*C6*R2+64.00*C8*R4
     C          -32.00*C10*R6)*EXPO
C
C
        DO 100 I = 1,3
          DO 90 L = I,3
            DO 80 J = L,3
              DO 70 K = 1,J
        XM1A(I,L,J,K) = 2.00*(X3+X1)*(D(L,K)*D(I,J)+D(J,L)*D(I,K))
     C          +4.00*X3*D(J,K)*D(I,L)+(X2+3.00*X4)*(D(I,J)*ES(L)*ES(K)
     C          +D(J,L)*ES(I)*ES(K)+D(L,K)*ES(I)*ES(J)+D(I,K)*ES(J)
     C          *ES(L))+4.00*X4*(D(I,L)*ES(J)*ES(K)+D(J,K)*ES(I)*ES(L))
     C          +4.00*X5*ES(I)*ES(J)*ES(K)*ES(L)
C
        XM1B(I,L,J,K) = 2.00*(D2X1+2.00*X2+6.00*X4+D2X3)*(D(J,L)*
     C          D(K,I)+D(K,L)*D(I,J))+4.00*(D2X3+4.00*X4)*D(J,K)*
     C          D(I,L)+4.00*(D2X4+2.00*X5+4.00*DX4)*(D(I,L)*ES(K)*
     C          ES(J)+D(J,K)*ES(I)*ES(L))+(3.00*(D2X4+2.00*X5
     C          +4.00*DX4)+4.00*DX2+D2X2+2.00*X5)*(D(I,K)*ES(L)*ES(J)
     C          +D(K,L)*ES(I)*ES(J)+D(J,L)*ES(I)*ES(K)+D(I,J)*ES(K)
     C          *ES(L))+4.00*(8.00*DX5+D2X5)*ES(L)*ES(K)*ES(I)*ES(J)
C
        IF (DK.EQ.0.00) GO TO 65
C
        XM2(I,L,J,K) = (1.00-0.200*DK2)*(EK(L)*EK(K)*(D(I,J)-
     C          EK(I)*EK(J))+EK(L)*EK(J)*(D(I,K)-EK(I)*EK(K))
     C          +EK(I)*EK(K)*(D(L,J)-EK(L)*EK(J))+EK(I)*EK(J)*
     C          (D(L,K)-EK(L)*EK(K)))*8.00*PI*(1.00+0.2500*XKC2
     C          +0.12500*(XKC2**2))*EXP(-0.2500*XKC2)
65      CONTINUE
        XM12T(I,L,J,K) =-(3.00/16.00)*R2*XM1A(I,L,J,K)+XM12T(I,L,J,K)
     C          -(3.00/80.00)*XM1B(I,L,J,K)+(3.00/16.00)*XM2(I,L,J,K)
     C          *COS(DK*(EK(1)*DX+EK(2)*DY+EK(3)*DZ))/W**3
70             CONTINUE
80            CONTINUE
90          CONTINUE
100     CONTINUE
        RETURN
        END
```

```
        SUBROUTINE ASSLE1
        COMMON/BLK 8/XM11(5,5),H11(3,5),G11(3,5),XM12(5,5),
     C          H12(3,5),G12(3,5),H12T(3,3,3),G12T(3,3,3),
     C          XM12T(3,3,3,3)
C
C       TWO DIMENSIONALIZE STRESSLET PIECES OF MOBILITY
C
        H12(1,1) = H12T(1,1,1) - H12T(3,3,1)
        H12(1,2) = 2.00*H12T(1,2,1)
        H12(1,3) = 2.00*H12T(1,3,1)
        H12(1,4) = 2.00*H12T(2,3,1)
        H12(1,5) = H12T(2,2,1)-H12T(3,3,1)
        H12(2,1) = H12T(1,1,2)-H12T(3,3,2)
        H12(2,2) = 2.00*H12T(1,2,2)
        H12(2,3) = 2.00*H12T(1,3,2)
        H12(2,4) = 2.00*H12T(2,3,2)
        H12(2,5) = H12T(2,2,2)-H12T(3,3,2)
        H12(3,1) = H12T(1,1,3) - H12T(3,3,3)
        H12(3,2) = 2.00*H12T(1,2,3)
        H12(3,3) = 2.00*H12T(1,3,3)
        H12(3,4) = 2.00*H12T(2,3,3)
        H12(3,5) = H12T(2,2,3) - H12T(3,3,3)
C
C       CREATE G12(3,5)
C
        G12(1,1) = G12T(1,1,1) - G12T(3,3,1)
        G12(1,2) = 2.00*G12T(1,2,1)
        G12(1,3) = 2.00*G12T(1,3,1)
        G12(1,4) = 2.00*G12T(2,3,1)
        G12(1,5) = G12T(2,2,1) - G12T(3,3,1)
        G12(2,1) = G12T(1,1,2) - G12T(3,3,2)
        G12(2,2) = 2.00*G12T(1,2,2)
        G12(2,3) = 2.00*G12T(1,3,2)
        G12(2,4) = 2.00*G12T(2,3,2)
        G12(2,5) = G12T(2,2,2) - G12T(3,3,2)
        G12(3,1) = G12T(1,1,3) - G12T(3,3,3)
        G12(3,2) = 2.00*G12T(1,2,3)
        G12(3,3) = 2.00*G12T(1,3,3)
        G12(3,4) = 2.00*G12T(2,3,3)
        G12(3,5) = G12T(2,2,3) - G12T(3,3,3)
C
        XM12(1,1) = XM12T(1,1,1,1)-2.00*XM12T(1,1,3,3)+XM12T(3,3,3,3)
        XM12(1,2) = 2.00*(XM12T(1,1,2,1)-XM12T(1,2,3,3))
        XM12(1,3) = 2.00*(XM12T(1,1,3,1)-XM12T(1,3,3,3))
        XM12(1,4) = 2.00*(XM12T(1,1,3,2)-XM12T(2,3,3,3))
        XM12(1,5) = XM12T(1,1,2,2)-XM12T(1,1,3,3)-XM12T(2,2,3,3)
     C          +XM12T(3,3,3,3)
        XM12(2,2) = 4.00*XM12T(1,2,2,1)
        XM12(2,3) = 4.00*XM12T(1,2,3,1)
        XM12(2,4) = 4.00*XM12T(1,2,3,2)
        XM12(2,5) = 2.00*(XM12T(1,2,2,2)-XM12T(1,2,3,3))
        XM12(3,3) = 4.00*(XM12T(1,3,3,1))
```

```
      XM12(3,4) = 4.00*XM12T(1,3,3,2)
      XM12(3,5) = 2.00*(XM12T(2,2,3,1)-XM12T(1,3,3,3))
      XM12(4,4) = 4.00*XM12T(2,3,3,2)
      XM12(4,5) = 2.00*(XM12T(2,2,3,2)-XM12T(2,3,3,3))
      XM12(5,5) = XM12T(2,2,2,2) - 2.00*XM12T(2,2,3,3)+XM12T(3,3,3,3)
C
      DO 120 I = 1,5
        DO 110 J = I,5
          XM12(J,I) = XM12(I,J)
110     CONTINUE
120   CONTINUE
      RETURN
      END
```

```
        SUBROUTINE ASSLE2(N)
        IMPLICIT INTEGER (I-N)
        COMMON/BLK 3/TEMP(12,12),DS
        COMMON/BLK 8/XM11(5,5),H11(3,5),G11(3,5),XM12(5,5),
     C          H12(3,5),G12(3,5),H12T(3,3,3),G12T(3,3,3),
     C          XM12T(3,3,3,3)
        COMMON/BLK 9/XMES(105,105),XMUS(126,105),XMOBMATA(63,63),
     C          XMOBMATB(63,63),XMOBMATC(63,63),RL(126,126),I,J
        COMMON/BLK 11/V,DX,DY,DZ,DRS,ES(3),A1N(3,3),DK,EK(3),
     C          B1N(3,3),C1N(3,3),PHI
C
          DO 250 K = 1,3
            DO 200 L = 1,3
             N1 = L+3*(J-1)
             N2 = K+3*(J-1)
             N3 = K+3*(I-1)
             N4 = L+3*(I-1)
C
             XMOBMATB(N3,N1) = B1N(K,L)
             XMOBMATB(N1,N3) = XMOBMATB(N3,N1)
             XMOBMATA(N3,N1) = A1N(K,L)
             XMOBMATC(N3,N1) = C1N(K,L)
C
             RL(N3,N4) = TEMP(K,L) + RL(N3,N4)
             RL(N3,N4+N) = TEMP(K,L+6) + RL(N3,N4+N)
             RL(N3,N1) = TEMP(K,L+3)
             RL(N3,N1+N) = TEMP(K,L+9)
             RL(N1,N3+N) =  RL(N3,N1+N)
             RL(N3+N,N4+N) = TEMP(K+6,L+6) + RL(N3+N,N4+N)
             RL(N3+N,N1+N) = TEMP(K+6,L+9)
C
             RL(N2,N1)= TEMP(K,L) + RL(N2,N1)
             RL(N2,N1+N) =-TEMP(K,L+6) + RL(N2,N1+N)
             RL(N2+N,N1+N) = TEMP(K+6,L+6) + RL(N2+N,N1+N)
200        CONTINUE
250       CONTINUE
C
C          ASSEMBLE XMUS(5NX6N) AND XMES(5NX5N) FOR FTS METHOD
C
           DO 280 K = 1,5
             DO 270 L = 1,5
               N1 = L+5*(J-1)
               N2 = K+5*(J-1)
               N3 = K+5*(I-1)
               N4 = L+5*(I-1)
C
               XMES(N3,N1) = XM12(K,L)
270          CONTINUE
280        CONTINUE
           DO 320 K = 1,3
             DO 310 L = 1,5
               N1 = L+5*(J-1)
```

```
            N2 = K+3*(J-1)
            N3 = K+3*(I-1)
            N4 = L+5*(I-1)
            XMUS(N3,N1) = G12(K,L)
            XMUS(N2,N4) = -G12(K,L)
            XMUS(N3+N,N1) = H12(K,L)
            XMUS(N2+N,N4) = H12(K,L)
310       CONTINUE
320     CONTINUE
      RETURN
      END
```

```
        SUBROUTINE SSI
        IMPLICIT INTEGER (I-N)
        COMMON/BLK 3/TEMP(12,12),DS
        COMMON/BLK 4/E(3),EP(3,3,3),D(3,3)
        COMMON/BLK 6/RSS(50),X11AS(50),X12AS(50),Y11AS(50),Y12AS(50),
     C              Y11BS(50),Y12BS(50),X11CS(50),X12CS(50),Y11CS(50),
     C              Y12CS(50)
        COMMON/BLK 7/X11ASINF(50),X12ASINF(50),Y11ASINF(50),
     C         Y12ASINF(50),Y11BSINF(50),Y12BSINF(50),
     C         Y11CSINF(50),Y12CSINF(50),X11CSINF(50),X12CSINF(50)
        COMMON/BLK 14/S1,S2,S3,S4,S5,S6,S7,S8,S9,S10,X11AR,Y11AR,
     C         Y11BR,X11CR,Y11CR
C
C       DETERMINE WHICH RANGE DR FALLS IN
C
        DR = DS
        S1 = 1.00/DR
        S2 = S1*S1
        S3 = S2*S1
        S4 = S2*S2
        S5 = S3*S2
        S6 = S4*S2
        S7 = S4*S3
        S8 = S4*S4
        S9 = S4*S5
        S10 = S5*S5
        R1 = S1
        R2 = S2
        R3 = S3
        R4 = S4
        R5 = S5
        R6 = S6
        R7 = S7
        R8 = S8
        R9 = S9
        R10 = S10
        IF (DR.GE.4.00) GO TO 20
        IF (DR.LE.2.0200) GO TO 125
        IF (DR.GE.2.100) GO TO 150
C
        IB = -1 + INT(100.00 * (DR - 2.00))
        GO TO 175
C
20      CONTINUE
C
        X11AR= 1.00+2.2500*R2+5.812500*R4+18.70300*R6
     C         +77.42600*R8
        Y11AR= 1.00+0.562500*R2+1.816400*R4+3.599900*R6
     C         +8.697800*R8
        Y11BR= -(0.7500*R3+1.421900*R5+5.737300*R7+20.70800*R9)
        Y11CR= 1.3333300+R4+5.895800*R6+15.56600*R8
        X11CR= 1.3333300 + 1.3333300*R6 + 4.00*R8
```

```
C       X12AR= -(1.500*R1+2.37500*R3+12.09400*R5+41.64800*R7
C    C           +148.6600*R9)
C       Y12AR= -(0.7500*R1+0.9218800*R3+2.206100*R5+5.471400*R7+
C    C           16.98100*R9)
C       Y12BR= R2+0.562500*R4+2.191400*R6+10.49800*R8
C       X12CR= -1.33333300*R3-1.3333300*R9
C       Y12CR= 0.66666700*R3+0.7500*R5+1.921900*R7+1.935200*R9
        DO 40 I = 1,12
          DO 35 J = 1,12
                TEMP(I,J) = 0.00
35        CONTINUE
40      CONTINUE
        GO TO 655
125     CONTINUE
        XI = DR - 2.00
        XI1 = 1.00/XI
        DLX = LOG(XI1)
        XDLX = XI*DLX
C
        X11AR= 0.2500*XI1+0.22500*DLX+0.9953800+0.02678600*XDLX
     C          - (2.2257900 - 1.86700*XI)
        Y11AR= 0.16666700*DLX+0.998300 - (1.3922400-1.03500*XI)
        Y11BR= -0.16666700*DLX+0.159400-0.083333*XDLX
     C          -(-0.24888600+0.800000*XI)
        X11CR= 1.4024000 + 0.16666700*XDLX
     C          -(1.354500-0.062500*XI)
        Y11CR= 0.26666700*DLX+0.937200+0.2506700*XDLX
     C          -(1.5426300-0.72600*XI)
        X12AR= -X11AR + 0.6451800-(-1.5837300+1.92500*XI)
     C          -(2.2257900 - 1.86700*XI)
        Y12AR= -Y11AR + 0.724600 -(-0.67227600+1.12900*XI)
     C          -(1.3922400-1.03500*XI)
        Y12BR= -Y11BR + 0.158300 -(0.40487800-0.89200*XI)
     C          -(-0.24888600+0.800000*XI)
        Y12CR= 0.066666700*DLX-0.0365300 + 0.500*0.1653300*XDLX
     C                  -(0.17550200-0.57300*XI)
        X12CR= -0.20034300+0.16666700*XDLX
     C                  -(-0.169312000+0.2565000*XI)
C
        Y11AR = Y11AR + 0.110800*XI
        Y12AR = Y12AR - 0.0236500*XI
        Y11BR = Y11BR - 0.192900*XI
        Y12BR = Y12BR + 0.0941800*XI
        GO TO 200
C
150     CONTINUE
        IB = 7+INT(20.00*(DR-2.00))
175     CONTINUE
        IA=IB +1
        C1=(DR-RSS(IB))/(RSS(IA)-RSS(IB))
        X11AR= (X11AS(IA)-X11AS(IB))*C1+X11AS(IB)
        Y11AR= (Y11AS(IA)-Y11AS(IB))*C1+Y11AS(IB)
```

```
      Y11BR= (Y11BS(IA)-Y11BS(IB))*C1+Y11BS(IB)
      X11CR= (X11CS(IA)-X11CS(IB))*C1+X11CS(IB)
      Y11CR= (Y11CS(IA)-Y11CS(IB))*C1+Y11CS(IB)
      X12AR= (X12AS(IA)-X12AS(IB))*C1+X12AS(IB)
      Y12AR= (Y12AS(IA)-Y12AS(IB))*C1+Y12AS(IB)
      Y12BR= (Y12BS(IA)-Y12BS(IB))*C1+Y12BS(IB)
      X12CR= (X12CS(IA)-X12CS(IB))*C1+X12CS(IB)
      Y12CR= (Y12CS(IA)-Y12CS(IB))*C1+Y12CS(IB)
C
      X11ARINF= (X11ASINF(IA)-X11ASINF(IB))*C1+X11ASINF(IB)
      Y11ARINF= (Y11ASINF(IA)-Y11ASINF(IB))*C1+Y11ASINF(IB)
      Y11BRINF= (Y11BSINF(IA)-Y11BSINF(IB))*C1+Y11BSINF(IB)
      X11CRINF= (X11CSINF(IA)-X11CSINF(IB))*C1+X11CSINF(IB)
      Y11CRINF= (Y11CSINF(IA)-Y11CSINF(IB))*C1+Y11CSINF(IB)
      X12ARINF= (X12ASINF(IA)-X12ASINF(IB))*C1+X12ASINF(IB)
      Y12ARINF= (Y12ASINF(IA)-Y12ASINF(IB))*C1+Y12ASINF(IB)
      Y12BRINF= (Y12BSINF(IA)-Y12BSINF(IB))*C1+Y12BSINF(IB)
      X12CRINF= (X12CSINF(IA)-X12CSINF(IB))*C1+X12CSINF(IB)
      Y12CRINF= (Y12CSINF(IA)-Y12CSINF(IB))*C1+Y12CSINF(IB)
C
      X11AR = X11AR - X11ARINF
      Y11AR = Y11AR - Y11ARINF
      Y11BR = Y11BR - Y11BRINF
      X11CR = X11CR - X11CRINF
      Y11CR = Y11CR - Y11CRINF
      X12AR = X12AR - X12ARINF
      Y12AR = Y12AR - Y12ARINF
      Y12BR = Y12BR - Y12BRINF
      X12CR = X12CR - X12CRINF
      Y12CR = Y12CR - Y12CRINF
200   CONTINUE
C
C     FILL TEMP MATRIX
C
      DO 400 I = 1,3
        DO 350 J = 1,3
        DOT = 0.00
        DO 300 K = 1,3
          SUM1 = EP(J,I,K)*E(K)
          DOT = DOT + SUM1
300     CONTINUE
        TEMP(I,J+6) = Y11BR*DOT
        TEMP(I,J+9) =-Y12BR*DOT
        TEMP(I+3,J+6) = -TEMP(I,J+9)
        TEMP(I+3,J+9) = -TEMP(I,J+6)
C
        TEMP(I,J) = X11AR*E(I)*E(J)+Y11AR*(D(I,J)-E(I)*E(J))
        TEMP(I,J+3) = X12AR*E(I)*E(J)+Y12AR*(D(I,J)-E(I)*E(J))
        TEMP(I+3,J+3) = TEMP(I,J)
C
        TEMP(I+6,J+6) = X11CR*E(I)*E(J)+Y11CR*(D(I,J)-E(I)*E(J))
        TEMP(I+6,J+9) = X12CR*E(I)*E(J)+Y12CR*(D(I,J)-E(I)*E(J))
```

```
            TEMP(I+9,J+9) = TEMP(I+6,J+6)
350         CONTINUE
400       CONTINUE
          DO 650 I = 1,12
            DO 625 J = I,12
               TEMP(J,I) = TEMP(I,J)
625         CONTINUE
650       CONTINUE
655       CONTINUE
C
C         SUBTRACT RINF FROM TEMP
C
C         DO 1000 I = 1,12
C           DO 950 J = 1,12
C             TEMP(I,J) = TEMP(I,J) - RINF(I,J)
C           CONTINUE
C         CONTINUE
          RETURN
          END
```